VERIFICATION OF COMPUTER SIMULATION METHODS FOR SLAB AND GIRDER BRIDGE SYSTEMS

by

A. F. Alani and J. E. Breen

PREFACE

This report summarizes a detailed investigation of the agreement
between previously developed computer simulation programs for slab and
girder bridge systems and the physical systems which they represent.
This report presents comparisons between physical test data and computer
results for a wide variety of typical slab and girder bridge systems.

In the development of the comparisons between the computer solu-
tions and physical tests it was often necessary to conduct physical tests
of certain types of slab and girder bridge systems, as well as to go
into great detail on comparisons with large numbers of specimens tested
by other investigators. Details of these physical tests and some of
the more repetitive data on computer simulations have been presented in
a series of MS theses which are referenced in this report. In addition,
a copy of each of these theses has been deposited with The University of
Texas Center for Highway Research and the Texas Highway Department Bridge
Division for use by readers seeking more details on physical tests and
comparisons.

The background theses which have been put on file are:

Bakir, N. N., "A Study of a 45° Skew Simply Supported Prestressed
    Concrete Bridge," MS thesis, The University of Texas at Austin,
    May 1970.

Barboza, N. J., "Load Distribution in a Skew Prestressed Concrete
    Bridge," MS thesis, The University of Texas at Austin, 1969.

Kaczmarek, J. A., "Comparison of Computer Analysis and Experimental
    Data for Concrete Slab and Steel Girder Bridges," MS thesis,
    The University of Texas at Austin, January 1970.

Repa, J. A., Jr., "Flexural Stiffness Redistribution in Typical
    Highway Bents," MS thesis, The University of Texas at Austin,
    August 1970.

This work is a part of Research Study 3-5-68-115, entitled "Experi-
mental Verification of Computer Simulation Methods for Slab and Girder

A B S T R A C T

Typical orthotropic slab and girder bridges were studied and the
correlation between reported test results and computerized analytical solu-
tions evaluated. Emphasis was given to a discrete element simulation
process developed in Project 3-5- 63-56. The range of application of the
previously developed computer programs was explored. Three types of slab
and girder bridge systems were studied. Prestressed concrete, reinforced
concrete and both composite and noncomposite steel girders with concrete
slabs were evaluated. These bridges included both simple and continuous
spans and included both normal and skew crossings.

The parameters involved in the analytical solutions were defined.
Evaluation of the range of these parameters and their effect on the final
results was outlined. The most important parameters studied included the
flexural and torsional stiffnesses of the girders. Effects of these param-
eters were studied thoroughly for each bridge system.

A computer program to generate realistic moment curvature relationships
for reinforced concrete members was developed. This program takes into
account the effect of crack formation on the behavior of members. The
study of crack formation shows that the steel percentage present in the
section has a large influence on the behavior of the concrete members.
Results from this computer program were compared with reported test values
of ten beams and four columns, and these show excellent correlation.

The computer simulation requirements for the slab and girder bridge
systems were presented and detailed procedures outlined to obtain good mathe-
matical models for the physical systems. This report includes the comparison
and analysis of test results for thirteen representative slab and girder
bridges. The parameters of the bridges were evaluated according to the
recommended methods presented in the study. In general, the correlation
with physical test results was excellent.

S U M M A R Y

This report presents a detailed comparison between typical test measurements and computerized analytical solutions for conventional slab and girder bridges. The accuracy of applying computer analysis techniques developed under Project 3-5-63-56 to prestressed concrete, reinforced concrete, and steel girder bridges with concrete deck slabs was confirmed by the high degree of correlation between test results and program calculations.

The method of inputting girder and slab physical properties was carefully examined and numerous recommendations were made for the proper values of stiffnesses to be input by designers. In addition, the effect of various inputs on accuracy was examined and guidelines were developed so that the designer would be given an indication of when a precise number was needed for an input and when an approximate number would suffice.

The bridges studied included both simple and continuous spans and normal and skew crossings. The analytical methods were shown to give a very accurate estimate of both load distribution characteristics and short-term deflections. The programs should be valuable in design of standard bridge systems and in investigation of special problems.

IMPLEMENTATION

This study indicates that the discrete element computer simulation programs for analysis of slab and girder bridges developed in Project 3-5-63-56 can be applied to a wide range of representative slab and girder bridges with a high degree of accuracy. While the present study established a reliability of the analytical procedures in order to arrive at an accurate estimate of bridge behavior (load distribution and deflections) under different kinds of loading and with various bridge configurations, design requirements will be best served by now using the verified computer programs to study a specific bridge class and to develop standard designs for that class. The computer procedures can also be utilized to study very specific bridge problems when the complexity of the problem wants special attention.

Guidelines for the evaluation of typical parameters such as the flexural and torsional stiffnesses of the girders and slabs are given and a method of generating realistic stiffnesses for reinforced concrete members is developed in detail. These procedures can be utilized by designers in selecting the input values to the computer programs in order to gain necessary accuracy. In a number of cases the sensitivity of the solution to various parameters is presented and recommendations are made so that the designer can choose the accuracy required for his input data according to the type of problem being solved.

In general the excellent correlation between the physical test results and the computer solutions should result in the Bridge Division having greater confidence in the reliability of the computer solutions and a clearer set of procedures for inputing physical constants. This will allow more accurate design procedures for slab and girder bridges with consequent improvement in design and greater reliability and economy.

CONTENTS

LIST OF NOTATIONS

A = cross-sectional area of the girder

A_s = area of tensile reinforcement

a = area of the rectangle inscribed in the joint

b = longer side of a rectangle

C = constant

c = shorter side of a rectangle

D $= \dfrac{Eh^3}{12(1 - \nu^2)}$ = flexural rigidity of plate, bar diameter in inches

D_{xy} = torsional rigidity

E = Young's modulus of elasticity

E_c = modulus of elasticity of concrete

E_s = modulus of elasticity of steel

FS = factor of safety

f_c = concrete stress

f'_c = compressive strength of concrete, psi

f''_c $= 0.85f'_c$

f_s = tensile stress in reinforcement

f'_t = ultimate tensile strength of concrete

f_y = yield strength of reinforcement

G $= \dfrac{E_c}{2(1 + \nu)}$, shear modulus

h = girder height, slab thickness

I = moment of inertia

I_c, I_s = moment of inertia of concrete and reinforcement, respectively, taken about the neutral axis

I_{cr} = cracked section moment of inertia

I_g = gross section moment of inertia

I_w = warping moment of inertia

K' = empirical coefficient to determine the correction in steel strain

K_r = torsional rigidity of the section

K_T = St. Venant's torsion constant

k_A = number of wheel loads to be carried by a girder

k_{GM} = longitudinal moment distribution factor (Guyon-Massonnet)

M = longitudinal moment in a specific girder

M_A = M_T/N_G = average longitudinal moment in all girders

M_{max} = maximum moment

M_{cr} = cracking moment

M_T = total longitudinal moment in all girders

M_x, M_y = bending moments per unit length

M_{xy} = $-M_{yx}$ = twisting moments per unit length

M_z = torsional moment

N_G = number of longitudinal girders

N_W = number of wheel lines on the bridge

P = load

p = reinforcement percentage

q = intensity of a continuously distributed load

S = average girder spacing in feet, mean crack spacing in inches

W_m = mean crack width

w = deflection of plate in z-direction

β = coefficient (0.141   0.333), which is a function of the ratio b/c

δ = deflection

ϵ_{cr} = steel strain at cracking moment

ϵ_m = mean steel strain

ϵ_s = steel strain

θ = rotation

ν = Poisson's ratio

τ = shearing stress

φ = angle of twist

CHAPTER I

INTRODUCTION

1.1 General

Slab and girder bridge systems are widely used for short and medium spans with lengths up to 200 feet. This span range represents a large percentage of bridges essential to modern transportation, especially highway structures.

The available analytical methods of solution for slab and girder bridge systems were reviewed by Leyendecker[34] and classified as (1) grillage method, (2) primary and secondary method, and (3) orthotropic plate method. Previous studies[34,39,49] showed the successful application of the orthotropic plate method to the analysis of such bridge systems. (The orthotropic plate method utilizes two different elastic parameters in two orthogonal directions.) This approach simulates the actual physical system by using an equivalent orthotropic elastic plate which is treated by the classical elasticity theory.[49,59,60]

Orthotropic plate systems have also been solved using discrete element mathematical models which allow point-to-point variations of parameters. Basically, this method involves the replacement of segments of the plate by finite elastic blocks connected to each other by rigid bars. These blocks have the same elastic properties as the idealized physical system. The equations describing the behavior of the system can then be obtained from a free body analysis of the model. This results in a very large set of simultaneous equations which are not adaptable to hand calculation. The use of digital computers make such methods of analysis possible. A series of computer programs entitled SLAB developed under the general supervision of H. Matlock has utilized the discrete element solution of the orthogonal plate to handle a variety of bridge and plate systems.[16,26,27,28,38,44,56,61]

1

1.2 Load Distribution Factors in Slab and Girder Bridge Systems

The standard AASHO[1] slab and girder bridge design distribution factor, k_A, specifies the fraction of a wheel load assigned to a girder, and can be stated as

$$k_A = \frac{S}{C} \tag{1.1}$$

where

> k_A = number of wheel loads to be carried by a girder
>
> S = average girder spacing in feet
>
> C = constant

The constant C depends on the type of slab and girder bridge system and the number of traffic lanes carried by the bridge. In the case of steel or prestressed concrete girders spaced at less than 10 ft. on centers, the constant is 7.0 for a one lane traffic bridge and 5.5 for two or more traffic lanes. Similarly, for a reinforced concrete girder, the values become 6.5 and 6.0, respectively.

The Guyon-Massonnet type longitudinal moment distribution factor, k_{GM} for a girder may be stated as

$$k_{GM} = \frac{M}{M_A} \tag{1.2}$$

where

> M = longitudinal moment in a specific girder
>
> $M_A = M_T/N_G$ = average longitudinal moment in all girders
>
> M_T = total longitudinal moment in all girders
>
> N_G = number of longitudinal girders

The Guyon-Massonnet distribution factor can be calculated from the final results of either physical tests or accurate analytical solutions of the system.

The relationship between Guyon-Massonnet and the AASHO distribution factors can be stated[34] as

$$k_A = \frac{S}{C} = k_{GM} \frac{N_W}{N_G} \qquad\qquad (1.3)$$

or

$$C = \frac{S}{k_{GM}} \frac{N_G}{N_W}$$

where

N_W = number of wheel lines on the bridge.

Previous studies[30,34] indicated that the comparison between the distribution factors as specified by AASHO and those obtained from either physical tests or analytical solutions are often not compatible. The AASHO factors are usually conservative when compared to more exact theories or documented test results.

The simple span, model bridges tested by Leyendecker[34] were pan-formed concrete type slab and girder bridge systems. The skew angle ranged between 0 degrees (no skew) and 45 degrees. The calculated factors k_A and k_{GM} from the tests and the factors specified by AASHO are given in Table 1.1 for two load cases.

TABLE 1.1. SERVICE LOAD SINGLE AASHO TRUCK DESIGN CRITERIA

Load Location	Girder	k_{GM} (test)	k_A (test)	AASHO Recommendation
Edge Truck Load	Exterior girder	3.91	S/4.5	Special Case*
	First interior girder	3.01	S/5.98	S/6.0
	Next interior girder	2.28	S/7.9	S/6.0
Central Truck Load	Girder to the left	1.56	S/11.55	S/6.0
	Central girder	2.07	S/8.6	S/6.0
	Girder to the right	1.83	S/9.85	S/6.0

*The exterior girder is designed by applying to the girder the reaction of the wheel load obtained by assuming the flooring to act as a simple beam between girders.

The AASHO criteria are in excellent agreement with the experimental factor of S/5.98 for the first interior girder for the edge truck load.

With the exception of this girder and the exterior girder, the AASHO factor is 20 to 43 percent conservative.

The study of steel girder bridges carried out by Kaczmarek[30] showed that the AASHO service load distribution factors for exterior girders for the simple span bridges analyzed were 31 to 46.5 percent conservative. Regardless of the skew angle in three bridges with 30 degrees skew and two bridges with 60 degrees skew, the factor for the central girder with a single truck load showed that AASHO values were 46.5 to 86 percent conservative.

The present study is aimed toward establishing the reliability of analytical procedures in order to arrive at an accurate estimate of bridge behavior under different kinds of loading and various bridge configurations. Verification of the accuracy of such a wide-ranging computational method would greatly facilitate comparative studies which could be used in more realistic design and analysis of slab and girder bridge systems. A generalized analytical method can handle broader ranges of bridge system variables such as angle of skew, continuity, and specific boundary conditions than can be specified by empirical methods. However, design requirements may still be best served by using the computer programs to study a bridge class and then developing simpler manual design rules and factors for that bridge class rather than using computer procedures to study each specific bridge to be designed.

This report is concerned only with the program verification and will not make specific design recommendations concerning the accuracy of AASHO type procedures. Such recommendations would stem from a detailed study of specific bridge types using the verified programs and are not in the scope of work of this project.

1.3 Scope and Objectives

Extensive electronic computation methods which permit rapid simulation of slab and girder bridge systems have been under development for a number of years. The rapidity of development in computer simulation has caused current analytical developments to outstrip experimental verification

in many areas. The mathematical models and programs were largely based on the assumption of elastic linear systems.

The overall objectives of this project were as follows:

(1) To verify the agreement between current computer simulation programs (such as DSLAB of Project 3-5-63-56) and the physical systems which they represent

    a) by carrying out library searches and literature reviews to to obtain correlation examples of well-documented typical highway bridge applications; and

    b) by constructing and testing several physical models of slab and girder bridge systems to obtain further comparative data in areas where such data are lacking.

(2) To study the most realistic ranges of input variables and to suggest guideline procedures for the designer's use in initially setting up the problem.

(3) To provide carefully documented data concerning behavior at moderate overloads and for ultimate loads of typical systems to assist the programming group in development of further simulation programs.

(4) To make recommendations regarding the adequacy and range of applicability of the present computer programs based on test and analysis results.

This report contains only summaries and representative samples of the many tests run and comparisons made under objectives 1 and 3. A great amount of further detail is contained in References 6, 7, 30, 34, and 47, copies of which have been made available as indicated in the Preface.

CHAPTER II

THEORY AND COMPUTER PROGRAM

2.1 Introduction

This chapter provides a brief presentation of the basis for the
solution of orthotropic plates based on the general theory of elasticity.
References are cited for detail. The link between elasticity solutions
and numerical methods is also illustrated in order to develop an under-
standing of the role of the different parameters involved in the solution.

2.2 Isotropic Plate Theory

For a complete solution of the state of stresses and deformations
exerted by external forces on an elastic homogeneous body, the solution
must satisfy both equilibrium and compatibility conditions for that body.
For the case of an isotropic plate subject to planar stress, Timoshenko[59]
has shown that plate moments, neglecting in-plane deformations, can be
stated as:

$$\frac{\partial^2 w}{\partial x^2} + \nu \frac{\partial^2 w}{\partial y^2} = - \frac{M_x}{D}$$

$$\frac{\partial^2 w}{\partial y^2} + \nu \frac{\partial^2 w}{\partial x^2} = - \frac{M_y}{D} \qquad (2.1)$$

$$\frac{\partial^2 w}{\partial x \partial y} = \frac{M_{xy}}{(1 - \nu)D}$$

where w = deflection of plate in z-direction

$D = \dfrac{Eh^3}{12(1 - \nu^2)}$ = flexural rigidity of plate

M_x, M_y = bending moments per unit length

7

$M_{xy} = - M_{yx} =$ twisting moments per unit length

E = Young's Modulus

ν = Poisson's ratio

h = plate thickness

The equation which relates the lateral loadings on a plate and the bending moments can be stated[58] as:

$$\frac{\partial^2 M_x}{\partial x^2} + \frac{\partial^2 M_y}{\partial y^2} - 2 \frac{\partial^2 M_{xy}}{\partial x \partial y} = - q(x,y) \qquad (2.2)$$

where q = intensity of a continuously distributed load.

Substituting Eq. 2.1 into 2.2,

$$\frac{\partial^4 w}{\partial x^4} + 2 \frac{\partial^4 w}{\partial x^2 \partial y^2} + \frac{\partial^4 w}{\partial y^4} = \frac{q(x,y)}{D} \qquad (2.3)$$

which defines the relation between applied loads and the displacement of an isotropic plate. Such a relation is very useful in solving structural problems.

2.3 Orthotropic Plate Theory

In order to define the relation between the stresses and strains for orthotropic materials, nine constants need to be determined,[55] instead of the two constants (Lame's constants) needed for isotropic materials. However, in the case of plane stress as in plates, the constants reduce to only four. Timoshenko[59] shows the derivation of the following moment equations

$$M_x = - (D_x \frac{\partial^2 w}{\partial x^2} + D_1 \frac{\partial^2 w}{\partial y^2})$$

$$M_y = - (D_y \frac{\partial^2 w}{\partial y^2} + D_1 \frac{\partial^2 w}{\partial x^2}) \qquad (2.4)$$

$$M_{xy} = 2D_{xy} \frac{\partial^2 w}{\partial x \partial y}$$

where

$$D_x = \frac{E_x' h^3}{12} \qquad\qquad D_1 = \frac{E'' h^3}{12}$$

$$D_y = \frac{E_y' h^3}{12} \qquad\qquad D_{xy} = \frac{G_{xy} h^3}{12}$$

and the four constants, E_x', E_y', E'', and G_{xy} are needed in order to define the elastic properties of an orthotropic material. For the particular case of isotropy, these constants reduce to

$$E_x' = E_y' = \frac{E}{1 - \nu^2}$$

$$E'' = \frac{\nu E}{1 - \nu^2}$$

$$G_{xy} = \frac{E}{2(1 + \nu)}$$

Introducing the notation

$$H = D_1 + 2D_{xy}$$

and substituting expressions 2.4 into Eq. 2.2 yields

$$D_x \frac{\partial^4 w}{\partial x^4} + 2H \frac{\partial^4 w}{\partial x^2 \partial y^2} + D_y \frac{\partial^4 w}{\partial y^4} = q(x,y) \qquad (2.5)$$

2.4 Determination of Rigidities

The four constants needed to define the elastic properties of an orthotropic plate can be stated as[55,58]

$$E_x' = \frac{E_x}{1 - \nu_x \nu_y}$$

$$E_y' = \frac{E_y}{1 - \nu_y \nu_x}$$

$$E'' = \frac{\nu_x E_y}{1 - \nu_x \nu_y} = \frac{\nu_y E_x}{1 - \nu_x \nu_y}$$

$$G_{xy} = \frac{E_x E_y}{E_x + (1 + 2\nu_{xy})E_y}$$

10

where $\nu_{xy} = \dfrac{E_x}{E_y} \nu_{yx}$

All variables involved in these expressions can be obtained by testing the material of the plate. If a reinforced concrete plate is to be considered as a particular case, then Timoshenko suggests that the following expressions for the rigidities are to be used.[59]

$$D_x = \frac{E_c}{1 - \nu_c^2} [I_{cx} + (\frac{E_s}{E_c} - 1) I_{sx}]$$

$$D_y = \frac{E_c}{1 - \nu_c^2} [I_{cy} + (\frac{E_s}{E_c} - 1) I_{sy}]$$

$$D_1 = \nu_c \sqrt{D_x D_y}$$

$$D_{xy} = \frac{1 - \nu_c}{2} \sqrt{D_x D_y}$$

where I_{cx}, I_{sx} = moment of inertia of concrete and reinforcement, respectively, taken about the neutral axis in the section where x = constant and I_{cy}, I_{sy} = the same but for y = constant.

The torsional rigidity D_{xy} should be regarded as a first approximation if it is based on theoretical analysis. More reliable values can be obtained by direct tests.[59,60] A simple idealized test to determine the torsional rigidity of a plate is shown in Fig. 2.1, where by measuring the angle of twist φ the torsional rigidity could be calculated as $2D_{xy} = \dfrac{1}{\varphi}$.

The expressions for the rigidities of a reinforced concrete plate are not independent of the state of the concrete. They may be especially in error when cracks form or steel begins to yield. A better expression could be obtained from the generation of the moment curvature relationship for the section which would define the rigidity for each level of moment applied to the section. Such a procedure will be discussed later in this study.
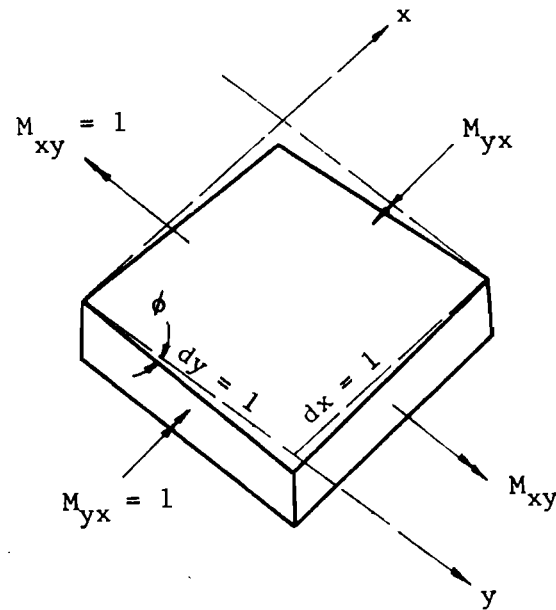
Fig. 2.1. Plate torsional test.

2.5 Discrete Element Method

2.5.1 **Numerical Methods**. The rigorous analytical solution for the differential equation of a plate such as Eq. 2.5 is too complicated to achieve for many practical problems since mathematically the function has to be continuous, and fourth order systems should have two continuous derivatives. These conditions cannot properly be fulfilled in many complex engineering problems. Hence the so-called numerical methods are used, where the differential equation is replaced by its finite difference equivalence, and in turn the problem reduces to the solution untilizing computers of a large number of simultaneous algebraic equations instead of the solution of a single complex one.

2.5.2 **The Physical Model**. Hudson[26] suggested a discrete element model for plates and slabs which includes a mesh of two principal sets of orthogonal beams connected at their nodal points. The bending stiffness and Poisson's ratio are represented by elastic blocks placed at the nodes. The torsional stiffness of the plate is modeled by torsion bars connecting the rigid bars which are running in both directions, as shown in Fig. 2.2.
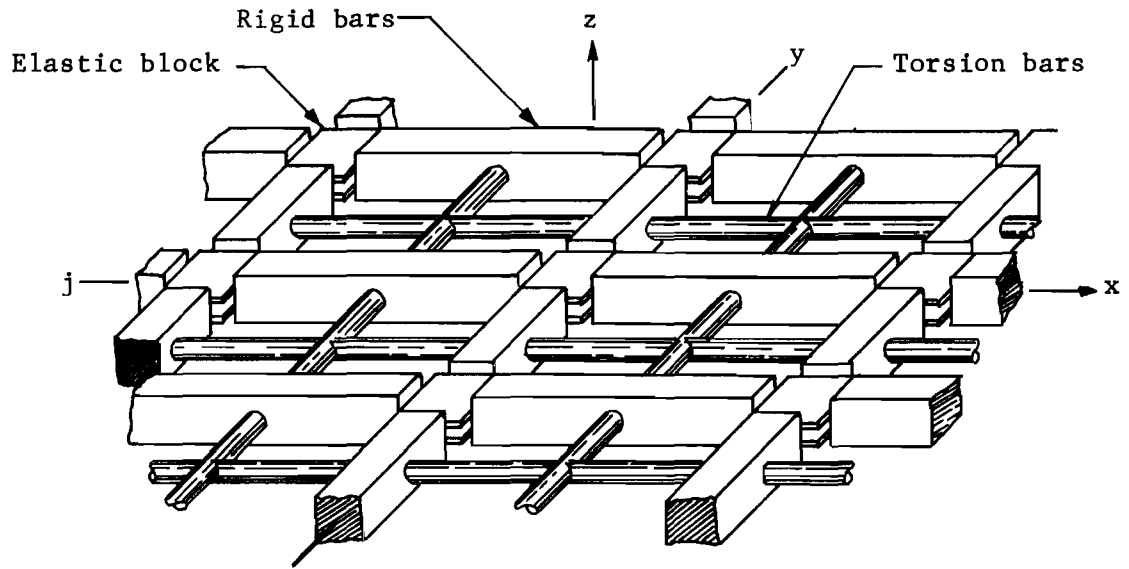
Fig. 2.2. Discrete-element model of a plate or slab.
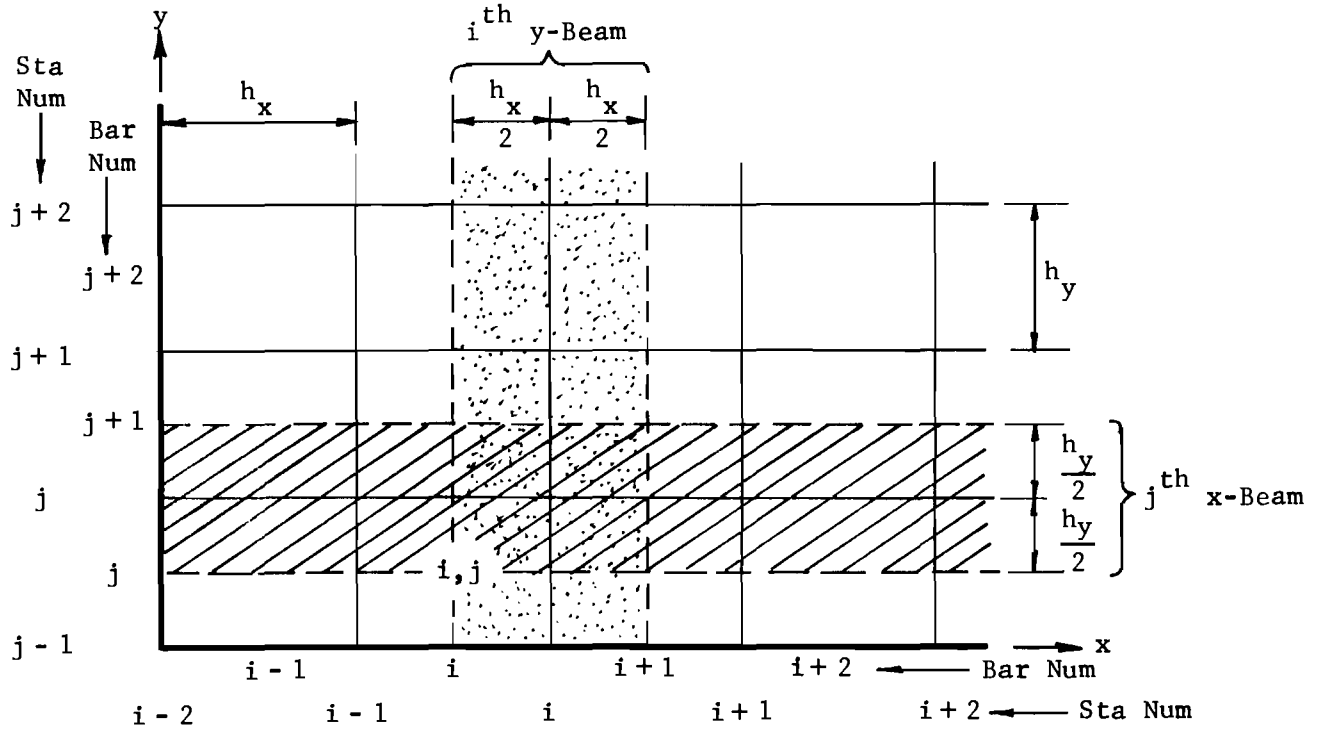
Fig. 2.3. Plan view of plate segment divided into x and y-beams.

A pictorial representation of the system with typical numbering procedure for nodes and bars is shown in Figs. 2.2 through 2.4.

2.5.3 <u>Formulation and Solution of Equations</u>. A typical joint (i,j) for the discrete element slab model is shown in Fig. 2.5 and the free body of a slab mesh node is shown in Fig. 2.6. Stelzer and Hudson[56] show the derivation of the general slab equation from the free body diagram and present the final form of that equation both in detailed form and matrix form.

A solution for the deflection matrix using the alternating-direction iteration method has been discussed and was used by Hudson[26] for the solution of his model. However, this method is not an efficient one and requires a parallel study to choose the closure spring constant which must be specified in that method in order to ensure convergence of the solution. A direct method for the solution was later developed by Stelzer and Hudson,[56] who presented the derivation of the equations for the solution.

2.6 The Computer Program

The formulation of the equations of the discrete element model is not really useful for hand calculation, yet the equations are very adaptable in conjunction with the use of digital computers. The development of a series of versatile computer programs called SLAB for the solution of slabs and plates of various types has been made at The University of Texas Center for Highway Research. The basic discrete element model was introduced by Hudson,[26] while solution procedures were developed by many authors, such as Matlock, Hudson, Ingram, Stelzer, Endres, and Panak.[27,28,56,16] The versions of the SLAB computer program used throughout this study were SLAB40 and SLAB43. The documentation of these and other versions was presented by Matlock and Panak.[38]

Figure 2.7 shows a summary flow chart for the SLAB program. Details and complete listings of the different versions of the programs can be seen in the references given above,

14
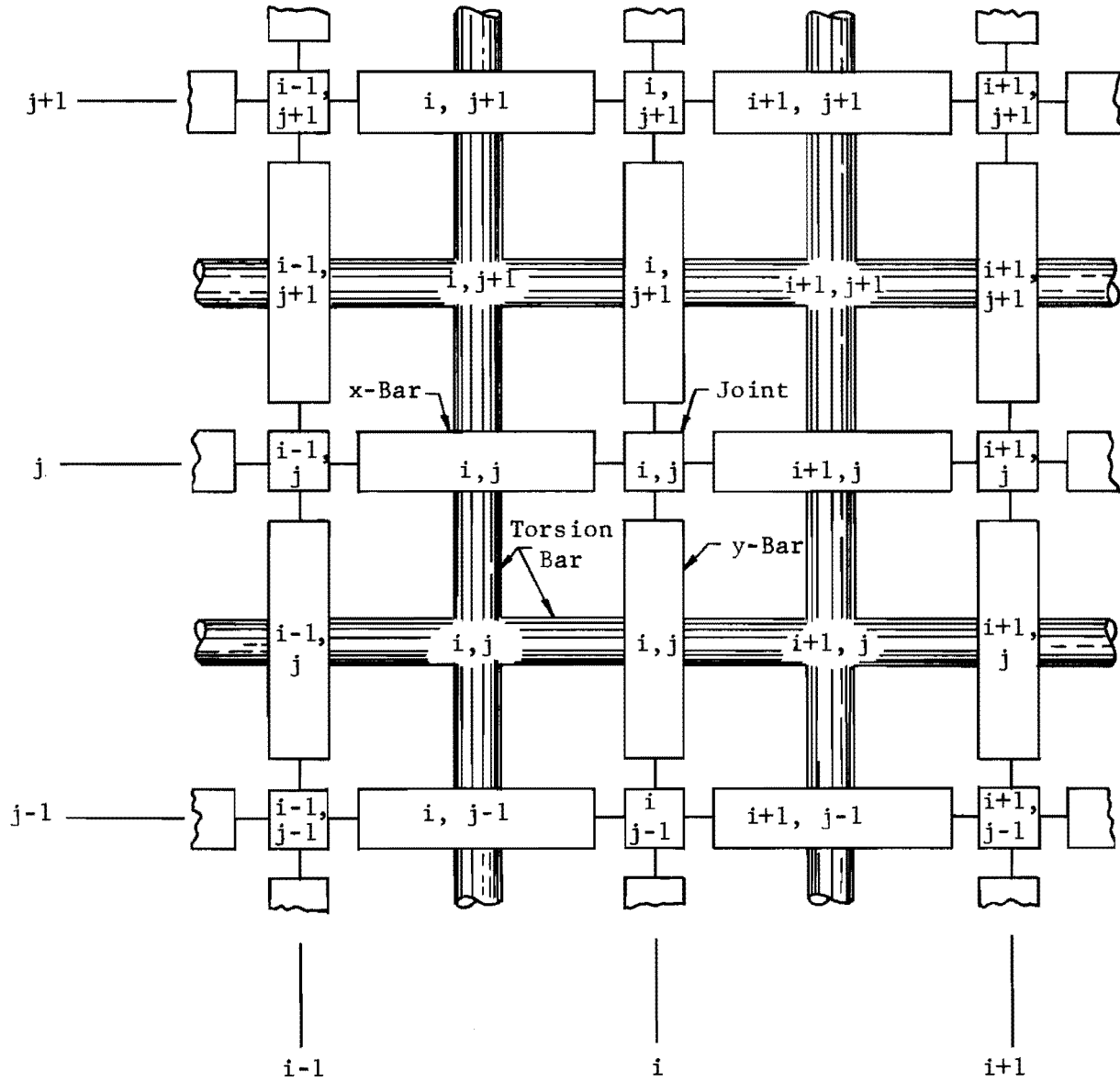
Fig. 2.4. Plan view of the slab model showing all parts with generalized numbering system.
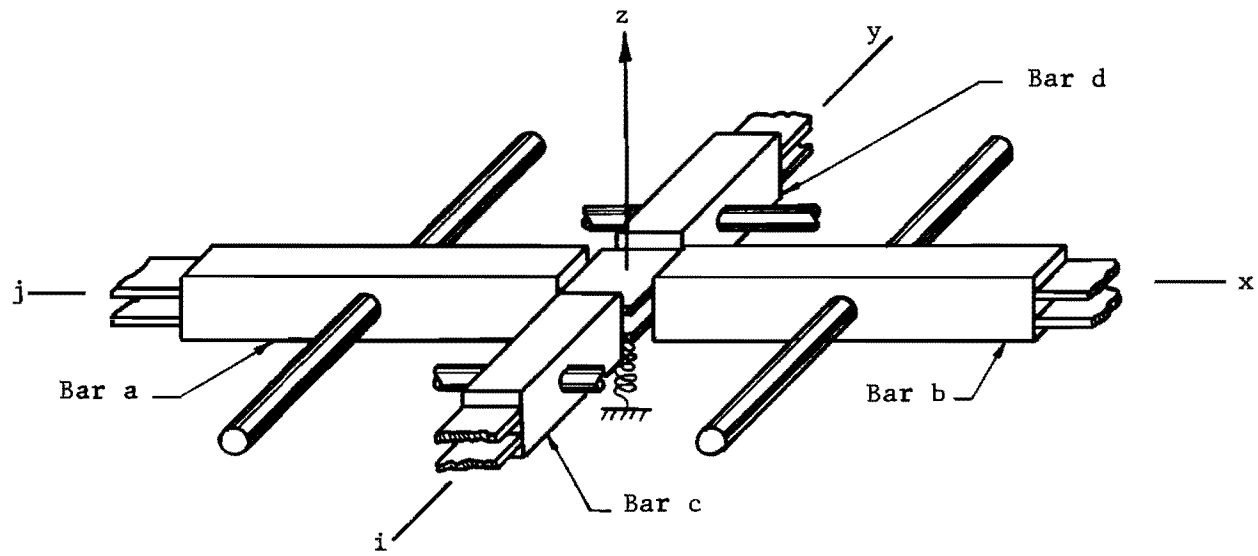
Fig. 2.5. Typical joint i,j taken from discrete-element slab model.
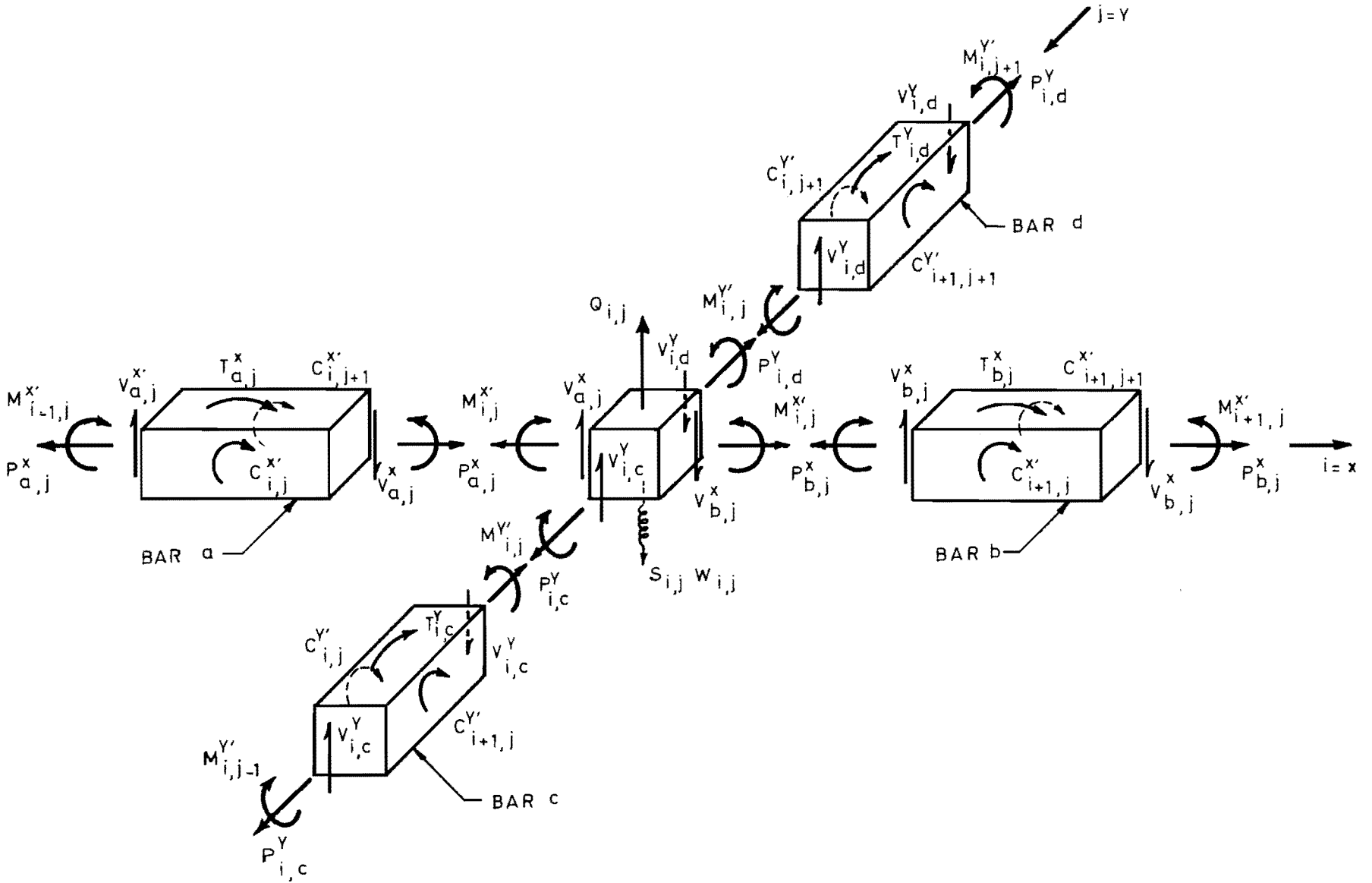
Fig. 2.6. Free-body of slab mesh point.
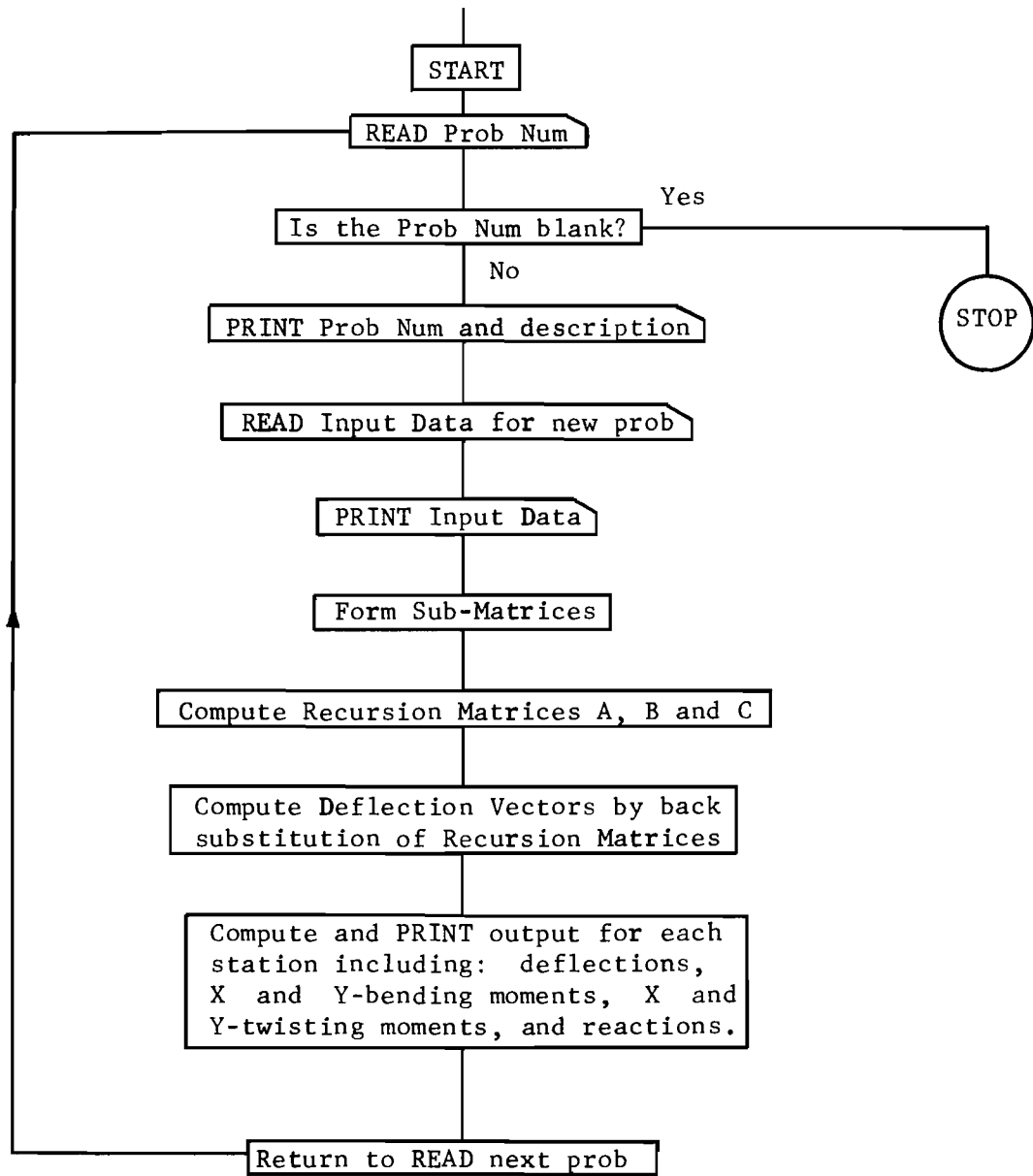
Fig. 2.7.   Summary flow chart of SLAB computer program.

CHAPTER III

COMPUTER SIMULATION OF PHYSICAL SYSTEMS

3.1 <u>General</u>

Any mathematical modeling of a physical system requires use of
various assumptions and approximations. These may include approximations
of the true material behavior, idealization of the loadings and typical
boundary conditions, and extension of theories derived for infinite media
to finite cases. Some assumptions are not strictly compatible with
actuality, but are imposed in order to simplify the modeling procedure
and/or the method of solution. Ideally, the assumptions used should not
significantly alter the analytical results from the comparable physical
results.

Two types of assumptions and approximations are used. The idealized
model discussed in Sec. 2.5.2 assumes in the analysis procedure that:

    a. Planes normal to the middle surface remain normal to the surface
        after bending.

    b. Stresses normal to the plate surface can be disregarded for the
        bending solution.

    c. No axial deformation of the neutral axis occurs.

    d. All deformations are small compared to the plate dimensions.

    e. The bar elements of the model are infinitely stiff and weightless.

    f. Each joint in the model is composed of an elastic, homogeneous, and
        orthotropic material which can be described by four independent
        elastic constants.

    g. Loads, masses, and bending strain occur only at the joints.

    h. Torsional stiffness of the plate element can be represented by
        torsion bars.

    i. The neutral axis lies in the same plane for all elements, even for
        nonuniform cross sections.

j. The spacing of the beams in the x and y directions (h_x and h_y) need not be equal but must be constant for all parallel beams.

k. The number of increments into which each beam is divided is equal to the length of the beam divided by the increment length.

Numerous comparisons to other analytical solutions of varied plate problems indicate that the primary solution errors are probably not due to these assumptions.

The other type of approximation tends to introduce most errors which stem from the evaluation procedure required to correctly input to the analytical programs accurate values for variables and parameters of the true systems. These inputs are required for the mathematical simulation of the physical system prior to obtaining the solution and include the following:

a. Flexural stiffness

b. Torsional stiffness

c. Poisson's ratio

d. Mesh size

e. Type and nature of boundary conditions

f. Type and nature of loadings

Evaluation of a, b, and c is confined to the type and properties of the materials used and also the kind and shape of the plate, while d, e, and f may be considered as general and applied to all kinds of plates. In this study particular emphasis will be placed on the thorough evaluation of these parameters and their effect on the modeling and on the results obtained.

3.2 Physical Systems Studied

Orthotropic plate theory has been widely used in the design and analysis of orthotropic bridges, although the slab and girder bridge has only lately been considered as an orthotropic plate. Slab and girder types are widely used for short and medium bridge spans. In this study they are classified as follows:

1. Prestressed concrete girders with concrete slabs.

2. Reinforced concrete girders and slabs.

3. a. Steel girders built compositely with concrete slabs

   b. Steel girders built noncompositely with concrete slabs.

In the following three chapters each type is studied separately. In each chapter comparisons of actual and idealized behavior are presented and recommendations for both design and analysis are discussed and presented. The study includes both simple and continuous span bridges and also considers a range of skewness. Comparisons with reported test results are made for the bridges listed in Table 3.1. These bridges are considered in more detail in case studies later in this text.

3.3 Nonlinear Problems

The derivation and development of the orthotropic plate theory, the later introduction of the discrete element methods and related mathematical models and the development of the computer solutions were all largely based on the assumption that the structure is linear.* This assumes a linear proportion between applied loads and resulting deformed configurations as well as that the materials are elastic and linear (obeying Hooke's Law). There is an apparent violation of logic which might possibly lead to significant errors in the results if these methods are used to seek solutions for widely used nonlinear materials such as reinforced concrete.

General stress-strain curves for concrete are shown in Fig. 3.1, and for reinforcing steel in Fig. 3.2. Knowing the behavior of the individual materials making up a reinforced concrete member is not enough to define the behavior of that member. Many factors influence the flexural stiffness which is the most important parameter needed to define the behavior of the member under the action of loads. The stiffness can be greatly affected by the type of applied loads, formation of cracks, percentage of steel, shape of the member, and the phenomenon of stress redistributions in the member at each level of loading.

---

*Although many methods were developed in a highly generalized form, practical examples, applications, and programs tended to be highly elastic and linear in nature.

TABLE 3.1. TESTED BRIDGES STUDIED

Bridge Type	Simple Span				Continuous Span			
	Bridge	Scale	Skew	Ref.	Bridge	Scale	Skew	Ref.
Reinforced concrete girders and deck	Chili Ave. (New York)	1/1	14°	5	Hillsboro (4-span)	1/1	30°	43
Prestressed concrete girders with concrete deck	UT (test)	1/5.5	30°	7	PCA (2-span)	1/2	0°	39
	UT (test)	1 5.5	45°	6	N. Ill. Toll Highway (4-span)	1/1	20°	29
	N. Ill. Toll Highway	1/1	20°	29				
Composite steel beams and concrete deck	U. of Ill. (S 15)	1/4	0°	42	Patuxent River Br. (3-span)	1/1	20°	22
	Patuxent River Br. (Maryland)	1/1	0°	51				
Noncomposite steel beams and concrete deck	U. of Ill. (30 N 15)	1/4	30°	41	U. of Ill. N 30 (2-span)	1/4	0°	52
	U. of Ill. (60 N 15)	1/4	60°	41				
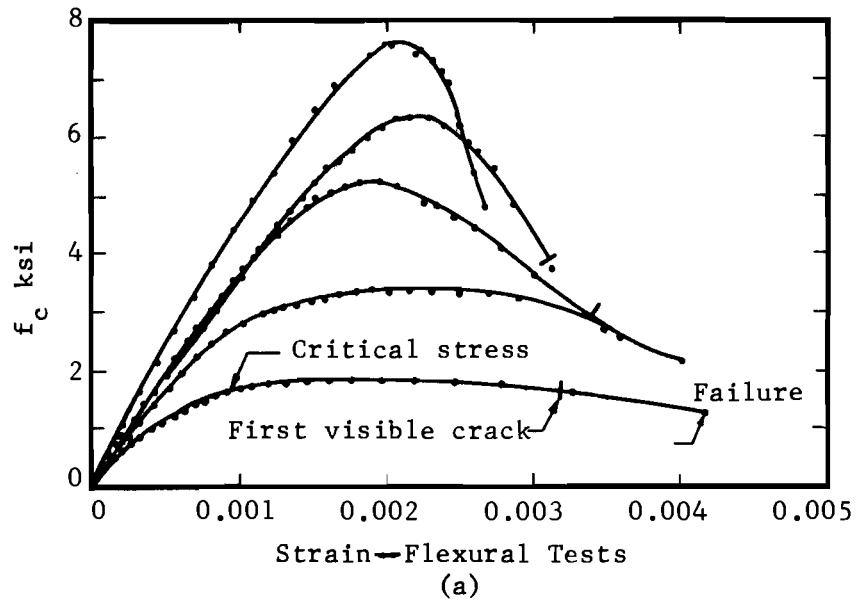
Fig. 3.1. Compression stress-strain curves at 28 days from flexural tests on 5 by 8 by 16 in. prisms.
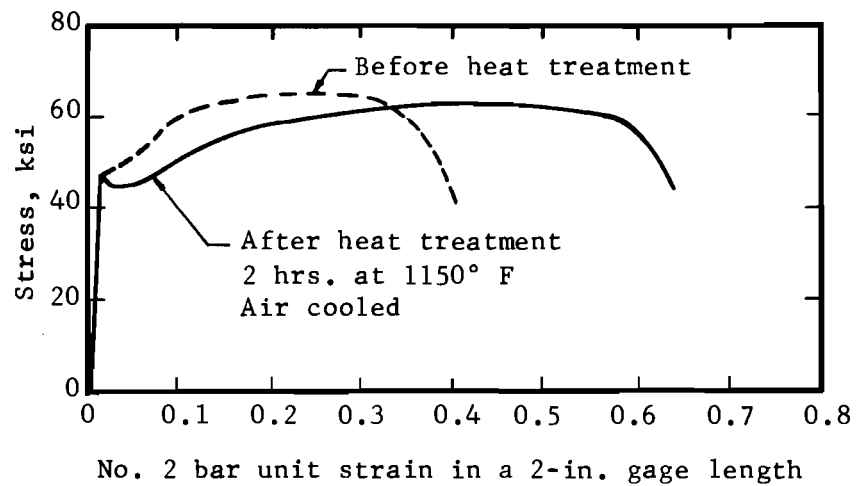
Fig. 3.2. Typical stress-strain curve for reinforcing steel bars.

The moment—curvature relationship gives the best estimate for the flexural stiffness of a beam. This relation would be a straight line for a linear member and the slope of such a line characterizes the stiffness. Figure 3.3 shows the actual moment--curvature relationship from a reinforced concrete beam test,[19] while Fig. 3.4 is from a concrete column test.[14] Presence of axial compression force in a concrete member can make the member behave linearly over a greater range of transverse load. In the case of prestressed concrete beams, the assumption of linear properties may be very justifiable in the working load range, as shown[31] in Fig. 3.5.

Two values of flexural stiffness for a reinforced concrete section are well-defined. These are assumed as strictly a property of the section with the initial modulus of elasticity of the concrete assumed unchanging and independent of loadings. One of these stiffnesses (EI) is based on the moment of inertia of the gross section and the other is based on the moment of inertia of the cracked transformed section. Both can be calculated easily for any section using procedures to be found in most elementary books dealing with reinforced concrete.

Using either value as an estimate for member stiffness could yield a significant error in results. This can be shown by the comparison of the observed and calculated midspan deflection of the simple span reinforced concrete beam (S-3) tested by Sinha.[54] The beam was 8 ft. in length and loaded with two point loads placed at 1.5 ft. on either side of the midspan. The measured deflection was 0.487 in. at a total load of 13.10 kips. The calculated deflection was 0.293 in., based on the gross moment of inertia, while a value of 0.852 in. is obtained when the cracked moment of inertia of the section is used in the calculation. Such comparisons indicated the need for a study of the proper use of theoretical solutions when dealing with the nonlinear problems such as those involving reinforced concrete.

In this study a computer subroutine called MPHI was developed to predict the moment-curvature relationship for a reinforced concrete section for use with the general solution. This subroutine considered many of the important parameters which influence the nonlinear behavior of the member. Details are given in Sec. 5.4. The program developed provides excellent
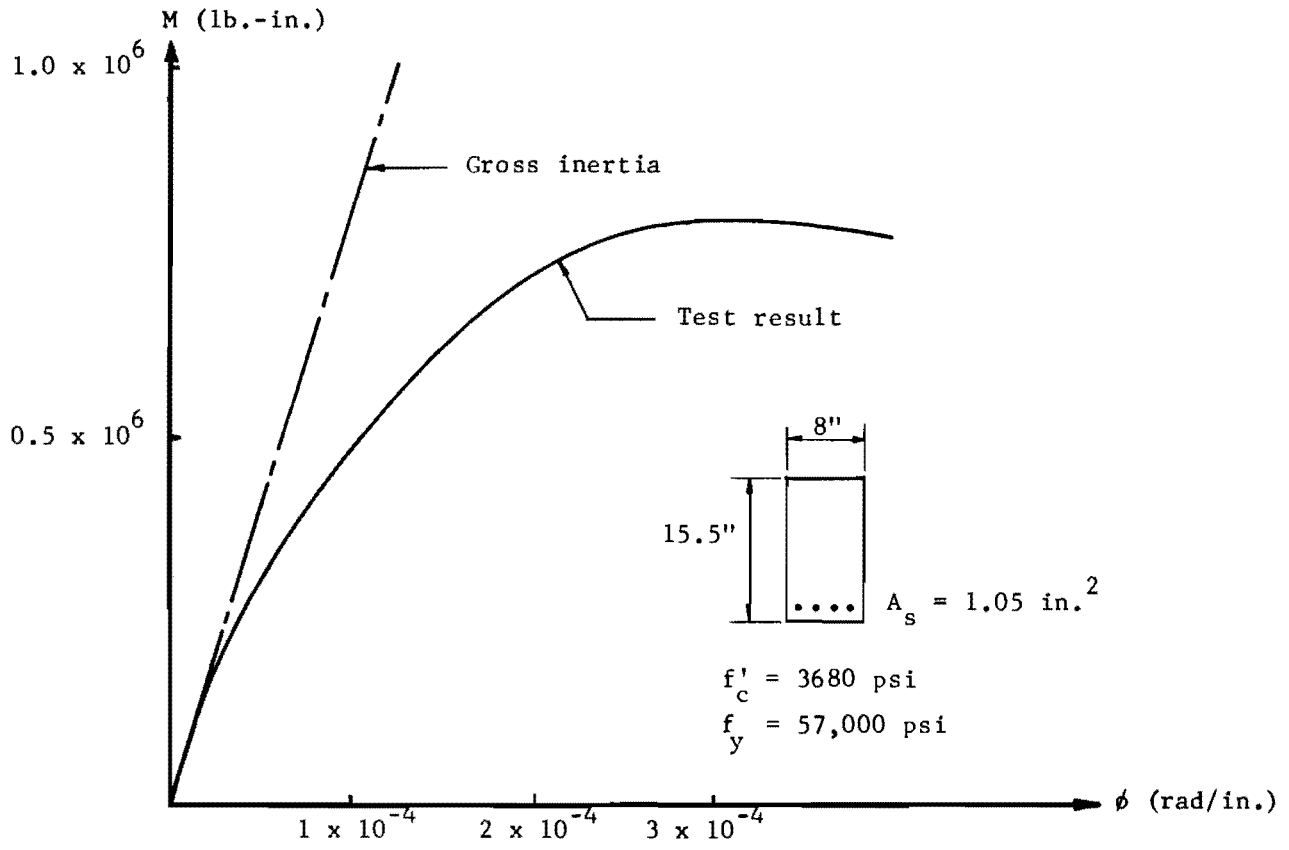
Fig. 3.3. Moment curvature for tested beam.
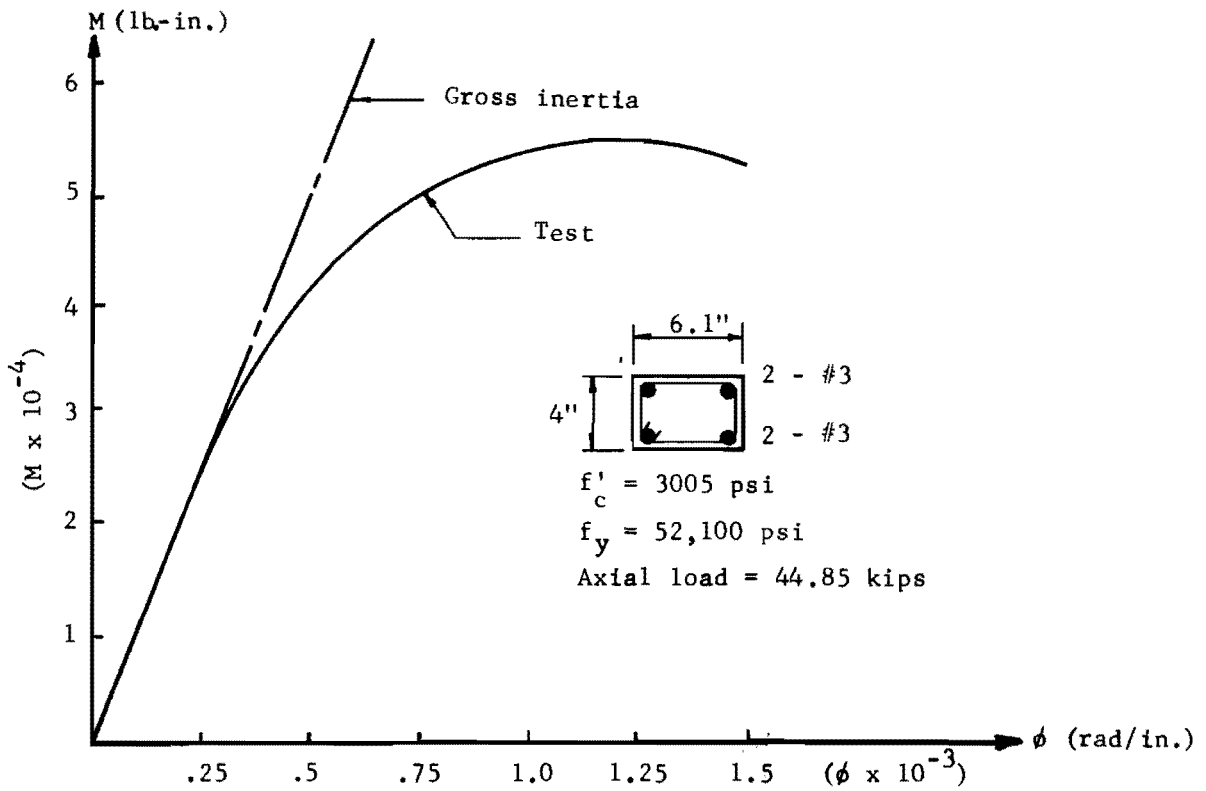
Fig. 3.4. Moment curvature for tested column.
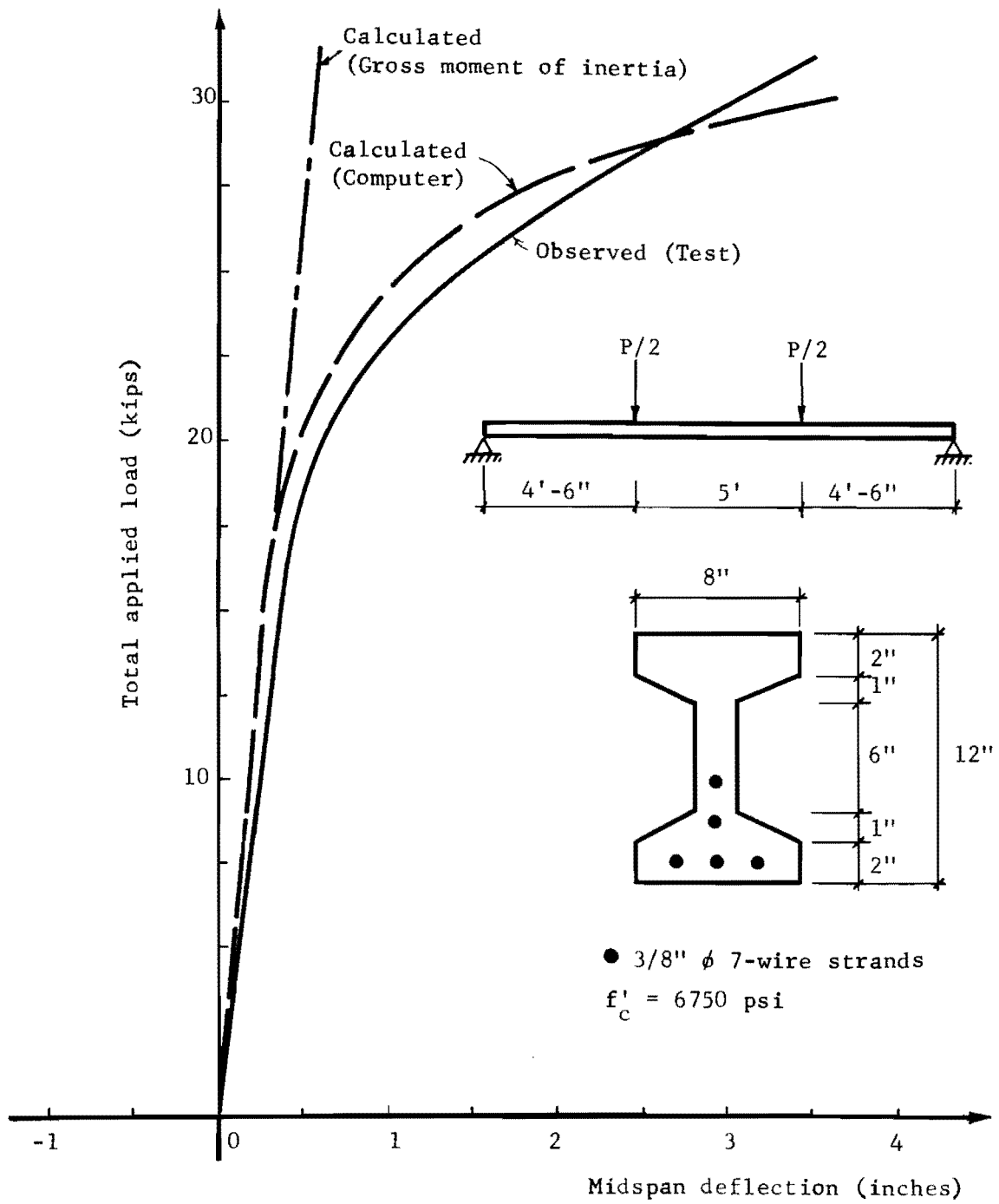
Fig. 3.5. Load-deflection curve.

predictions for the moment-curvature relationship of concrete beams when compared with many test results.

In general, nonlinearity is common for many engineering materials. The stress-strain curves of some common engineering metals[21] are quite nonlinear at higher load levels. Even though a great range of the curves could be taken as linear, this will not necessarily be the case for the stiffness of members built from such materials, since there are other factors affecting member stiffness such as the shape of the section, residual stresses, stress concentrations and types of loads applied on the member.

Residual stresses can be quite high in comparison to the yield stress of the material.[9] Presence of residual stresses in a member make some part of the section yield at a lower level of loading, and thus the member will lose some of its stiffness at such a level of loading. Hence, a nonlinear behavior for that member will result. Beedle[8] discussed the effect of the residual stresses on the moment-curvature relationship of a hypothetical rolled section where all materials were placed in the flanges, as shown in Fig. 3.6a. Assuming a value of residual stresses of the pattern shown in Fig. 3.6b, the calculated moment-curvature curve would be similar to Fig. 3.6d, where the numerical figure refers to the level of loadings shown by Fig. 3.6c. Stress concentration has a similar effect on the moment-curvature relationship.

The effect of such parameters on the behavior of members built of metals usually starts at relatively higher levels of loading and their influence needs to be considered only for loadings which are normally beyond the working loads of the member. Therefore, the consideration of linear behavior for such members is well-justified for the usual range of service loads on structures.

3.4 The Problem of Skew

The number of skew bridges built is very considerable. Rowe[49] has stated that in England their number is greater than the number of right bridges. This is probably the case in other countries. Skew angle is considered throughout this study as that angle between the abutment line and the perpendicular to the traffic path over the bridge deck. Rowe has also indicated that there is no rigorous analytical method for either isotropic

28

(a)

(b)

(c)

(d)
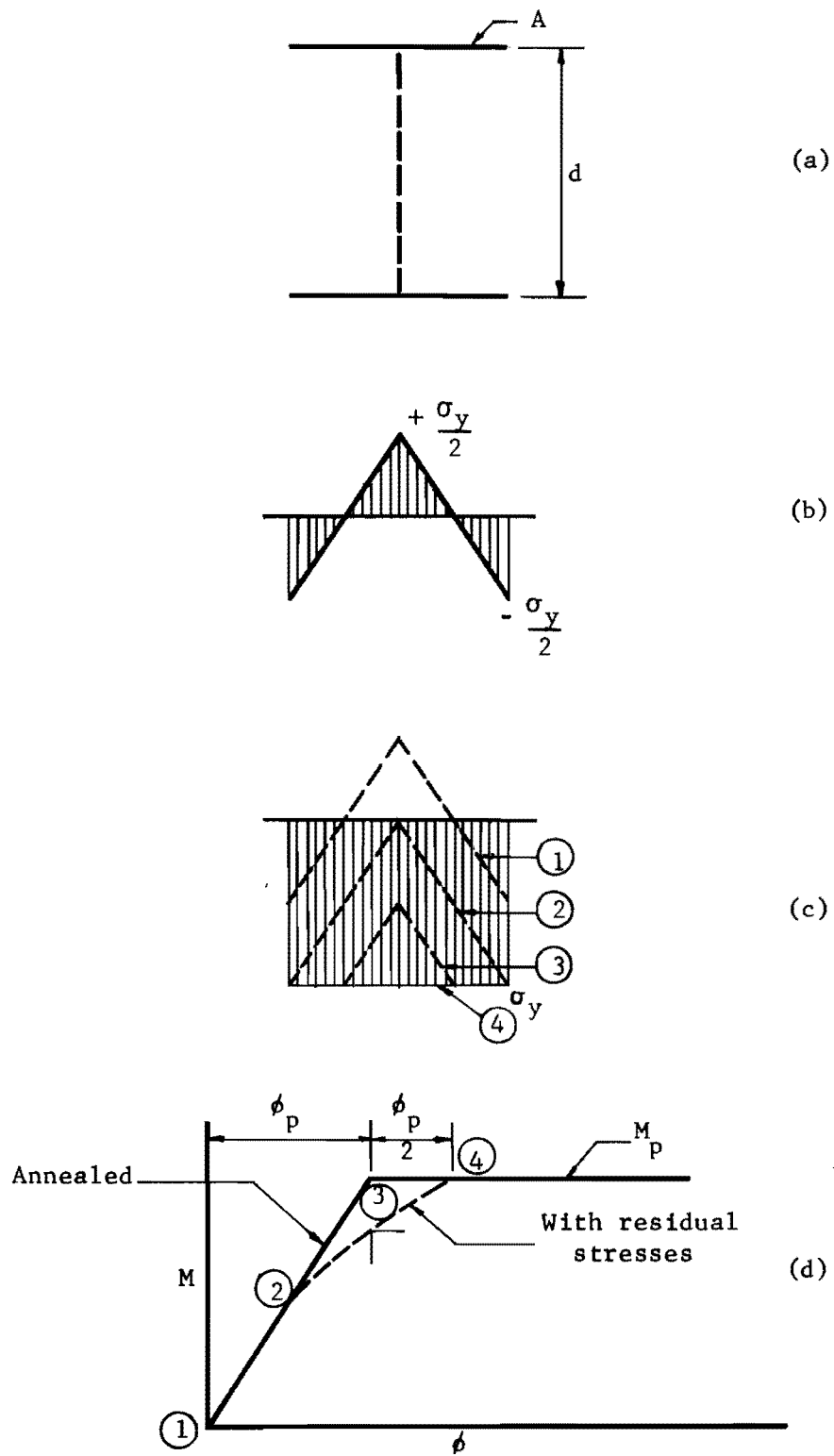
Fig. 3.6. Representation of the influence of residual stresses upon the moment—curvature relationship of a beam in bending (idealized).

or orthotropic skew plates. He showed the application of finite difference for certain cases of isotropic skew plates while he indicated the limited theoretical approach for orthotropic skew plates.

The method of solution used in the SLAB program has an advantage in this respect as it can readily deal with orthotropic skew bridges. For all bridges studied, this variable was handled by careful modeling of the supporting lines in choosing the mesh increments in both the x and y directions, as shown in Fig. 3.7a. The skew edge of the slab can be taken as a series of stairstep lines following the grid lines. When modeling a skewed supporting edge for a girder and slab bridge, no supporting points should be used for slab nodes along the skewed edge. The only support input used should be that for the girder ends. The validity of this procedure was shown when Leyendecker[34] input both slab and girder supports as shown in Fig. 3.7c and found extremely large errors in calculated midspan deflections of some skew bridges tested. Later, Kaczmarek[30] reran the same bridge examples with supporting points only under the girder ends and found excellent results.

A physical interpretation for this error is indicated in Fig. 3.7c, d, and e, which shows a typical skew support. In the case shown, supports are used for both girders and slab end nodes. Note that compatibility demands that the deflection must be the same for the modeled beams running in both directions when they intersect at a node. Thus, when mesh beam i+2 is considered in the y direction, the deflection profile indicates that it is very close to a fixed end condition. This would provide a large restraint for beams running in the x direction, such as beam j+4. This restraint induces appreciable computed negative bending moments near the ends of this beam which do not exist in reality. This can lead to tremendous errors in some cases, such as in the bridges studied by Leyendecker. This false fixity reduced the computed midspan deflection to as little as one-fourth of the test value as shown by Kaczmarek.

Vora and Matlock[61] suggested a model which may deal directly with skew problems. This model consists of a tri-directional system of rigid bars and elastic joints in order to simulate an anisotropic skew plate and

(a) Grid system with correct supports.

(b) Bridge section.

(c) Grid system with incorrect supports.
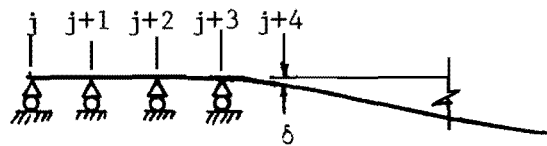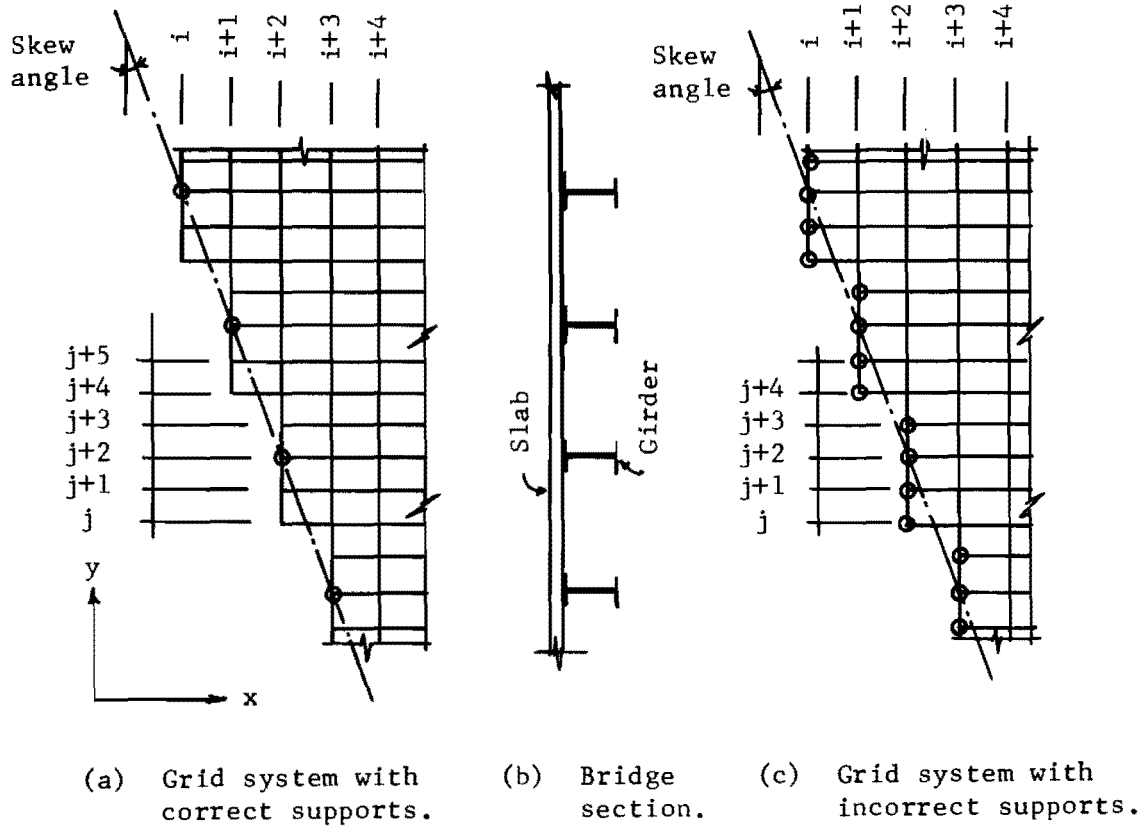
(d) Mesh beam i+2 for grid system shown in (c).
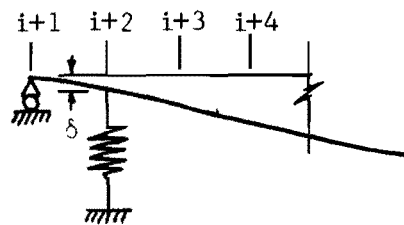
(e) Mesh beam j+4 for grid system shown in (c).

Fig. 3.7. Modeling of a typical skew edge.

slab-and-beam system where the beams may run in any three directions. This model is a direct step toward fitting the boundary condition of a skew plate, since the angle between the simulated beam could be selected to fit the required angle of skew in the problem.

3.5 Evaluation of General Parameters

3.5.1 Mesh Size. As a general rule with discrete element models, the finer the mesh size the closer the model represents the physical system. Therefore, higher accuracy can be obtained using finer meshes. In many engineering problems such higher accuracy does not mean much practically. Usually even the third significant figure is not really significant in applying the results in actual designs. Added digits require a finer mesh and make the solution more costly, requiring larger computer storage and longer computer time. Panak and Matlock[44] report the storage required for the SLAB30 program using the CDC 6600 computer as

$$Storage = 8m^2 + 11mn + 100m + 33n + 12,200 \qquad (3.1)$$

where m and n are the number of increments in the x and y directions, respectively. The time required to run SLAB programs is proportional to some power of the mesh size. Stelzer and Hudson[56] reported that for SLAB5, a problem with 8 by 8 increments can be solved in four seconds, while 16 by 16 increments require twenty seconds.

For an optimum solution where accuracy and economy are involved, it is necessary to define the range of mesh size which would yield reasonably accurate solutions. For the case of orthotropic bridges of the type presented in this study, where the main longitudinal stiffness of the bridge is provided by the girders, it is important to consider the number of increments. Additional segments between girders give a better approximation for the curved deflected shape of the connecting slab. Experience indicates that less than four segments between girders usually gives too crude an approximation of the shape.

Likewise, a smaller number of segments increases the possibility of wheel type live loads occurring inside the increments while the method of solution requires that all loads be input on the nodes. Hence, with small

numbers of increments additional approximation for the load distribution on the adjacent nodes is necessary and this has some influence on the results, as will be discussed in Sec. 3.5.3. For all cases studied herein, a range of 4 to 7 increments between girders was used and found to be satisfactory.

The number of segments in the longitudinal direction of the bridge depends on the span length and the number of spans in the case of continuous bridges. Hence, an increment of 16 to 40 was used for each actual span. This was a good range for both straight and skew bridges with the higher number more likely required for the skew cases. In addition, the skew case will often require more total increments because of the need to enclose the skew bridge parallelogram in an analytical rectangle.

3.5.2 <u>Type and Nature of Boundary Conditions</u>. Boundary conditions such as supporting points, axial loads, external couples, rotational restraints, and skew edges can be modeled and input for the SLAB programs. Supporting points are modeled by springs having the same characteristics as the physical supports. These are defined by the spring constants which are chosen to give the behavior of the true supports under the action of loads. The value of the spring constants of such supports are input at the nodes only. Where data are lacking on the behavior of the supports a value of 1×10^8 lb./in. or higher may be used to model a nonyielding support.

External couples and rotational restraints must be defined in both magnitude and location throughout the system. These loads should be applied and input on the mesh joints. All these data are input in Tables 3, 4, and 6 of the guide for data input for SLAB programs. Input details for skew edges were discussed in Sec. 3.4.

3.5.3 <u>Type and Nature of Loadings</u>. Two kinds of static loads may be analyzed; dead loads which are usually uniformly distributed, and live loads such as traffic loads which usually are represented as point loads. All loads must be input on the nodes of the mesh. Therefore, dead loads should be calculated so that each node will carry all loads which fall inside the tributary area of that node. Point loads are input directly if they fall on the nodes. In the case of loads which fall inside the mesh, the load should be distributed to the four nodes which bound the specific grid. This distribution is based on the assumption that the grid is very stiff and is

simply supported on the nodes. Figure 3.11 shows such distribution of a point load P to the four point nodes P_1, P_2, P_3, and P_4.

$$P_1 = (1 - a - b + ab) \, P$$

$$P_2 = (b - ab) \, P$$

$$P_3 = (ab) \, P$$

$$P_4 = (a - ab) \, P$$
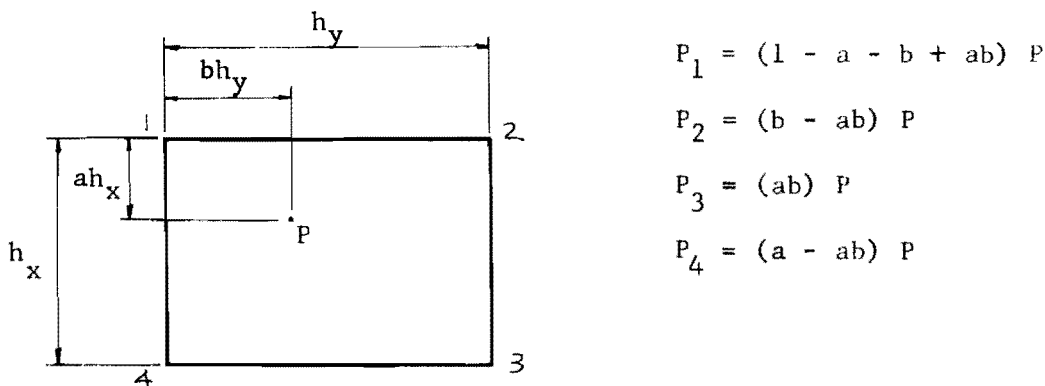
Fig. 3.8. Distribution of a load which falls inside a mesh to the four nodes.

This approximation works well with fine meshes, but it has some deficiency when applied for coarser meshes. Therefore, it is preferable to avoid such approximations during the system modeling by attempting to choose a mesh size which matches such loads with the nodes whenever possible.

3.5.4 Poisson's Ratio. Poisson's ratio of concrete is highly variable and has been studied thoroughly by Simmons.[53] He discussed the methods of measurement of both dynamic and static values and indicated average values of 0.21 dynamically and 0.16 statically.

A simple expression to approximate the Poisson's ratio of the concrete is presented in the German Code (DIN 4227) as

$$\nu = \sqrt{f_c'}/350 \tag{3.2}$$

where f_c' is the compressive strength of the concrete at 28 days in psi. For 3000 psi concrete Eq. 3.2 indicates ν as 0.16.

Poisson's ratio for steel is ordinarily found as close to 0.3.[32]

It can be seen from the equations presented in Chapter II that the magnitude of the bending and twisting moments in a plate may be affected by the numerical value of Poisson's ratio. For the orthotropic bridges and for the solutions obtained by SLAB this effect was shown to be very small, and Bakir[6] reported that a change of 100 percent in Poisson's ratio did not introduce an error greater than 1 percent in the results of a prestressed concrete girder and concrete slab bridge. For the Patuxant River Bridge, which is composed of steel girders and reinforced concrete slab, the effect was even less. Ignoring Poisson's ratio for the slab did not introduce any appreciable change in either total moment or deflection at the midspan of the girders. The maximum reductions were 0.5 percent in the maximum moment and 0.8 percent for the maximum deflection. Therefore, it could be concluded that use of the mean value of the Poisson's ratios, as given above, could be considered as a reasonable uncertainty as to the actual Poisson's ratio in the material to be used in a given bridge.

CHAPTER IV

PRESTRESSED GIRDER BRIDGES

4.1 Introduction

All bridges studied in this chapter are prestressed I-shaped concrete girders with reinforced concrete decks. This type of bridge is the most common shape for spans from 40 to 120 ft.[35] The study consists of the evaluation of parameters for such structures and then a correlation study of the DSLAB computer solution with physical test results. The test bridges include both simple and continuous span bridges. Three tests are considered for the first type and two for the second, with some range of skew angle in both types.

4.2 Evaluation of Stiffnesses

4.2.1 Slab Flexural Stiffness. Section 2.4 presented the equations for flexural stiffness of reinforced concrete plates, assuming concrete an elastic homogeneous material. While not valid over the whole loading range, it is a good estimate for uncracked sections. Neglecting the small contribution of the reinforcing steel, the expression for slab stiffness per unit width reduces to

$$D_x = D_y = \frac{E_c I_c}{1 - \nu_c^2} = \frac{E_c t^3}{12(1 - \nu_c^2)} \qquad (4.1)$$

where t is the thickness of the slab. This expression does not correctly represent the stiffness of cracked sections, as indicated by accurate non-linear moment-curvature relations.

For typical slab and girder bridges the slab stiffness is usually very small (say 1/1000) compared to girder stiffness. Thus, use of elaborate moment-curvature procedures to define the slab stiffness at each level of loading is unnecessary. Figure 4.1 shows that doubling and even tripling

36

D = Slab flexural stiffness

D_o = Reference stiffness
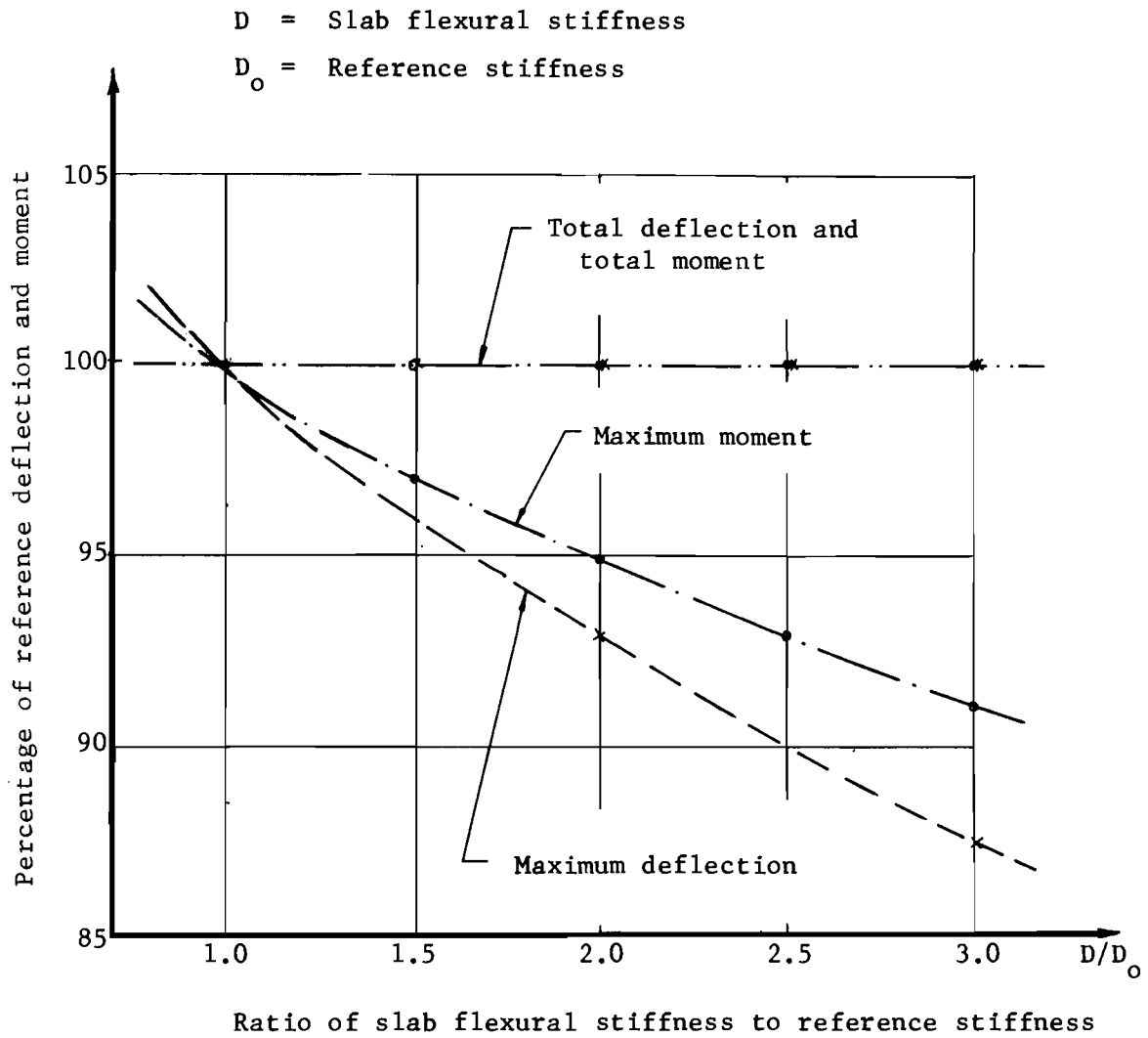
Fig. 4.1. The effect of slab stiffness on deflections and moments.

the value of slab stiffness did not appreciably change either total deflection or total moment at midspan of the bridge (Sec. 4.3.2) tested by Bakir,[6] and had only a relatively small influence on both maximum values. The slabs usually act compositely with the girders and under service loads most of the slab is not appreciably affected by the formation of flexural cracks. Exceptions might be found over interior supports in a continuous bridge and in the immediate vicinity of point loads. Since calculations beyond Eq. 4.1 will not improve the final results by an order of magnitude which justifies such rigorous calculations, it is recommended that the slabs be assumed to have the stiffness of the uncracked section throughout the bridge.

4.2.2 <u>Slab Torsional Stiffness</u>. The importance of this parameter depends on its role in the distribution of loads and deflections transversely across the bridge. This effect actually is of small magnitude, as can be seen from Fig. 4.2, which is a case study for the bridge tested by Bakir.[6] Doubling the value of the slab torsional stiffness causes less than 1 percent error in the total deflection and moment and 3 percent error in the maximum girder deflection and moment. Furthermore, the error was about the same magnitude when the whole value was neglected.

Section 2.4 indicated that the theoretical values for the torsional stiffness of plates should be considered as first approximations, while more reliable values could be obtained from tests. Actually, this precision is unnecessary for this application of orthotropic plate theory, since the loads are mainly carried by the girders. Thus, the theoretical values are quite adequate.

The expression for torsional rigidity of a reinforced concrete plate was given in Sec. 2.4 as

$$D_{xy} = \frac{1 - \nu_c}{2} \sqrt{D_x D_y}$$

By substituting for D_x and D_y, their values from Eq. 4.1

$$D_{xy} = \frac{E_c t^3}{24(1 + \nu_c)} \tag{4.2}$$

C - Slab torsional stiffness

C_o - Reference torsional stiffness
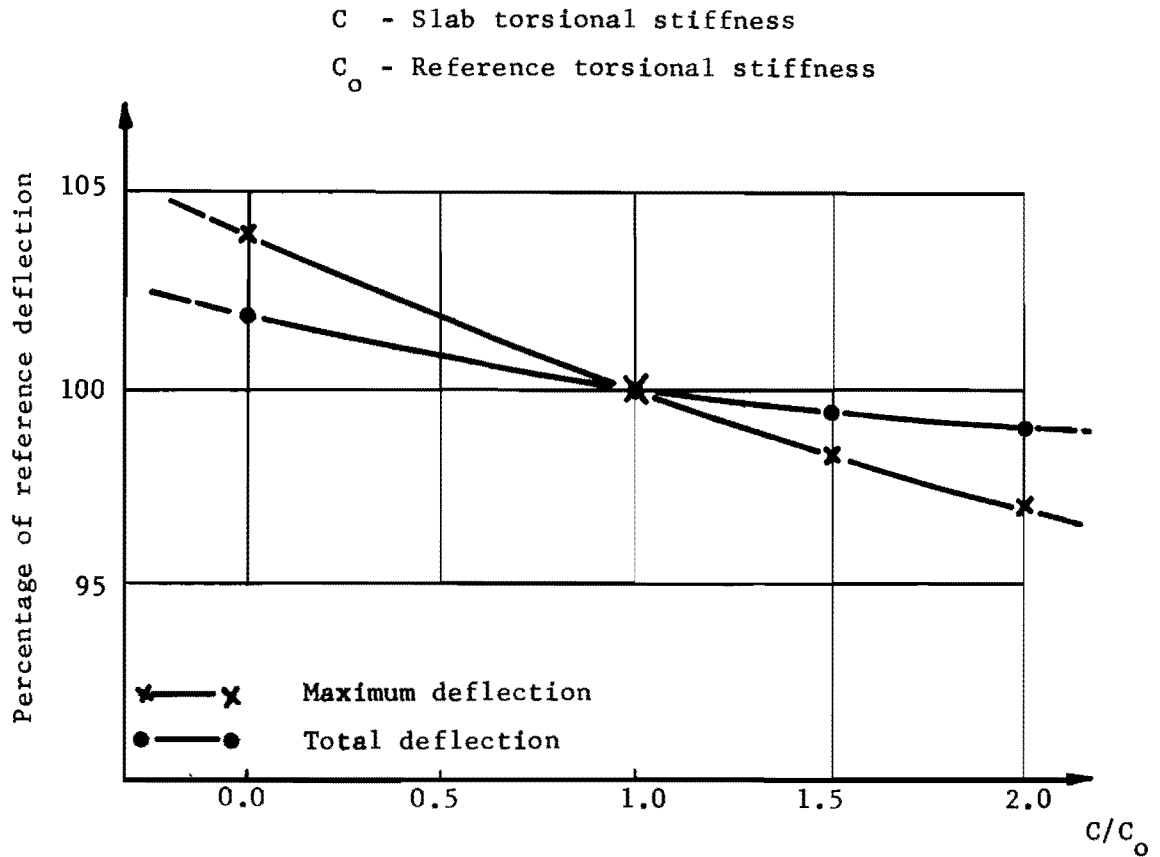
Fig. 4.2a. The effect of slab torsional stiffness on deflections.
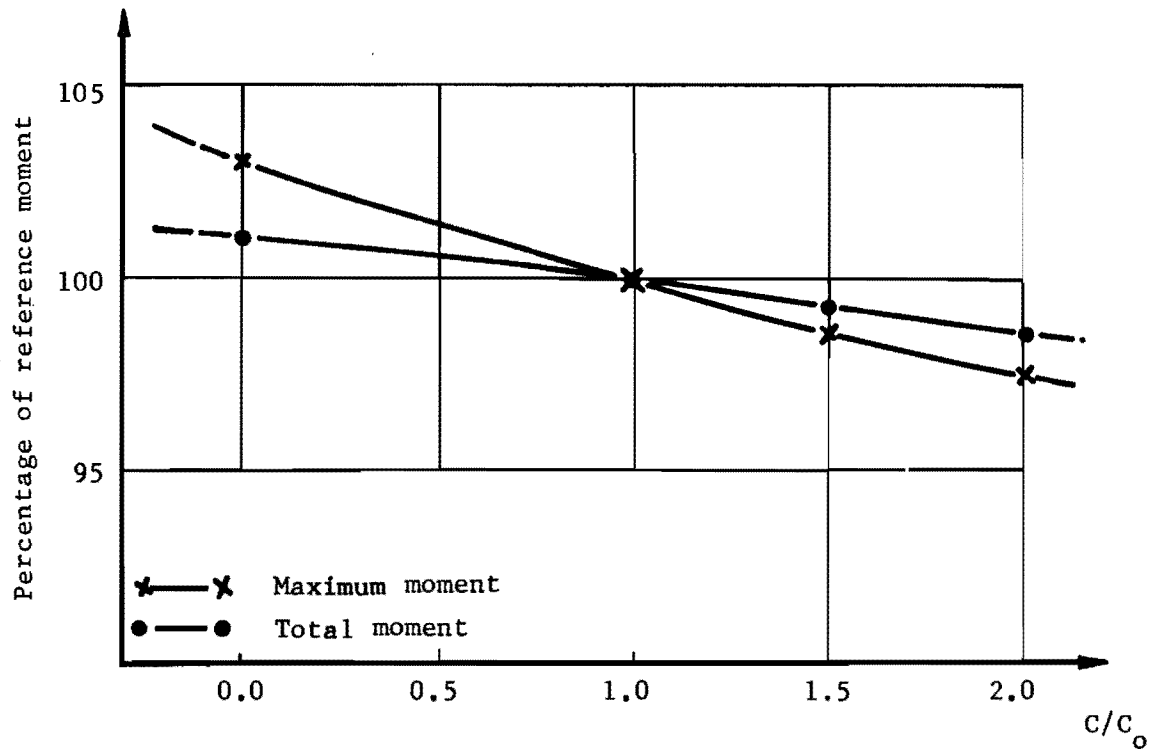
Fig. 4.2b. The effect of slab torsional stiffness on girder moments.

Hudson[26] used the notation of C_x and C_y for the torsional rigidities of the bars, which represent mesh rigidities in both x and y directions, as

$$C_x = C_y = 2D_{xy} = \frac{E_c t^3}{12(1 + \nu_c)} \qquad (4.3)$$

4.2.3 <u>Girder Flexural Stiffness</u>. The flexural stiffness of the girders is the most dominant parameter affecting the results. In one-dimensional problems, like beams and plane frames, the final displacements are directly proportional to member stiffness. In two-dimensional problems such as plates, the influence of load distribution in both directions somewhat reduces the impact of the variation of stiffness in one direction on the final results.

Figure 4.3 shows the effect of variation of girder flexural stiffness on moments and deflections for the bridge presented by Bakir.[6] Increasing girder flexural stiffness by 20 percent causes a decrease of 16 percent in the total girder deflection at midspan, and a decrease of 12 percent in the maximum girder deflection. The effect on moments is much less, since they depend more on relative stiffness relationships. A 20 percent increase in girder stiffness results in an increase of not more than 1 percent for total moment and 4 percent for maximum moment. Although the effect on deflection is not of the same order as in one-dimensional problems, actually it is of considerable effect, and, hence, a limitation on the expected range of errors in the estimation of the flexural stiffness of girders is necessary in order to limit the errors in the final deflection results. An estimate of flexural stiffness within about 10 percent is required in order to limit the error in the final results to a narrow range for positive comparisons.

As is usually the case, tests can provide the best measures for variables. However, quite good estimates can be obtained by simpler methods involving only analytical calculations. Highly accurate stiffnesses can be obtained from the moment-curvature relationships generated by digital computers. A comparison of test results and computer analysis for a prestressed beam tested by Keyder,[31] is shown in Fig. 3.5. The computer analysis for the beam is presented by Chang.[15] The manually calculated
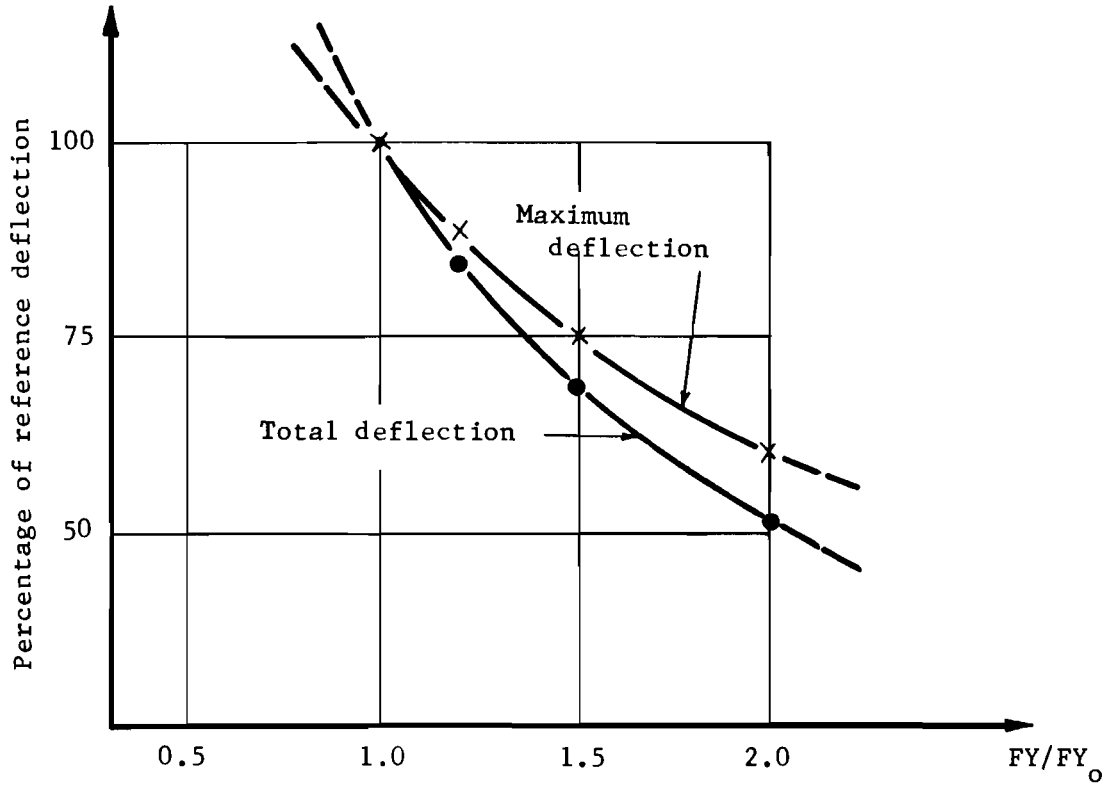
Fig. 4.3a. The effect of girder flexural stiffness on deflections.

FY = Flexural stiffness

FY_o = Reference stiffness
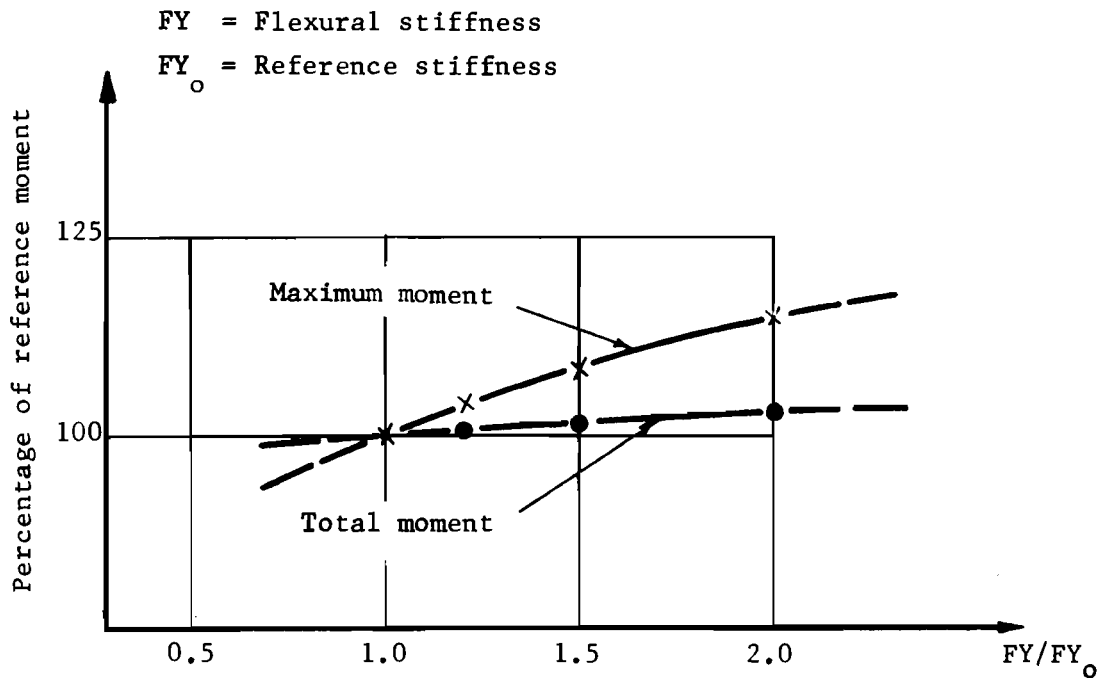
Fig. 4.3b. The effect of girder flexural stiffness on girder moments.

straight-line behavior is based on EI using the gross moment of inertia and the 1963 ACI Code[2] formula for the modulus of elasticity of the concrete. The response is very close to linear over a large range of loads, including service loads and moderate overloads. Thus, for service loads an extensive computer analysis for stiffness is not justified. This same observation was reported by Janney and Eney[29] for their field test on a prototype pre-stressed concrete girder from the Northern Illinois toll highway. The design criteria which limit tensile stresses in prestressed concrete to values below those which might cause cracks ensure that at service loads the section behaves elastically so that both gross and transformed gross moments of inertia are adequate estimates of stiffness.

The flexural stiffnesses of ten prestressed girders tested by Mattock and Karr[39] are presented in Table 4.1. Typical cross sections of the girder and the test setup are shown in Fig. 4.4. Comparisons of test results with stiffnesses calculated both on the basis of gross and trans-formed gross moment of inertia of the section are also presented. The comparison shows that using gross moment of inertia the average error was - 8.5 percent, while using the gross transformed moment of inertia is somewhat more accurate with an average of -5.4 percent. This indicates that the required level of accuracy can be obtained by such relatively simple methods of calculation for the service load region.

4.2.4 <u>Girder Torsional Stiffness</u>. The analysis of girder and slab bridges using SLAB computer programs is much less sensitive to the tor-sional stiffness of the girders than to flexural stiffness. This can be seen in Fig. 4.5 for the bridge tested by Bakir[6] with a single load at mid-span of the edge girder. Neglecting torsional stiffness completely causes the maximum deflection to increase by 24 percent and the total deflection by 8 percent, while maximum girder moment increases by 18 percent and total moment by 7 percent. When half of the torsional stiffness is used, the error is slightly less than one-half of the previous percentages. These values are for a 45° skew, and they decrease for smaller angles. From this it is concluded that an estimate of torsional stiffness of girders within 25 percent will limit the error in the maximum values of moment and deflec-tion to about 5 percent.

42

2 - #2
2 strand ½" ⌀

8"

1.75

3.5
2.75

26 strands
½" ⌀ (1" on
center
vertically)

2.25

9.5   22.5"

3.75

3.75
3.5

2"

11"

Test Setup
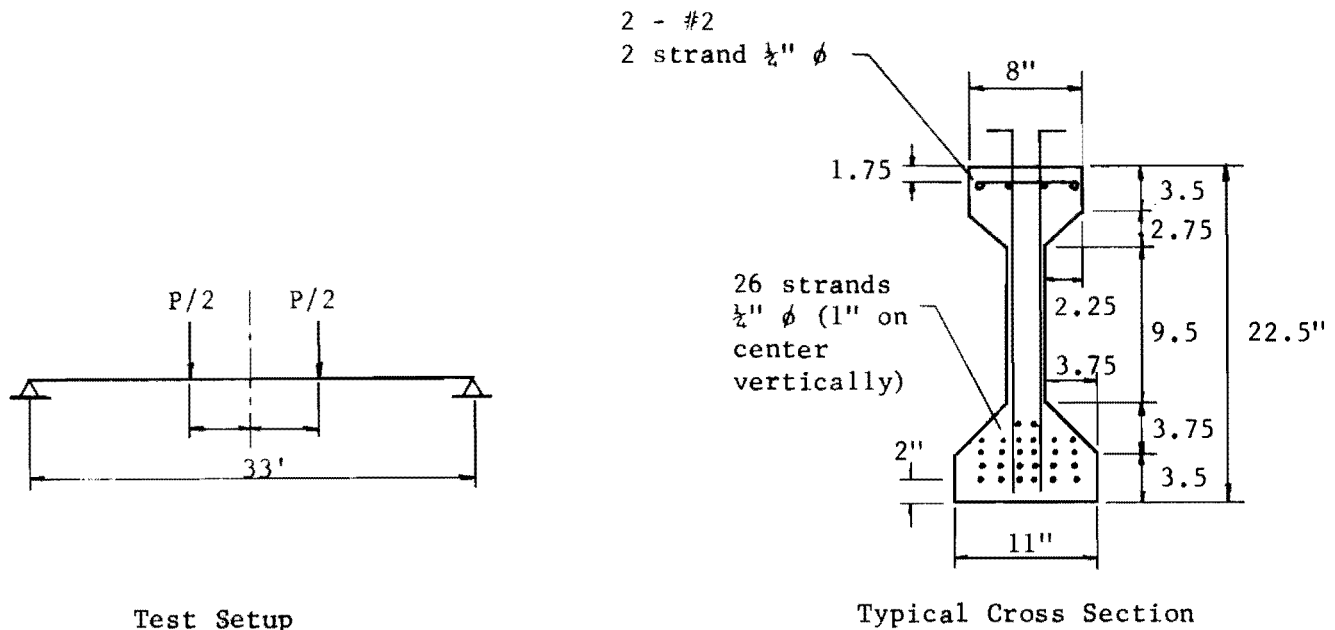
Typical Cross Section

Gross I   = 7826 in.^{4}

Transformed gross I   =   8098 in.^{4}

Fig. 4.4.   Typical setup and cross section details of the tested
            precast, prestressed beams.

TABLE 4.1.   COMPARISON OF MEASURED AND CALCULATED FLEXURAL
              STIFFNESS OF PRESTRESSED CONCRETE BEAMS

Girder	Measured E_c (lb./in.^{2} x 10^6)	Measured EI (lb.-in.^{2} x 10^6)	Computed EI (gross) (lb.-in.^{2} x 10^6)	% error	Computed EI (tran) (lb.-in.^{2} x 10^6)	% error
1	4.02	37,680	31,500	-16.4	32,600	-13.5
2	4.55	37,220	35,600	- 4.3	36,800	- 1.1
3	4.46	39,190	34,900	-10.9	36,100	- 7.9
4	4.35	39,650	34,100	-14.0	35,250	-11.0
5	4.35	35,940	34,100	- 5.1	35,250	- 1.9
6	4.35	35,120	34,100	- 3.2	35,250	+ .4
7	4.39	36,170	34,400	- 4.9	35,600	- 1.6
8	4.59	37,910	36,000	- 5.0	37,200	- 1.9
9	4.32	36,170	33,800	- 6.5	35,000	- 3.2
10	3.90	35,820	30,600	-14.5	31,600	-11.8
			Average	- 8.5		- 5.4
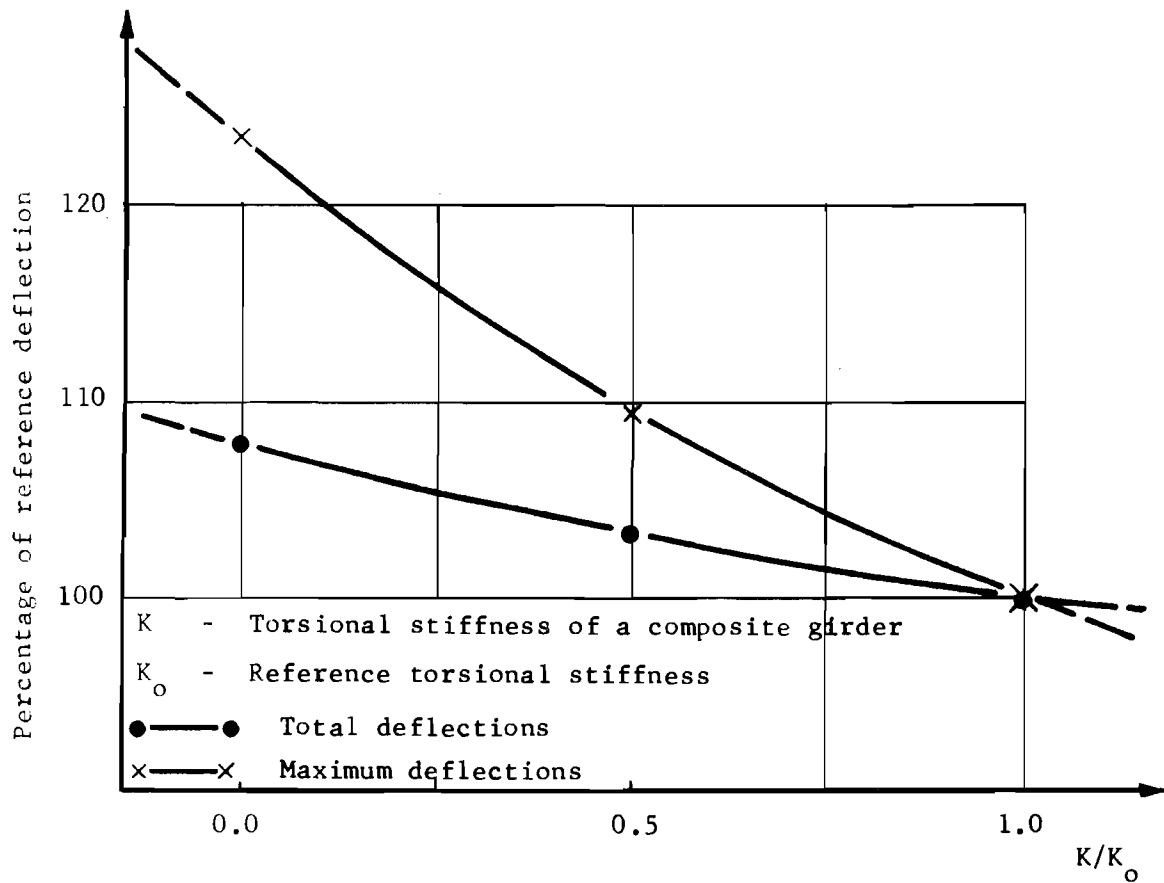
Fig. 4.5a. The effect of girder torsional stiffness on deflections.
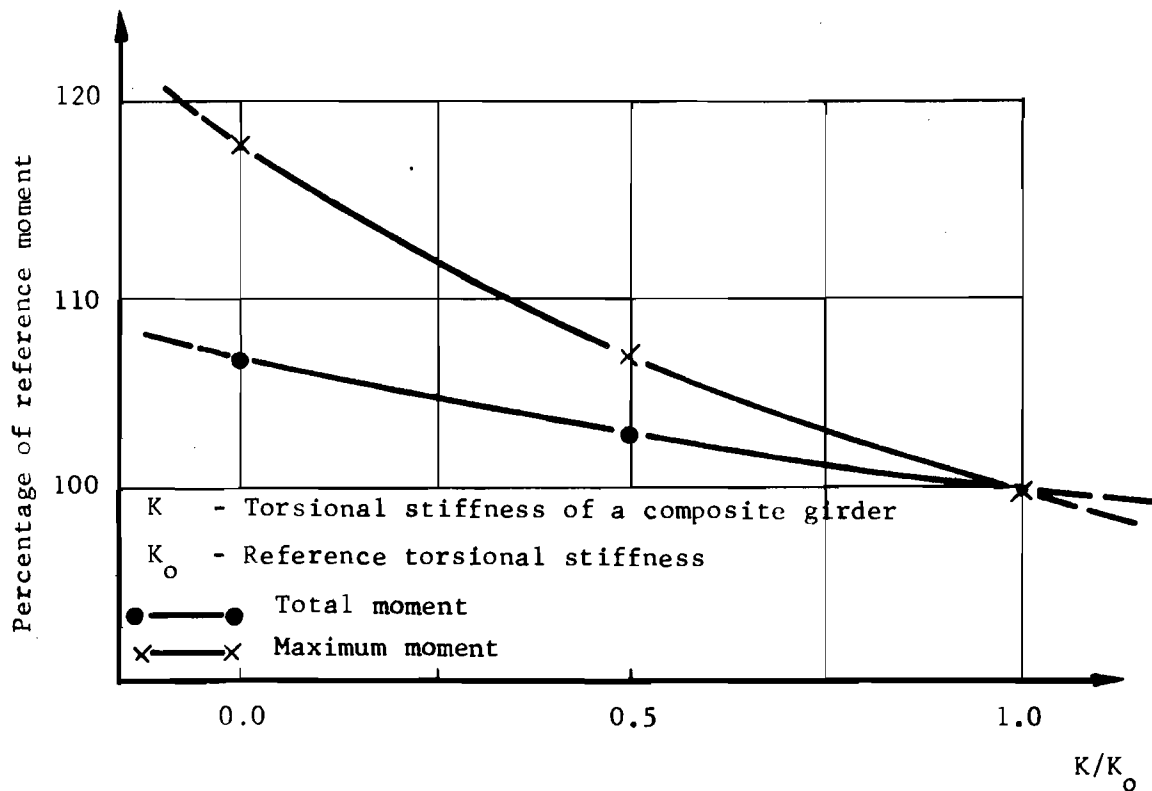
Fig. 4.5b. The effect of girder torsional stiffness on girder moments.

44

A theoretical study accompanied by physical tests was carried out at The University of Texas at Austin[45] for a common I-shaped prestressed concrete girder, as used in highway bridges. The study showed that an estimate of torsional stiffness could be obtained within about 10 percent accuracy. The following procedures may be used for isolated and composite girders.

4.2.4.1 Torsional stiffness of prestressed girders. The torsional stiffness can be calculated based on an equivalent rectangular cross section for the I-shaped girder using the St. Venant formula. The equivalent rectangle shown in Fig. 4.6a is assumed to have the following sides:

$$b = h$$
$$c = 0.9 \, A/h$$

(4.4)

where

b = the longer side of the rectangle

c = the shorter side of the rectangle (see Fig. 4.6a)

h = height of the girder

A = cross-sectional area of the girder

The St. Venant formula is

$$K_r = \beta b c^3$$

(4.5)

where

K_r = torsional rigidity of the section

β = coefficient $(0.141 \leq \beta \leq 0.333)$, which is a function of the ratio b/c (see Fig. 4.7).

Multiplying K_r by the shear modulus of the section the torsional stiffness is

$$\text{Torsional stiffness} = K_r G$$

where

$$G = \frac{E_c}{2(1 + \nu)}$$

4.2.4.2 Torsional stiffness of composite section. Composite sections gain their torsional stiffnesses from three different sources, i.e., the girder stiffness, the slab stiffness, and the joint effect. To calculate the stiffness within the required accuracy:

$$c = 0.9 \frac{A}{h}$$

$h = b$ Area = A

(a)   Common shape of prestressed concrete girder.

Area = a

Slab

Girder

(b)   Composite section of slab and girder.
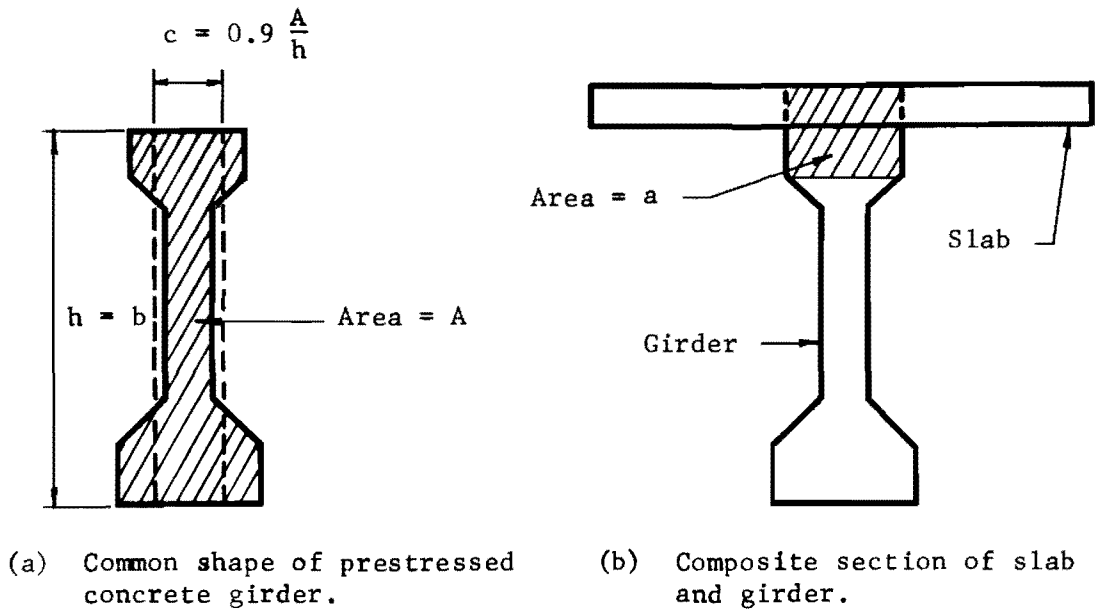
Fig. 4.6.   Isolated and composite section of typical prestressed concrete I-shaped beam.

$$\beta = \frac{1}{3} - 0.21 \frac{b}{c} \left(1 - \frac{b^4}{12c^4}\right)$$

$$K = \beta \, bc^3$$
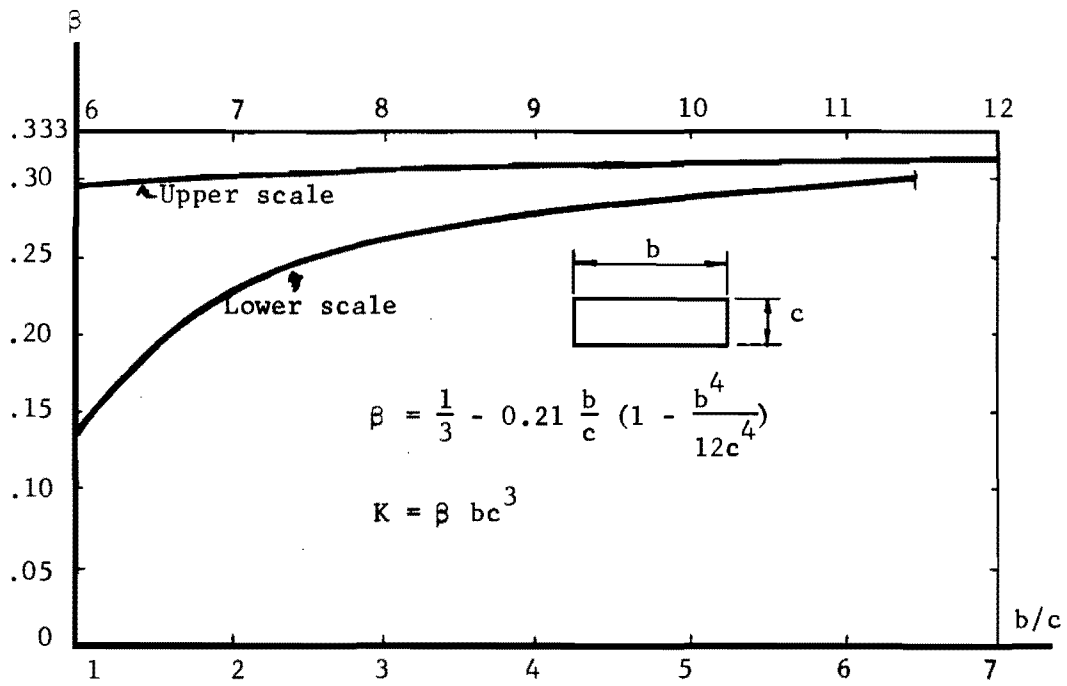
Fig. 4.7.   Coefficient β.

(1) The girder torsional stiffness is calculated as in Sec. 4.2.4.1.

(2) The slab torsional stiffness is obtained in the same way except it must be multiplied by the ratio of (G_s/G_g) which represents the shear modulus of slab materials related to girder material.

(3) For the joint effect, the following empirical expression was found to be a very good approximation when compared with test results[45]:

$$K_{joint} = 0.156 \ a^2 \qquad (4.6)$$

where

$$a = \text{the area of the rectangle inscribed in the joint,}$$
as shown in Fig. 4.6b.

(4) Therefore, the torsional rigidity of the composite section is

$$K_{comp} = K_{girder} + K_{slab} \cdot G_s/G_g + K_{joint} \qquad (4.7)$$

The torsional stiffness is obtained by multiplying this expression by the shear modulus of the girder. The girder torsional stiffness is then divided by two to transform it to the correct equivalent plate element torsional stiffness.

4.3 Comparison of Test Results--Simple Span Bridges

4.3.1 The University of Texas Test, 30° Skew Bridge. An accurate microconcrete model of a standard 80 ft. span prestressed girder bridge was built and tested at the Balcones Research Center of The University of Texas at Austin. The scale factor was 5.5. Details of building and testing this model were presented by Barboza.[7] Figure 4.8 shows a plan view and cross section of the bridge model, which had six prestressed precast concrete girders and a reinforced cast-in-place concrete slab. The bridge had a 30° skew angle.

In the SLAB analysis the bridge is simulated by a mesh which has 22 stations of 4.14" in the x direction and 93 stations in the y direction, each of which has an increment length of 2.39". The increments in the x direction were chosen in order to have a minimum of four stations between girders, while in the y direction the increments were based on the consideration of the skew angle and location of supporting points. Later experience indicated that satisfactory results could have been obtained with substantially fewer stations in the y direction.

Flexural and torsional stiffnesses of the slab were calculated as recommended in Secs. 4.2.1 and 4.2.2, while the girder values were obtained
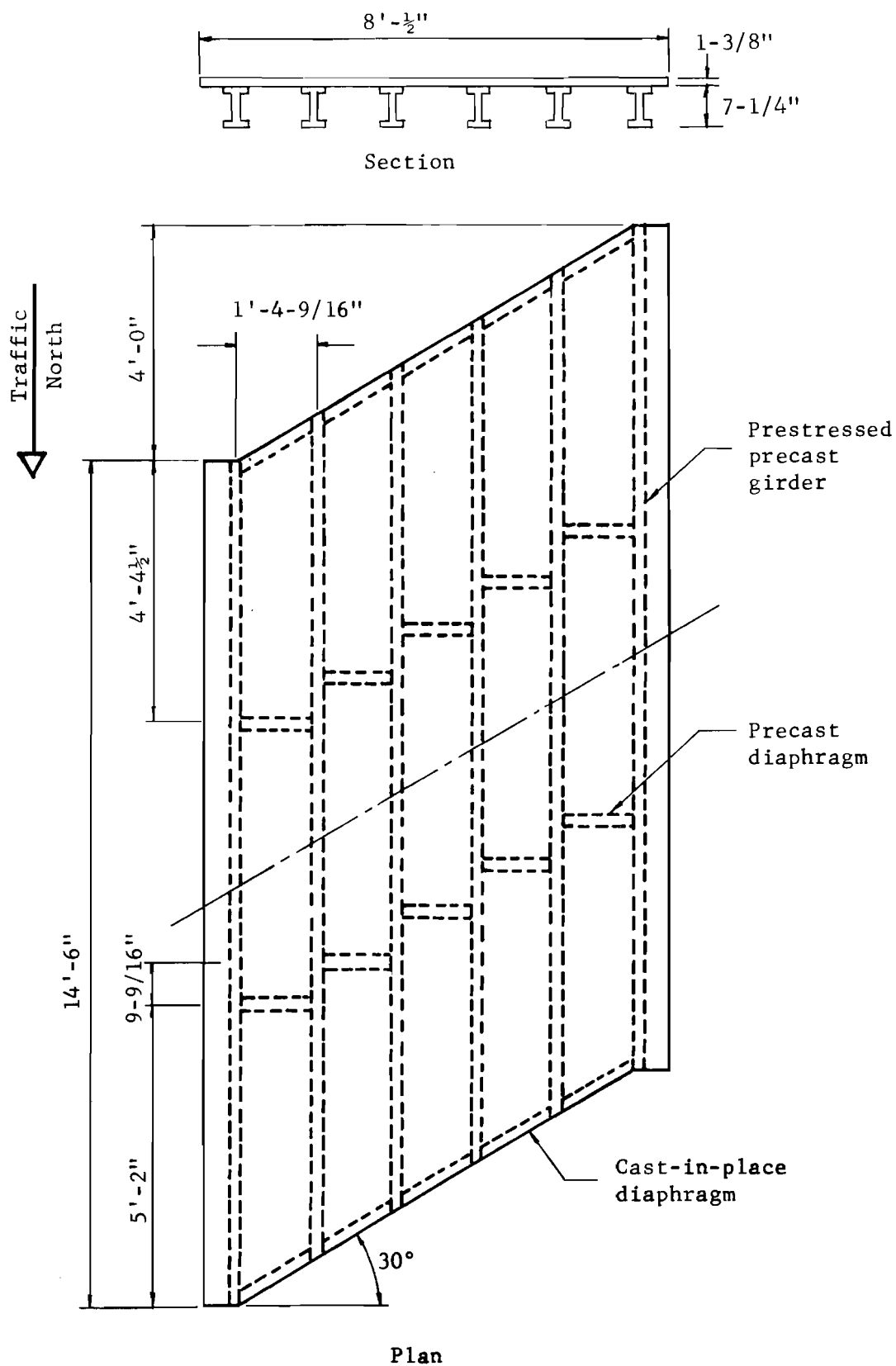
Fig. 4. 8. The University of Texas—30° skew angle model
bridge.

from auxiliary tests done on similar girders. The calculated girder flexural stiffness as recommended in Sec. 4.2.3 was within 5.5 percent of the tested values. All the parameters required for the computer simulation are presented in Table 4.2. Girder flexural stiffness is input along its axis in the mesh, while the composite girder torsional stiffness is added to the two slab increments which adjoin the girders. Supporting points are simulated with springs having constants of 1×10^6 lb./in. A model truck which had the same scale factor of 5.5 to simulate a H20-S16 standard truck, plus 25 percent impact load was used. The loads were applied by hydraulic jacks fixed to a loading frame with rubber pads used at loading points to simulate the wheels. The bridge was instrumented with 42 strain gages in addition to 30 deflection dial gages.

Two typical load cases are compared with analytical solutions using SLAB (SLAB36 version). These cases are an edge loading representing an extreme case of load distribution and a central loading. The truck was positioned in the longitudinal direction to have the west drive wheel fall on the midspan at that location. Figures 4.9 and 4.10 show comparisons of tests and analytical results for both deflection and moment in the girders for these load cases. The multiplier x shown in the figures corresponds to the number of truck overloads. The comparisons show excellent correlation results at service load levels, which may be considered up to twice design truck load. Such a range of loading represents the elastic range of the bridge and no appreciable changes in stiffnesses occur. However, deviation between tests and analytical results becomes apparent at three times design truck load, at which the bridge is into the nonlinear region. Some cracks in the beams were noticed at this load level, which means that stiffnesses decreased from the original values, and, therefore, test results should be greater than analytical results, based on the original stiffness values. These figures show clearly that the discrete element method is very useful and yielded results with high accuracy in obtaining solutions for this bridge.

The discontinuous interior diaphragm has a flexural stiffness equivalent to a slab width of 31 in. The analytical analysis showed that such diaphragms had negligible effect on the final results when comparative solutions were run considering and ignoring diaphragm stiffness.

TABLE 4.2. 30° SKEW BRIDGE, THE UNIVERSITY OF TEXAS

DATA SHEET

Mesh size

$m = 22$

$n = 93$

Increment length

$h_x = 4.14$ in.

$h_y = 2.39$ in.

Poisson's ratio $= 0.167$

Slab stiffnesses

$$D_x = D_y = \frac{Et^3}{12(1 - \nu^2)} = 7.46 \times 10^5 \ (lb.-in.^2)/in.$$

$$C_x = C_y = (1 - \nu) \ D_x = 6.2 \times 10^5 \ (lb.-in.^2)/rad./in.$$

Girder stiffnesses

EI (from test) $= 1.78 \times 10^9 \ (lb.-in.^2)$

EI (calculated) $= 1.88 \times 10^9 \ (lb.-in.^2)$

Torsion (from test) $= 6 \times 10^7 \ (lb.-in.^2)/in./rad.$

Diaphragms

$D_x = 2.34 \times 10^7 \ lb.-in.^2$

Supporting springs

$S = 1 \times 10^6 \ lb./in.$

Loading

Standard truck (H20-S16) + Impact (25%)
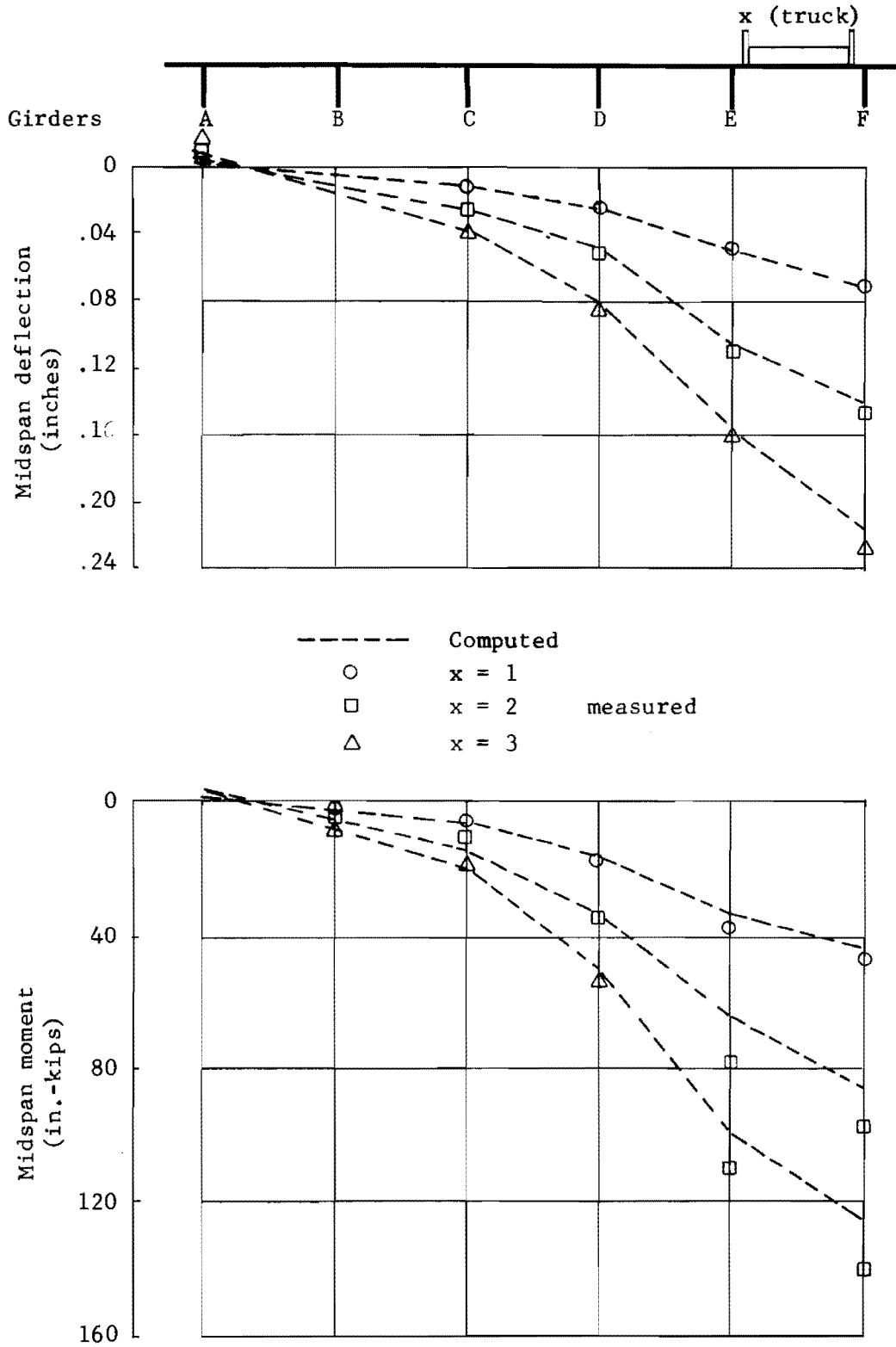
Fig. 4.9. Girder deflections and moments for an edge truck overload (30° skew bridge).

51
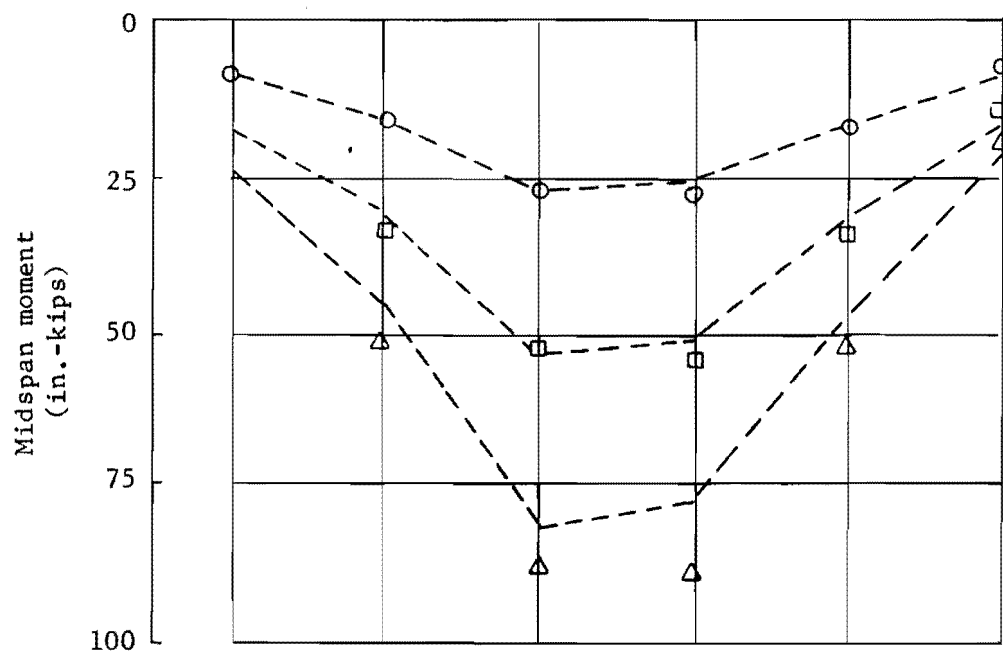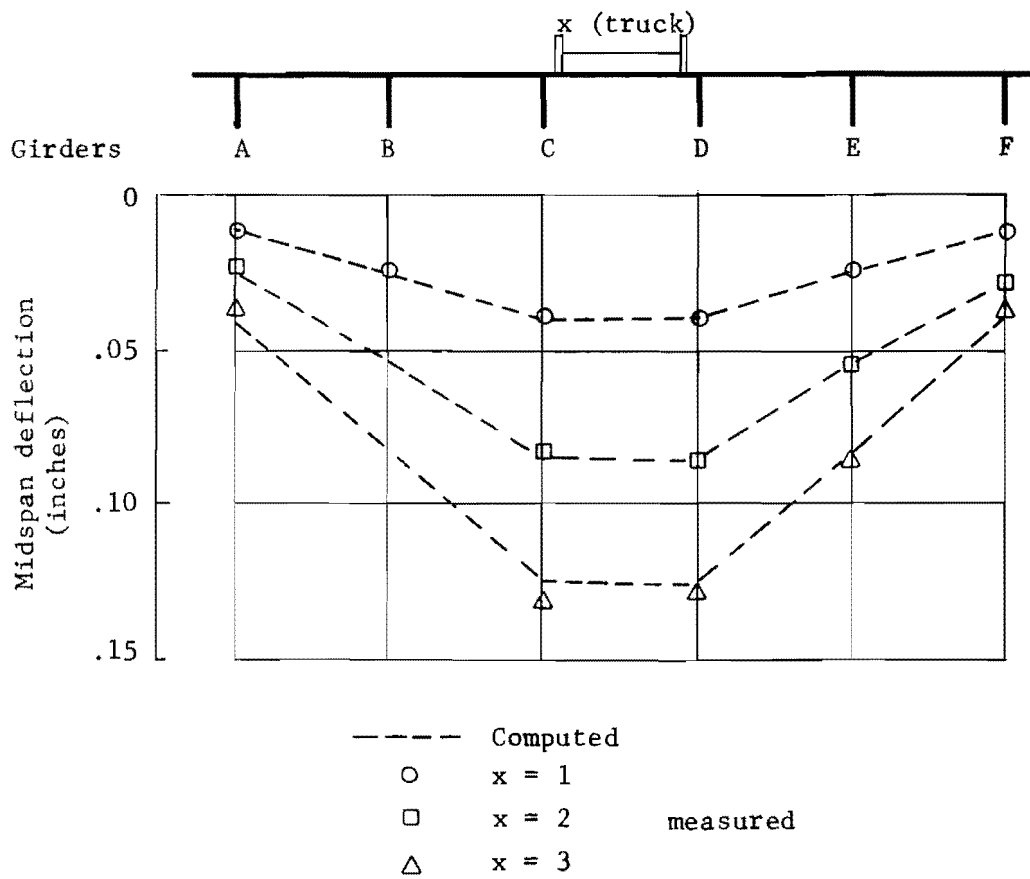
Fig. 4.10. Girder deflections and moments for a central truck overload (30° skew bridge).

52

4.3.2 <u>The University of Texas Test, 45° Skew Bridge</u>. This bridge
model is the same type as that presented in the previous section, but it
had a skew angle of 45°. It was built and tested at The University of
Texas Civil Engineering Structures Research Laboratory at the Balcones
Research Center. Details of instrumentation and testing technique were
presented by Bakir.[6] A plan view and a section are shown in Fig. 4.11. All
information presented in Table 4.2 is applicable for this bridge except for
the number of stations and increment lengths in the y direction, where 63
stations with lengths of 4.13 in. were used. (Note - only 42 stations are
used to model any girder span.)

The purpose of this model was to study the effect of skew angle on
the efficiency and accuracy of the discrete element method. Loading trucks
and their locations in the longitudinal direction are generally the same as
in the previous bridge. Figures 4.12 and 4.13 show the comparison of typical
test results with the analytical values for two load cases. One truck was
positioned at the middle of the cross section in the first case. In another
loading case the same truck, plus an extra one placed at the edge, acted
simultaneously on the bridge. Comparison of the results shows a good pre-
diction for the discrete element method for the elastic linear region up
to twice the design truck loads for the first case and to design truck load
for the two trucks of the second case. From these figures it is concluded
that the efficiency of the computer program did not change due to the
increase of the skew angle of the bridge. The results at design loads were
excellent and highly accurate.

Ignoring the stiffness of the interior discontinuous diaphragms had
negligible effect on the final analytical results when comparative runs
were made.

4.3.3 <u>A Bridge on Northern Illinois Toll Highway</u>. A full-scale
test was performed by Janney and Eney[29] on a bridge located on the Northern
Illinois Toll Highway. The two-lane bridge was tested as a single span,
and was an interior panel of a four-span continuous bridge when construction
was completed. The span was 70'-5", with a 20° skew angle. The cross section
was composed of six prestressed, precast I-shaped concrete girders spaced at
7'-6" center-to-center. A precast prestressed slab 2-1/2 in. thick was placed

Plan

Section showing interior diaphragms   Section showing end diaphragms
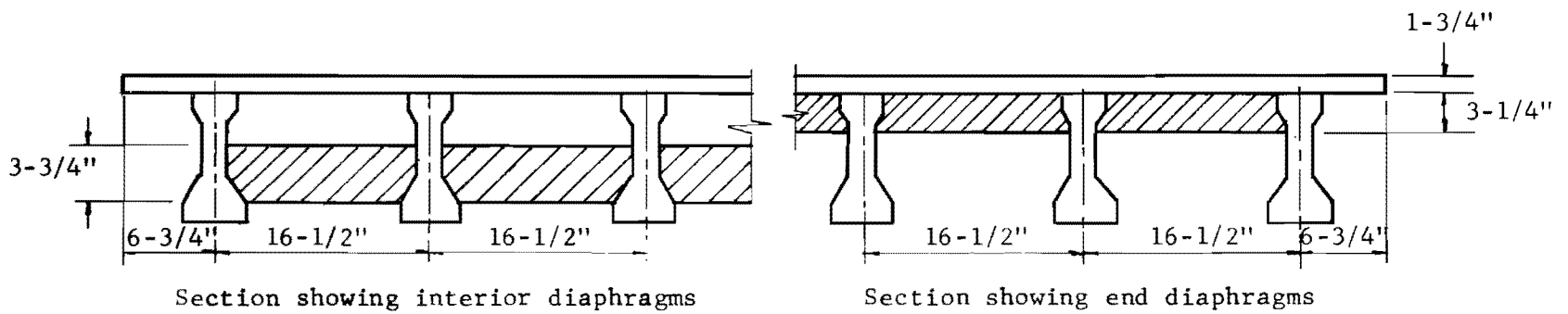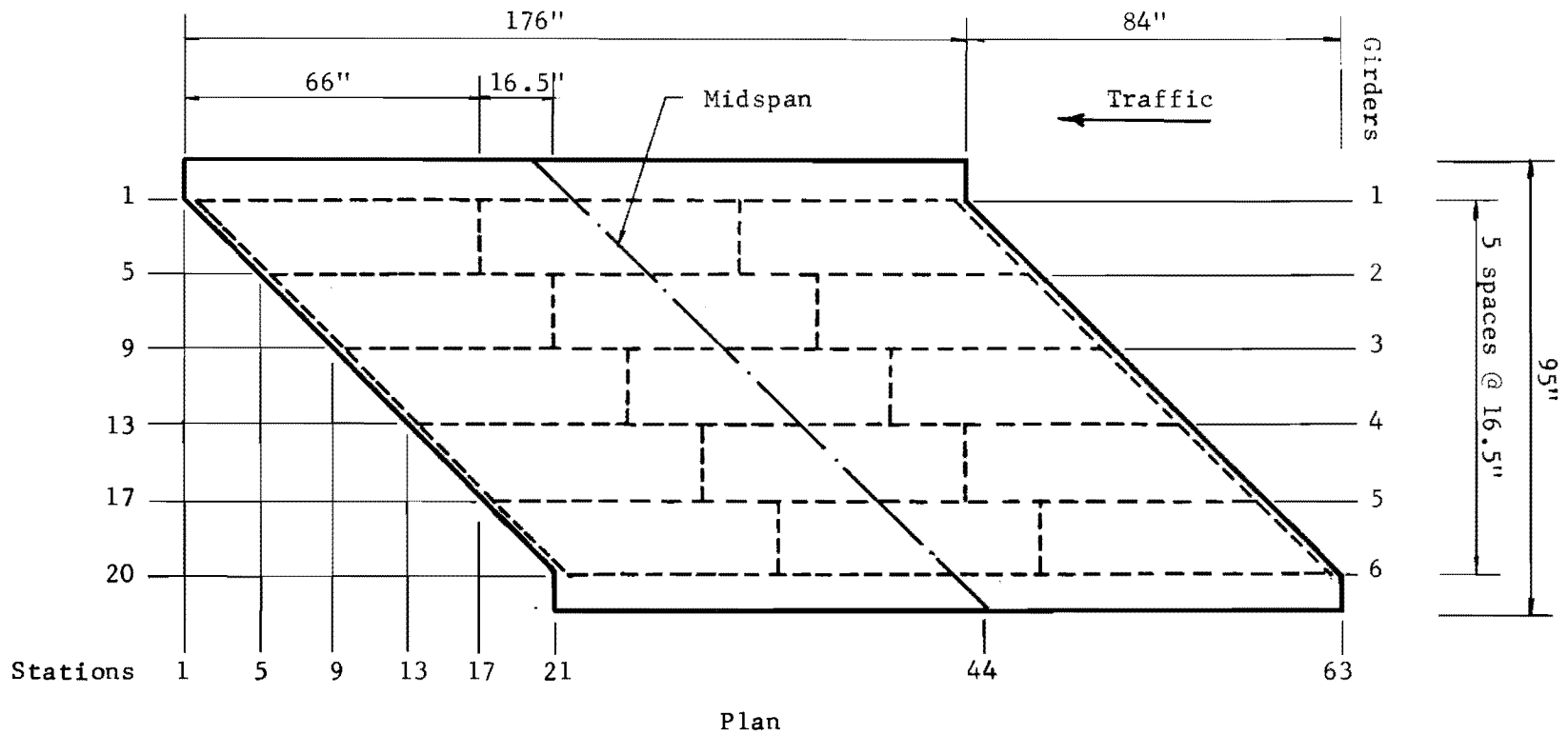
Fig. 4.11 . The University of Texas test--45° skew bridge.
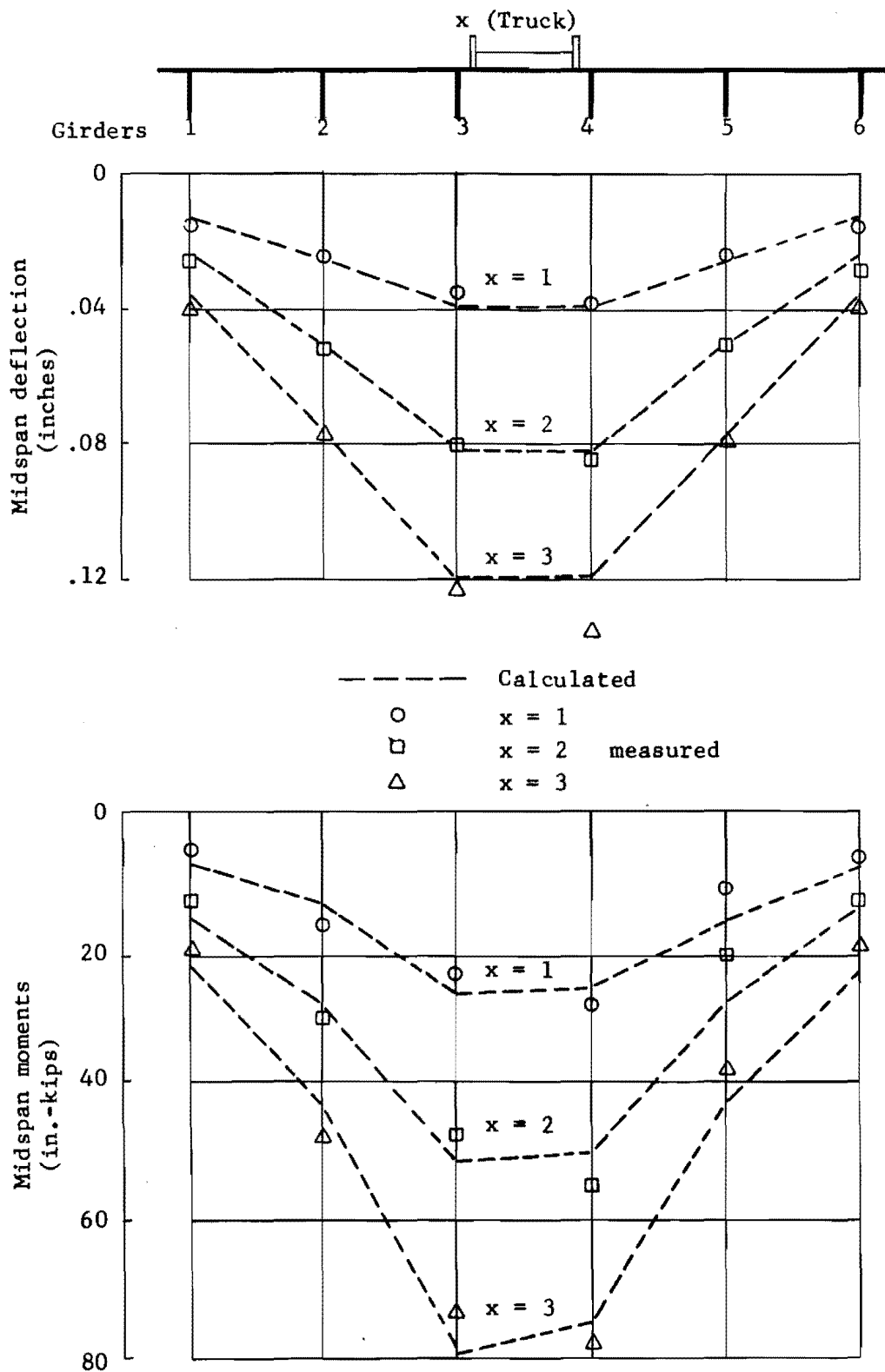
Fig. 4.12. Girder deflections and moments for a single truck overload (45° skew bridge).
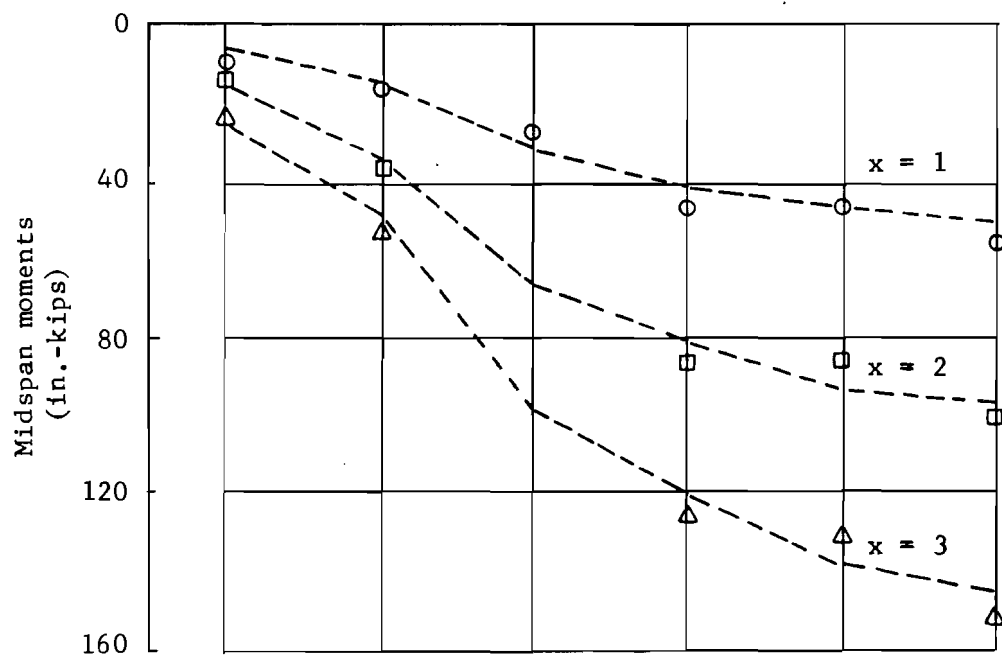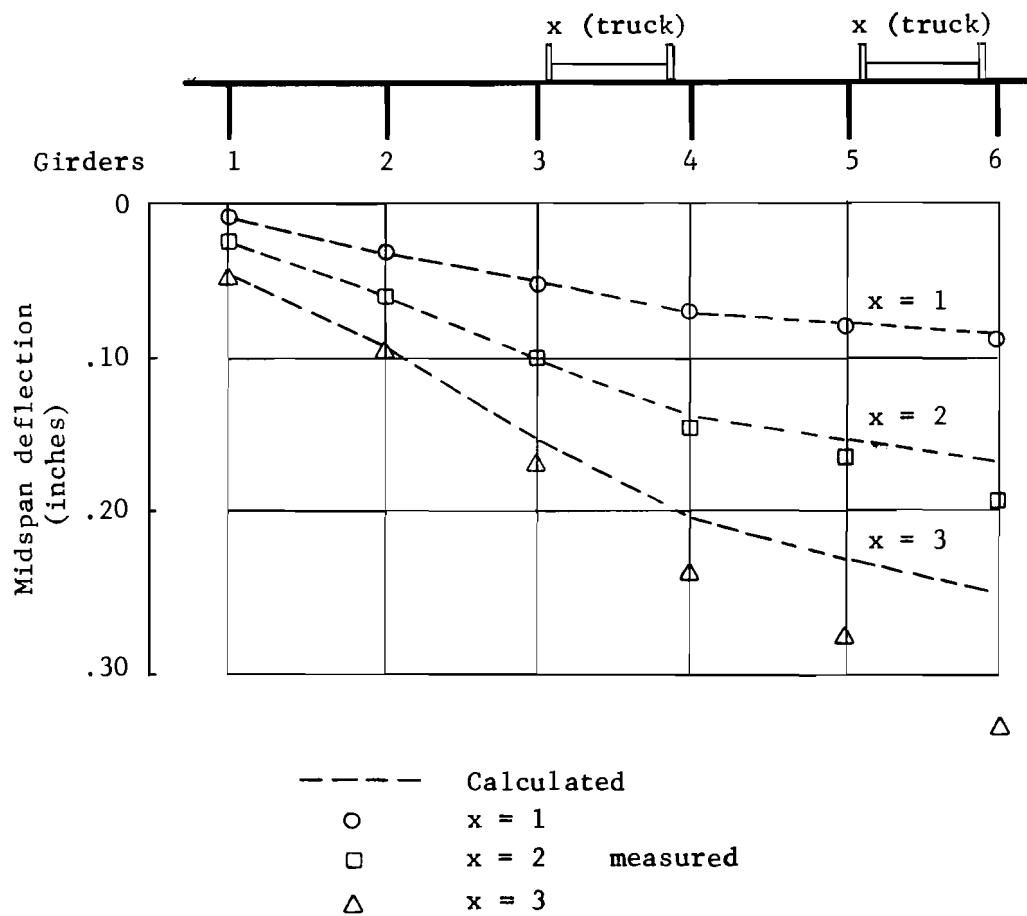
Fig. 4.13. Girder deflections. and moments for a double truck
overload (45° skew bridge).

to span between the girders and rested on a bed of mortar along each supporting edge. These panels were jointed with each other with a groove-type joint along the common joint. The top face of the panels was rake finished to supply enough bond for the 5-in. thick cast-in-place reinforced concrete slab. The precast elements served as formwork for the cast-in-place deck.

The plan view and a cross section of the bridge and girders are shown in Fig. 4.14. The prestressed steel used in the girders was forty-six 7/16 in. strands with an ultimate tensile strength of 255,000 psi. The concrete strength of the prestressed slab panels was 6000 psi. The cylinder strength of the cast-in-place deck was 1700 psi and the compressive strength of cores taken from the test span was 2000 psi.

Stiffnesses of girders were derived from tests performed as part of the study, and a value of the moment of inertia of the T-section was given as 584,000 in.^{4}, with an average modulus of elasticity of 4.12 x 10^6 psi. The stiffnesses of the slab were based on the calculation of the gross moment of inertia of the total thickness of 7-1/2 in., with an average modulus of elasticity of 3.84 x 10^6 psi. The loading system was composed of two concentrated loads, each spaced 8 ft. on either side of the midspan of the loaded girder. The loads were applied with hydraulic rams manifolded together in order to have an equal load furnished by each ram.

Two girders were chosen to represent the two load cases. Girder 1 represented an edge loading and Girder 4 represented a general interior load case. Figure 4.14 shows the numbering of the girders and the simulation of the bridge by a mesh. Stations in each direction are also shown. SLAB40 was used in the analysis.

A total load of 112,000 lb. was applied for each load case and a measurement of deflections and moments at the midspan of each girder was obtained. Figure 4.15 shows a comparison of test and theoretical results for the edge load. Figure 4.16 shows the same comparison for the interior load case. The fine correlation indicates the prediction of the discrete element model is very good.

Plan

Typical Section
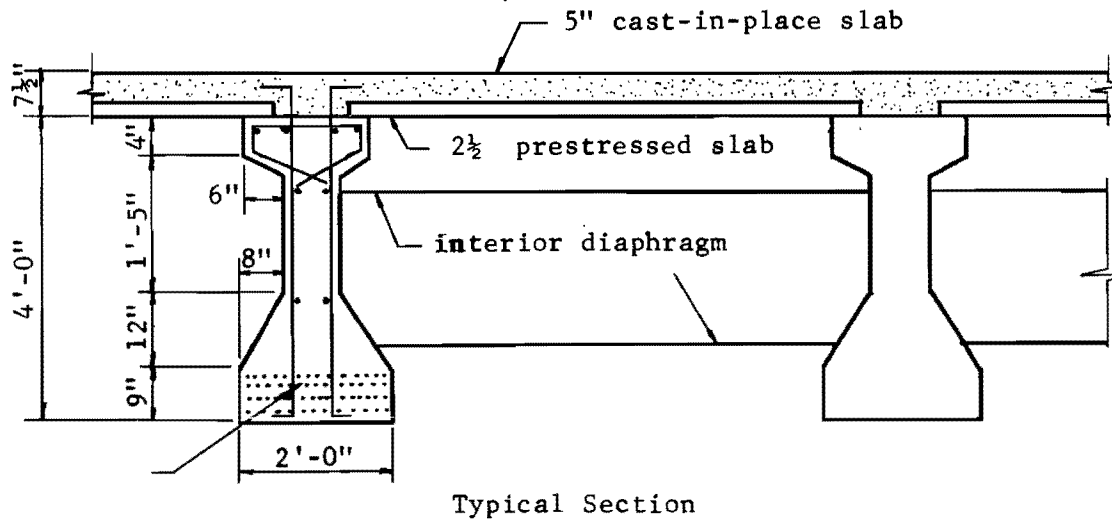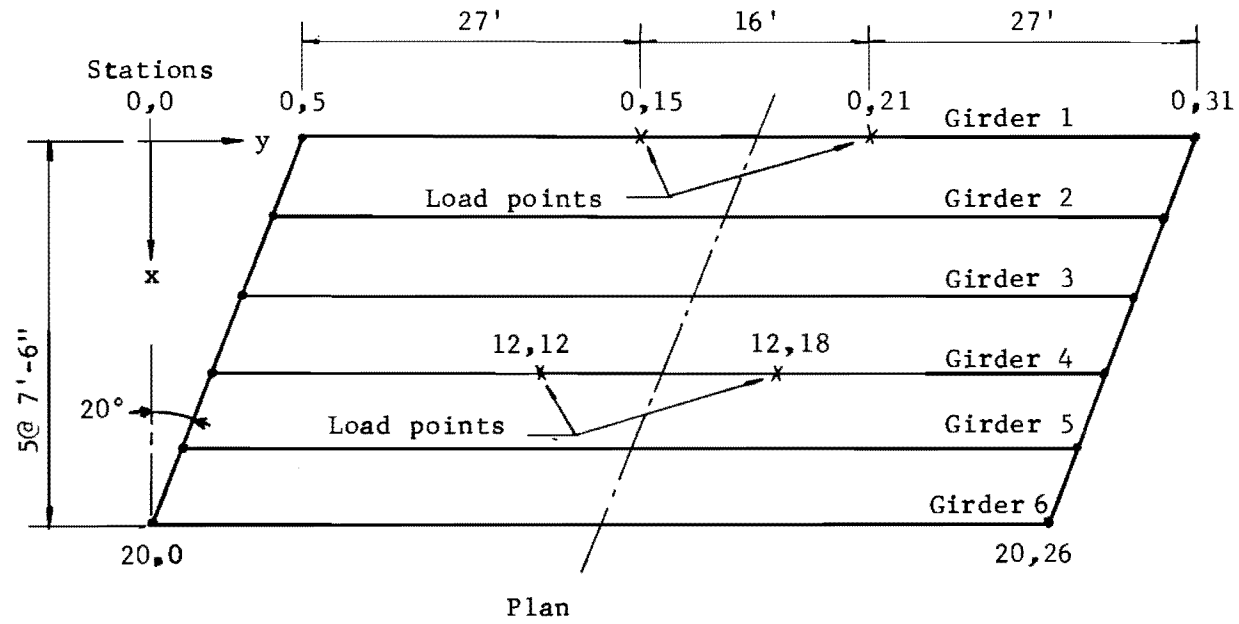
Fig. 4.14. Northern Illinois Toll Highway--A simple span bridge detail.

58
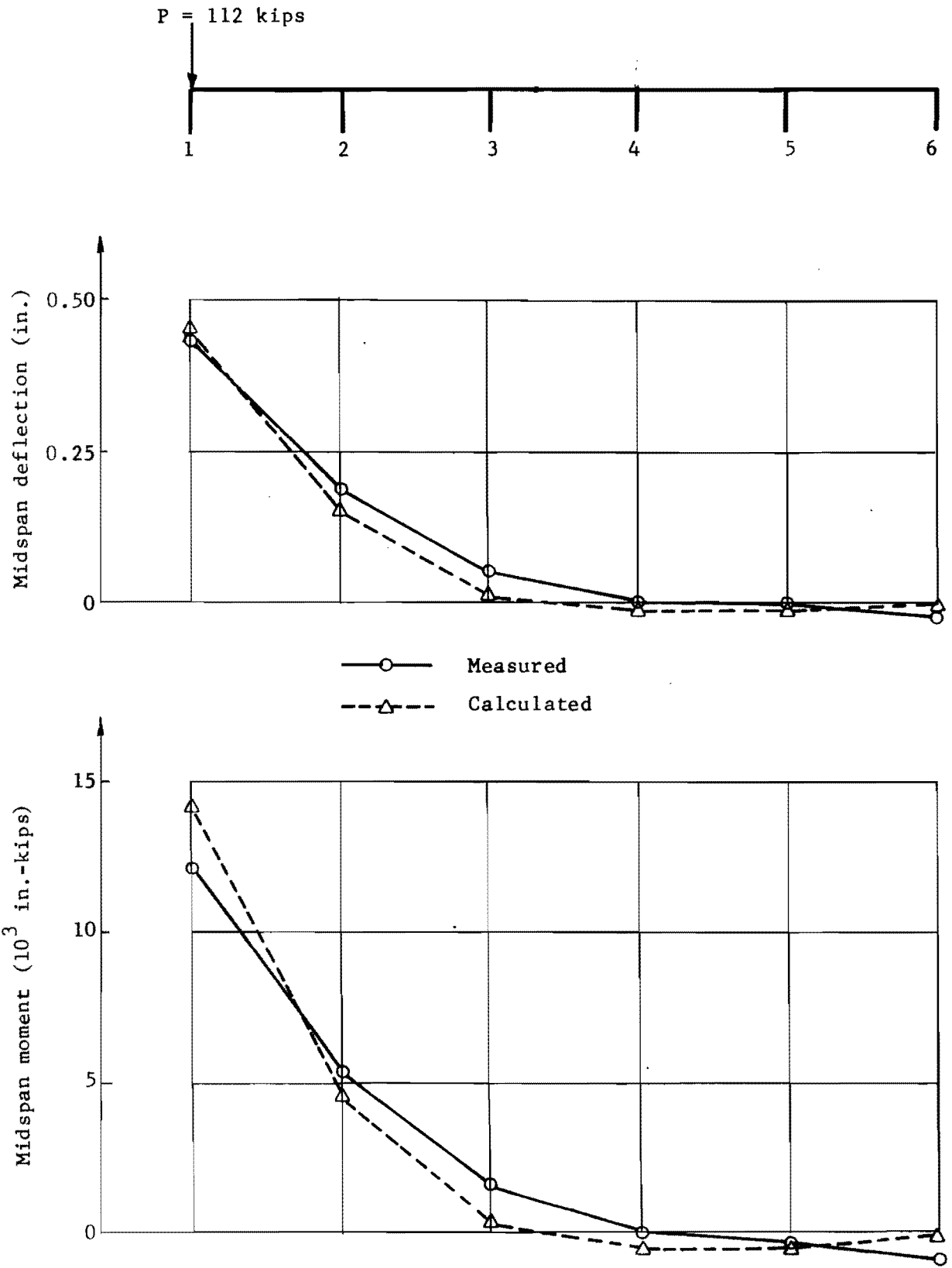
Fig. 4.15. Measured and calculated midspan deflection and moment of girders under edge loading.
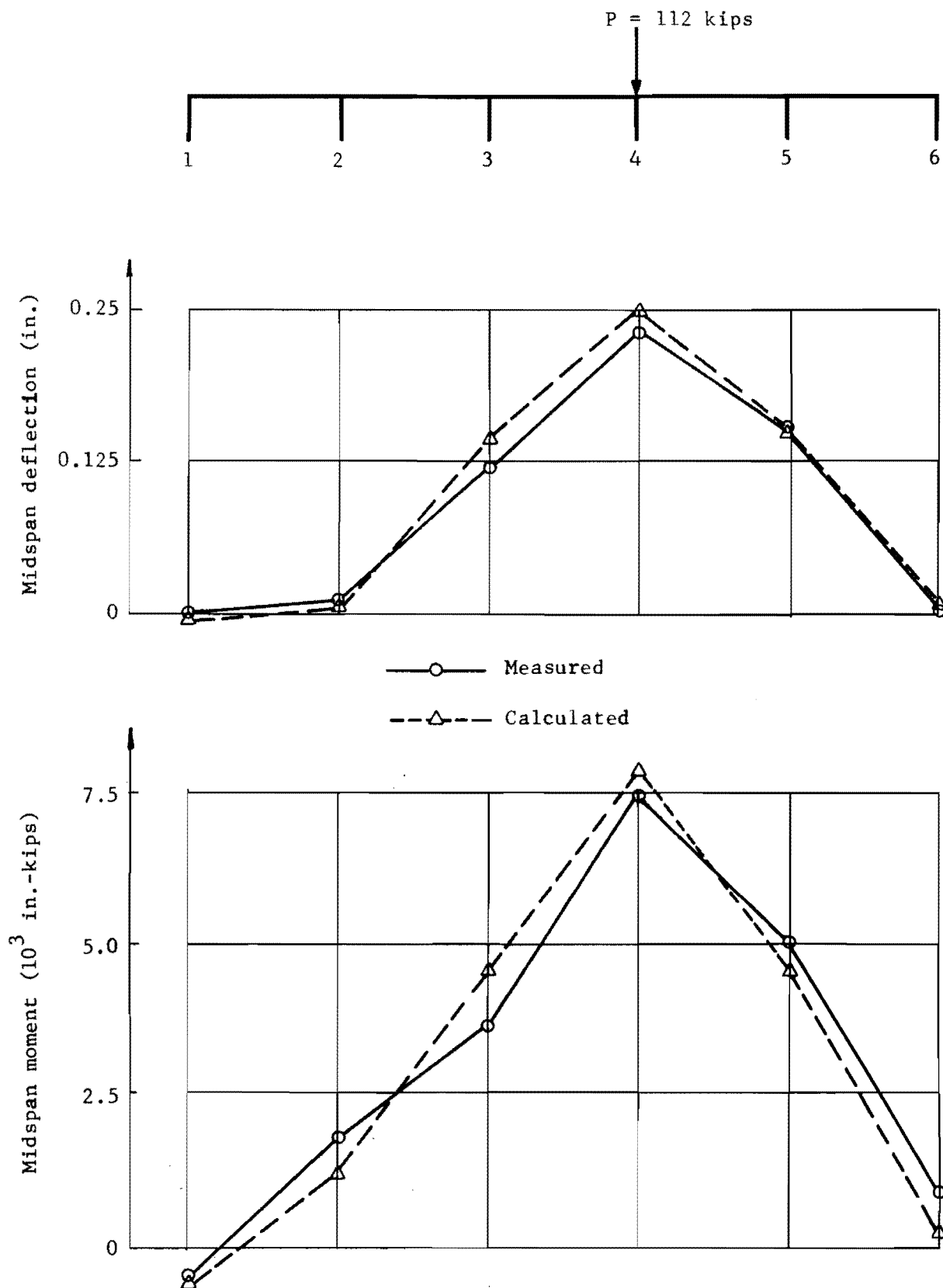
Fig. 4.16. Measured and calculated midspan deflection and moment of girders under interior loading.

4.4 Continuous Span Bridges

Two study cases were considered for this type of bridge. The first is a two-span, straight, half-scale bridge, and the second is a four-span, skewed full-scale test.

4.4.1 PCA Test, A Two-Span Continuous Bridge. The Portland Cement Association test was a two-span continuous, no skew, half-scale model bridge. The bridge was built and tested at the PCA Research and Development Laboratories. Details on construction and test results are presented by Mattock and Kaar.[39] Figure 4.17 shows details of the bridge. The two equal spans were each 33 ft. long. The cross section was composed of five prestressed precast concrete girders spaced at 3'-3" on their centers, while the deck was a cast-in-place reinforced concrete slab 3 in. thick. Continuity was provided by both the cast-in-place concrete deck and the central diaphragm. The prestressing steel used was seven-wire strand of 1/4 in. diameter with a yield stress of 254,000 psi at 1 percent offset. The continuity reinforcement was #4 deformed bars with a yield point of 48,500 psi, and the transverse bars were deformed #3 with a yield point of 44,400 psi. The average strength of the concrete in the ten girders was 5300 psi at 7 days, and the average strength of the cast-in-place slab was 3520 psi at 28 days.

Flexural and torsional stiffnesses of the composite girders were obtained by companion tests performed on a matching precast girder with a deck slab, 3 ft.-3 in. wide and 3 in. thick. The test flexural stiffness was found to be 9.219×10^{10} lb.-in.^{2} This stiffness is very close to 8.917×10^{10} lb.-in.^{2} as calculated from the gross transformed moment of inertia of the section coupled with the measured concrete modulus. The torsional stiffness of 3.410×10^9 lb.-in.^{2} was obtained from the torsional test and is in excellent agreement with the value of 3.290×10^9 lb.-in.^{2} which is computed using the procedure outlined in Sec. 4.2.4.2. The flexural and torsional stiffnesses of the slab were calculated using the elasticity expressions. SLAB36 program was used in the analysis.[6]

Two load cases were studied. One thousand pounds were placed at the midspan of an edge girder (A), and the same load was then placed at the midspan of the central girder (C). Comparison of the distribution of girder
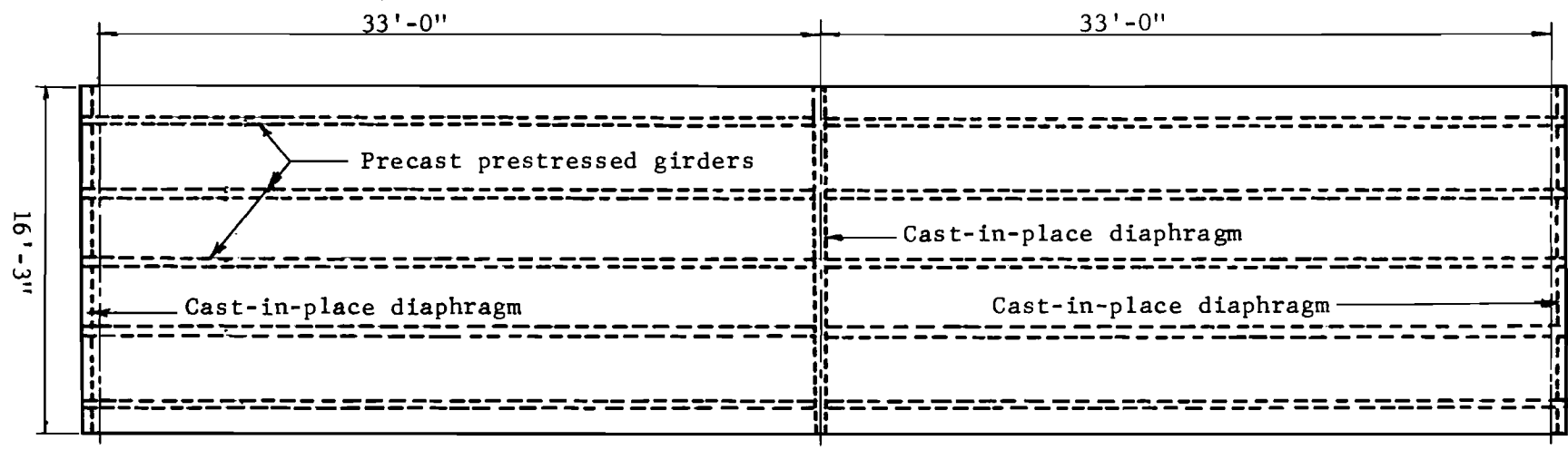
Plan
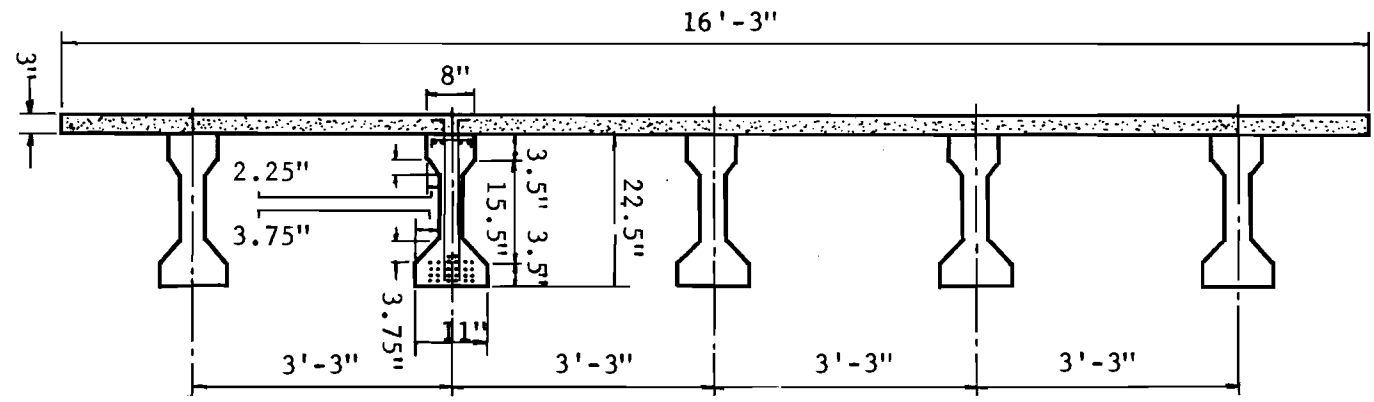
Typical Cross Section

Fig. 4.17. The PCA test--two span continuous half-scale bridge.

62

deflections and moments obtained from tests and theory for both load cases
are shown in Fig. 4.18 through Fig. 4.20. These figures show the useful-
ness and the accuracy of the analytical results for continuous bridges
when parameters involved in the solution are evaluated properly. This
comparison is especially useful in evaluating the accuracy of the analyti-
cal results for the case of a continuous bridge, since test results are
well-documented and are accompanied by comprehensive data on the behavior
of the different elements of the bridge.

4.4.2 A Bridge on Northern Illinois Toll Highway. This bridge,
shown in Fig. 4.21, is one of many grade separation structures on the
Illinois Toll Highway. It is composed of four continuous spans of 43'-
70'-70'43', with a 20° skew angle. The bridge was constructed using precast
prestressed concrete girders to span between piers and continuity was pro-
vided by both the cast-in-place reinforced concrete deck and the interior
diaphragms over the supports. Some of the details of the bridge are pre-
sented in Sec. 4.3.3 where the single span bridge presented in that section
is part of this continuous bridge. Other details and test results are
reported by Janney and Eney.[29] Evaluation of stiffnesses are the same as
in Sec. 4.3.3. The SLAB40 computer program was used to analyze this bridge
for two concentrated loads applied at 8 ft. on either side of the midspan
of Girder 4 in Span 2. Simulation of the bridge into a mesh with 4 incre-
ments between girders and 16 or 26 increments per span is shown in Fig. 4.21.

The overall four-span bridge was divided into 20 stations in the
x direction and to 89 stations in the y direction. The slab stiffnesses were
input for the whole rectangular shape which bounds the actual skew shape,
while girder stiffnesses and supporting points were input only where they
actually existed in the rectangle. This means that two imaginary triangular
wedges were added to the deck to complete the rectangle, as shown in Fig. 4.21.
This alteration considerably reduces the number of cards in the input data,
thus reducing the designer's time. This type of simulation for a skew deck
is not valid when analyzing dead load on the bridge, since the incorrect
dead load of these wedges usually creates a large amount of actually non-
existent negative bending moment along the skew edge. If dead loads are
input only on the actual skew shape of the deck, there will be no saving of
work for the designer. To evaluate the effect of addition of the deck wedges
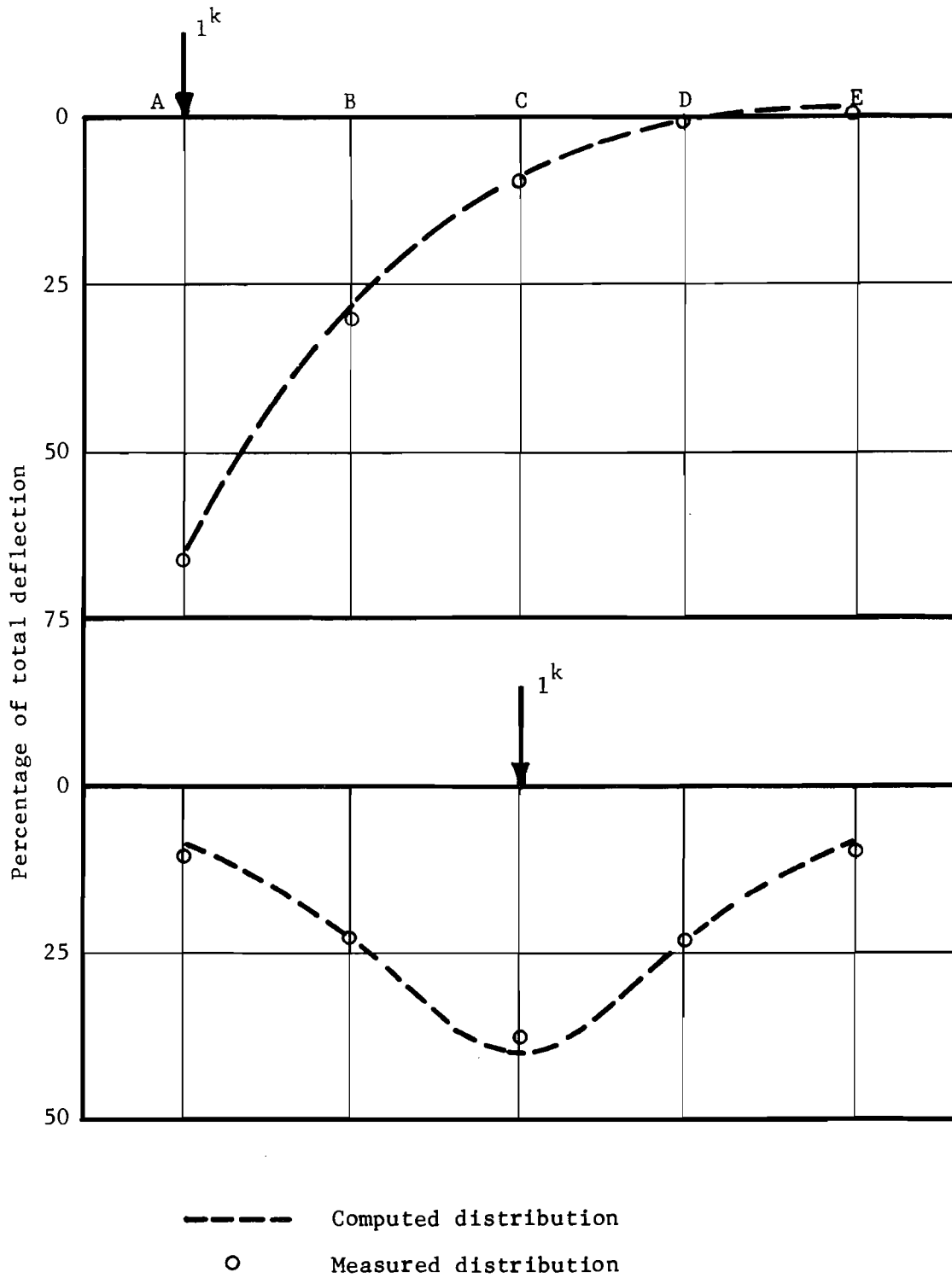
Fig. 4.18. Distribution of midspan deflections in the loaded
span--load at midspan.
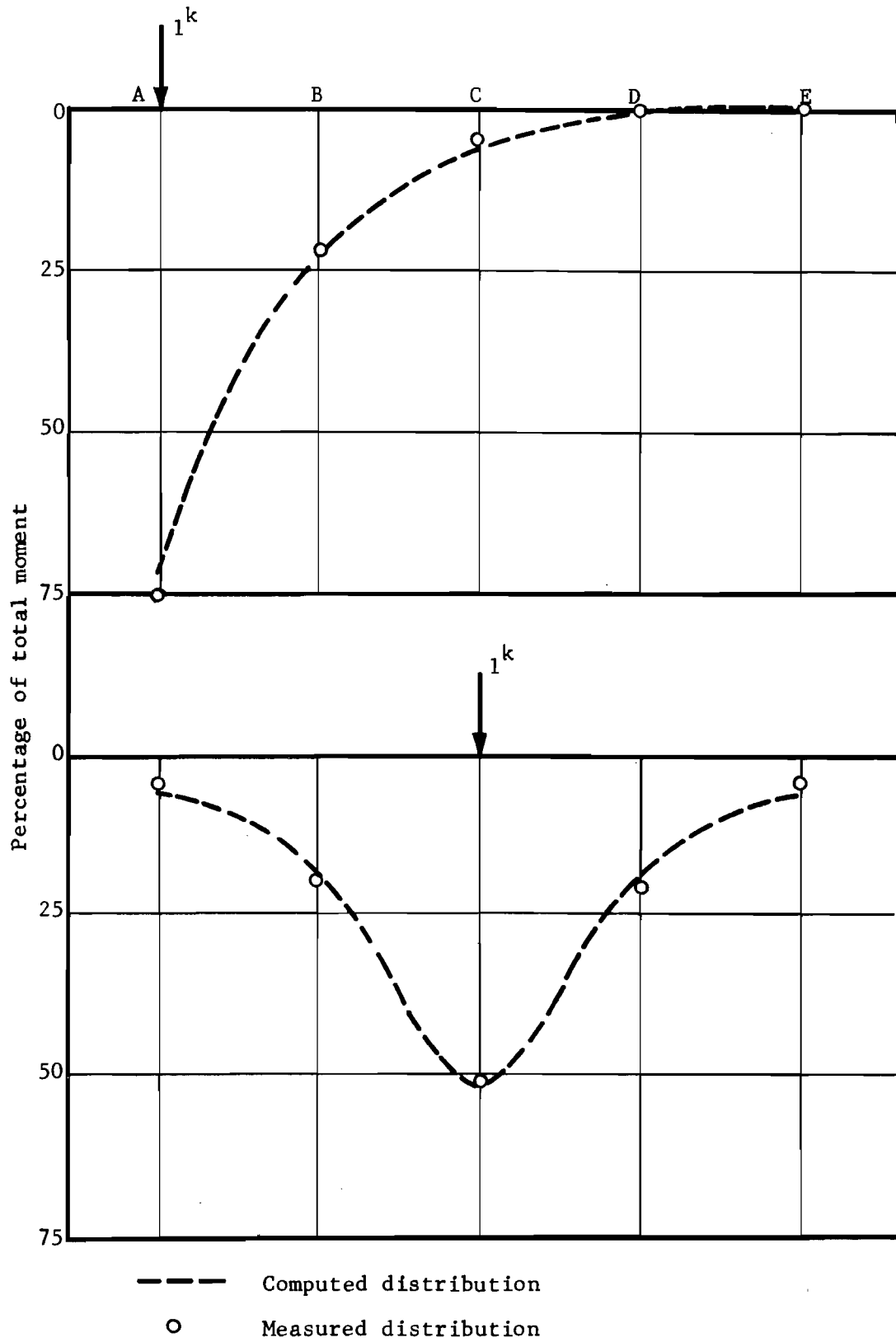
Fig. 4.19. Distribution of midspan girder moments in the loaded
span load at midspan.
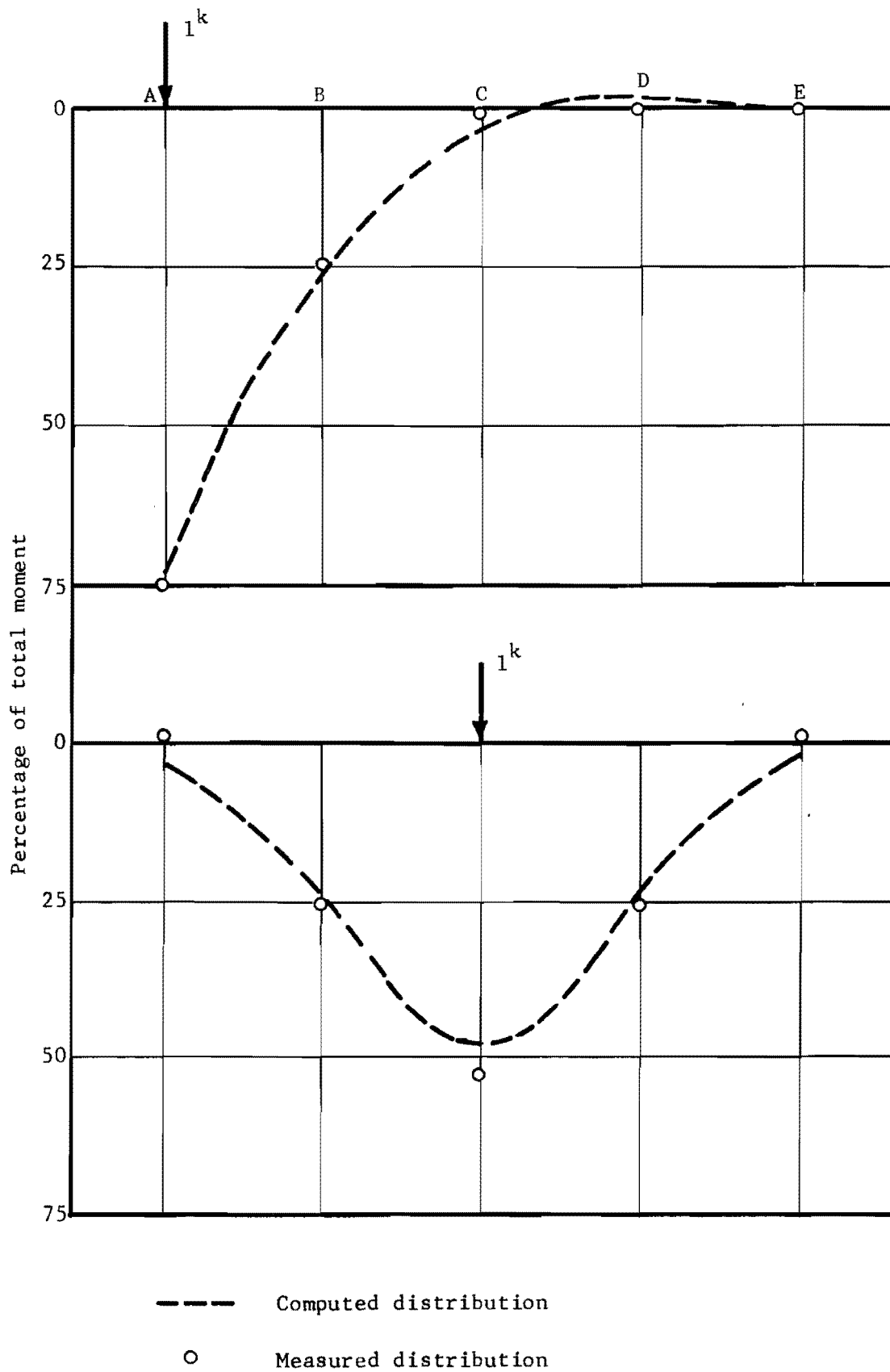
Fig. 4.20. Distribution of girder moments along center support load at midspan.
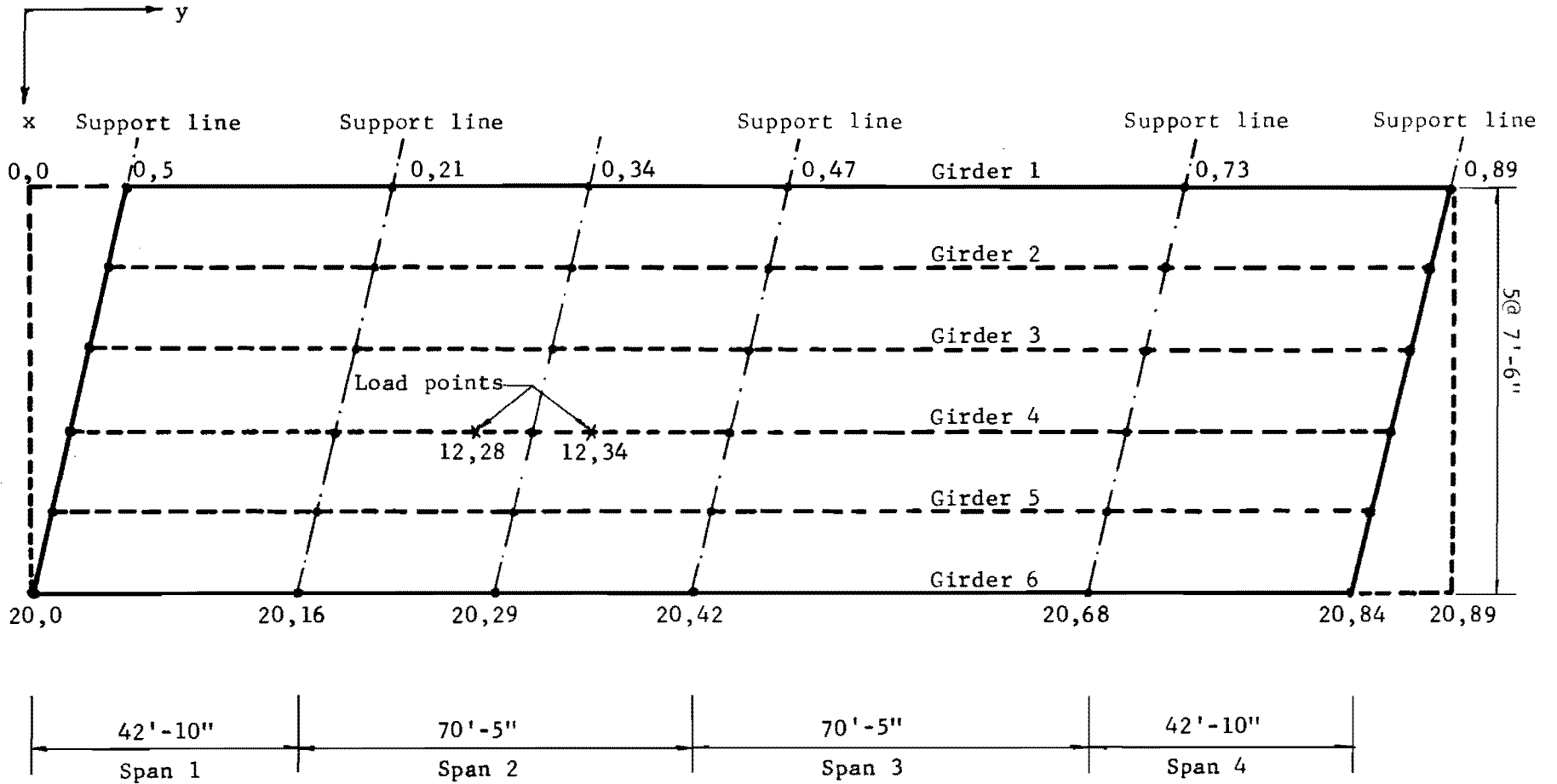
Fig. 4.21. A plan view of the Northern Illinois Toll Highway Bridge.

in the analysis of live loads, the amount of negative moment at the end of the loaded girder (station 12, 2 girder 4), was found to be only 23 lb.-in., as compared to the moment on the first interior support (station 12, 18) of 4,446 lb.-in. All other girder ends had much smaller error moments.

The comparison of test results and analytical values is shown in Fig. 4.22 for both midspan deflection and moment for the girders in Span 2 of the bridge, when a load of 112 kips was applied on Girder 4. The comparison was very satisfactory and indicated the accuracy and ease of SLAB in handling a continuous bridge.

4.5 Recommendations for Computer Simulation of Prestressed Concrete Girder and Slab Bridges

The accurate computer simulation of prestressed concrete girder and slab bridges requires two basic items:

a. Correct simulation of the bridge by a gridwork system.

b. Realistic evaluation of bridge parameters.

4.5.1 Correct Simulation of the Bridge by a Gridwork System. In selecting the gridwork proper attention must be paid to mesh size, boundary conditions, type of loading, and location of supporting points.

(a) Mesh Size. Choice of mesh size is the first step in the simulation and it is an important one, since an improper choice can lead to either a costly solution or a crude one, as indicated in Sec. 3.5.1. The size of the mesh in the transverse direction is a function of the number of girders. Four to seven increments between girders are found to be adequate. An increment less than four should not be used. The increments in the longitudinal direction are a function of skew angle and the number of spans in the bridge. Increments of 16 to 40 for each span usually yield very good results.

(b) Boundary Conditions. These include skew edges and presence of external loads or restraints along the boundaries, such as axial forces, external couples, and restraining ends. While these can be handled easily and input directly, the methods suggested in Sec. 3.4 should be used for skew edges. When analyzing live loads, the slab
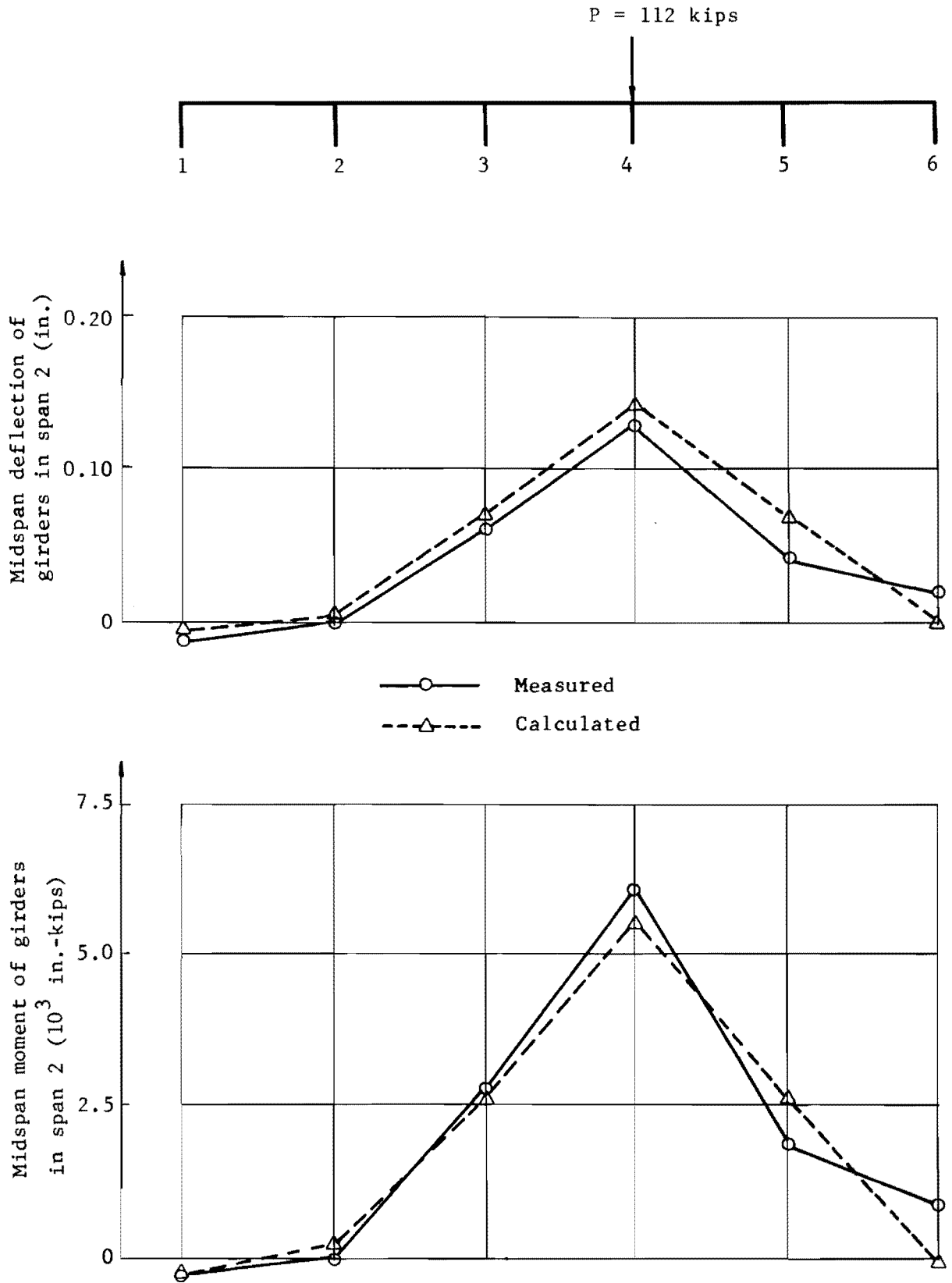
Fig. 4.22. Girder deflections and moments with load in Span 2.

can be considered as a rectangular plate with skewed supports to greatly simplify the simulation without really affecting the results.

(c) Loadings. All loadings must be input on the mesh nodes. For live load cases when wheel loads fall inside a grid, the distribution of the loads to the four nodes which bond the grid can be approximated by the values given in Fig. 3.8.

(d) Supports. In the absence of reliable data to describe the behavior of supports, a spring constant of the order of 1×10^8 lb./in. or more may be used to simulate a nonyielding support. Supporting points are input on nodes only and, for the case of nonskew edges, such points may be input along the whole edge which includes both slab and girder nodes. It is important to reemphasize that on skew edges, supports must be input only for those nodes on the girders that fall along the skew lines, as shown in Sec. 3.4.

4.5.2 Realistic Evaluation of Bridge Parameters. Parameters such as stiffnesses, involved in the analytical solution, can be of great importance and may greatly influence the results of the solution. When authenticated test values of the parameters cannot be obtained (as usual in design stages), the following procedures are suggested:

(a) Poisson's Ratio. Poisson's ratio is a function of many variables. An average value of this ratio for concrete is 0.16, and for steel is 0.3. These values may be generally used, since girder and slab type orthotropic bridges are not sensitive to Poisson's ratio.

(b) Slab Flexural Stiffness. Since the solution is generally not sensitive to this parameter, it can be calculated as

$$D_x = D_y = \frac{E_c t^3}{12(1 - \nu_c^2)}$$

While this expression is derived for an elastic homogeneous material, it works well as an estimate for the concrete slab.

(c) Slab Torsional Stiffness. Again, since the solution is generally not sensitive to it, the elasticity expression may be used. In the input in the SLAB program, the stiffness of the torsional bars represents

the torsional stiffness of the slab mesh. The value is calculated as

$$C_x = C_y = \frac{E_c t^3}{12(1 + \nu_c)}$$

(d) <u>Girder Flexural Stiffness</u>. This is a very important parameter greatly affecting the results. Hence, an estimate within 10 percent accuracy is suggested in Sec. 4.2.3 in the evaluation of girder flexural stiffness. Such accuracy can be obtained by calculating the gross transformed moment of inertia of the section and multiplying it by the modulus of elasticity of concrete. For the girders in a bridge, the composite section of the girders and the effective slab should be used. The composite girder stiffness value can be input along the line in the simulated mesh where the girders lie.

(e) <u>Girder Torsional Stiffness</u>. The solution is not very sensitive to girder torsional stiffness. Section 4.2.4 discussed the approximation of such stiffness within about 10 percent of test values. In the same section a method is suggested which can be used for both I-shaped cross sections and composite sections. When the girder torsional stiffnesses are input in the SLAB program, the girder stiffness must be added to the slab torsional stiffness. In order to do this properly the girder (or line element) torsional stiffness must be divided by two to transform it to the correct equivalent plate element torsional stiffness. This transformed plate stiffness is then added to the slab stiffness. If the girder falls at the midpoint of a slab increment width, the transformed plate stiffness is divided by the width of the element and the unit stiffness is added to the slab stiffness. However, if the grid line lies along the girder axis, the transformed plate stiffness is divided into two equal parts. Each part is then divided by the slab increment width and added to the slab torsional stiffness of the adjacent meshes.

C H A P T E R   V

REINFORCED CONCRETE GIRDER BRIDGES

5.1 Introduction

Reinforced concrete girder bridges are extensively used for spans between 25 and 100 ft.[10] The statically determinate simple span bridges are easier to design, but do not always represent the most economical solution of the problem. Continuity and monolithic construction have great advantages, resulting in lighter, stronger, and more rigid structures.

Design and analysis of reinforced concrete structures can be complicated if their nonlinear behavior is considered. Flexural rigidity is a variable function which depends mainly on load levels, state of the member, and composition of the material properties of the section. For a reinforced concrete girder bridge, the main stiffness is always provided by the girders and, therefore, any error in estimating girder stiffnesses has a great influence on final results. Such influences could reach an error level of doubling or even tripling the true value. This was shown in Sec. 3.3 for the deflection of a simply supported beam.

To improve the accuracy of such computations, further development in the method of estimating the girder stiffness is necessary. Such development, based on the characteristics and properties of the section, was achieved during this study by the generation of an accurate moment-curvature relationship for a reinforced concrete section on a digital computer. A program called MPHI was written to define the stiffness for the whole range of loading and then the MPHI results were incorporated into the analysis of bridges using SLAB programs. Two physical tests were considered for such comparison. The first test is a single span bridge and the second is a continuous girder bridge. Both were loaded with H20-S16 truck loads.

5.2 The Formation of Flexural Cracks
in Reinforced Concrete Members

An important feature that greatly influences the behavior of a
reinforced concrete member is the formation of cracks. Cracks are formed
when the tensile force at any point exceeds the tensile strength of the
concrete, or when the strain exceeds its ductility. The uniform distribu-
tion of stresses in both concrete and steel in the tension zone along the
reinforcing bars becomes different after cracks occur and a wave shape
distribution of stresses results after cracks stabilize, as shown in
Fig. 5.1. When cracks form the local concrete stress suddenly drops to
zero, while steel stresses have a sudden increase. Then a redistribution
of stresses and strains in the vicinity of the cracks takes place, due to
the progressive slipping of the steel, and, therefore, the wave-shaped
distribution usually results.[10] The dashed lines in Fig. 5.1b, c, d, and e
represent the instantaneous distribution immediately after the cracks form.

Crack opening is due to differential elongation between steel and
surrounding concrete. It is a function of steel area, bar diameter, stress
level, concrete cover and bond between concrete and steel. After a
stabilization of cracks is reached, it is found that a strong relationship
between the crack spacing and the ratio between bar diameter and steel per-
centage exists. Borges and Lima[11] studied such relationships in an experi-
mental program, where 26 reinforced concrete beams were tested and analyzed
to determine what governs the spacing and width of cracks. The beams were
cast from the same quality concrete but different kinds of reinforcement
were used. The mean distance between cracks was given by Eq. 5.1, where K_1
is obtained experimentally.

$$S = 2 + K_1 \frac{D}{p} \qquad (5.1)$$

where

S = mean crack spacing in inches

D = bar diameter in inches

$p = \dfrac{\text{area of tensile steel}}{\text{concrete area}}$

K_1 = 0.10 for plain mild steel
0.05 for high tensile and twisted plain steel
0.025 for deformed high tensile steel.

The figures given above for K_1 are obtained for $\dfrac{D}{p} < 240$.
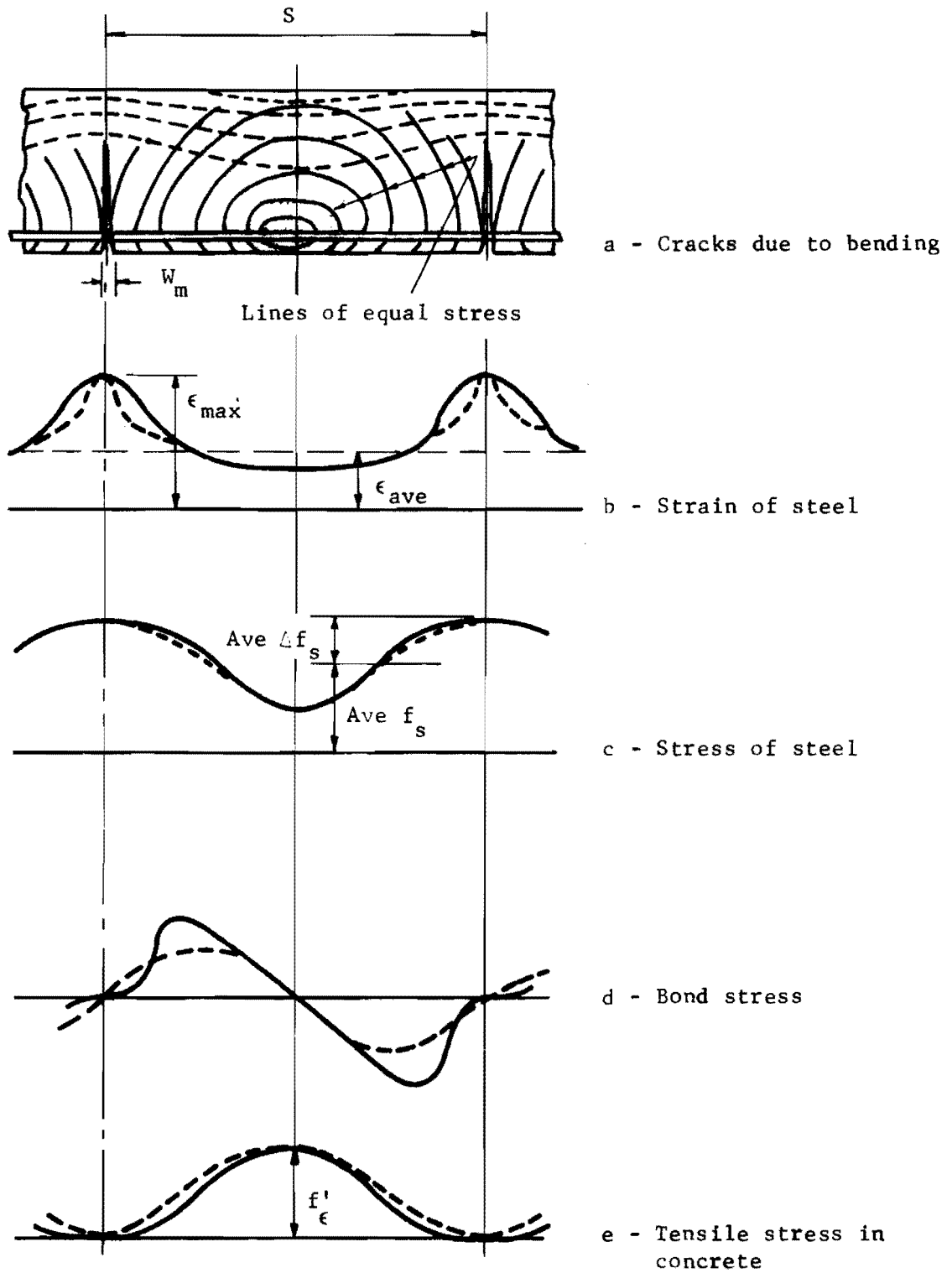
Fig.5.1. Formation of cracks due to bending moment.

When concrete strains in the region of tensile stress between cracks and shrinkage effects are neglected as minor compared to steel strains, then the mean width is

$$W_m = \epsilon_m \cdot S \qquad (5.2)$$

where

W_m = mean crack width.

ϵ_m = mean steel strain.

Both beam test and tensile tests of bars embedded in concrete showed the strong effect of steel percentage (p) on the relation between the calculated steel stresses (f_s) and the mean strain (ϵ_m). In this relation the strain corresponding to a given stress decreases as steel percentage decreases. Such variation becomes more pronounced for steel percentage less than 1 percent. This relation can be expressed as

$$\epsilon_m = \frac{f_s}{E_s} \left(1 - \frac{K'}{pf_s}\right) \qquad (5.3)$$

where K' is an empirical coefficient to determine the correction in steel strain. A value of K' = 57 was adopted during the study. This value of K' leads to strains slightly smaller than those observed for steel stresses lower than 43,000 psi, and, therefore, the following expressions may be used to estimate the mean crack width.

$$W_m = \frac{f_s}{E_s} \left(2 + K_1 \frac{D}{P}\right)\left(1 - \frac{57}{pf_s}\right) \qquad (5.4a)$$

for f_s < 43,000 psi.
Otherwise,

$$W_m = \frac{f_s}{E} \left(2 + K_1 \frac{D}{P}\right) \qquad (5.4b)$$

where all units are in pounds and inches.

Another study by Rao[46] to evaluate the effects of cracks on the steel strain distribution in the tension zone is represented schematically in Fig. 5.2. The expression used to arrive at the mean steel strain is that of Eq. 5.5. This equation is similar in nature to that of Eq. 5.3.
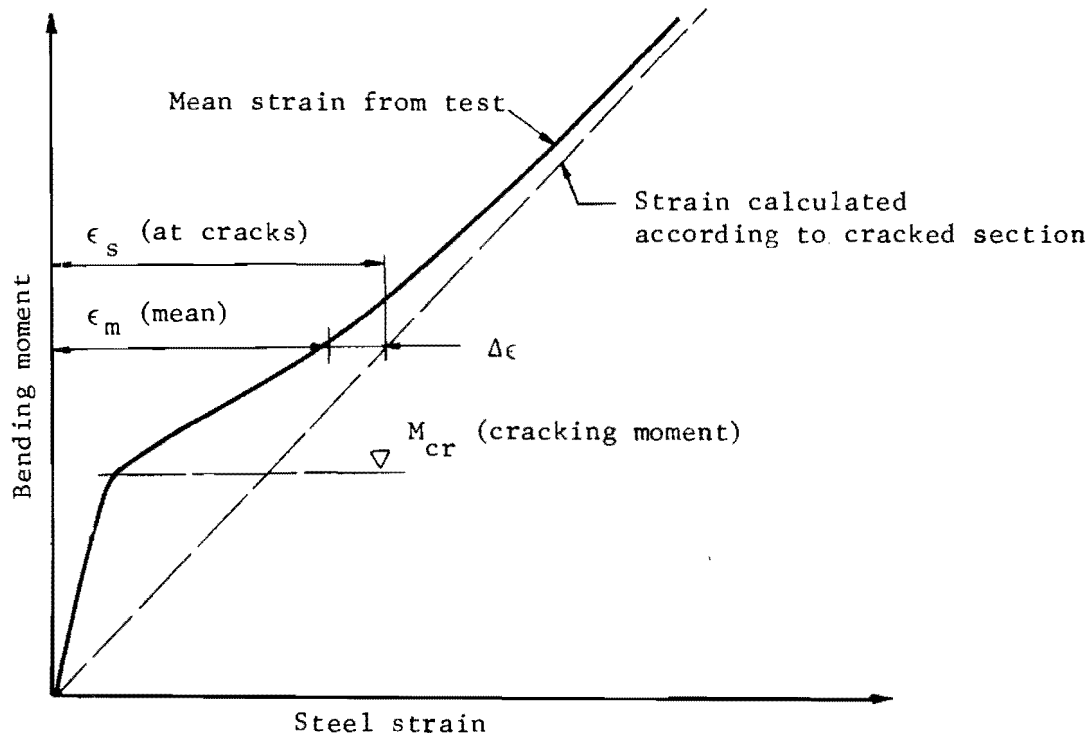
Fig. 5.2. Steel strain as a function of moment.

$$\epsilon_m = \epsilon_s - K \frac{f_t'}{E_s p} \qquad (5.5)$$

where

$$K = \frac{(\epsilon_s - \epsilon_m)}{f_t'} E_s p, \text{ and}$$

$f_t' =$ ultimate tensile strength of concrete.

The study, which relied on experimental work to evaluate the factor K, showed that its value could be estimated as

$$K = 0.18 \frac{\epsilon_{cr}}{\epsilon_s} \qquad (5.6)$$

where

$\epsilon_{cr} =$ steel strain at cracking moment based on cracked section

$\epsilon_s =$ steel strain at the level of moment under consideration based on cracked section.

5.3 Theoretical Analysis of Moment-Curvature
     Relationships for a Reinforced Concrete
     Member

     5.3.1 Steel Stress-Strain Relationship. In order to determine the
true behavior of reinforcement in a concrete section, the effect of cracks
on steel stresses and strains must be considered. This dictates that mean
steel stresses be considered. Thus, in order to take into account crack
effects, a family of curves must be used instead of a single curve to repre-
sent the relationship of the reinforcement stress-strain characteristics.
This approach has been shown to be very effective in dealing with nonlinear
analysis of reinforced concrete structures.[12,13] Equation 5.3 can be written
as

$$\epsilon_m = \epsilon_s - \frac{57}{pE_s} \qquad\qquad (5.7)$$

     The second term on the right-hand side of the equation represents
the amount of strain correction needed in order to arrive at the mean
strain. To establish the stress-strain relationship describing the behavior
of the reinforcing bar in a concrete member, the effect of tension cracks
is considered by defining the strain in terms of mean steel strain throughout
a cracked region. Obviously the mean steel strain is not only a function
of the physical properties of the steel observed from tension tests performed
on bar specimens but is also a function of the cross section of the rein-
forced member. Therefore, different stress-strain curves result from the
same kind of reinforcement when used in different members. The expression
of mean steel strain given in Eq. 5.7 can be used to establish the curves
shown in Fig. 5.3 for different steel percentages and different types of
steel. Similarly, other curves could be calculated for different steel
percentages. This method can be easily handled by computers which generate
the required curves needed for the problem under consideration.

     5.3.2 Concrete Stress-Strain Relationship. Compressive stress-
strain relationships obtained from tests on different quality concretes are
shown in Fig. 3.1. Many theoretical curves have been proposed by different
authors. Fowler[18] compared theoretical shapes proposed by Kriz and Lee,
Rüsch, Todeschini, et al., and Hognestad. The curves look similar in shape
with some relatively minor differences in the descending parts of the
stress-strain relationship.
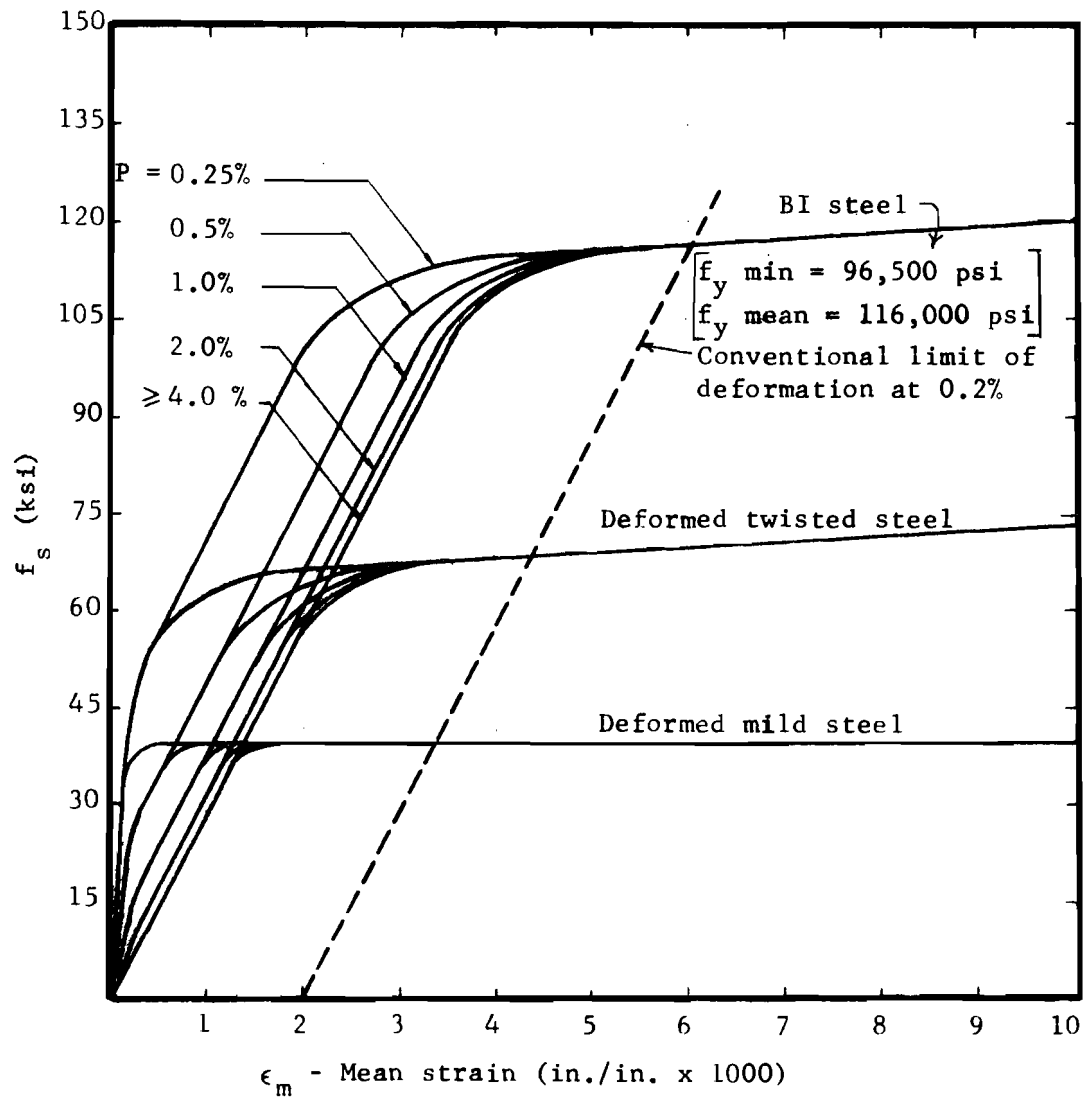
Fig. 5.3   Stress-strain characteristics of steel taking into account the correction in steel strain. (Ref. 13)

The Hognestad stress-strain curve[25] has been widely accepted as reasonably describing the relationship of the stress-strain curve for concrete in flexural compression and so was used in the MPHI program.

The tensile strength of concrete varies with the method of test. The stress-strain curve of concrete in tension obtained from different kinds of loading for the same quality of concrete is shown in Fig. 5.4. These specimens[50] have dimensions of 6 in. by 3.5 in. by 24 in. Tests were carried out at a concrete age of three days, and the average concrete compression strength was an abnormally low 1650 psi. The tensile strength of concrete can be expressed as a function of its compressive strength. Ferguson[17] has stated that tensile strength of concrete is about 10 to 15 percent of the compressive strength. ACI Committee 435[3] suggests

$$f_t' = 7.5 \sqrt{f_c'} \text{ to } 12 \sqrt{f_c'} \qquad (5.8)$$

where the smaller factor applies to higher strength concrete and larger factor to lower strength concrete. The smaller factor is recommended by ACI Committee 435 for general use.[3]
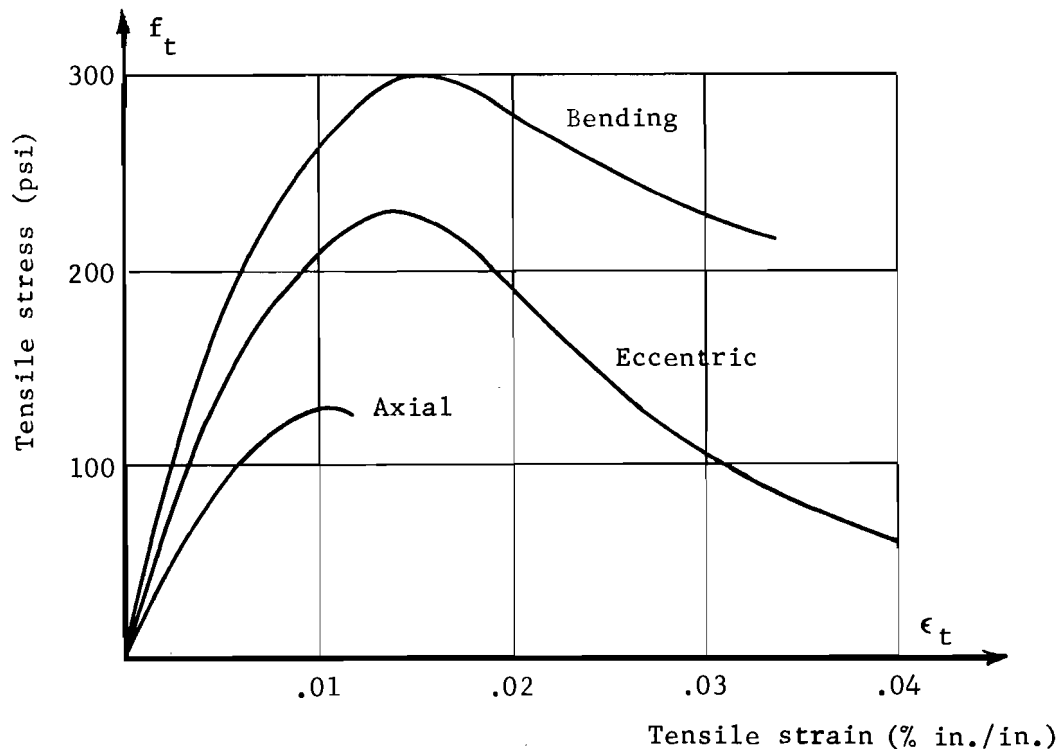
Fig. 5.4. Tensile stress-strain relationships.

5.3.3 <u>Generation of Theoretical Moment-Curvature Relationships</u>.
The moment-curvature relationship is the most useful curve for defining the
flexural stiffness of the member for the whole range of loadings. At any
level of loading the stiffness is merely equal to the slope of the curve.

$$\text{Stiffness} = EI = \frac{M}{\phi} \tag{5.9}$$

For a reinforced concrete member, both E and I vary with load. While the
moment of inertia has a distinct decrease as cracks form, the change in
modulus of elasticity corresponds mainly to the load level. Flexural cracks
usually occur at relatively low loads compared to the ultimate strength.
Such low levels of loading have only a small effect on the modulus. Thus,
the reduction in stiffness is mainly due to cracking for load levels up
to one-half of the ultimate strength.

The moment of inertia of the section may drop suddenly to about
one-third or even less of its gross value as soon as cracks occur. For any
section the uncracked and cracked values can easily be calculated. ACI Com-
mittee 435[3,57] suggested an empirical expression based on a statistical study
of test results to estimate the effective moment of inertia of the section
after cracks form as

$$I_{eff} = I_{cr} + \left(\frac{M_{cr}}{M_{max}}\right)^3 (I_g - I_{cr}) \tag{5.10}$$

in which $M_{cr} = \dfrac{f_t' I_g}{y_t}$

and $f_t' = 7.5 \sqrt{f_c'}$

where M_{cr} = cracking moment

M_{max} = maximum moment.

Equation 5.10 is valid when $M_{max} > M_{cr}$. Otherwise, the gross moment of
inertia is to be used.

Moment-curvature relationships for a cross section may be generated
on a computer by integrating stress-strain curves for both concrete and
steel. Different theoretical stress-strain relationships for the materials
used by various programs yield different shapes of the moment-curvature
relationship. To illustrate the difference possible, three programs

MOMPHI,[15] GMC,[47] and MPHI will be compared, both in the input and output, and in relation to test results.

While all programs used the same Hognestad stress-strain curve for concrete in compression, the stress blocks for concrete in tension were different from each other. Figure 5.5 shows the tensile stress block used in each program.

The relationship used in program MPHI is assumed to initially be parabolic, with the initial slope equal to E_c. The parabola passes through a specified point of maximum stress at an assumed strain of 0.0001. This assumption seems to agree quite well with the general shape of the stress-strain relationship of the concrete under tension, as shown in Fig. 5.4. The assumed descending branch of the tensile block was chosen to approximate the tensile stress distribution in the concrete block bounded by two flexural cracks. The latter branch was found from a best fit with the test results. The concrete tensile block used by program MOMPHI makes allowance for inelasticity in the tension zone. The tensile block used in program GMC is generally similar to that in MPHI.

The steel stress-strain relationship used with program MPHI is a family of curves similar to those shown in Fig. 5.3, which makes allowance for mean steel strain while for other programs a single curve is used which makes no allowance for tension between cracks. The moment-curvature relationship obtained from a beam test reported by Macchi[36] is shown in Fig. 5.6, where the theoretical curves from all three programs are also shown. The curve of ACI Committee 435 is calculated by coupling the effective moment of inertia given by Eq. 5.10 with the 1963 ACI Building Code[2] concrete modulus. The two straight lines represent the stiffnesses based on the elastic gross section and the elastic transformed cracked section. The comparison shows clearly the effectiveness of program MPHI in predicting the moment curvature relation for the beam. It shows the best agreement with the test data.

5.4 MPHI Computer Program

The computer program MPHI, written in FORTRAN language, generates the moment-curvature relationship for a reinforced concrete member where

$$f_t' = \frac{3000}{(3 + 12{,}000/f_c')}$$

$$E_c = 33w^{1.5}\sqrt{f_c'}$$

a. Program MOMPHI

$$f_t' = 5\sqrt{f_c'}$$

$$f_t = 2f_t' \cdot \frac{\epsilon_t}{\epsilon_{ot}} \cdot \frac{1}{1 + (\epsilon_t/\epsilon_{ot})^3}$$

$$f_t = 2f_t' \cdot \frac{\epsilon_t}{\epsilon_{ot}} \cdot \frac{1}{1 + (\epsilon_t/\epsilon_{ot})^2}$$

$$\epsilon_{ot} = .0001$$

b. Program GMC

$$f_t' = 5\sqrt{f_c'}$$

$$f_t = \epsilon_t E_c - (f_t' - \epsilon_{ot} \cdot E_c)\left(\frac{\epsilon_t}{\epsilon_{ot}}\right)^2$$
(parabola)

$$f_t = f_t'\left(\frac{\epsilon_{ot}}{\epsilon_t}\right)$$

$$E_c = 33w^{1.5}\sqrt{f_c'}$$

$$\epsilon_{ot} = .0001$$
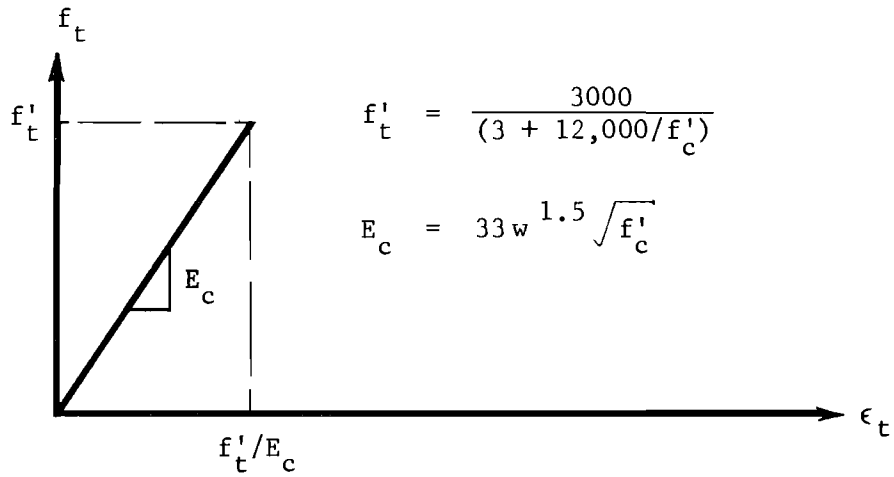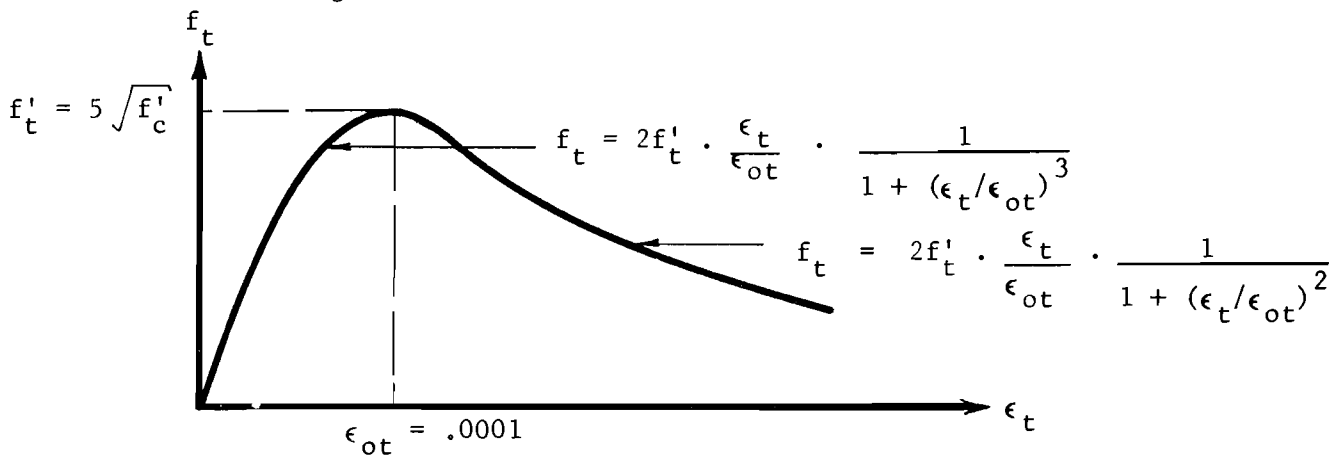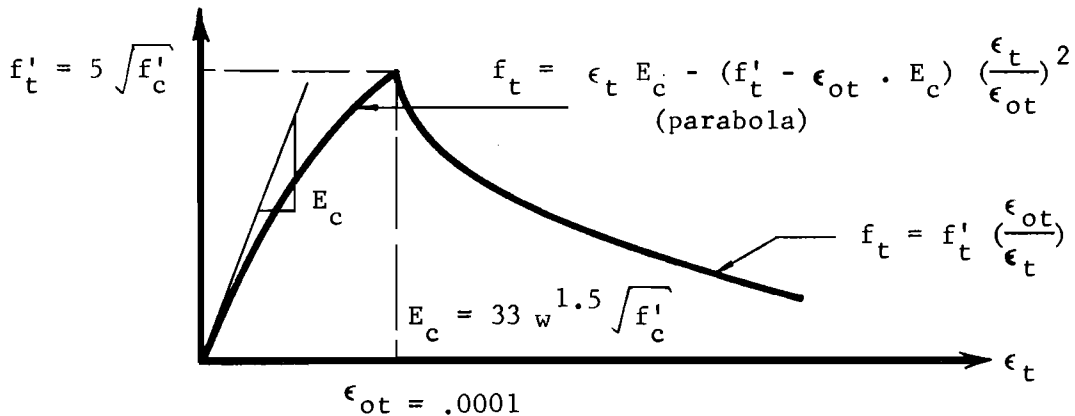
c. Program MPHI

Fig. 5.5. Assumed tensile block used by different programs.
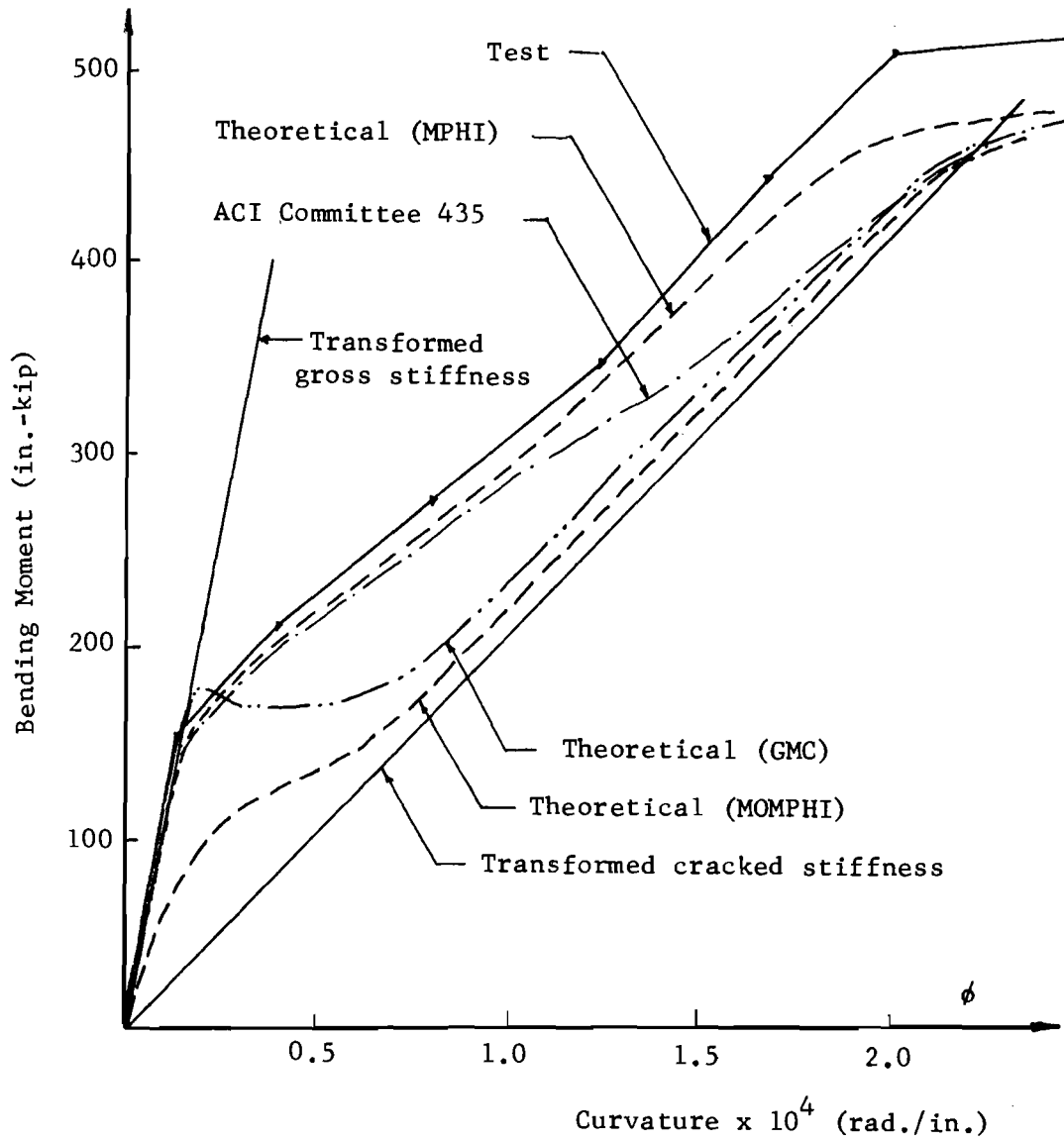
Fig. 5.6. Experimental and theoretical comparison of moment-curvature of reinforced concrete beam (TP1).

cracks are anticipated in the section. The computation is based on numerical methods with the member cross section divided into finite rectangular segments. Each of these segments has the area of the strip it replaces in the cross section. The stress distribution across the section is considered as piecewise linear. The calculation of stress in both concrete and steel is based on the theoretical stress-strain curves of the materials. The Hognestad curve is used for the concrete in compression and the stress block shown in Fig. 5.5c is used for concrete in tension. The stress-strain curve for steel in tension is calculated by the program on the basis of the mean steel strain. This is influenced by the crack formation when the applied moment exceeds the cracking moment. The amount of correction is discussed in Sec. 5.3.1, where it is shown that a family of curves should be used instead of the single curve usually obtained from bar specimen tests. The family of curves for steel in tension need not be stored or input, since the program establishes the required curve according to the strength of the steel and the reinforcement percentage. For steel in compression the stress-strain curve is considered a bilinear curve with a flat top. This is the usual case when an annealed bar specimen is tested.

The program begins by calculating the elastic center of the section. This is the point at which an applied axial load will produce no bending moment so that the section remains under uniform strain. Each point on the moment-curvature relationship is found by determining the proper strain profile which produces static equilibrium of forces on the section. The program utilizes the bisection method in calculating the appropriate strain profile. This method is often used in numerical analysis to find the roots of a given function. The number of iterations in this program is limited to twenty for each point. This suggests that if all iterations are executed for an interval strain of $\Delta\epsilon$, the final results will be as close to the true value as

$$\text{Strain closure} = \frac{\Delta\epsilon}{2^{20}} \simeq \Delta\epsilon \cdot 10^{-6}$$

Such a strain closure will yield extremely low levels of stress increments in both steel and concrete so that the program can also cut off iteration at an optional load closure, as specified by the user. If not input, the

program will consider the smallest value of either 1/1000 of the applied
axial load, if any, or a load which gives a uniform stress on the gross
section of 1 psi as the closure values. The flow chart is shown in Fig. 5.7,
while the listing of the program is given in Appendix A.

Comparisons of moment-curvature relationships obtained from tests
with those from the MPHI program were made for a wide range of both rein-
forced concrete beams and columns as listed in Table 5.1. The table includes
a wide range of tensile steel percentage in the beams, ranging between 0.32
and 1.52 percent and includes concrete quality ranging from 3070 to 5250 psi.
The steel yield point is between 40,000 and 70,000 psi. This seems to be a
good range for practical reinforced concrete beams. The four columns listed
in the table are similar in dimensions, steel percentage, and yield points
of steel, with some variation in concrete quality. The main difference is
in the level of axial load applied on each column. This ranged between
14.65 kips and 60.2 kips, which is from 14.6 to 69.4 percent of the axial
load crushing strength of the columns. Comparisons between test results
and MPHI predictions for each member are shown in Figs. 5.8 through 5.20.
On these diagrams additional information is shown about test setup and other
member properties. The predictions of the program seem to be excellent for
all the members listed in Table 5.1. No reduction factor for ultimate con-
crete strength was used $(f''_c = f'_c)$, since all members were tested under
laboratory control. A comparison with a reduction factor of 0.85 was shown
for the columns shown in Figs. 5.17 through 5.20.

5.5 Evaluation of Stiffnesses

5.5.1 Flexural and Torsional Slab Stiffnesses. The reinforced con-
crete slab stiffnesses can be evaluated in the same manner as presented in
Sec. 4.2.1 and 4.2.2.

5.5.2. Girder Flexural Stiffness. The flexural stiffness of girders
is the most influential parameter affecting the solution results, and, hence,
it should be carefully evaluated. The text of Secs. 5.2 and 5.3 described
the behavior of a reinforced concrete member with flexural loading, and it
was found in Sec. 5.4 that a theoretical moment-curvature relationship for
the member can be generated with high accuracy. Comparisons were made with
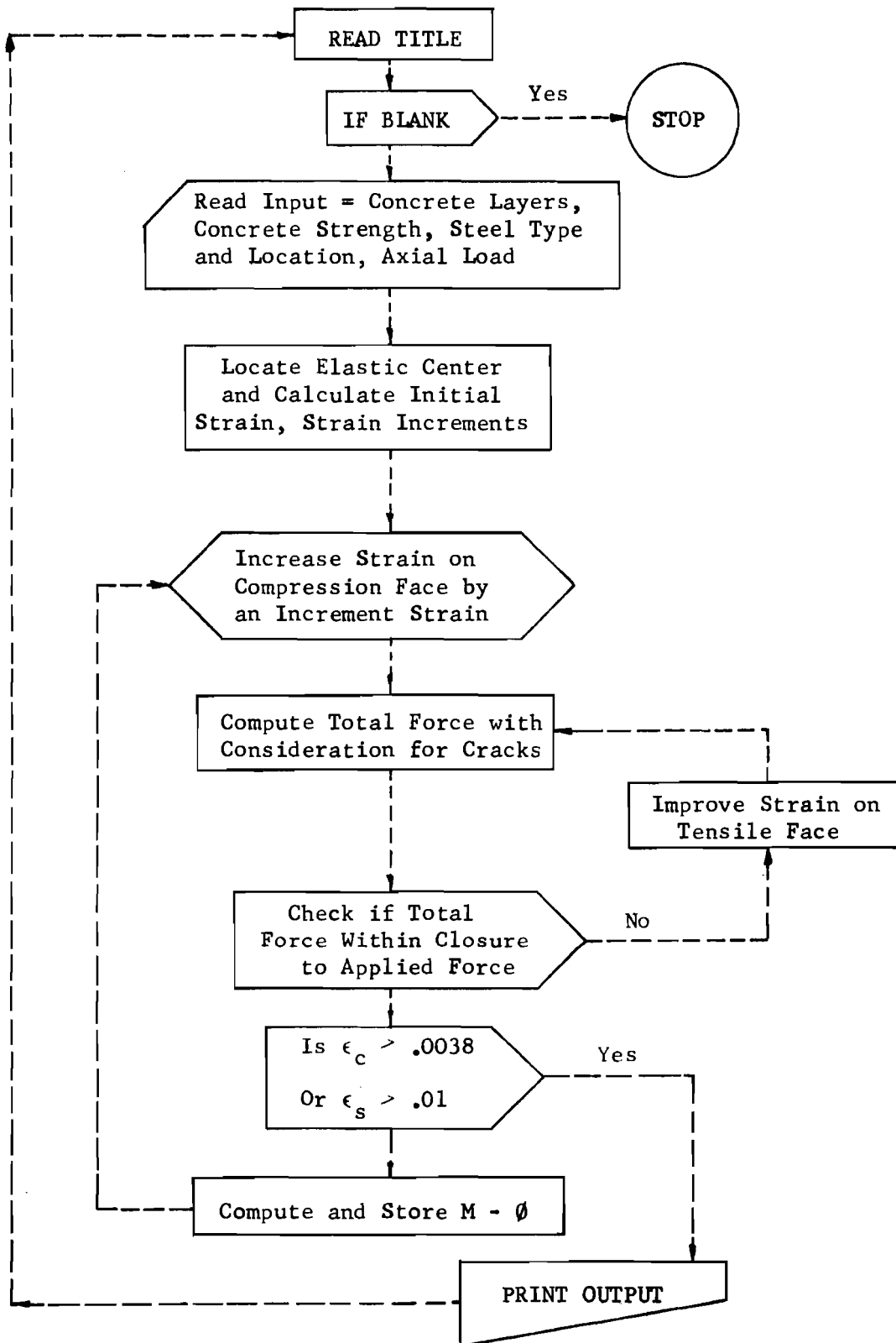
Fig. 5.7. MPHI Flow Chart.

TABLE 5.1.

PRINCIPAL PROPERTIES OF TESTED REINFORCED CONCRETE MEMBERS

(all units are inches and pounds, as required)

Member	Symbol	Section		P%	f'_c (psi)	f_y (psi)	See Fig.	Ref.
		b(in.)	h(in.)					
Beam	P_o & Q_o	5.9	11.0	0.81	4080	60500	5.8	37
Beam	TP1	6.0	15.8	0.56	5250	70000	5.6	36
Beam	A1	7.9	15.8	1.50	3070	40000	5.9	19
Beam	B1	7.9	15.4	0.92	3220	40000	5.10	19
Beam	A2a	8.0	15.6	1.47	3300	57000	5.11	19
Beam	A2b	7.8	15.6	1.52	4730	57000	5.16	19
Beam	B2a	7.9	15.4	0.94	3680	57000	5.13	19
Beam	C2b	7.9	15.2	0.32	5000	57000	5.14	19
Beam	C2c	7.8	15.3	0.32	3760	57000	5.15	19
Beam	C3	7.9	15.2	0.32	3200	57000	5.16	19
Column	C3	6.1	4.0	1.06	4150	51800	5.17	14
Column	C5	6.1	4.0	1.06	3005	52100	5.18	14
Column	C6	6.1	4.0	1.06	3030	50175	5.19	14
Column	C7	6.1	4.0	1.06	3670	51800	5.20	14
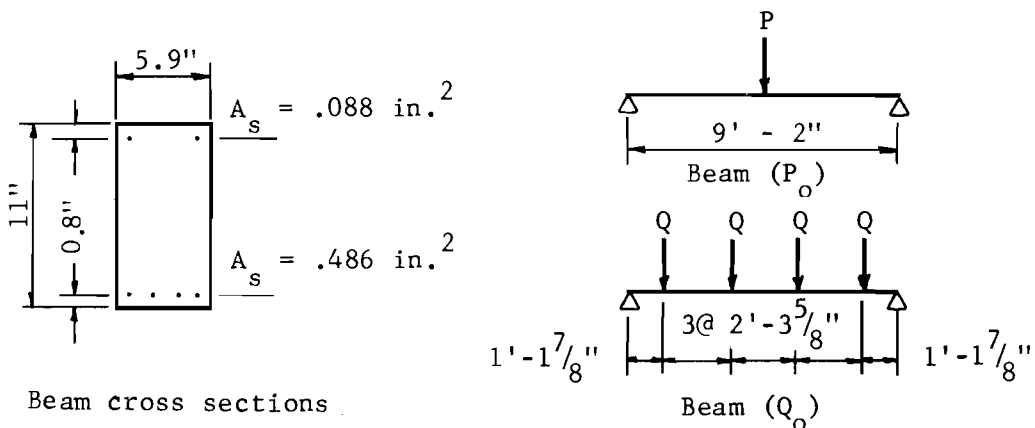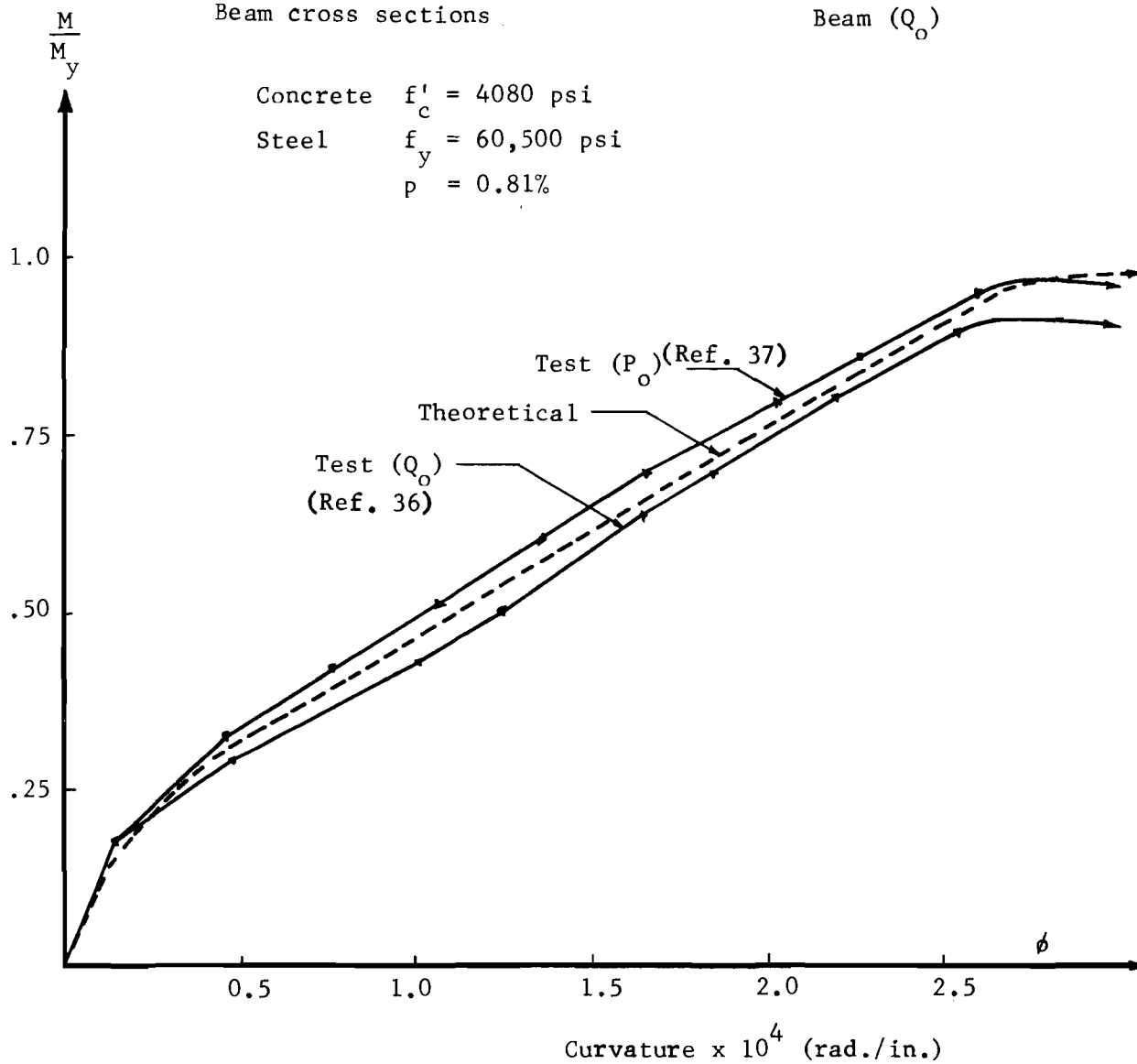
Fig. 5.8.   Moment-curvature relationship of Beams P_o and Q_o .
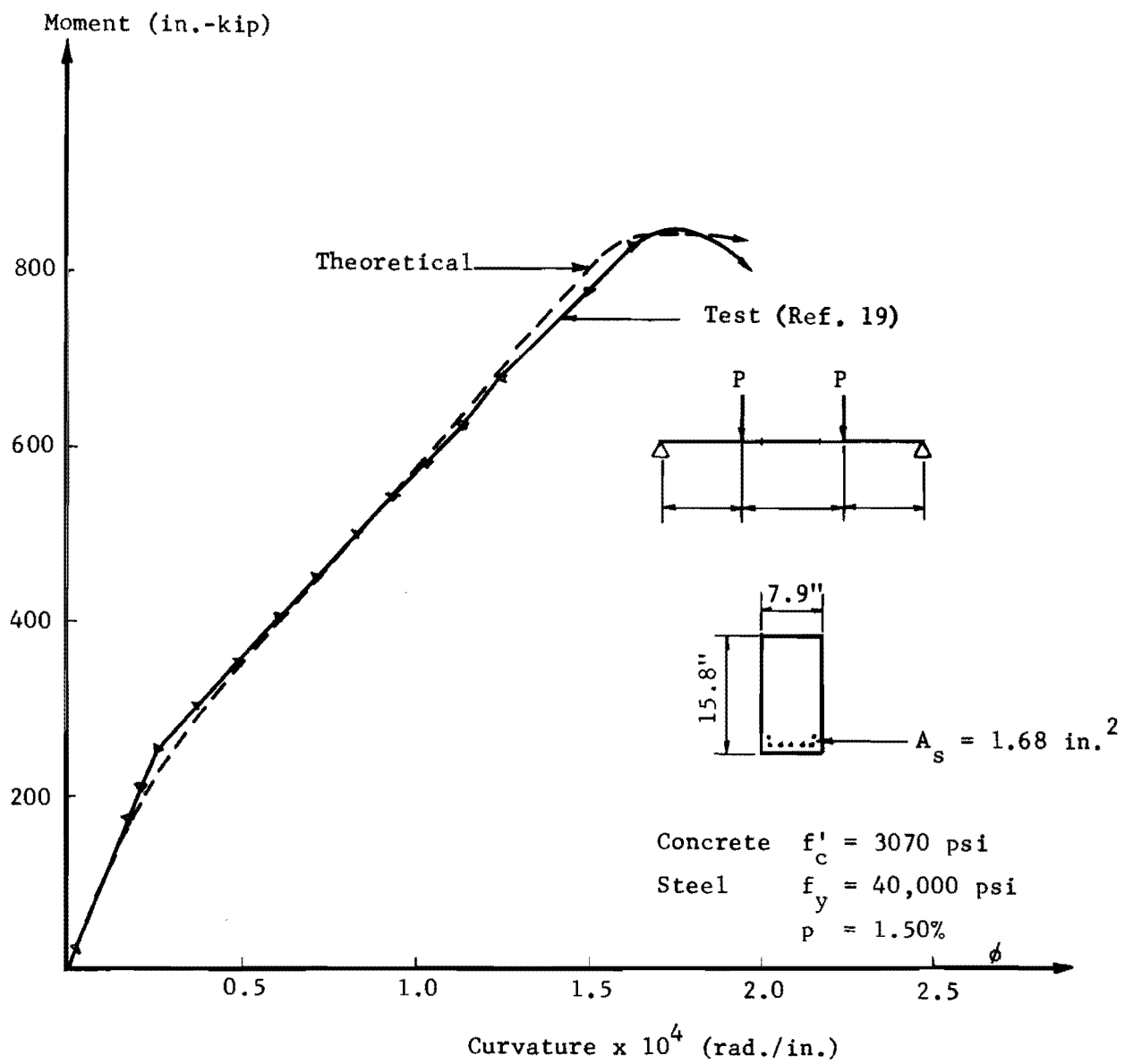
Fig. 5.9.   Moment-curvature relationship of Beam A1.
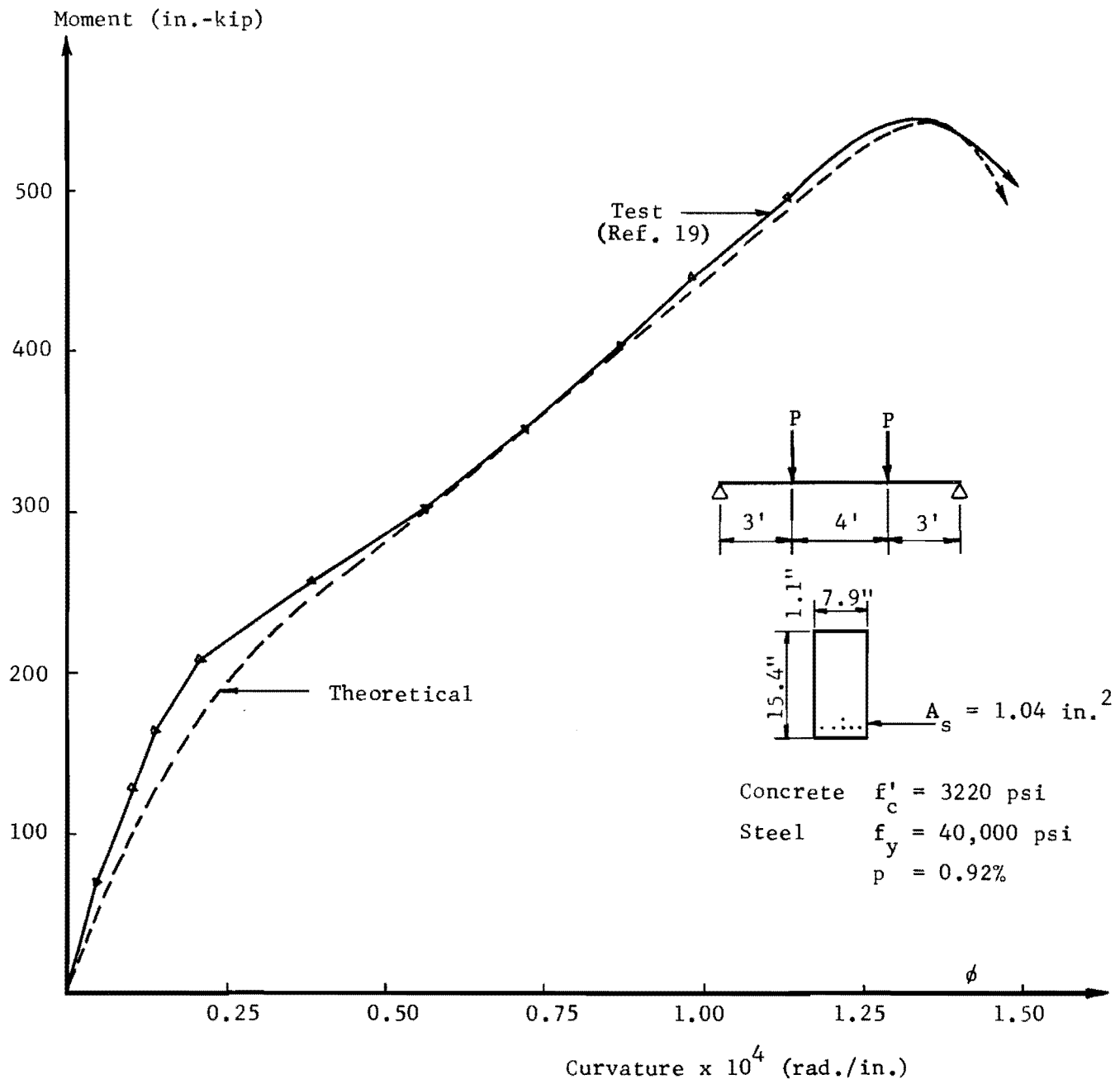
Fig. 5.10. Moment-curvature relationship of Beam B1.
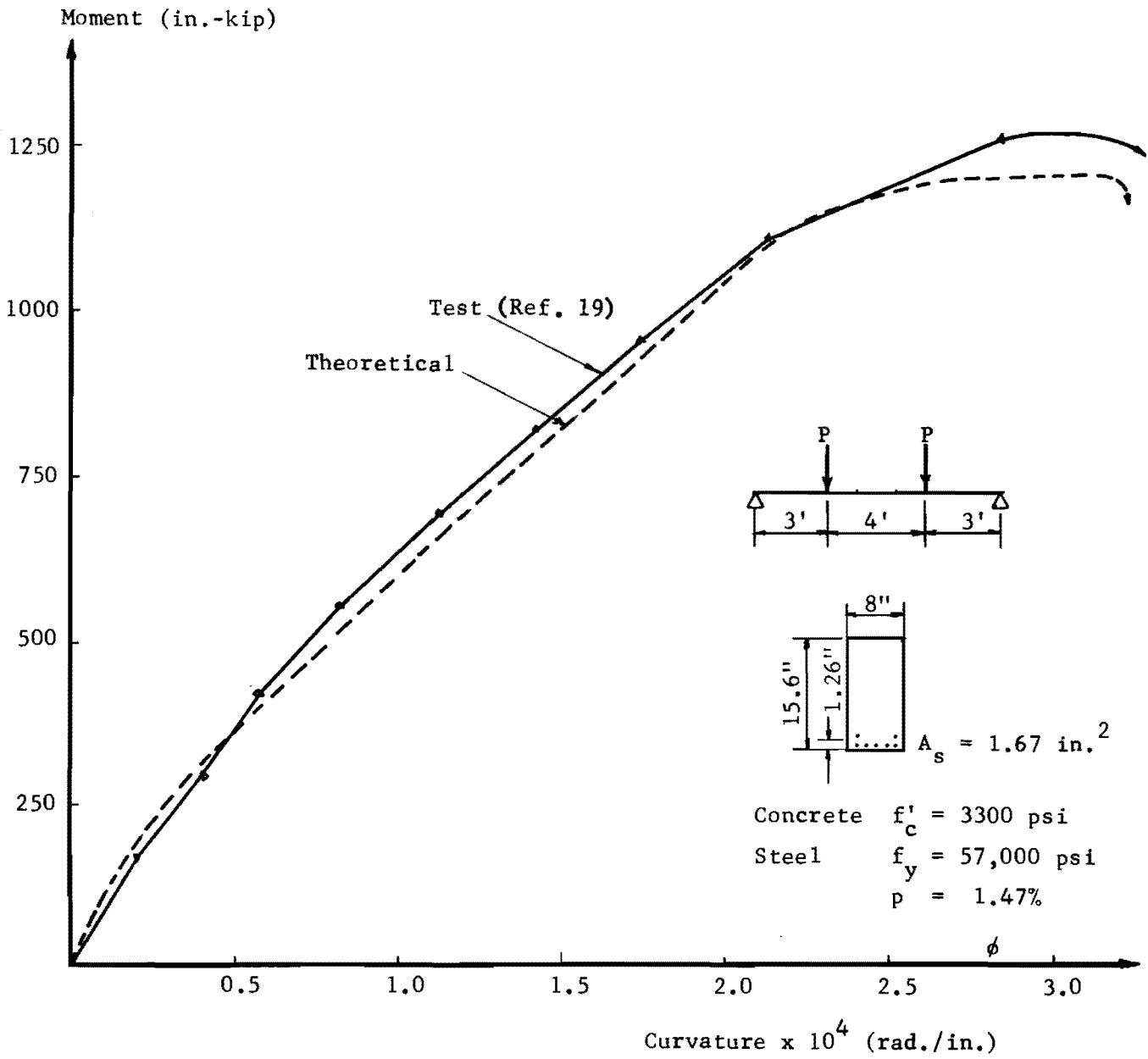
Fig. 5.11. Moment-curvature relationship for Beam A2a.
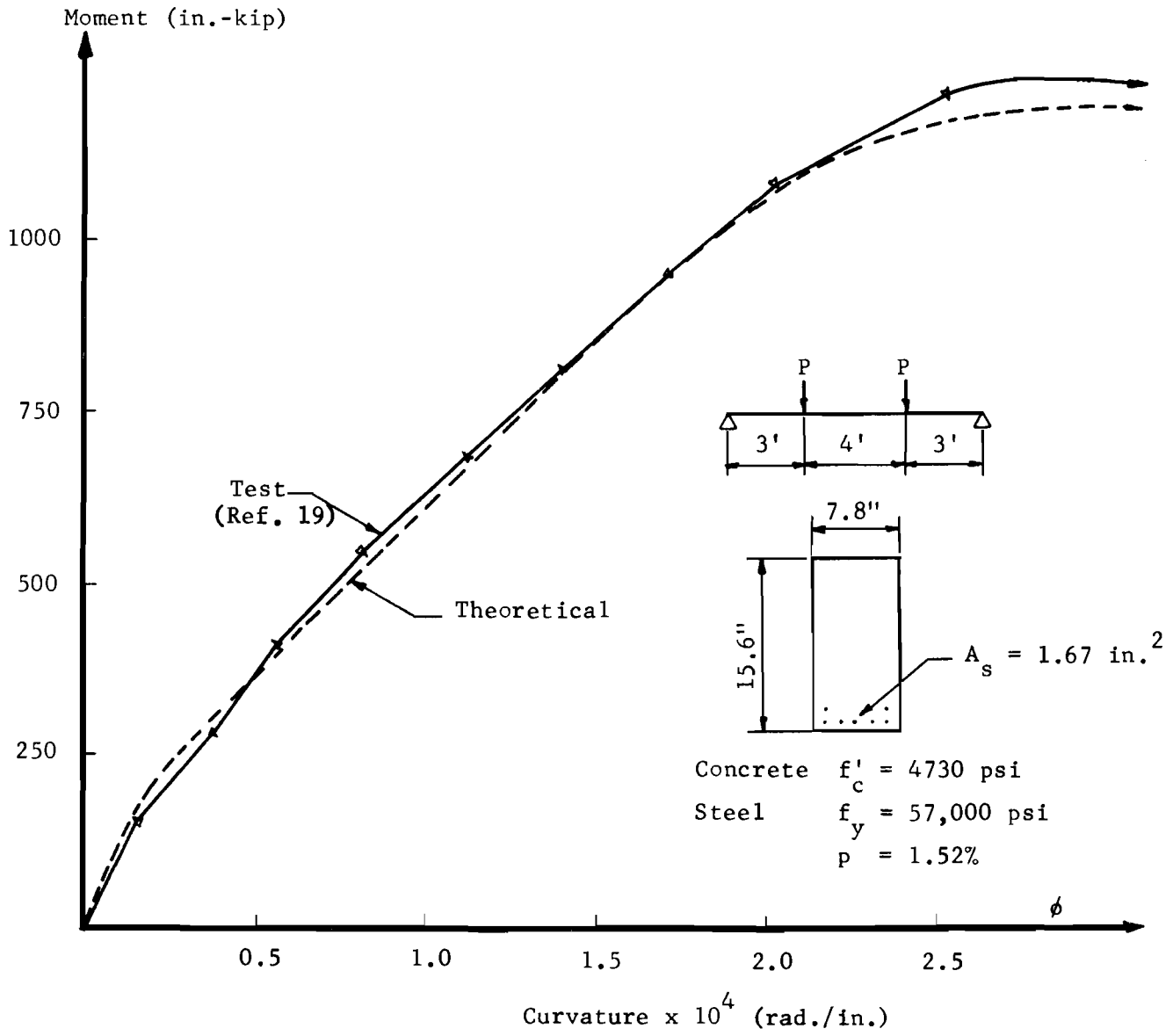
Fig. 5.12. Moment-curvature relationship of Beam A2b.
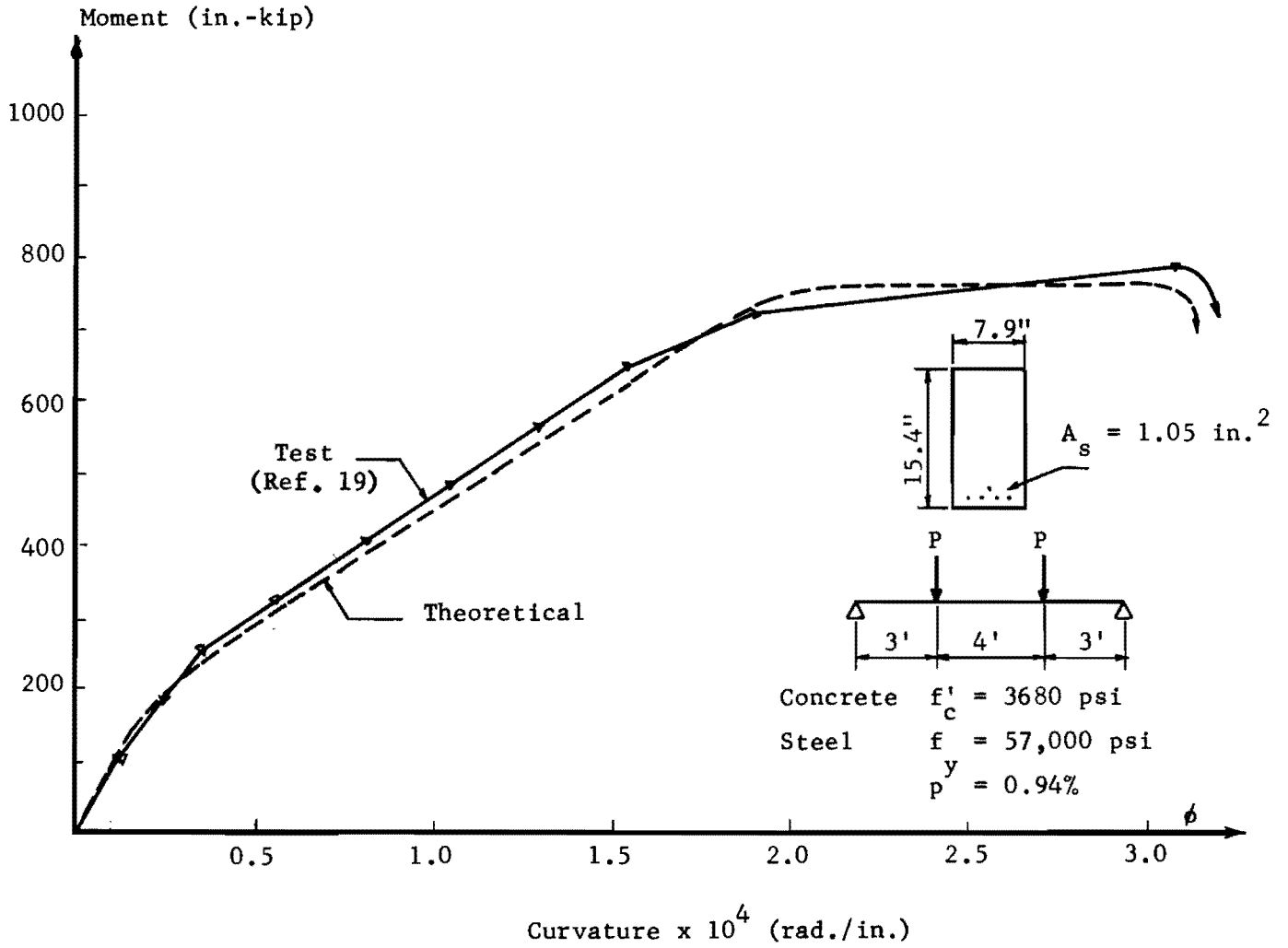
Fig. 5.13. Moment-curvature relationship of Beam B2a.

Moment (in.-kip)
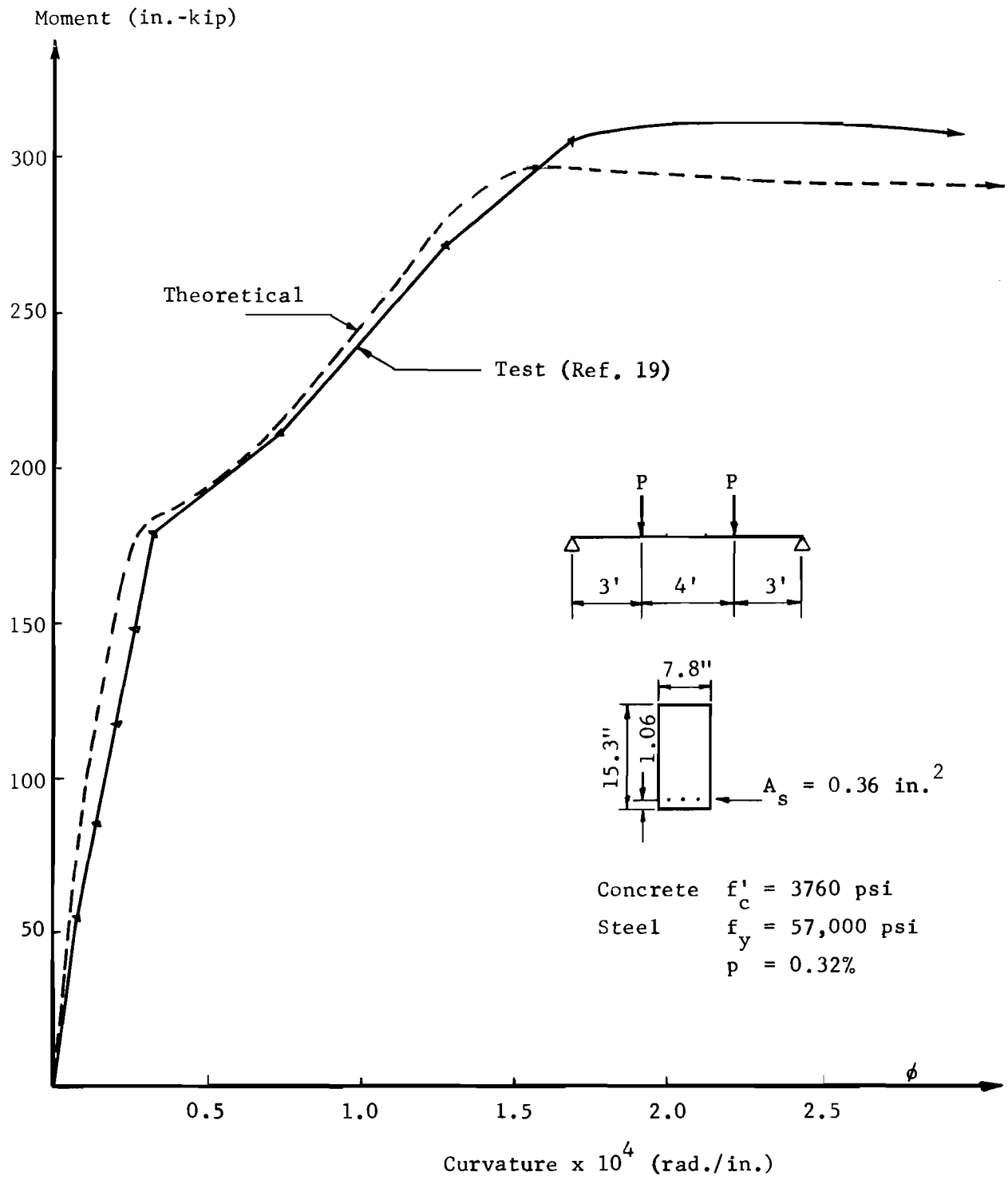
Fig. 5.14. Moment-curvature relationship of Beam C2b.

94
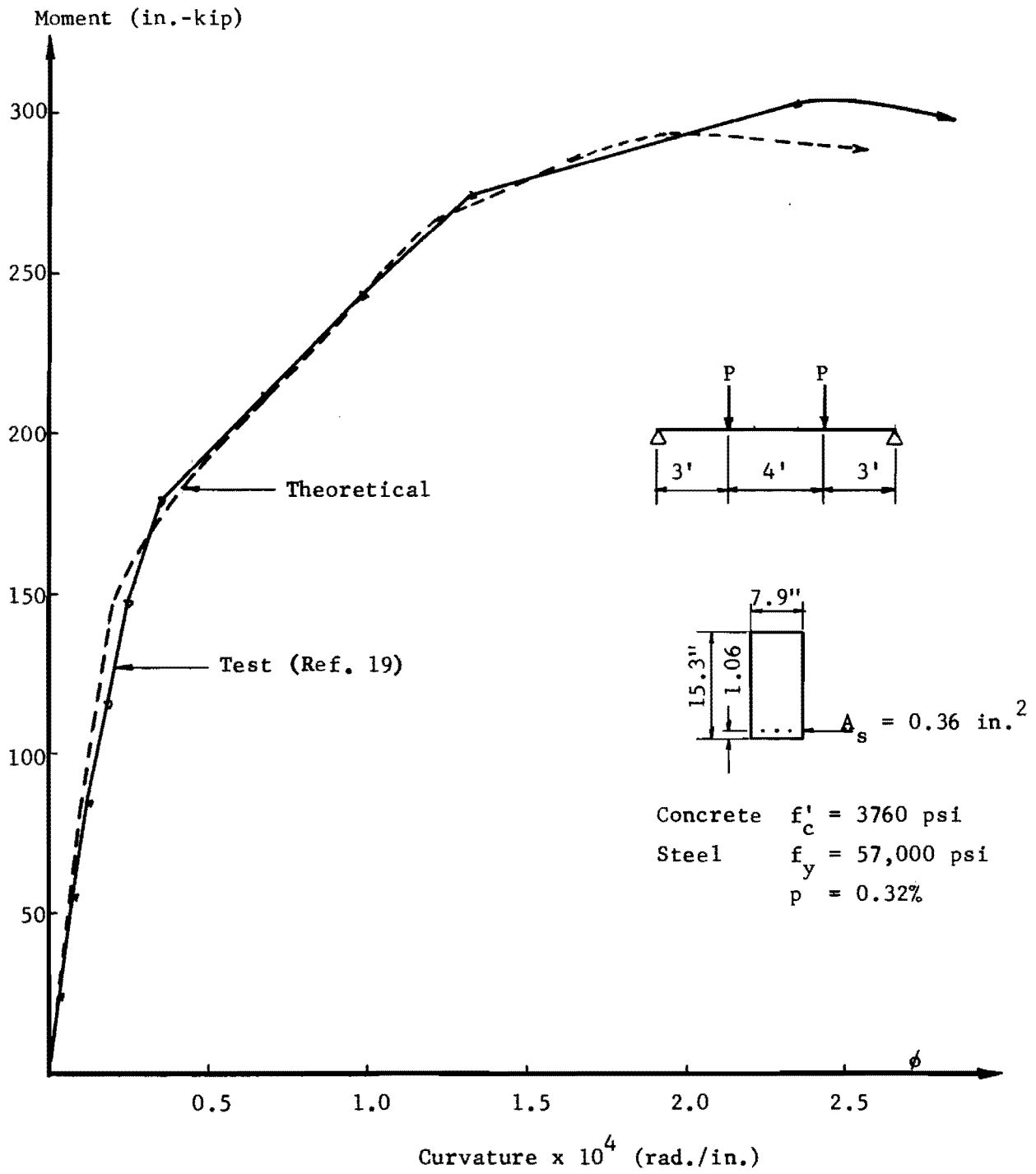
Fig. 5.15. Moment-curvature relationship of Beam C2c.
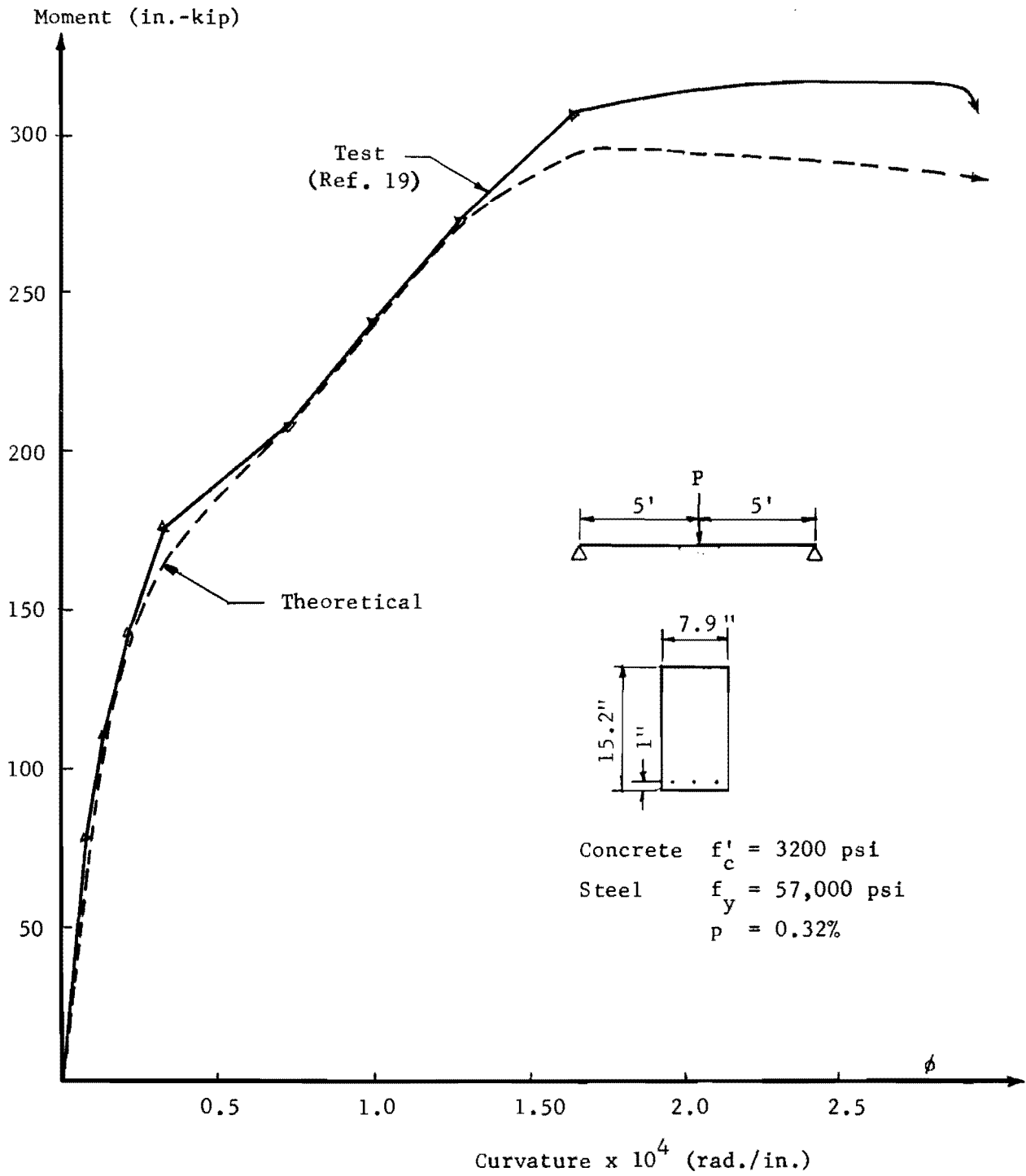
Fig. 5.16. Moment-curvature relationship of Beam C3.
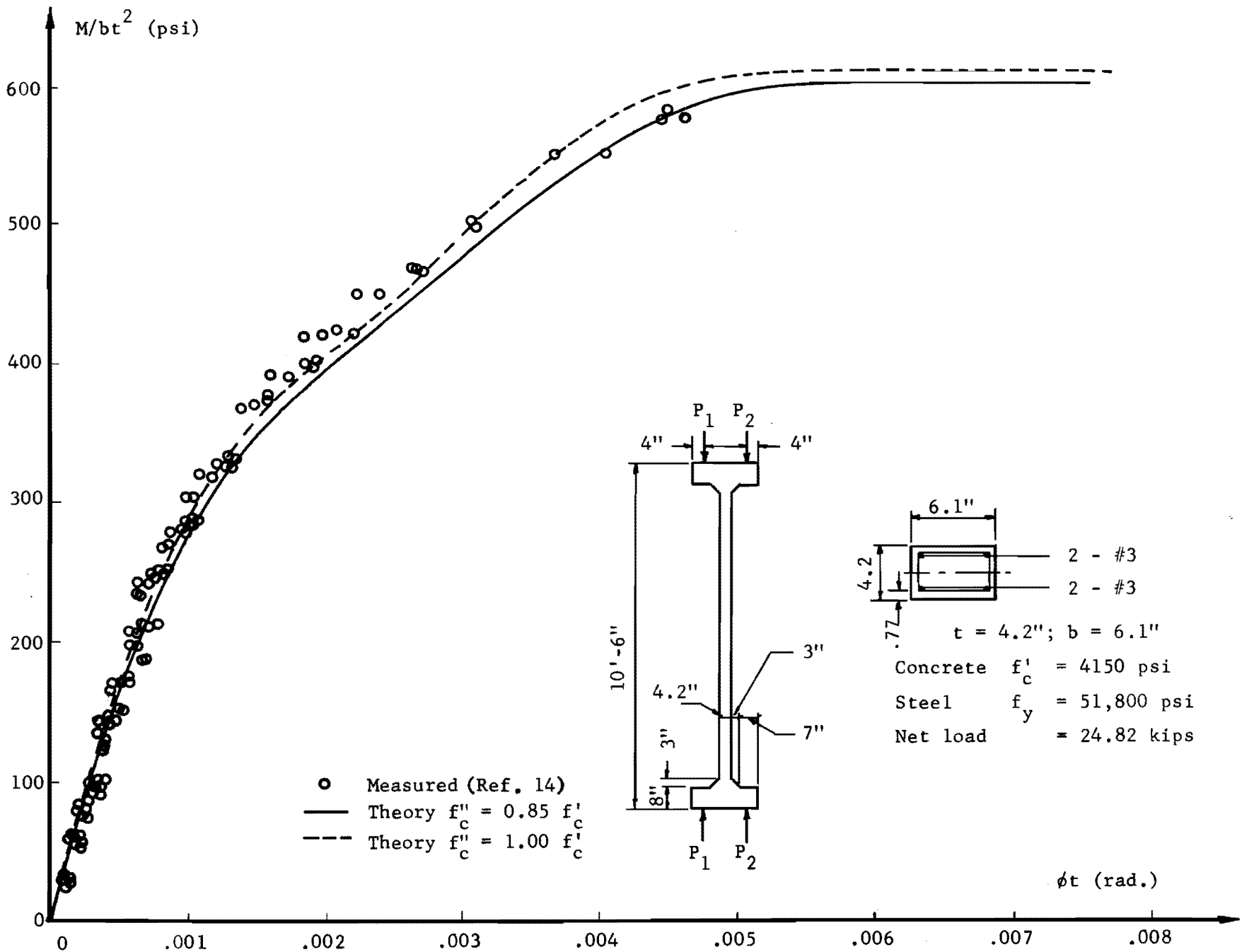
Fig. 5.17. M/bt^2 vs ϕt relationship (column C3).
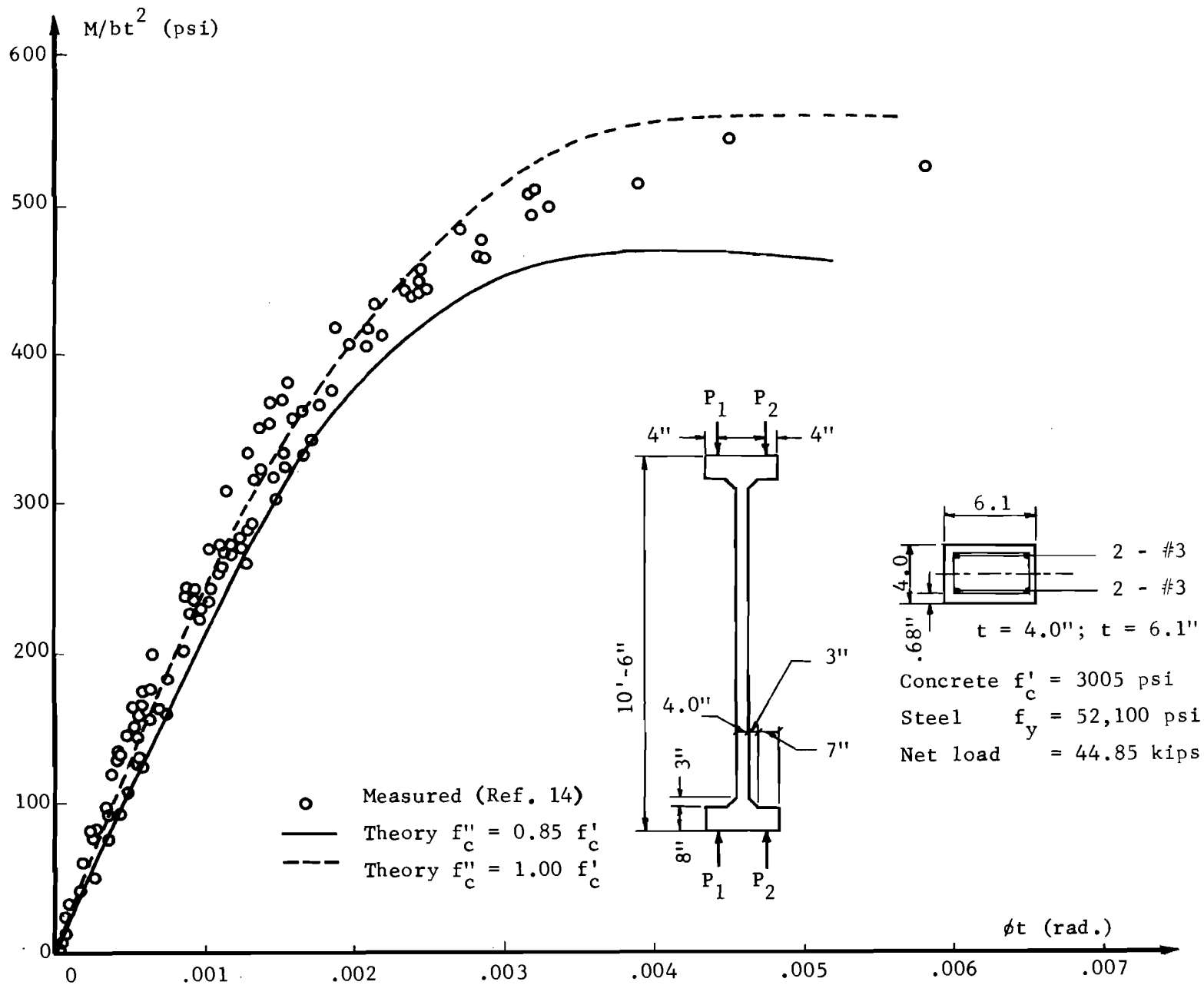
Fig. 5.18. M/bt^2 vs ϕt relationship (column C5).
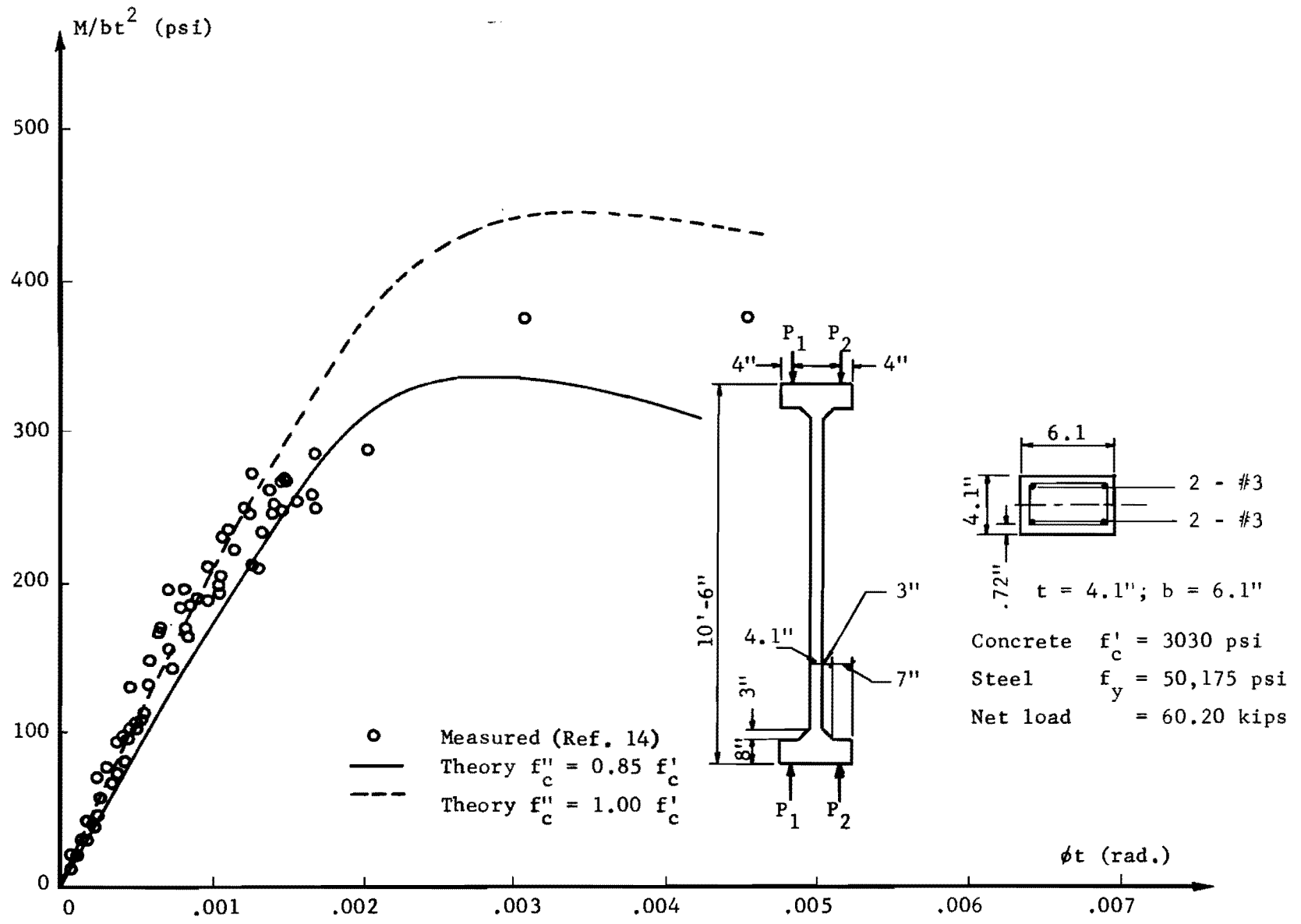
Fig. 5.19. M/bt^2 vs ϕt relationship (column C6).
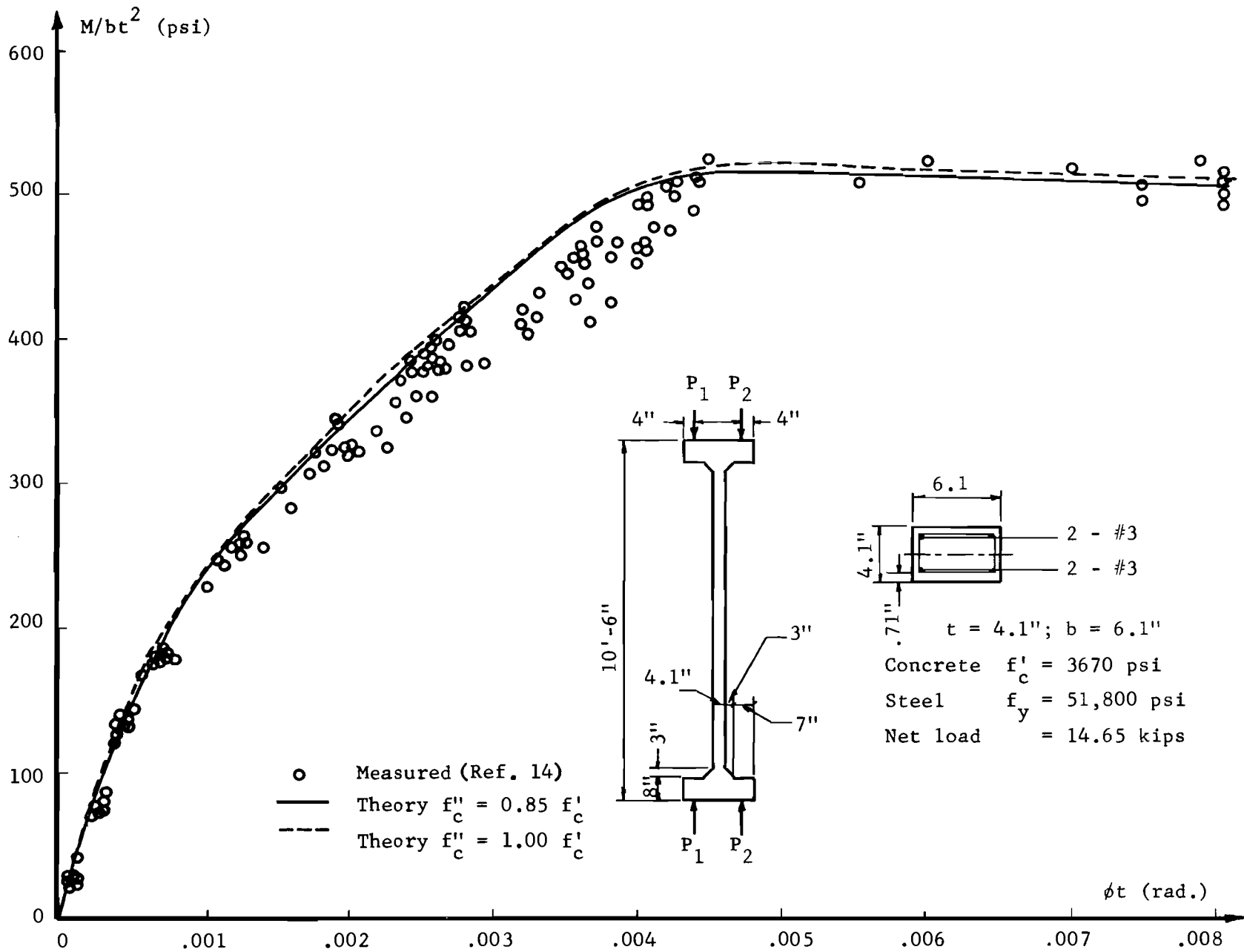
Fig. 5.20. M/bt^2 vs ϕt relationship (column C7).

test results for those members described in Table 5.1. A single run of the MPHI program will provide the required stiffness at various sections along the girder length if reinforcement or dimensions vary. The program also calculates the gross moment of inertia of each section and the modulus of elasticity of the concrete.

The SLAB program ought to be used in an iterative manner in the analysis of continuous reinforced concrete bridges. In the first cycle the stiffnesses of girders along their length can be input based on the gross moment of inertia of the sections. Then revised stiffnesses can be determined based on the moments carried by the members as found from the output of MPHI program. For the two bridge studies (comparison with test results is shown in Sec. 5.6), good theoretical results are obtained with only a single iteration after the first solution.

In the first solution it is clear that an overestimate of bridge stiffness will usually result, since the gross moment of inertia of the sections is used for the entire bridge. This would be a fairly good approximation if there were no flexural cracks in the bridge. This rarely occurs in a reinforced concrete bridge unless specific attempts are made to design to prevent cracking under service loads. The amount of such an overestimation of flexural stiffness when the gross moment of inertia is used depends mainly on the level of loading on the bridge and the portion of the bridge which is loaded beyond its cracking moment.

In the Hillsboro Bridge, the measured deflection for the load case (presented in Table 5.2) was 0.372 in.[43] The computed result from the first (gross section) approximation of stiffnesses gave a deflection of 0.294 in., which is 21 percent too low. A value of 0.384 in. is obtained by refining the stiffnesses using the MPHI program. However, an overestimated value of 0.560 in. was obtained when stiffnesses were refined according to those given by the GMC program which approaches the cracked section stiffness.

It is clear, however, that highly accurate results could be obtained for even a complex reinforced concrete bridge if the stiffnesses were evaluated correctly. Hence, since the flexural stiffnesses calculated using the MPHI program provide the best estimate for such parameters for all members studied in testing the program, girder flexural stiffnesses should be determined using the MPHI program.

5.5.3 <u>Girder Torsional Stiffness</u>. The importance of the girders' torsional stiffness is in the distribution of applied loads on the bridge as carried by the girders across the section. Therefore, torsional shear stresses usually occur in girders. The level of such stresses in reality is low, and, hence, the section can be analyzed elastically. The torsional stiffness of a section composed of a number of rectangles can be obtained by summing up the torsional stiffness of the individual rectangles.[49] An isolated typical section of a reinforced concrete girder in a bridge is shown as the T-beam of Fig. 5.21a. It should be noted that the flange of the beam is part of the continuous slab and such continuity would reduce the stiffness of the member. The torsional stiffness of a rectangular section as shown in Fig. 5.21b can be obtained using St. Venant's formula (see Sec. 4.2.4).

$$\text{Torsional stiffness} = \beta bc^3 G \qquad (5.11)$$

where the factor β may be obtained from Fig. 4.7.

The membrane analogy gives a simple interpretation of the torsion problem. If a thin membrane covers the section and a uniform pressure is applied on the membrane, then twice the volume swept by the membrane is equal to the torque, provided that $F/S = 2G\theta$.[58] The slope at any point on the membrane corresponds to the shear stress. For a rectangular section the equilibrium of the parabolic shape of the membrane shown in Fig. 5.21c yields

$$\delta = \frac{qc^2}{8S}$$

$$\text{Volume} = \frac{2}{3} c\delta b = \frac{qbc^3}{12S}$$

$$\text{Torque} = 2V = \frac{qbc^3}{6S}$$

$$= \frac{1}{3} bc^3 \theta G$$

$$\text{and torsional stiffness} = \frac{1}{3} bc^3 G \qquad (5.12)$$

This stiffness can be calculated from the integration of shear stresses across the section. The stress distribution is shown in Fig. 5.21d. The deflected shape of the parabola is obtained as
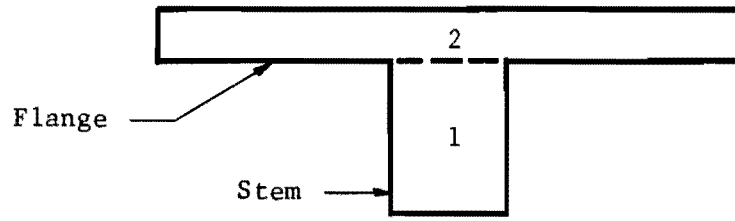
a. Typical concrete T-beam
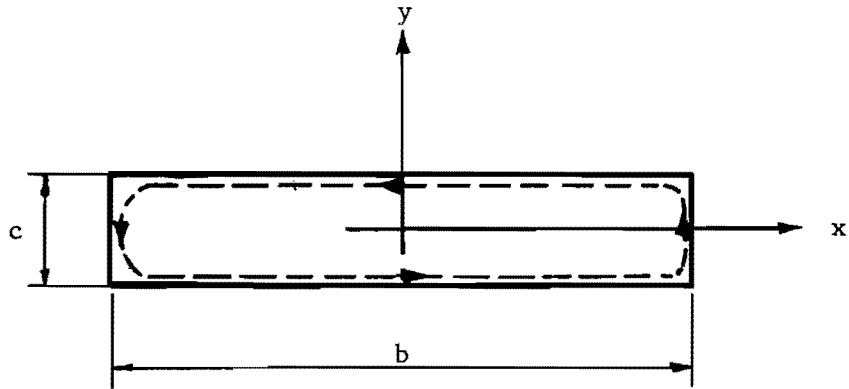
b. Shear flow in a rectangle section under torsion
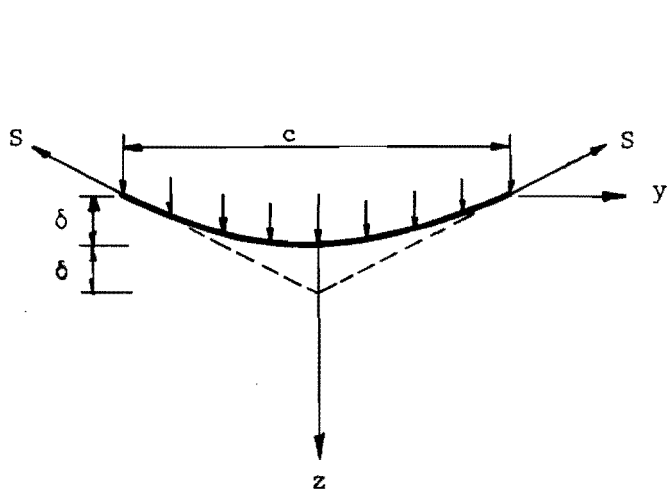
c. Deflected shape of membrane
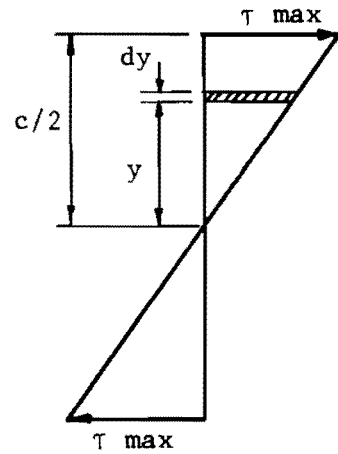
d. Stress distribution

Fig. 5.21. Torsion analysis.

$$Z = \frac{4\delta}{c^2} \left(\frac{c^2}{4} - x^2 \right)$$

$$\frac{dz}{dx} = - \frac{8\delta x}{c^2} = - \frac{q}{S} x$$

The corresponding stress $= 2G\theta x$

$$\text{Torque} = \int_{-c/2}^{c/2} 2G\theta x^2 bd_x$$

$$= \frac{1}{6} bc^3 \theta G$$

and torsional stiffness $= \frac{1}{6} bc^3 G$ \hfill (5.13)

This stiffness is one-half the previous value of Eq. 5.12. The difference is due to neglecting the shear stresses at the ends of the rectangle which have a large lever arm, since such stresses are not present in a continuous section. This suggests that only one-half of the torsional stiffness of flanges of the isolated T-beam should be included in the calculation of the torsional stiffness and, hence, the following expression can be used to estimate such stiffness

$$\text{Torsional stiffness} = \beta_1 b_1 c^3 G + \frac{1}{2} \beta_2 b_2 c_2^3 G \hfill (5.14)$$

where β_1 and β_2 are shape factors to be calculated from Fig. 4.7.

5.6 Comparison of Analytical and Test Results

   5.6.1 The Chili Avenue Bridge--A Simple Span Structure.[5] This prototype, a cast-in-place, reinforced concrete bridge, was designed, constructed, and instrumented under the supervision of the New York State Department of Transportation. The Bureau of Public Roads furnished the recording equipment and the personnel required for the test. Located in Rochester, New York, the structure (see Fig. 5.22) is the middle span of a simply supported three-span, four-lane, one-way traffic bridge. The span is 66 ft. with a skew angle of 14°-$20'$. The cross section is composed of seven monolithic beams having a stem width of 10 in. The beams are spaced at 7'-11" on centers. The reinforced concrete deck has a thickness of 7"
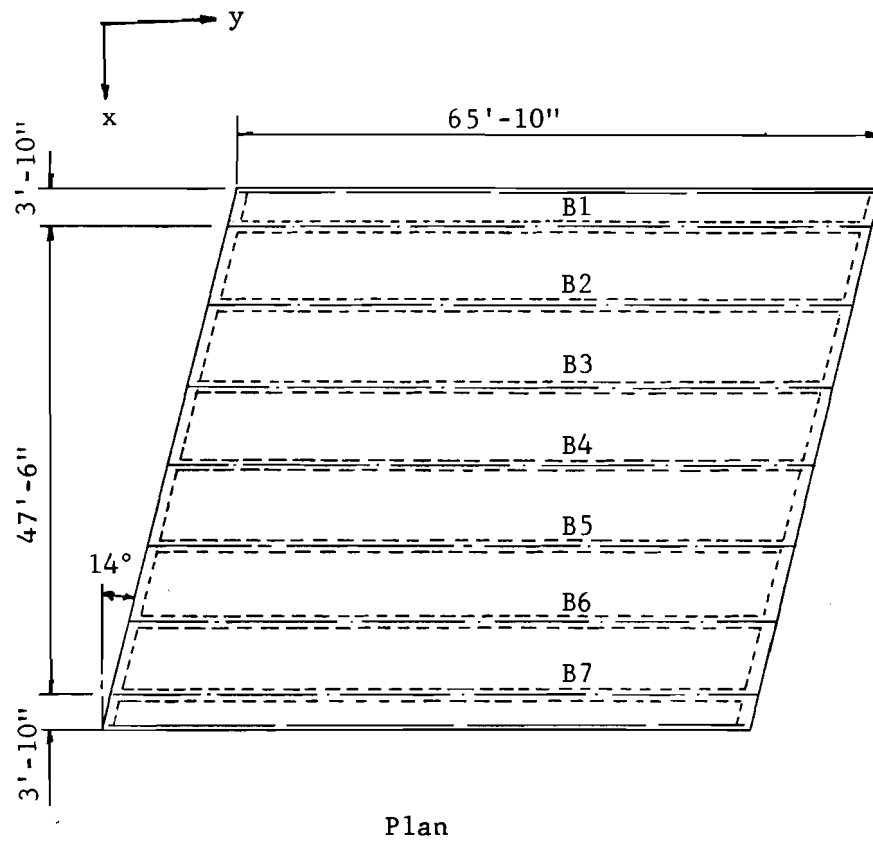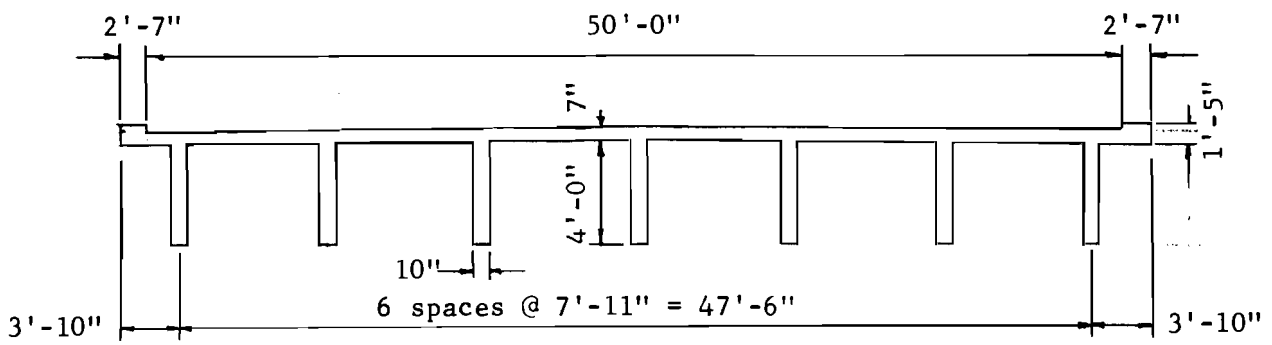
Fig. 5.22   Chili Avenue Bridge--Plan and a cross section detail.

which forms the 50 ft. road width. A plan view and a cross section of the bridge are shown in Fig. 5.22. A432 high strength steel ($f_y >$ 60 ksi) reinforcement was used with the cast-in-place concrete having a minimum 28 days compressive strength of 4000 psi.

The structure was simulated by a mesh size of 28 increments in the x direction which gave a 4-increment spacing between beams. For the y direction 39 increments were used. Increment lengths were 23.75 and 24.00 in., respectively. Stiffness of the deck was evaluated as explained in Secs. 4.2.1 and 4.2.2. Torsional stiffness of girders was evaluated as in Sec. 5.5.3. The flexural stiffnesses of girders were obtained from the generation of the moment-curvature curves for the sections, using the MPHI program with a reduction factor of 0.85, i.e. ($f_c'' = 0.85f_c'$). Two curves are shown in Fig. 5.23 for typical interior and exterior beams. Two load cases were considered in the comparison of analytical and test results. These cases are positions 4 and 5 for the H20-S16 truck load when its centerline passed over Beams B3 and B2, respectively.

In the analysis program SLAB40 was used in an iterative manner where the flexural stiffness of the girder was the variable. In the first run of the program the elastic gross flexural stiffnesses were used to find initial moments. From this first approximation the values of the flexural stiffnesses were refined by entering the established moment curvature curves for the beams obtained from the MPHI program using the initial solution moments. Revised stiffnesses were used for a new solution. Two iterations of SLAB40 were found to be sufficient for the analysis, since very close results were obtained from the second solution. The comparison of computed and measured girder deflections and load distributions for both load cases are shown in Figs. 5.24 and 5.25. The distribution of truck loads to girders was based on the measured steel stresses at the bottom of the girders, while in the analytical analysis the load distribution was based on the bending moment computed for each girder. Both girder deflections and load distribution patterns showed excellent agreement with test results after the flexural stiffnesses of beams were refined according to the results of MPHI program using two iterative cycles.
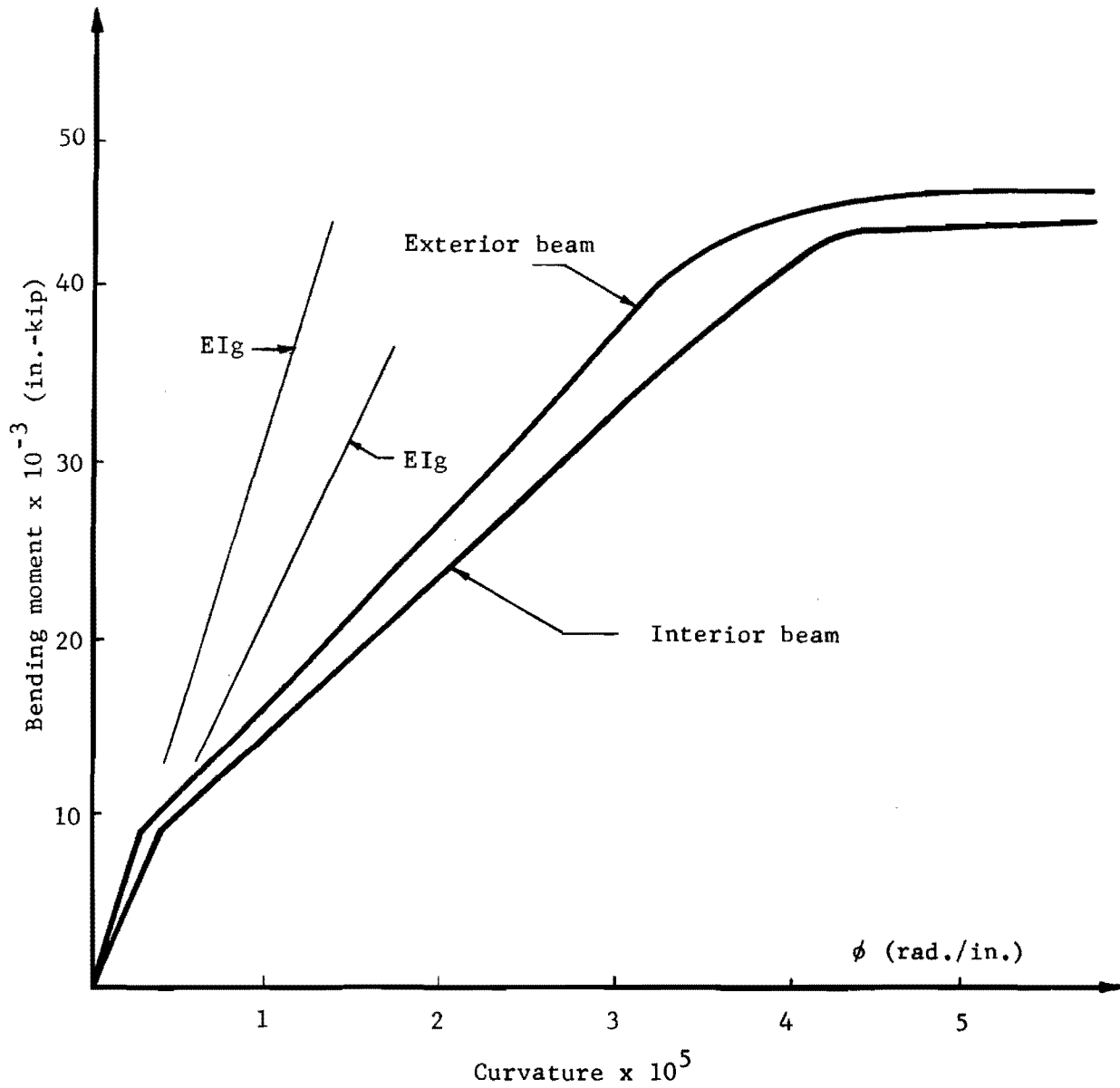
Fig. 5.23. Moment-curvature relationship for an interior and exterior beam of Chili Avenue Bridge.
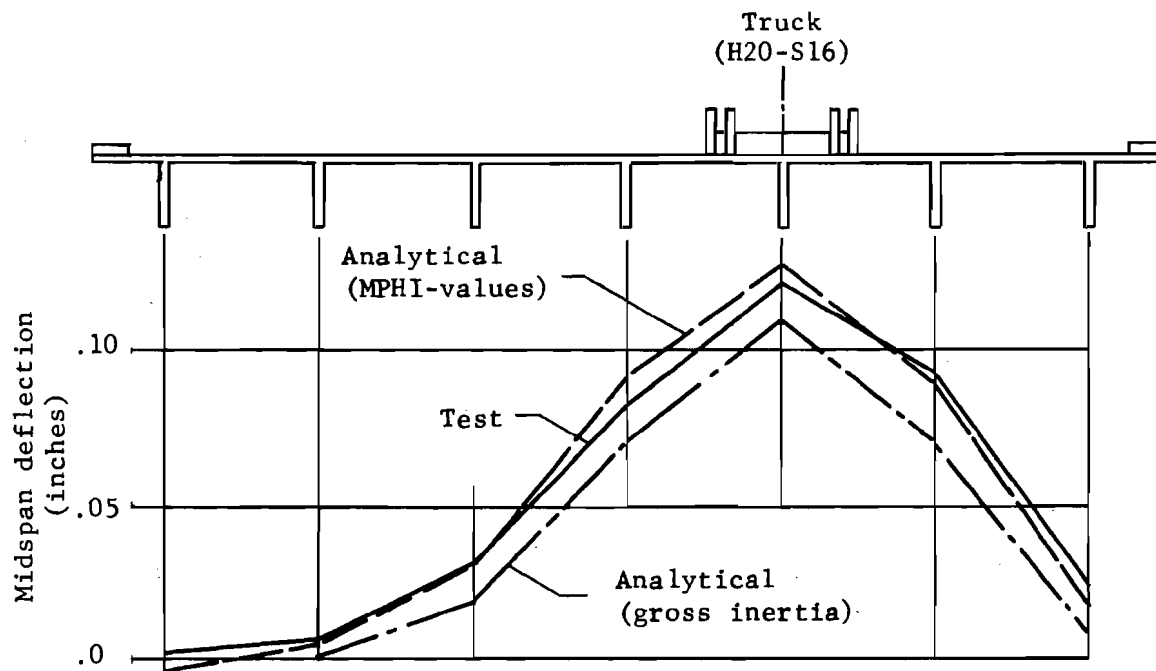
Fig. 5.24a.   Comparison of measured midspan deflection with calculated
               values.
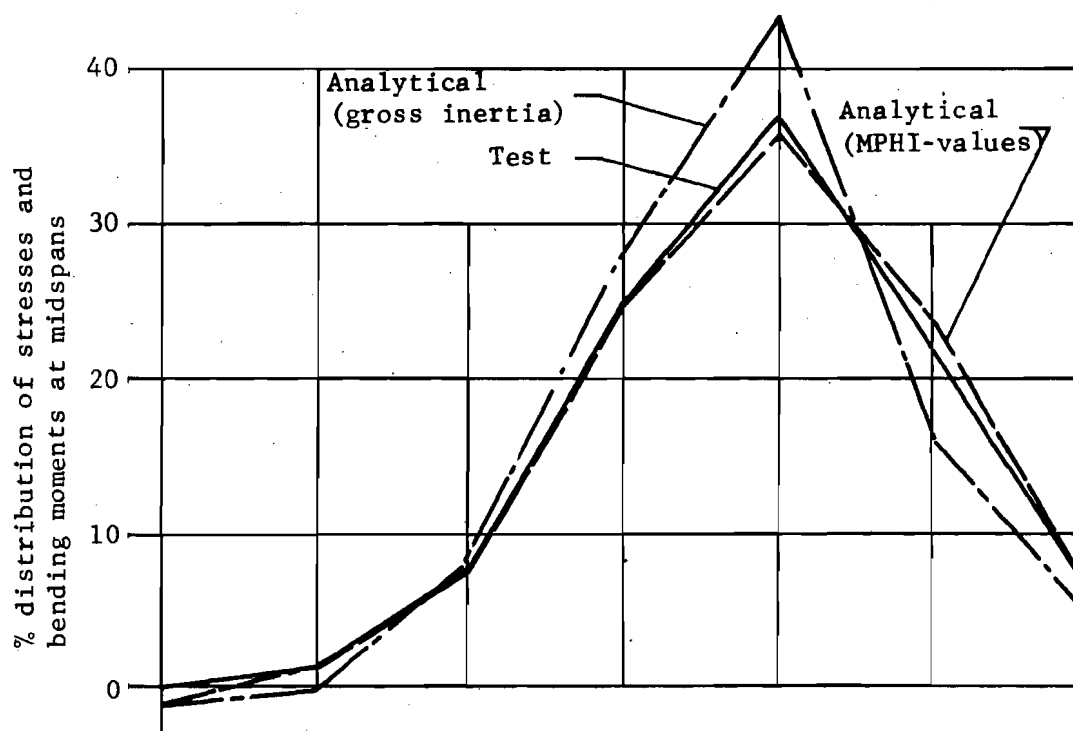
Fig. 5.24b.   Comparison of measured stress distribution in the beams
               with the calculated moment distribution.
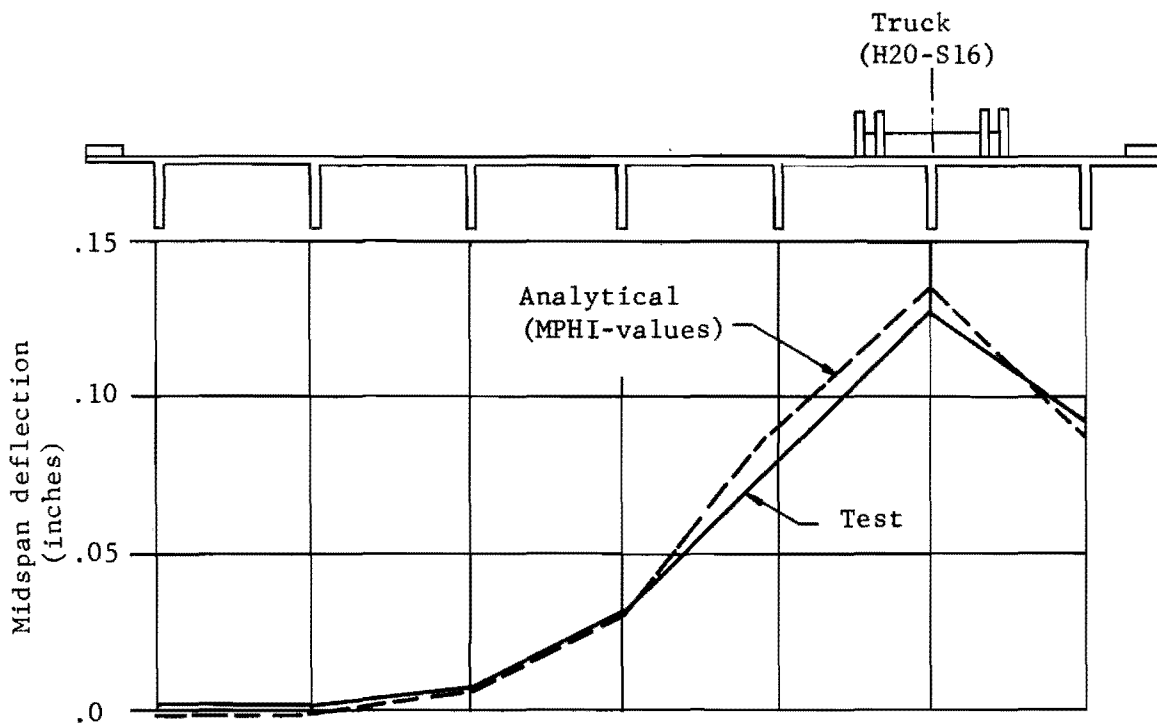
Fig. 5.25a.   Comparison of measured midspan deflection with calculated values.
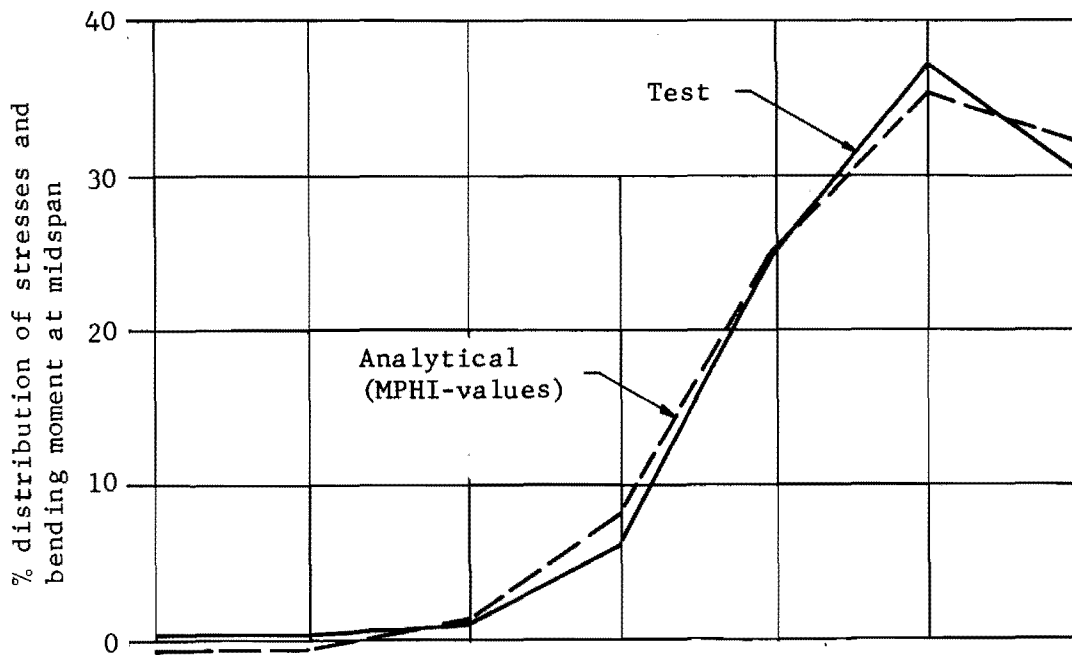
Fig. 5.25b.   Comparison of measured stress distribution in the beams with the calculated moment distribution.

5.6.2 <u>The Hillsboro Bridge--A Four-Span Continuous Structure</u>.[43]

The Texas Highway Department initiated the test of this prototype crossroad structure over Interstate Highway 35 near Hillsboro, Texas. The experimental phases were performed with the cooperation of the U. S. Bureau of Public Roads. This haunched girder bridge, shown in Fig. 5.26, was built of cast-in-place concrete having an average 28-day strength of 5000 psi, and reinforced with A432 high strength steel having a minimum yield point of 60,000 psi. The girders are continuous over four spans of lengths 55'-88'-88'-55'. The stem of the girders is of uniform width of 2 ft.-4-1/2 in. The total depth is 2 ft.-3 in. in the uniform thickness regions and is increased to 4 ft.-9 in. over the interior supports. The slab was cast monolithically with the girders and has a thickness of 6-1/2 in. This formed a two-lane roadway 24 ft. wide. The structure had a skew angle of 30°-22'. A plan view with a longitudinal elevation and a cross section is shown in Fig. 5.26.

The simulation of the bridge into an orthotropic mesh is made by choosing a mesh size of 14 increments in the transverse x direction and 118 increments in the longitudinal y direction. The increment lengths are 21.3 in. and 30 in., respectively. Slab stiffnesses are calculated as in Secs. 4.2.1 and 4.2.2. The stiffness of the girders is evaluated at each section along the span as shown in Fig. 5.26b. The torsional stiffness is calculated as in Sec. 5.3 for the same sections. The girder flexural stiffness is evaluated from the theoretical moment-curvature relationships at each section using $f''_c = 0.85f'_c$. Figure 5.27 shows the positive moment-curvature relationships of the beams at section 7, as described by both MPHI and GMC programs. The relationship for the negative moment of beams at section 12 is shown in Fig. 5.28. In these figures the gross stiffnesses of the sections are shown as a linear relationship. The two theoretical curves of the moment-curvature relationship obtained from the MPHI and GMC computer programs are used separately to obtain a solution and a comparison between the results is made.

SLAB40 is used in the analysis in an iterative process. In the first run the flexural stiffness of girders based on elastic gross section moments of inertia was used and then a refinement of the stiffness based on the moment-curvature characteristics of the sections, as described by
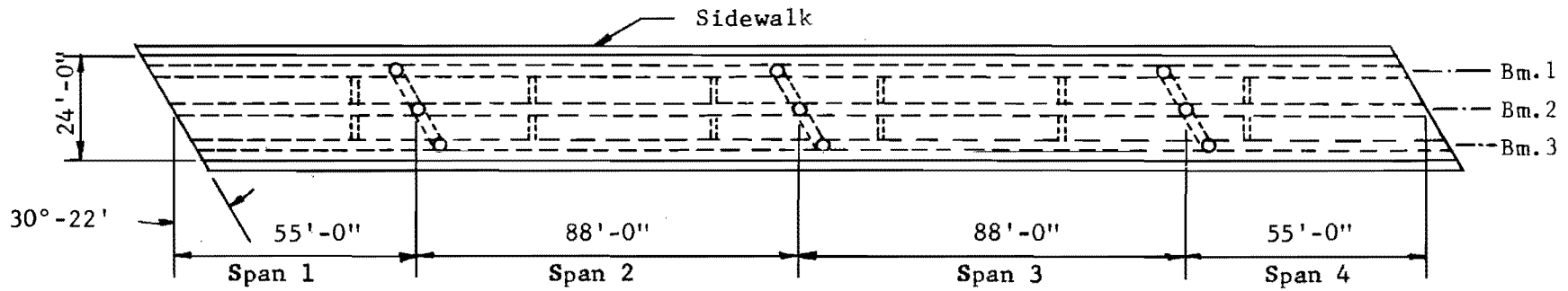
Fig. 5.26a Plan view of Hillsboro Bridge.
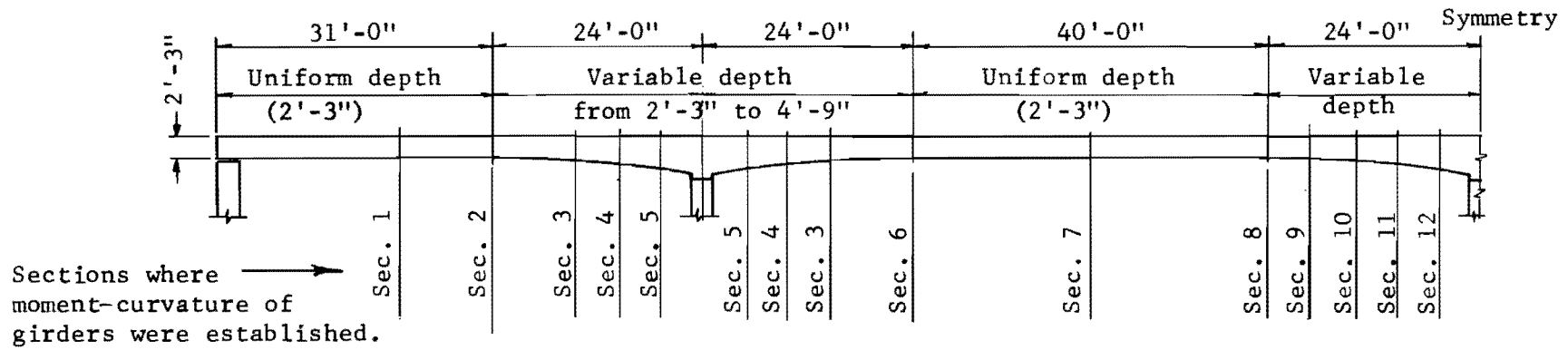
Fig. 5.26b Typical elevation of girders.
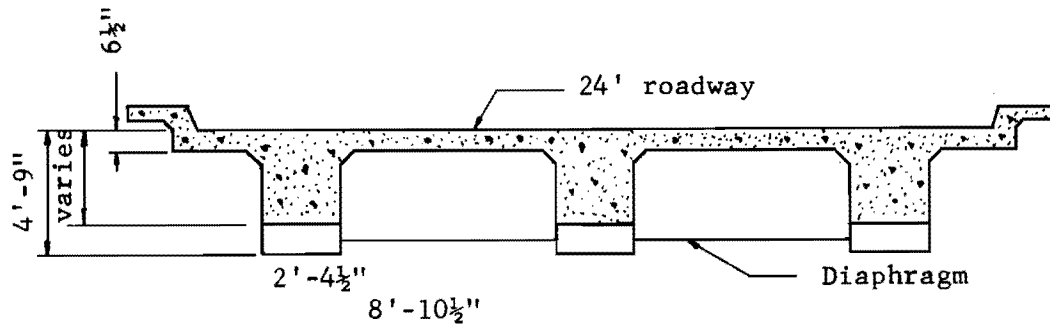
Fig. 5.26c. Typical orthogonal section of the bridge.
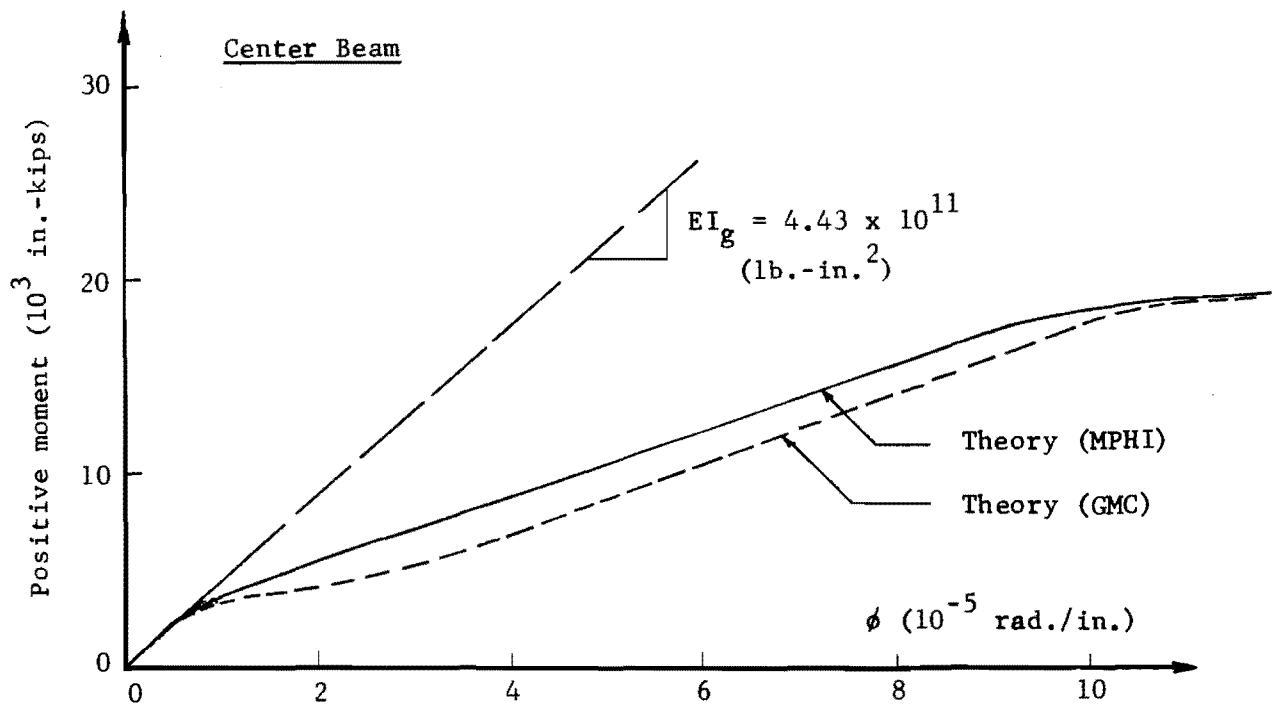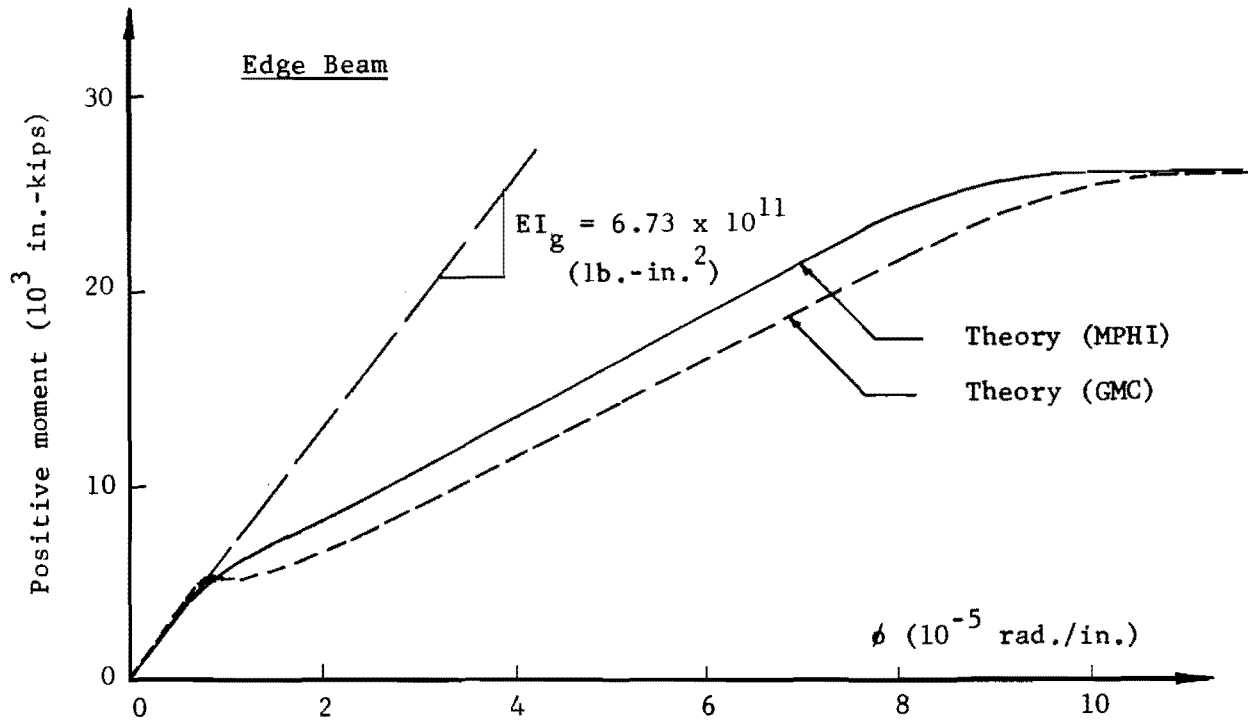
Fig. 5.27. Theoretical moment--curvature relationship of Section 7.
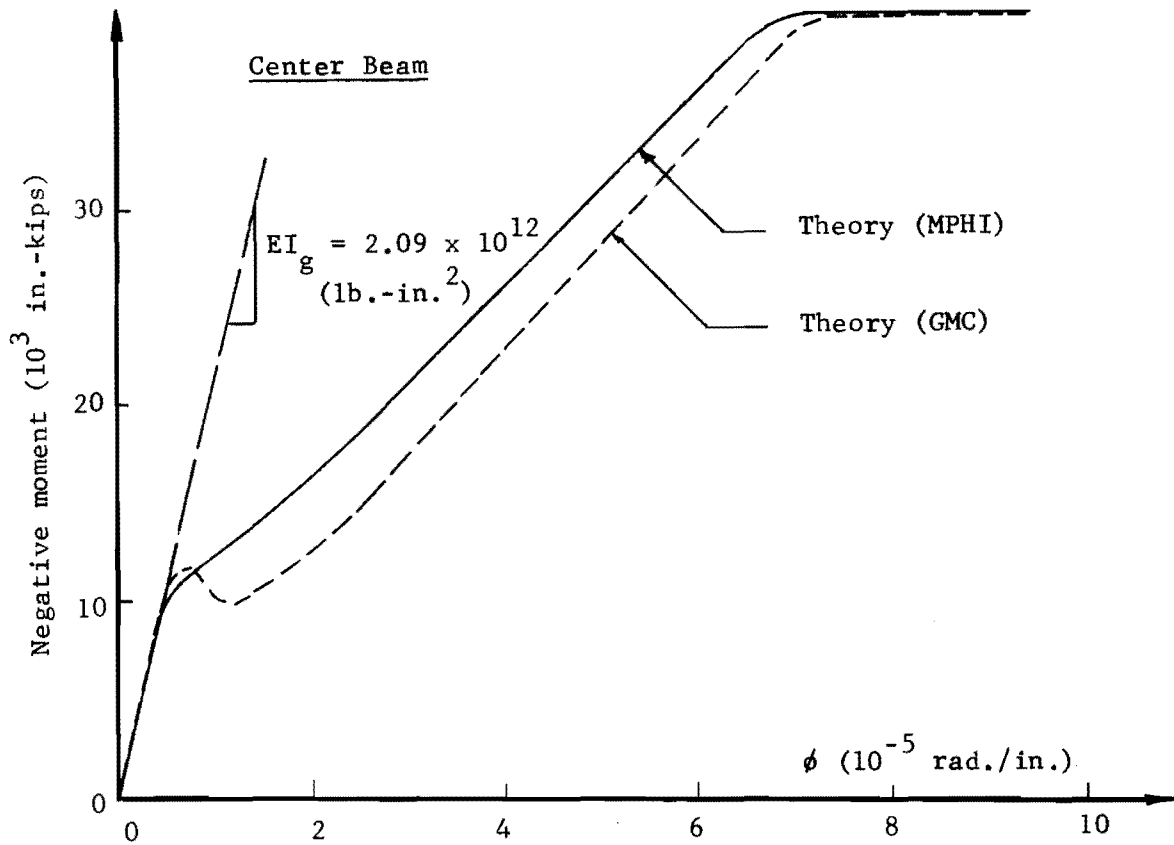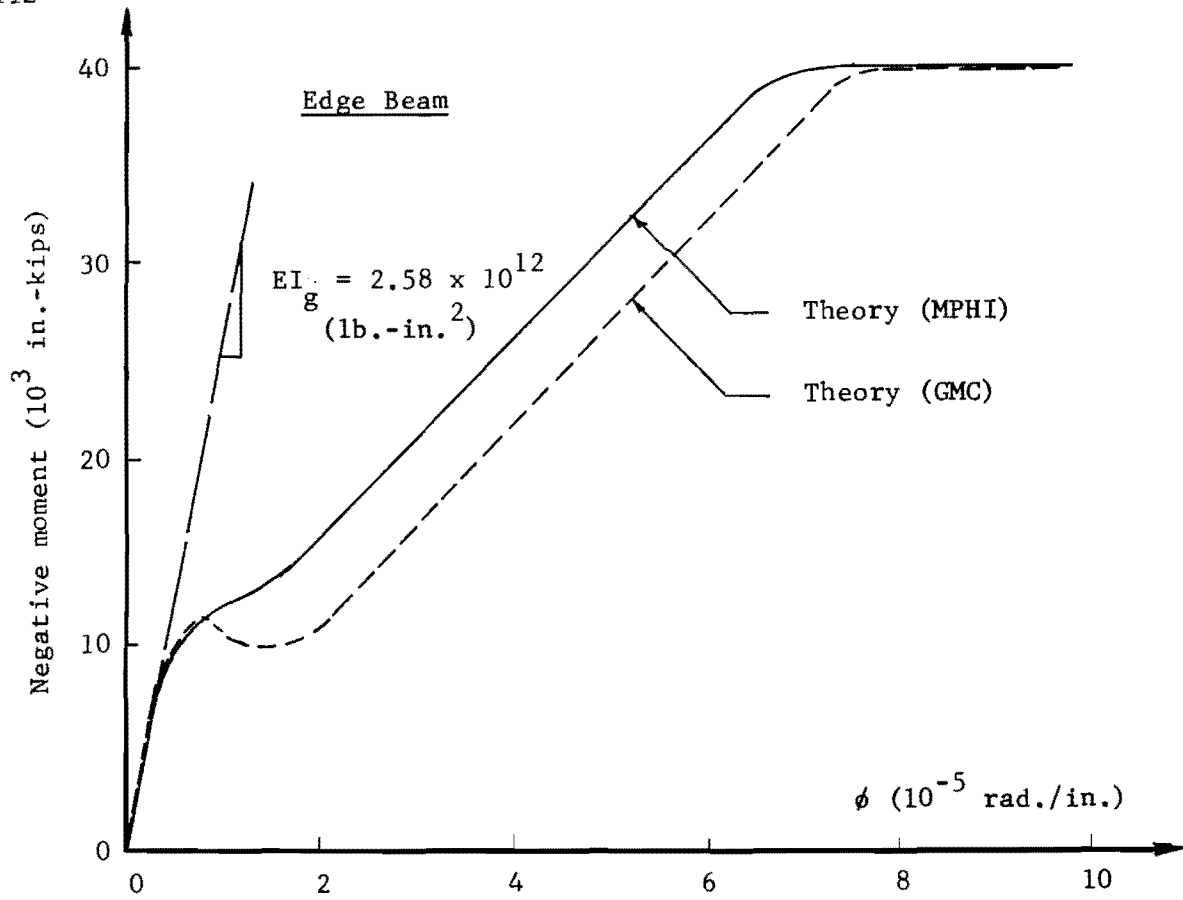
Fig. 5.28. Theoretical moment—curvature relationship of Section 12.

the two theoretical curves, was input for a second run. Test results and the corresponding analytical values for the midspan deflection of girder 2 for lane 3 loading are compared in Table 5.2. The only variable in the analytical results is the source of the flexural stiffnesses of the girders. The load case considered is the H20-S16 truck load passing over the longitudinal median line of the bridge. The comparison shows clearly the effectiveness of the predictions of section stiffness by using MPHI program.

Another load case considered was the normal traffic lane in lane 2, as specified in the report of the Texas Highway Department.[43] The comparison between tested values and analytical results of the midspan deflection obtained by using stiffnesses provided by MPHI program is shown in Fig. 5.29. The comparison shows very good agreement between test and computer results.

5.7 Recommendation for Computer Simulation of Reinforced Concrete Girder Bridges

The detailed recommendations for simulation of girder and slab bridges by gridwork systems, presented in Sec. 4.5.1 is fully applicable for reinforced concrete bridges. In Sec. 4.5.2 the torsional and flexural stiffness of girders should be evaluated according to the findings of this chapter, while the rest of the parameters are applicable without change.

The torsional stiffness of a reinforced concrete girder is presented in Sec. 5.5.3, and an evaluation method for this parameter is suggested. The stiffness may be obtained on the basis of summing up the stiffness of the individual rectangles which comprise the cross section of the girder. Half of the calculated stiffness of the rectangles which comprise the girder flanges should be considered. This reduction is due to the fact that such flanges are usually a part of a continuous deck. The stiffness of the individual rectangle may be calculated as follows:

$$\text{Torsional stiffness} = \beta bc^3 G$$

where

        β = a factor may be calculated from Fig. 4.7

        b = longer side of the rectangle

        c = shorter side of the rectangle

        G = shear modulus of the material

TABLE 5.2. MIDSPAN DEFLECTION AND STRESS OF THE CENTRAL
BEAM AT THE THIRD SPAN OF THE BRIDGE DUE TO
CENTRAL TRUCK LOAD.

	Deflection (in.)	% deviation from tested 5 mph
Test (5 mph)	0.372	0
Test (10 mph)	0.386	+4
Theory (gross inertia of beams)	0.294	-26
Theory (stiffness from MPHI)	0.384	+3
Theory (stiffness from GMC)	0.56	+51
Theory (cracked inertia of beams)	0.955	+157

	Stress (psi)	% deviation from test (5 mph)
Test (5 mph)	4850	0
Test (10 mph)	4600	-5
Theory (gross inertia for beams)	5600	+15
Theory (stiffness from MPHI)	5300	+9
Theory (stiffness from GMC)	6500	+34
Theory (cracked inertia of beams)	7080	+46

Deflection (inches) at Midspan

	B1	B2	B3
Test (5 mph)	0.37	0.34	0.25
Test (10 mph)	0.405	0.395	0.30
Theory (static)	0.428	0.361	0.241
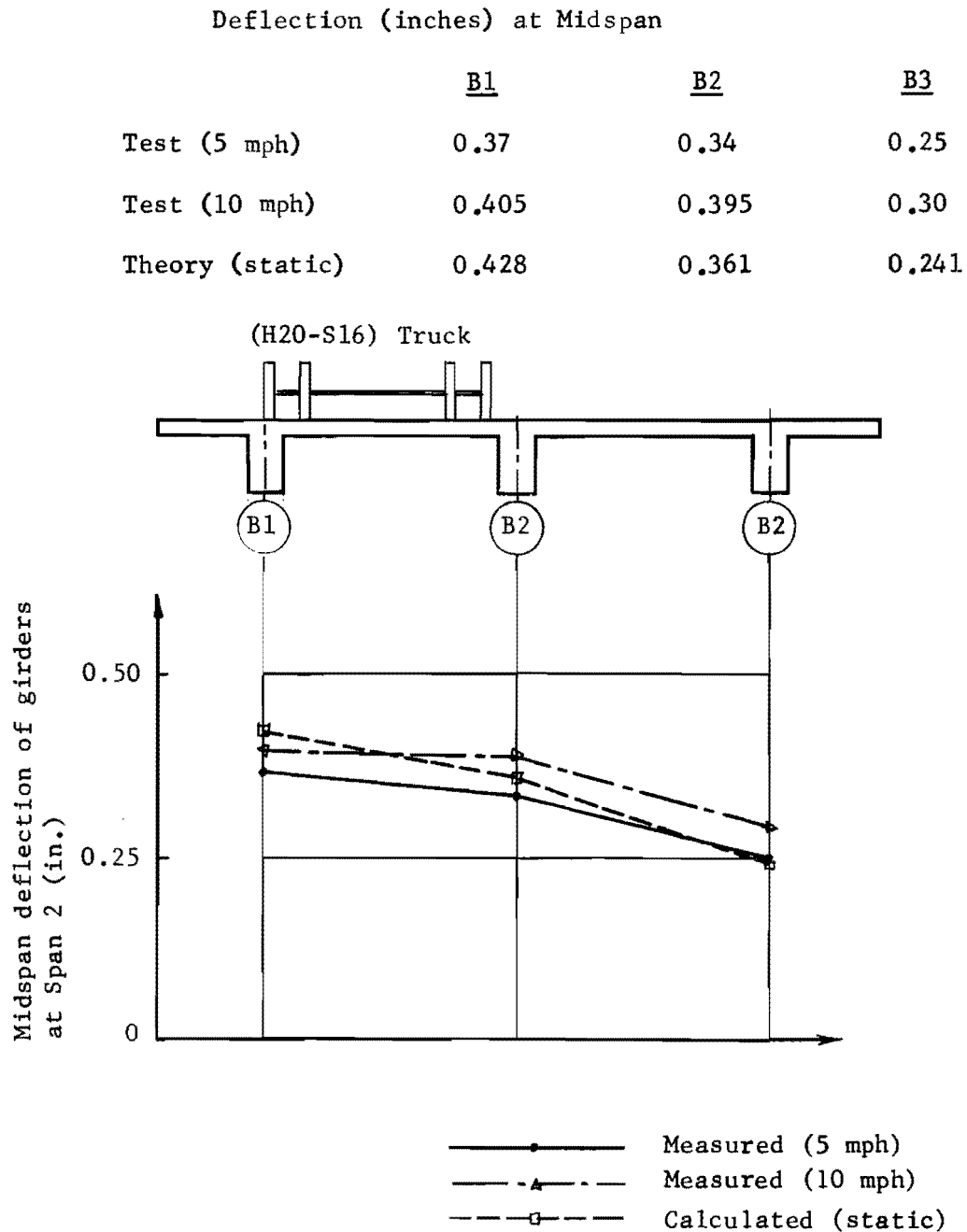
Fig. 5.29. Measured and calculated midspan deflection of girders at
Span 2 due to load case Lane 2 Span 2 (Hillsboro Bridge).

The flexural stiffness of the girders is to be evaluated from the moment-curvature relationships as described by the MPHI program. Such relationships should be established for the different sections of the girder when the dimensions or reinforcements are varied. At this stage all parameters are defined for the input in the SLAB program. The complete solution is obtained in an iteration method, where the flexural stiffness of girders is the only input variable. The elastic gross flexural stiffnesses are used in the first run with SLAB then refined values of stiffness are found from the moment-curvature curves for each value of moment and these are used in the iterations. It was found that a single iteration, after the first gross section run, gave good results for the load cases studied for both bridges presented in this chapter. The stiffnesses should be refined according to the total bending moment imposed on the sections, which naturally includes the dead load moments in addition to any other live loads under consideration.

CHAPTER VI

STEEL GIRDER BRIDGES

6.1 Introduction

Concrete deck and steel girder bridges are often built from plate girders or rolled steel sections with or without stiffening cover plates. Fully composite action between the top flanges of the steel girders and the concrete slab is usually ensured by shear connectors attached to the flanges and embedded in the deck. The performance of bridges built compositely is much better than with noncomposite construction. A comparison (see Table 6.1) between the performance of two bridges, B3 and A4, as reported by the Highway Research Board,[24] indicates the effectiveness of composite action. Both bridges are nearly similar in properties, except that bridge B3 was built compositely while no shear connectors were added to bridge A4.

In this chapter methods for computer simulation of both composite and noncomposite steel girder bridges are presented. Computer solutions are compared with physical tests of both simple and continuous span structures and recommendations are made for evaluation of certain parameters.

6.2 Stiffnesses of Composite Bridges

6.2.1 Flexural Stiffness of Composite Sections. Ordinary elastic analysis transformed section theory for the entire composite section was used to estimate girder flexural stiffness for a composite bridge. Kaczmarek[30] showed good agreement between this analytical method and test results. This method was also used to evaluate the girder flexural stiffness in this study and was found to be an effective measure yielding very good correlation between analytical and test results.

The elastic stiffness of a composite beam is calculated by replacing the effective width of the concrete slab with its equivalent "steel" value

117

TABLE 6.1. PROPERTIES AND PERFORMANCE DATA OF B3 AND A4
BRIDGES[24]

	Bridge B3 Composite	Bridge A4 Noncomposite
Beam size (3 Beams)	18WF60	18WF60
Cover plate (bottom only)	18'-6"	19'-0"
Slab thickness (in.)	6.45	6.45
Mean compression strength at beginning of the test (psi)	5740	5460
Stiffness of bridge at midspan (kip-in.^{2})	384.3×10^6	126.5×10^6
Computed natural frequency (cps)	4.52	2.64
Live load deflection at midspan of central beam (in.)	0.79	2.37
Permanent set deflection at midspan of central beam (in.)	0.06	3.36*
Average impact (percent)	12.8	29.2

*Permanent set caused due to the yield of the flanges of the beams.

as transformed by the modular ratio of steel and concrete. The moment of inertia of the hypothetical section is obtained and the elastic stiffness (EI) determined using the steel modulus of elasticity. This stiffness (EI) is not valid near yielding but may generally be used for the analysis of bridges at service loads. The nonlinear effect on the flexural stiffness of composite bridges discussed in Sec. 3.3 indicates that appreciable errors do not occur at service load levels.

6.2.2 Torsional Stiffness of Composite Sections. The differential equation for an open section subjected to nonuniform torsion (warping torsion) may be written as[20,23]

$$\varphi''' - \lambda^2 \varphi' = \frac{-M_z}{EI_w} \tag{6.1}$$

where

$$\lambda^2 = \frac{GK_T}{EI_w}$$

and M_z = torsional moment

φ = angle of twist

G = modulus of rigidity of the material

K_T = St. Venant torsion constant

E = modulus of elasticity of the material

I_w = warping moment of inertia.

A general solution of Eq. 6.1 can be written as

$$\varphi = C_1 + C_2 \cosh(\lambda z) + C_3 \sinh(\lambda z) + \frac{M_z}{\lambda^2 EI_w} \tag{6.2}$$

where

C_1, C_2, and C_3 are constants which can be found from the boundary conditions of the problem, and Z is the longitudinal axis of the member.

The boundary conditions and the complete solution of the differential equation are presented in Table 6.2 for three cases of beam end conditions. Other cases may be found in Ref. 23.

The application of Eq. 6.2 requires the evaluation of the properties of the particular section under consideration. The sectional parameters affecting torsion are (GK_T) and (EI_w).

TABLE 6.2. WARPING TORSION FOR SOME END CONDITION CASES OF BEAMS

Type of Beam	Pinned Ends	Cantilever	Fixed Ends
	$M_z \xleftarrow{\quad L \quad} M_z$ $\vdash\!\!\rightarrow z$	$\xleftarrow{\quad L \quad} M_z$ $\vdash\!\!\rightarrow z$	$M_z \xleftarrow{\quad L \quad} M_z$ $\vdash\!\!\rightarrow z$
Boundary Conditions	at $z = 0$ $\phi = 0$ $\phi'' = 0$ at $z = L$ $\phi'' = 0$	at $z = 0$ $\phi = 0$ $\phi' = 0$ at $z = L$ $\phi'' = 0$	at $z = 0$ $\phi = 0$ $\phi' = 0$ at $z = L$ $\phi' = 0$
Solution	ϕ_1	ϕ_2	ϕ_3

where $\phi_1 = \dfrac{M_z z}{GK_T}$

$\phi_2 = \dfrac{M_z}{\lambda GK_T} [\lambda z - \sinh (\lambda z) + \tanh (\lambda L)(\cosh (\lambda z) - 1)]$

$\phi_3 = \dfrac{M_z}{GK_T} [(\dfrac{\cosh (\lambda L) - 1}{\lambda \sinh (\lambda L)})(\cosh (\lambda z) - 1) + (z - \dfrac{\sinh (\lambda z)}{\lambda})]$

The problem of nonuniform torsion in open, thin-walled members, composed of any number of different materials has been studied by McManus and Culver.[40] The particular case of a composite steel beam with concrete slab is considered as a special case. The sectional properties of a member composed of two materials can be written as

$$GK_T = \frac{1}{3} (2 G_s b_s t_f^3 + G_s h t_w^3 + G_c b_c t_c^3) \tag{6.3}$$

$$EI_w = \frac{1}{3} \left[\left(\frac{E_s t_f b_s^3 d^2}{4} + \frac{E_c t_c b_s^3 (a + b - c - d)^2}{4} + \right. \right.$$

$$\frac{E_s t_f b_s^3 (a + b - c - d)^2}{4} + \frac{E_c t_c (b_c - b_s)}{4} \left[(b_s c - b_c (a + b - d))^2 \right.$$

$$+ (b_s c - b_c (a + b - d)) (b_s (a + b - c - d))$$

$$\left. \left. + (b_s (a + b - c - d))^2 \right] \right] \tag{6.4}$$

where all variables of Eq. 6.3 are shown in Fig. 6.1.

S = shear center

B = centroid

$a = \bar{y}' - t_f/2$

$b = h + \frac{t_c}{2} + 2 t_f - \bar{y}'$

$c = - \frac{1}{2} t_f$

$d = a - Y_0$

Fig. 6.1. Geometrical parameters of a T-section.

Location of the centroid of the hypothetical section with plates related to their modulus of elasticity is

$$\bar{y}' = \frac{b_c t_c E_c (h + 2t_f + \frac{t_c}{2}) + b_s t_f E_s (h + 2t_f) + ht_w E_s [(\frac{h}{2}) + t_f]}{b_c t_c E_c + 2b_s t_f E_s + ht_w E_s} \qquad (6.5)$$

The shear center S is found as[40]

$$Y_o = \frac{2E_s t_f b_s^3 (a - b + c) - E_c t_c (2b_c^3 b + b_c^3 c - 3b_s^3 c - 3b_c^3 b_s c)}{2(2E_s t_f b_s^3 + E_c t_c b_c^3)} \qquad (6.6)$$

The above expressions define the geometrical parameters for a composite section. These equations together with those of Table 6.2 governing the torsion problem are troublesome for hand calculation. Hence, a computer program called TORSION has been written to evaluate the angle of twist and the rigidity of a composite beam along its length. The program solves the three cases specified in Table 6.2. The listing of the program is given in Appendix A.

Any significant effect of the girder torsional sitffness would occur in the distribution of the lateral loads to the various girders across the bridge. The effect of ignoring the torsional stiffness of the girders was studied (see Sec. 6.4.1) for a typical composite bridge (Bridge S15 of Ref. 42). This study showed that completely neglecting torsional stiffness caused a deviation for the calculated maximum deflection of 3 percent for an edge-point load and of 7 percent for a central load from a set of reference calculations considering the full stiffness. The corresponding values for bending moments were 6 percent and 4 percent, respectively. The load case was a single point load placed at girder midspan. Similar studies for the Patuxent Bridge[51] showed the same order of magnitude error in the final results. The effect of fully neglecting torsional stiffness on maximum deflection with an edge truck loading was calculated to be 4 percent and was almost the same as for a central truck loading. The corresponding values for maximum beam bending moments were 2 percent and 5 percent, respectively.

It is apparent that girder torsional stiffness does not represent the critical parameter in obtaining usable final results for most routine cases. The torsional stiffness of a restrained composite member varies

along the length due to the warping effect. The influence of warping
tends to increase the stiffness in the vicinity of the restraining points.
This increase diminishes rapidly along the length of the member. The
relative portion of span length affected by the warping becomes smaller
with longer spans. In cases where torsional stiffness is important, the
program TORSION can be used to evaluate the stiffness for any number of
sections along the girder. The number of 21 stations was arbitrarily used
in the program. The average value of these calculated torsional stiffnesses
can be used in the input of the SLAB program to obtain the final solution
for the bridge.

6.3 Stiffnesses of Noncomposite Bridges

6.3.1 Flexural Stiffness of Noncomposite Sections. Calculations
based on the addition of stiffnesses contributed by the individual component
subsectional material are used to evaluate the flexural stiffness of the
full noncomposite section. This estimate of the section's stiffness actually
represents the hypothetical case of completely ignoring the contribution
of the interaction between the slab deck and the top flange of the steel
section. Some amount of additional stiffness will ordinarily be present
from the friction which exists between the two surfaces when the members
bend. Such interaction usually is not of a large magnitude and depends not
only on the natural bond between the steel and concrete but also on the
roughness of the surfaces. It is particularly difficult to justify even
the existence of the natural bond in a bridge which has been in service for
a period of time and where the vibration and impact of the traffic on the
structure should be enough to destroy any such bond.

In designing noncomposite bridges the interactions between the con-
crete and steel section are assumed irrelevant and it is common practice
to ignore their effect on the stiffness. Therefore, the sum of the stiff-
nesses of the individual components represents a lower bond for the actual
stiffness of the member and is slightly on the conservative side.

6.3.2 Torsional Stiffness of Noncomposite Sections. The torsional
rigidity of a thin-walled open section may be calculated from Eq. 4.5 using
values of the function (K) for the section from Roark's tables[48] or using
Fig. 4.7. The torsional stiffness is then obtained as the value of (KG),

124

where G is the modulus of rigidity. The concrete and the steel section which form a noncomposite section may each be considered as an open thin-walled section. The torsional properties of rolled steel sections can be picked up directly from a handbook.[23] The corresponding values for built up steel sections and concrete decks can be calculated with the use of the St. Venant formula for an open thin-walled section.[48] In general, for a steel section, the ratio of plate widths to the thickness is large and, hence, Eq. 4.5 may be approximated as

$$K = \frac{1}{3} \sum_{i=1}^{n} b_i t_i^3 \qquad (6.7)$$

where

b_i = width of the ith plate

t_i = thickness of the ith plate

n = number of plates in the section.

Therefore, the summation of the torsional stiffness (KG) of each component of the section gives the stiffness of the noncomposite member.

6.4 Comparison of Analytical and Test Results

6.4.1 University of Illinois-Composite Single Span Bridge S15. This quarter-scale model, nonskew, single span, composite bridge was tested at the University of Illinois Experimental Station. Results of the test were reported by Newmark, Siess, and Penman.[42] The bridge is composed of five 10JB9.0 girders, spaced at 18 in. on centers. The reinforced concrete slab is 1.75 in. thick and the span length is 15 ft. The composite action was provided by shear connectors attached to the top flanges of the steel girders and embedded in the concrete deck.

A mesh size of 16 by 18 increments was used to simulate this structure. The 16 increments across the bridge were used to give a 4 increment spacing between the girders. The flexural and torsional stiffnesses of the girders were computed using Secs. 6.2.1 and 6.2.2. Other parameters were evaluated from the physical properties of the structure. Point loads were used to test this bridge model.

The excellent correlation between the influence lines obtained from test and from theory is shown in Figs. 6.2 and 6.3. These influence lines
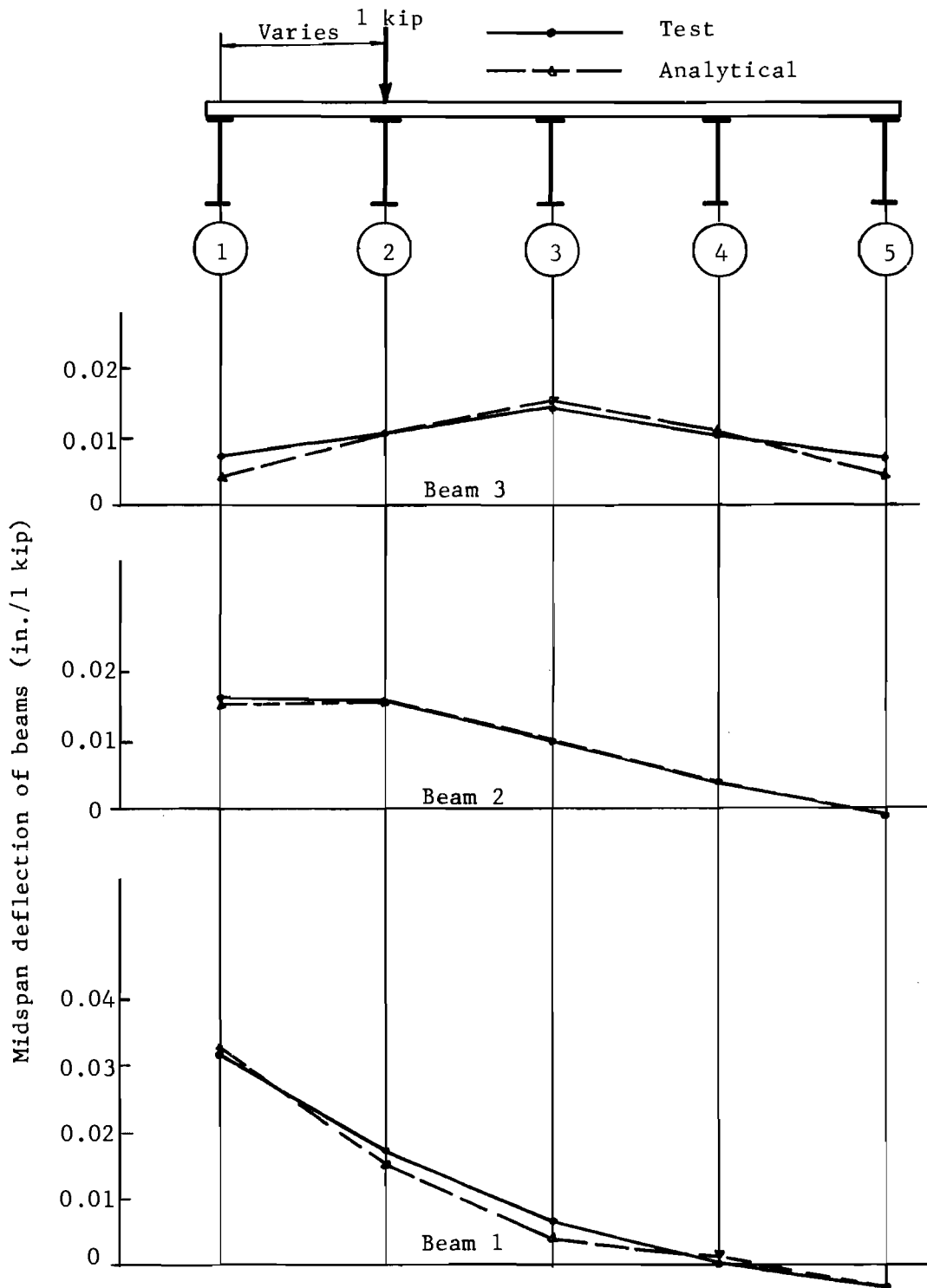
Fig. 6.2. Influence ordinates for deflection in beams at midspan
for load moving transversely across the bridge at midspan.

126
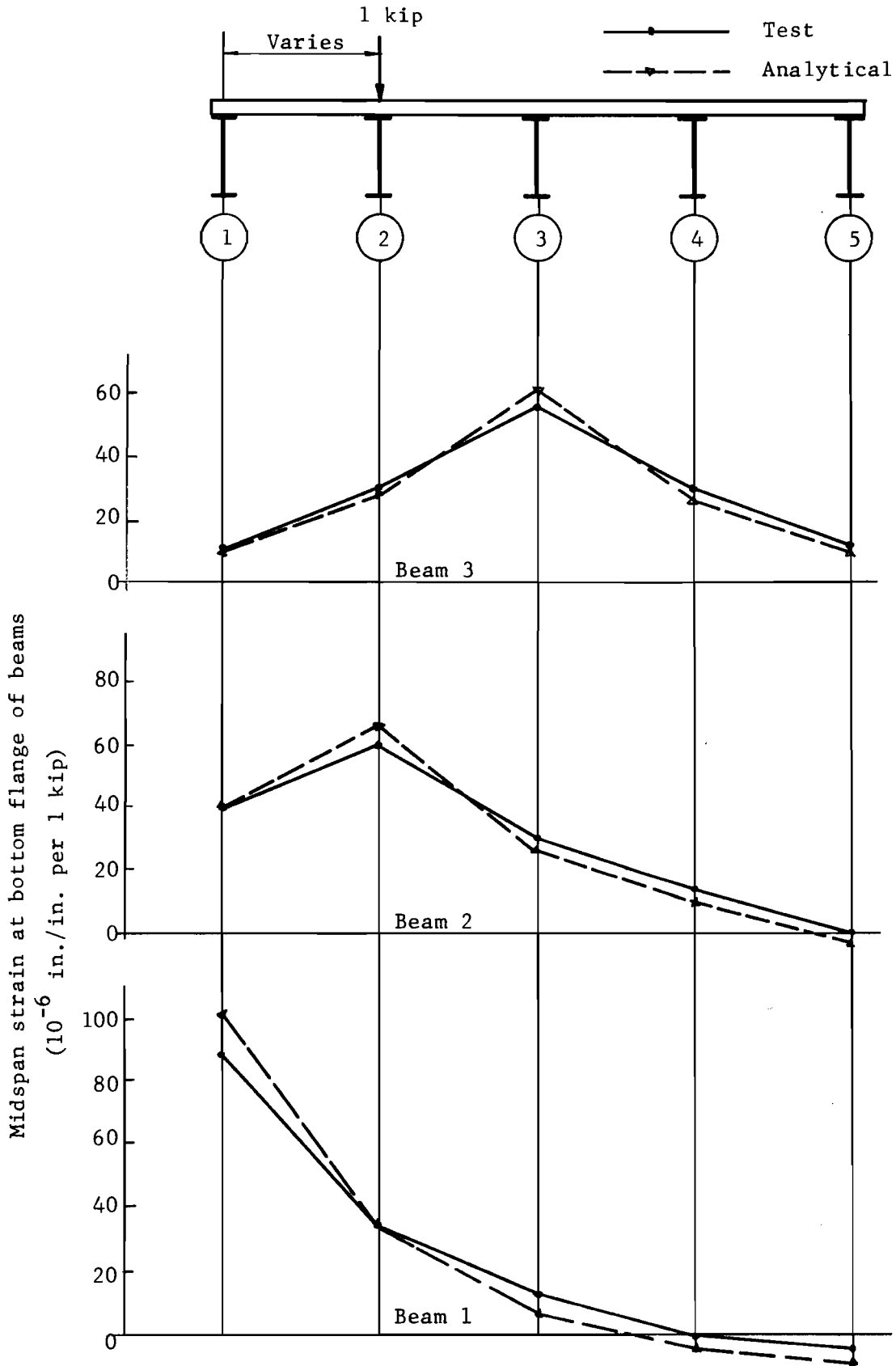
Fig. 6.3. Influence ordinate for strains in beams at midspan for
load moving transversely across the bridge at midspan.

are for a 1 kip load moving across the midspan of the bridge. Figure 6.4 shows a comparison between the measured and computed midspan girder deflections for the four point loads of 5 kips each applied at midspan. Table 6.3 shows the relatively minor effect of ignoring the girder torsional stiffnesses on the theoretical results for a single load at the midspan of beam 1, as compared with test values.

TABLE 6.3. INFLUENCE OF GIRDER TORSIONAL STIFFNESS ON FINAL RESULTS FOR A SINGLE LOAD AT MIDSPAN OF B1.

	B1	B2	B3	B4	B5
Deflection (in./1 kip)					
Test	.032	.017	.007	.00	-.004
Theory with Torsion	.031	.015	.005	.00	-.003
Theory without Torsion	.034	.015	.004	.001	-.004
Strain (10^{-6} in./in./kip)					
Test	90	40	10	0	-5
Theory with Torsion	97	39	11	0	-6
Theory without Torsion	103	40	10	-3	-8

6.4.2 Patuxent River Bridge--A Composite Single Span Structure. This nonskew bridge consists of three simply supported spans. The single span adjacent to the west bank of the Patuxent River was tested.[51] The bridge is located over the Patuxent River, on Maryland Route 4. A plan view and a cross section are shown in Fig. 6.5. The span is 80 ft. in length and the cross section is composed of five rolled steel beams with welded cover plates at their central portions. The composite action was provided by shear connectors attached to the steel beams and embedded in the 7 in. concrete deck slab. A BPR vehicle was used to load the bridge. This vehicle closely approximated the standard AASHO (H20-S16) truck load.
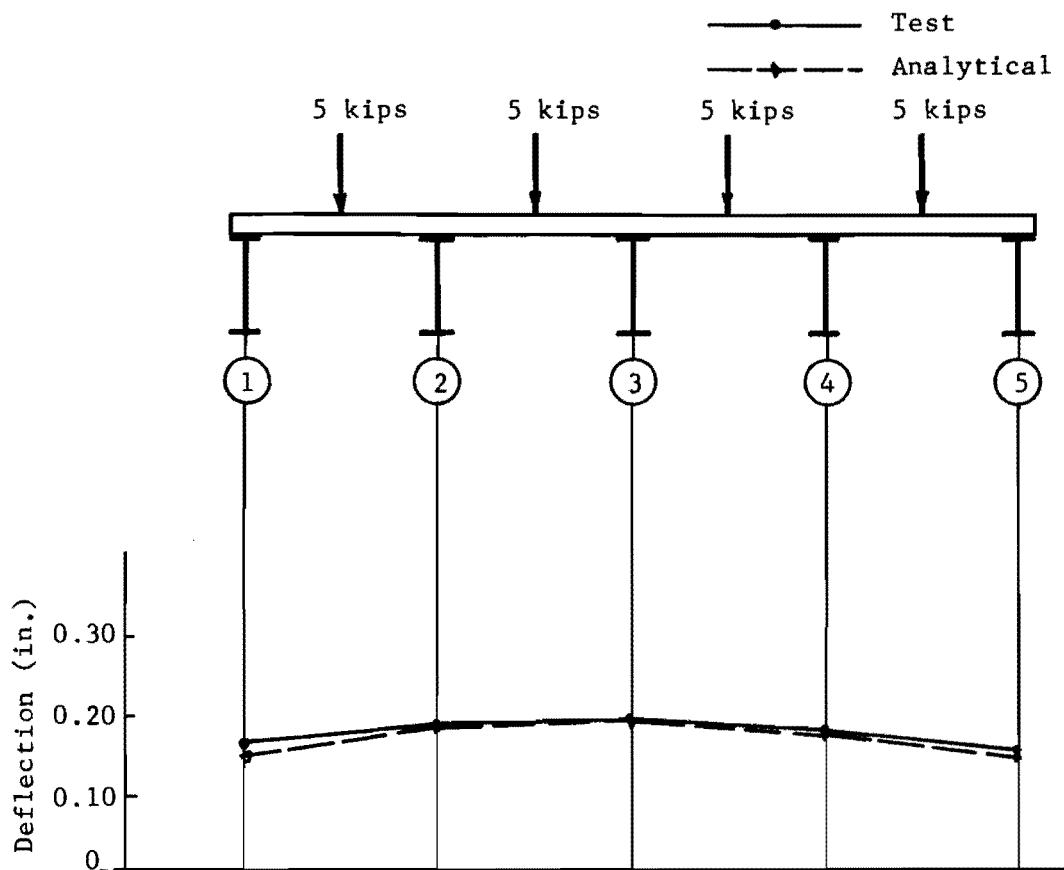
Fig. 6.4. Deflection of beams at midspan for four loads at midspan.

Plan View
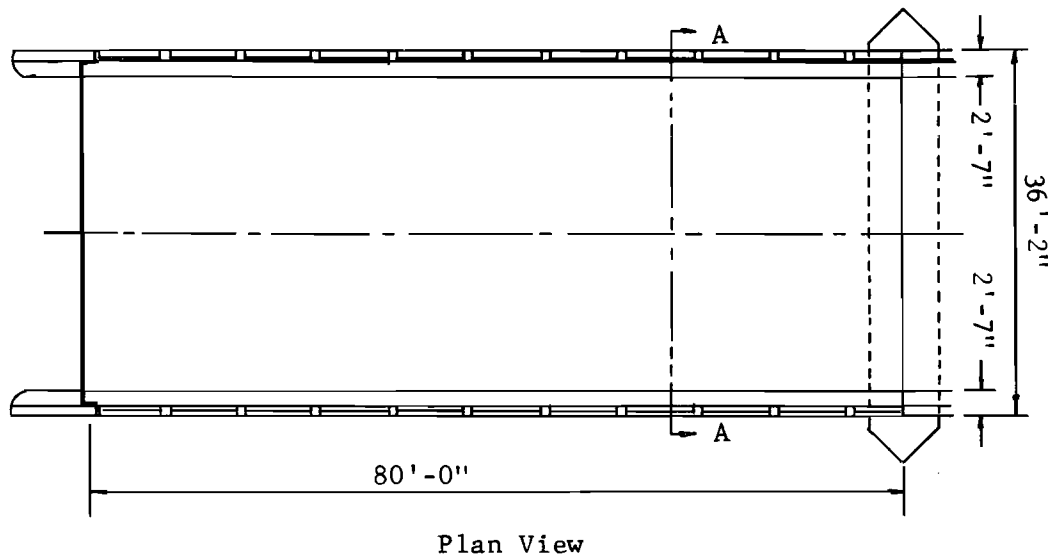
36 WF 230 Girders
with 14" x 1" x 52'
cover PL.

18 ⊏ 42.7 diaphragms
at quarter points

14'-0" 52'-0" 14'-0"

Elevation

9" 31'-0" 1'-7" 1'-0"

1'-2"
1'-0"
0'-7"

1 2 3 4 5

5@ 8'-1½" = 32'-6"
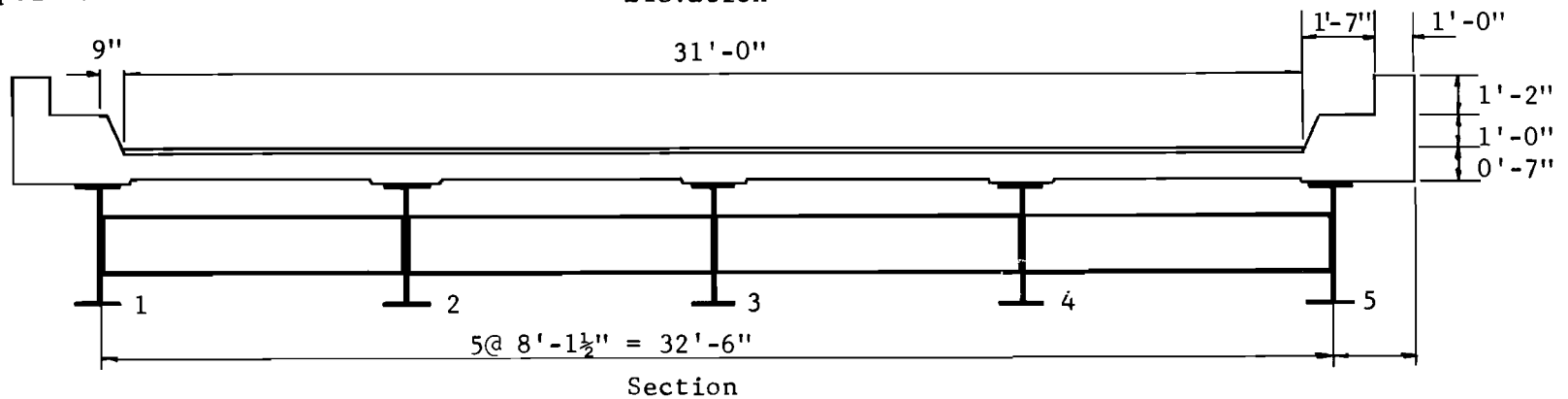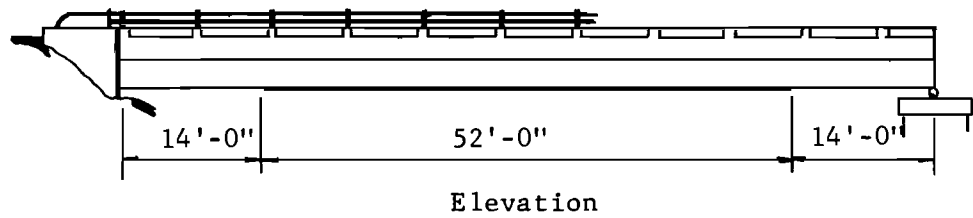
Section

Fig. 6.5. Girder bridge over Patuxent River at MD Route 4.

36'-2"

2'-7"

2'-7"

80'-0"

A

A

A mesh of 16 by 32 increments was used for computer simulation. The smaller number of increments was applied in the transverse direction. The computer study of this structure included (a) two assumptions for evaluating the flexural stiffness of the composite girders, (b) the effect of ignoring Poisson's ratio, (c) the effect of ignoring the girder torsional stiffness, and (d) the effect of the interior diaphragms. The girder flexural stiffnesses were evaluated for two different assumptions as to the effective width of the concrete slab. In one analysis, an effective slab width of only 12 slab thicknesses, according to AASHO specifications,[1] was used to evaluate the girder stiffness. In the other case, girder stiffnesses were obtained for an effective slab width equal to the full spacing distance between beams (14 slab thickness).

Two load cases were considered in the analysis. They are CD12 and CD3, as they were designated in the report.[51] The first load case corresponded to an edge loading while the other case was for a central loading on the bridge. Comparison of tests and analytical results for midspan strains and deflections of beams are shown in Figs. 6.6 and 6.7. The effect of Poisson's ratio on the final results is summarized in Table 6.4.

TABLE 6.4. EFFECT OF POISSON'S RATIO ON FINAL RESULTS

Calculated Function	Load Case	Considering Poisson's Ratio	Ignoring Poisson's Ratio	Error
Maximum Deflection (in.)	CD12	0.2474	0.2487	+0.52%
	CD3	0.2535	0.2505	-1.2%
Maximum Moment (in.-kips)	CD12	6623	6654	+0.52%
	CD3	4256	4211	-1.07%

SLAB40 was used to obtain the theoretical results. The analytical results, as calculated for full center-to-center slab effectiveness in computing girder stiffnesses, were in good agreement with test values. The torsional stiffness of beams had a minor effect on the final theoretical
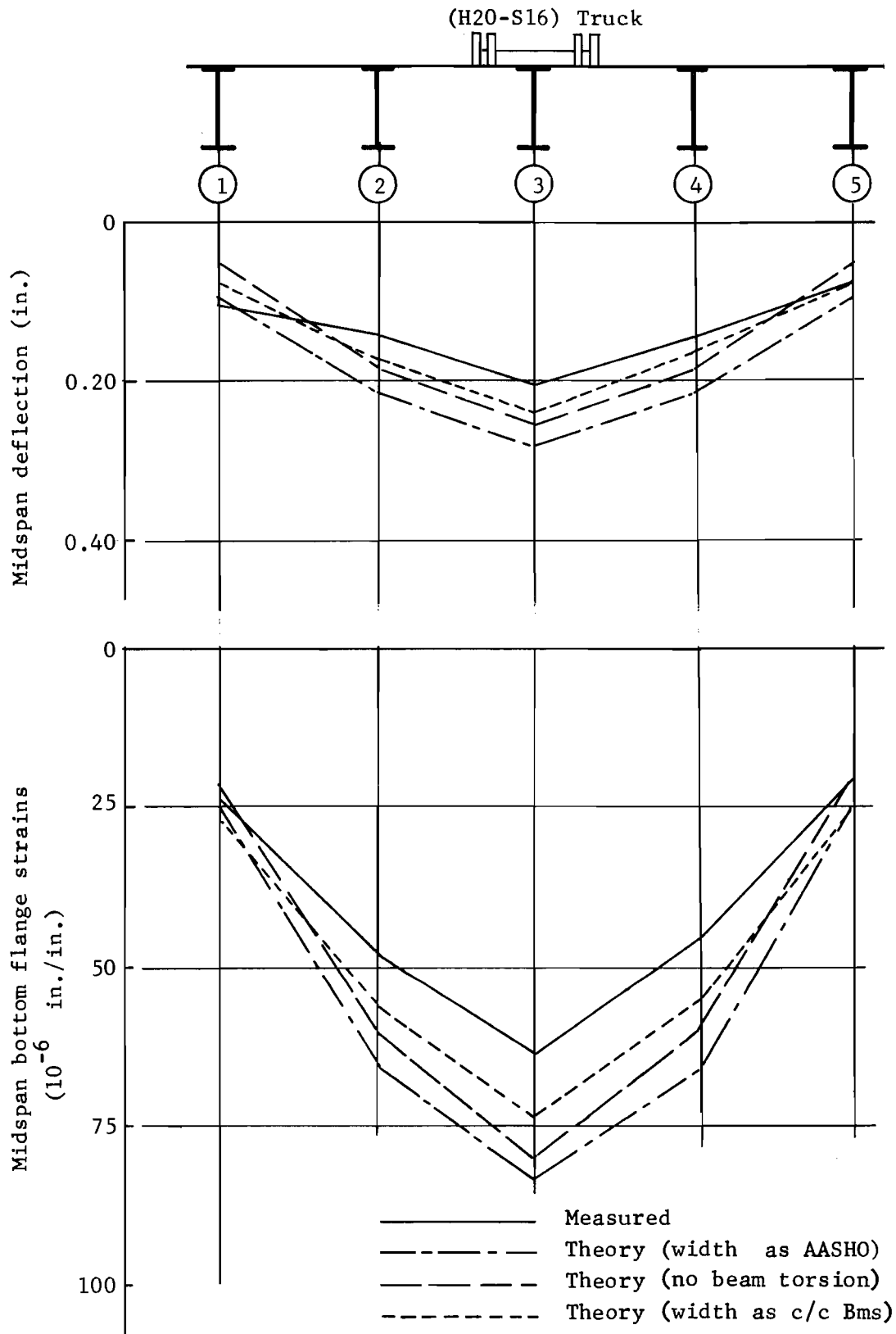
Fig. 6.6. Measured and computed deflection and strain of beams for a central loading truck.
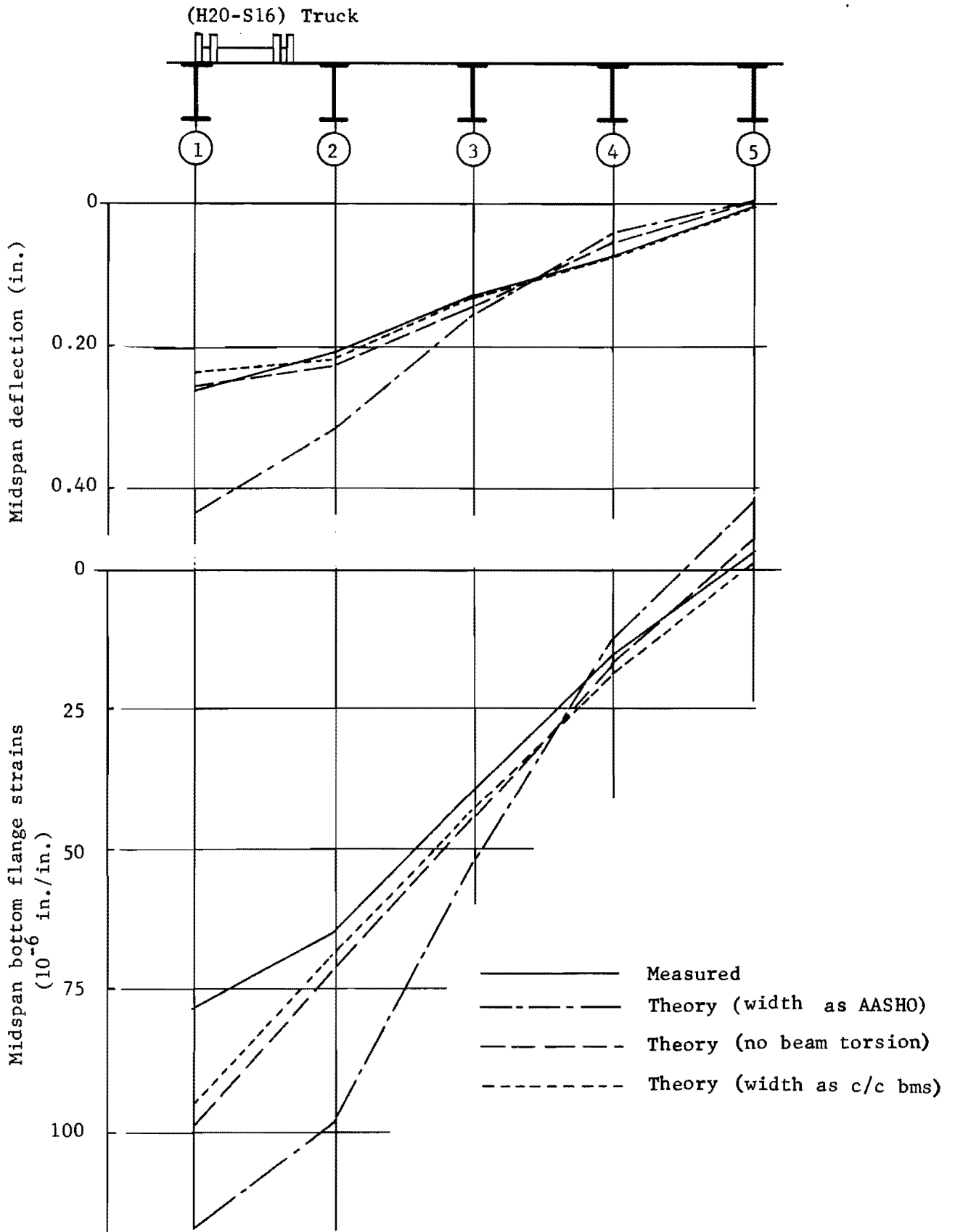
Fig. 6.7. Measured and computed deflection and strain of beams for a
curb loading truck.

results which ranged between 2 and 8 percent when such stiffnesses were
ignored completely. The effect of Poisson's ratio was much lower and could
be considered as negligible, as shown in Table 6.4.

The interior diaphragms between girders were continuous across the
bridge and placed at the quarter points along the span. The flexural
stiffness was calculated as being 1.65 x 10^7 (kip-in.^{2}). This stiffness
is equivalent to a slab strip having a width of 115 in. Ignoring the
stiffness of these diaphragms in the computations changed the final analyti-
cal results approximately 2 percent in terms of maximum deflection and
approximately 2.4 percent in terms of the maximum moment with an edge truck
load (CD 12). Corresponding changes with a central truck load (CD 3) were
6 and 8 percent, respectively. It is obvious that the effectiveness of
the interior diaphragms is greater for the central loading, since the dia-
phragms tend to distribute the load in both directions on either side of
the loaded girders. It should be noted that in this case the diaphragm
stiffnesses are relatively high when compared to the slab stiffness.

The comparison of the theoretical and test results of girder deflec-
tions and strains shown in Fig. 6.6 indicates that the tested bridge was
stiffer than the calculated values. The analytical results show an over-
estimation of the test values by 14 percent in the maximum deflection and
17 percent in the maximum strain. The calculated girder flexural stiffness
was based on assumptions regarding the shape and properties of the concrete
deck. There were no test data reported for the concrete but an assumed
modulus of elasticity of 5000 ksi was presented in the report.[51] The bridge
cross section shows undimensioned haunches in the deck which increased the
slab thickness over the top flange of the girders. This thickness increase
was ignored in the calculation of the girder flexural stiffness used in the
analysis. Taking into account these haunches would increase the girder
stiffness and would yield lower calculated results, the magnitude of such
effects was simulated by an assumed drop of the top steel flange 1.5 in.
below the bottom of the deck with an assumed elasticity of the concrete of
5500 ksi. This caused an increase in the calculated flexural stiffness of
the composite girders by as much as 11 percent. This increase in stiffness
could make the theoretical results very close to the test values and an

excellent correlation would then be obtained. In view of these uncertainties, the accuracy actually obtained is acceptable.

6.4.3 <u>Patuxent River Bridge--Composite Three-Span Continuous</u> <u>Structure</u>. A plan view and a section are shown in Fig. 6.8. The three spans which form this composite, continuous, skew bridge are 65'-85'-65'. The skew angle is 21°-09'. This structure carries the north bound traffic on U.S. Route 1 over the Patuxent River at Laurel, Maryland. The cross section is composed of seven rolled steel beams with additional welded cover plates over the interior supports. The spiral type shear connectors attached to the top flange of beams were embedded in the 7 in. deck slab to ensure composite action. The test results and more details are reported in Ref. 22.

A 24 by 112 increment mesh was used in the simulation of the bridge. The stiffnesses were evaluated from the reported physical properties of the structure. Using the procedures of Secs. 6.2.1 and 6.2.2, the composite action of the sidewalks was considered in the calculation of the flexural stiffness of the exterior girders. Two load cases with BPR trucks were considered in the analysis. They are B1 and F1 as referred to in the report.[22] The BPR truck closely approximated the standard AASHO (H20-S16) truck. Section B is at the middle of the south span, while section F is at the middle of the central span. The number which appears in the load cases refer to a curb loading lane, where the truck passed as close as feasible to the east curb of the bridge.

Figures 6.9 through 6.12 show the comparison of test and calculated results. The measured strains on the girder bottom flanges across section F1 (as shown in Fig. 6.10) indicate a probable defect or mistake in reading or reporting the strain gages for girders 2, 3, and 4. A possible mistake in the values of reported strains for girder 4 is more likely, since there was inconsistency in the values of this point when compared to the same position taken from the distribution of strain along the beam, as shown in the same report.[22] Otherwise, the comparison of tested and calculated results were generally good for both load cases considered in the study.

6.4.4 <u>The University of Illinois Tests 30N15 and 60N15--Noncomposite</u> <u>Simple Span Bridges</u>. Both 30N15 and 60N15 bridge models were one-quarter scale, noncomposite, skewed angle, single-span structures. They were built

North ⟹

Support   Support   ⌐ Steel girder   Support   Support

20°─|9.5'

|←── 65'-0" ──→|←──── 85'-0" ────→|←── 65'-0" ──→|

B   F

Plan View

| | Exterior   Interior

1'-0" ─→|←─ 5'-0" ─→|

Girder Section   36WF160   30WF116

Cover Plate Over Interior Supports

Top   5/16" x 18" x 23.0'   1/2" x 12" x 21.0'

Bottom   1"   x 18" x 23.0'   7/8" x 12" x 21.0'

7"

|←─ 6'-4" ─→|←──── 6 @ 5'-4" = 32'-0" ────→|←─ 6'-4" ─→|

2   3   4   5   6   7   8

3'-1"   11"   4'-9"
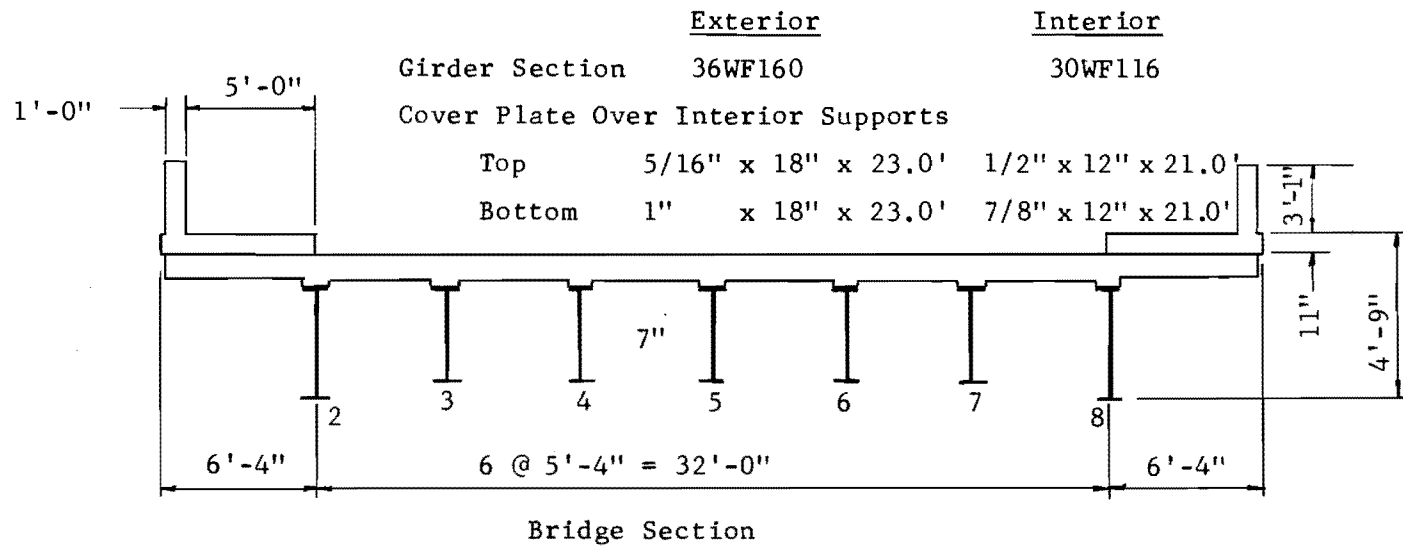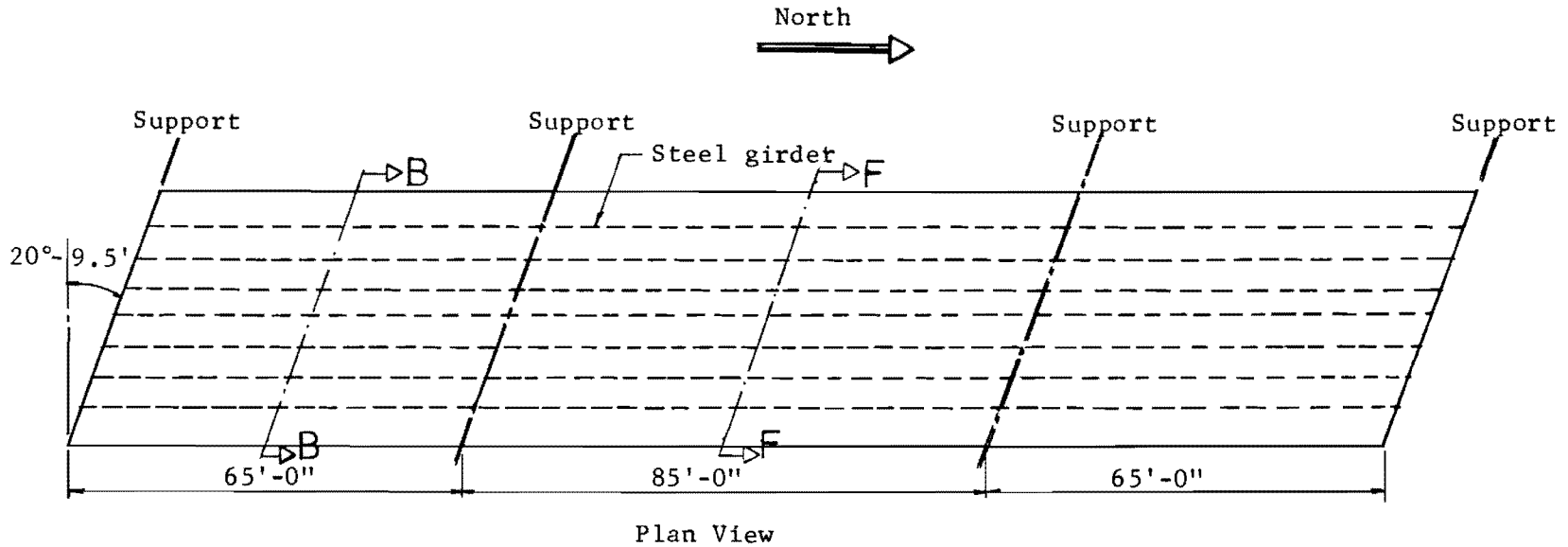
Bridge Section

Fig. 6.8   Patuxent River Bridge--Three-span continuous composite bridge.
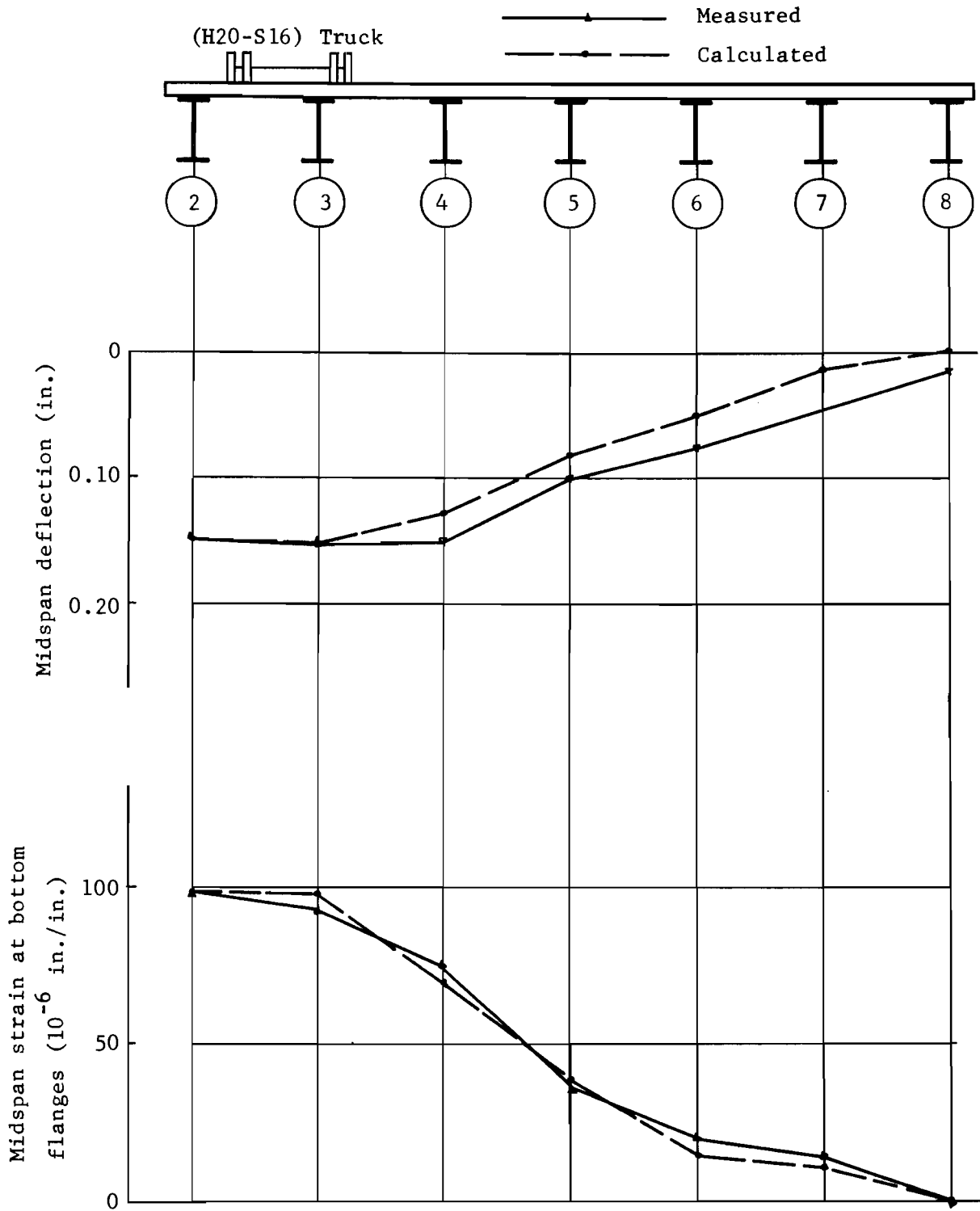
Fig. 6.9 Midspan deflections and strains of girders at section B due
to load case F1 (Pataxent River Bridge).
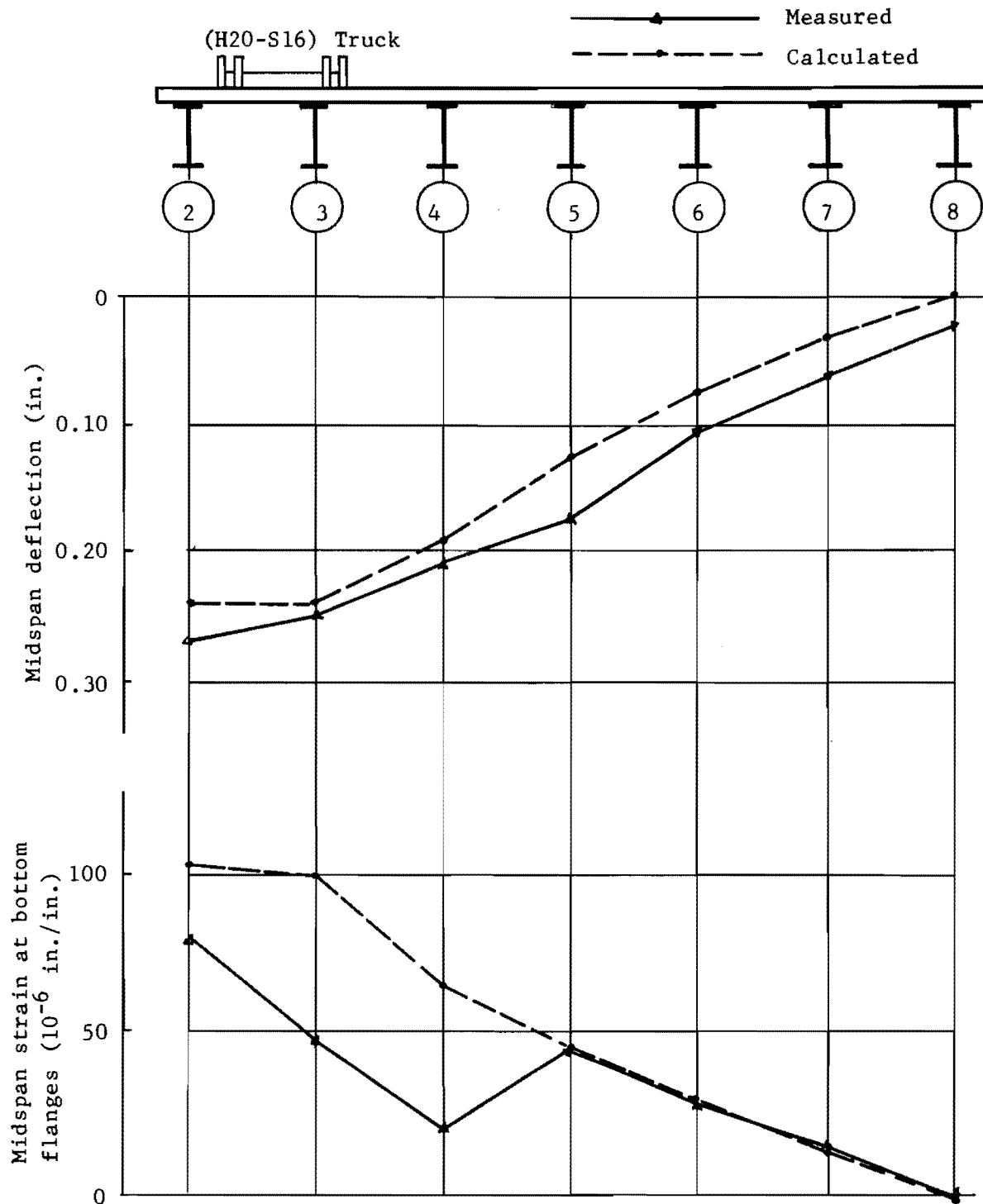
Fig. 6.10 Midspan deflections and strains of girders at section F due to load case Fl (Patuxent River Bridge).
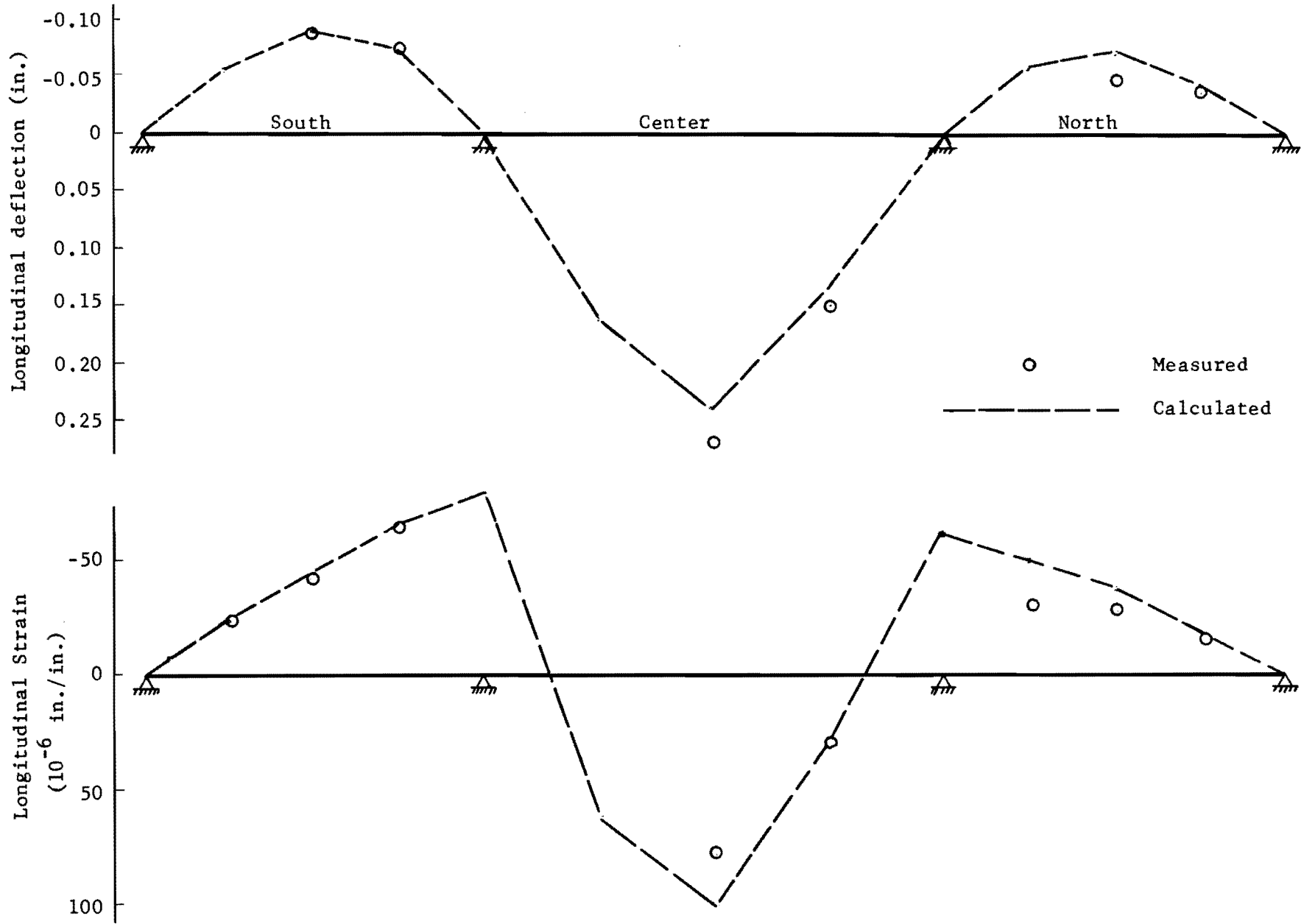
Fig. 6.11 Longitudinal deflection and strain distribution of girder 2 due to load case F1.
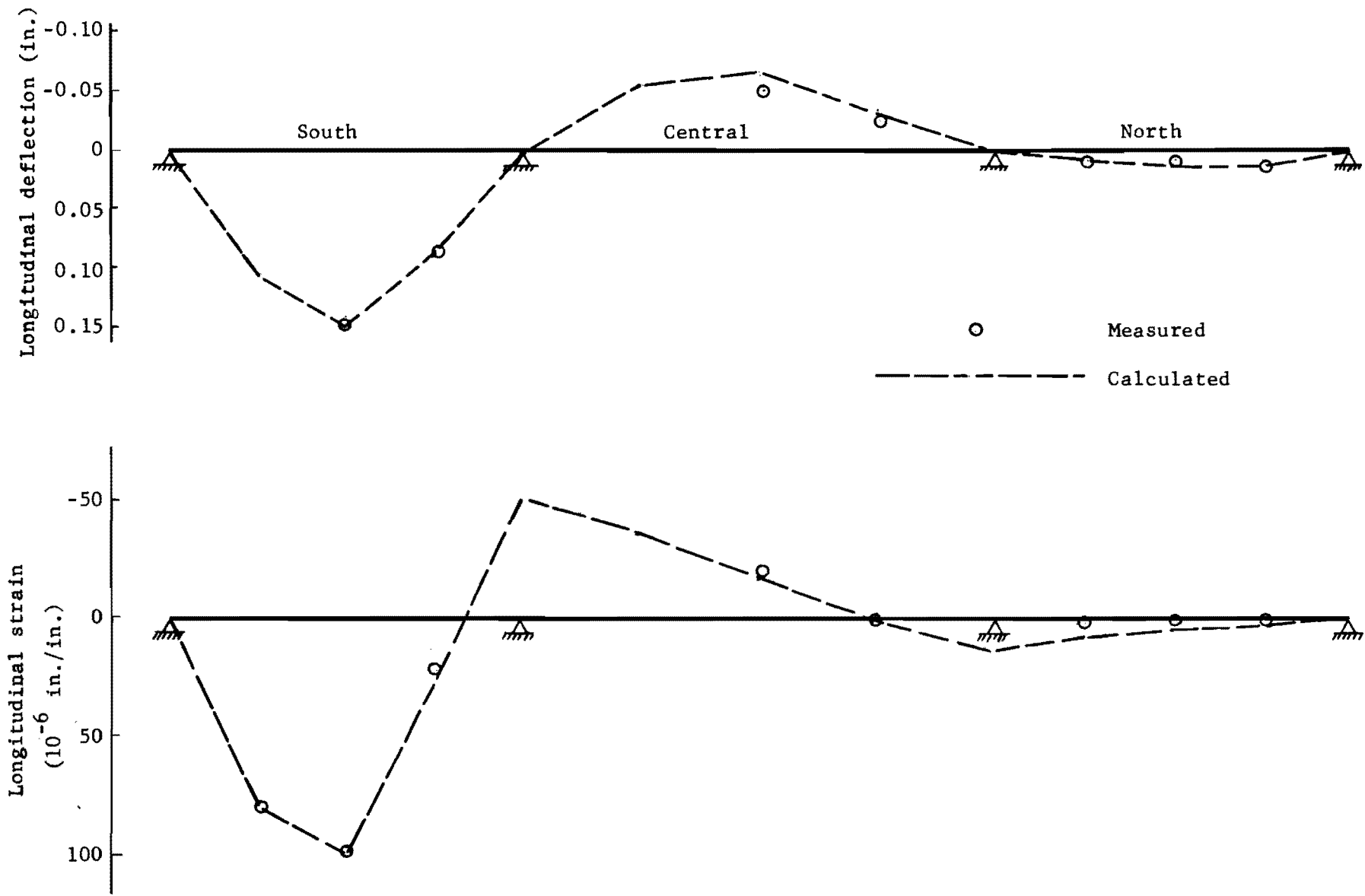
Fig. 6.12 Longitudinal deflection and strain distribution of girder 2 due to load case B1.

140

and tested at the University of Illinois Engineering Experiment Station.[41]
The plan view of each bridge with typical cross section is shown in Fig. 6.13.
The skew angles of the two bridges were 30 and 60 degrees, respectively. A
typical cross section was composed of five identical steel beams of 15 ft.
span length and spaced at 18 in. on centers. No mechanical shear connectors
were attached on the top flanges of the beams. The cast-in-place mortar
reinforced concrete slab had a uniform thickness of 1.75 in.

The mesh used to simulate the bridges had 16 by 22 increments for
model 30N15 and 16 by 20 increments for model 60N15. The flexural and
torsional stiffnesses of the girders were evaluated using Secs. 6.3.1 and
6.3.2. Similar parameters for the slab were evaluated using Secs. 4.2.1
and 4.2.2. Program SLAB43 was used in the solution for the two load cases
considered for a comparison with the test results.

Figures 6.14 and 6.15 show the analytical solution and the test
results for the deflection across section 0 (see Fig. 6.13) of both bridges.
The comparison is very good for bridge 30N15. For bridge 60N15 some devia-
tions resulted in the absolute values, but the shape of the deflection
envelope was very similar.

6.4.5 The University of Illinois Test N30--Noncomposite Continuous
Span Bridge. Bridge N30 was a quarter-scale, two-span continuous, nonskew,
noncomposite bridge. It was built and tested at the University of Illinois
Engineering Experiment Station. The plan view and a cross section of the
bridge are shown in Fig. 6.16. The bridge was composed of five steel beams
spaced at 18 in. on centers and spanning the two continuous spans of 15 ft.
each. No mechanical shear connectors were inserted between the top flanges
and the 1.75 in. cast-in-place mortar reinforced concrete slab. Two load
cases are considered for the comparison of test results with the analytical
solution. All point loads were applied along a section designated as W5 as
shown in the same figure.

SLAB43 was used to obtain the analytical results. The bridge was
simulated with a mesh of 16 by 36 increments. The flexural and torsional
stiffnesses of the girders were evaluated according to Secs. 6.3.1 and 6.3.2.
The same parameters for the slab were evaluated according to Secs. 4.2.1 and
4.2.2. The comparison of test and analytical results is shown for two
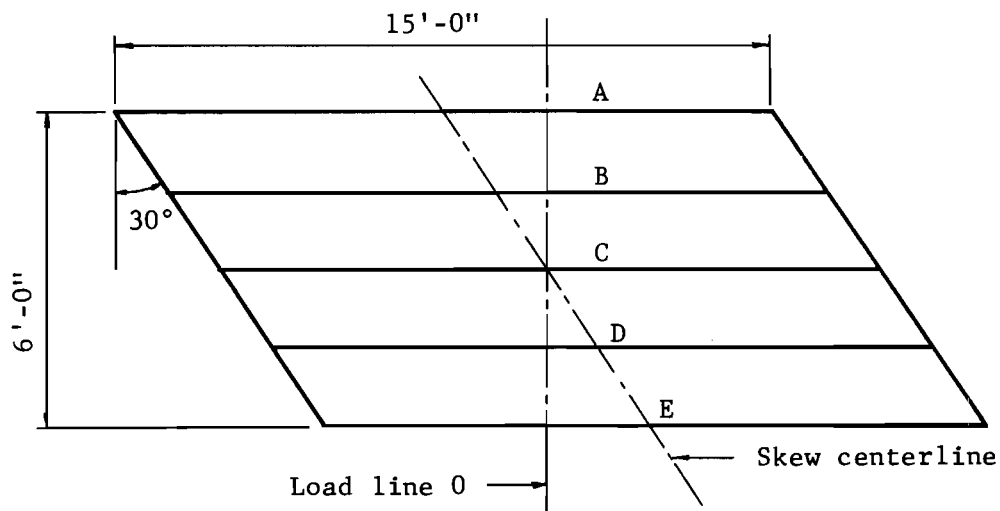
Fig. 6.13a. Layout of bridge 30N15.
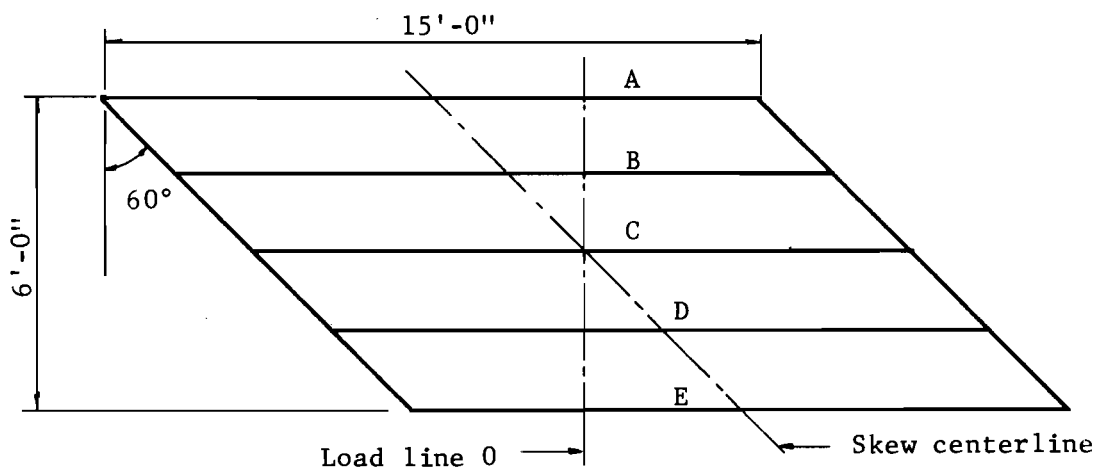
Fig. 6.13b. Layout of bridge 60N15.
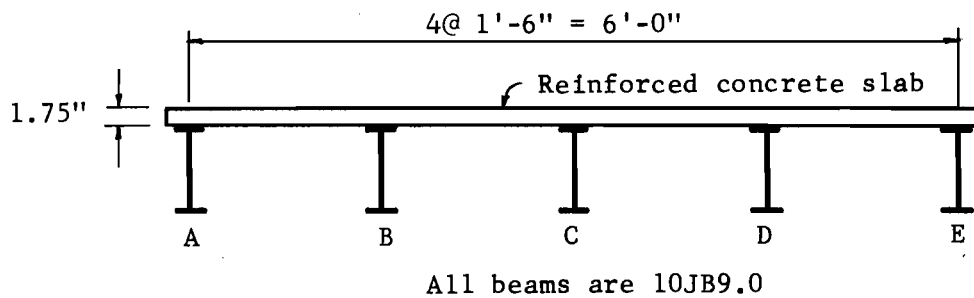
Fig. 6.13c. Typical cross section of bridges along line 0.

P = 3000 lbs

O   Measured
— — — — Calculated
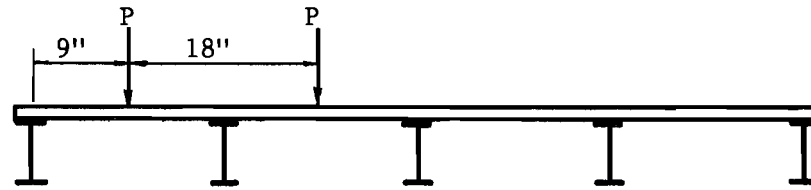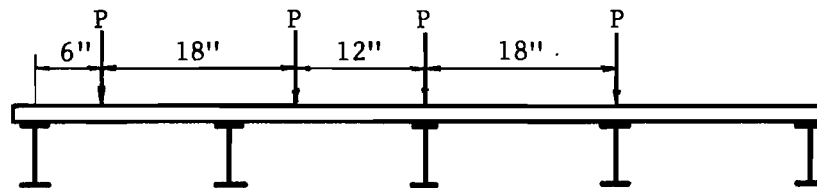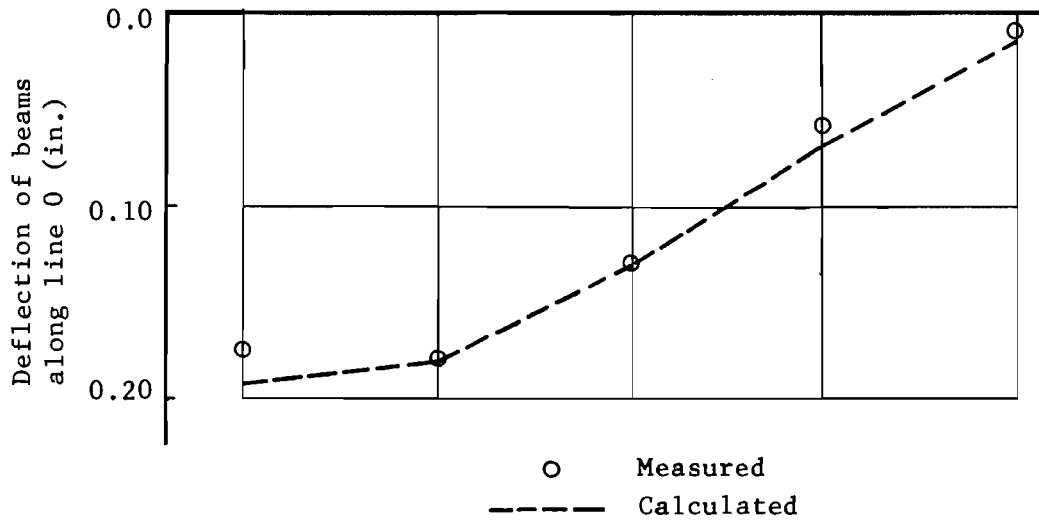
P = 3000 lbs
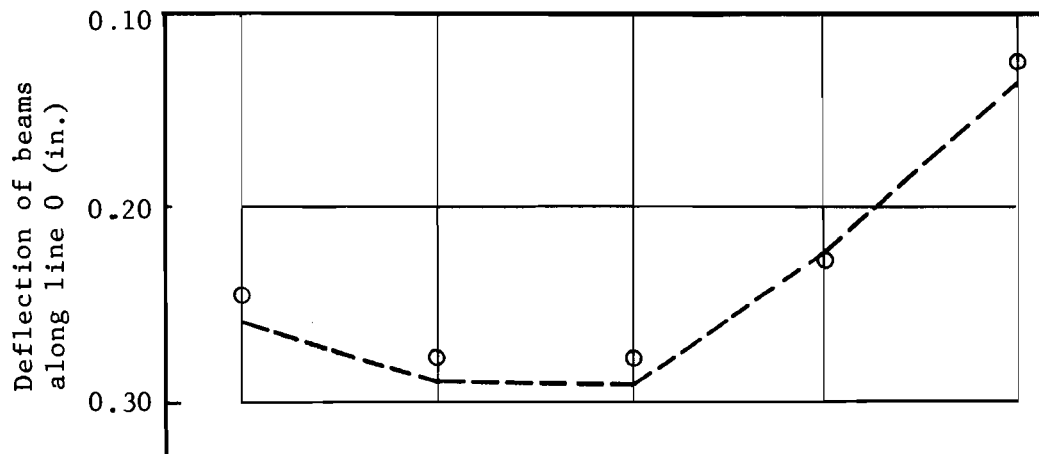
Fig.6.14   Comparison of girder deflection for loads on line)
(Bridge 30N15).

P = 3000 lbs.

O   Measured
— — — Calculated

P = 3000 lbs.
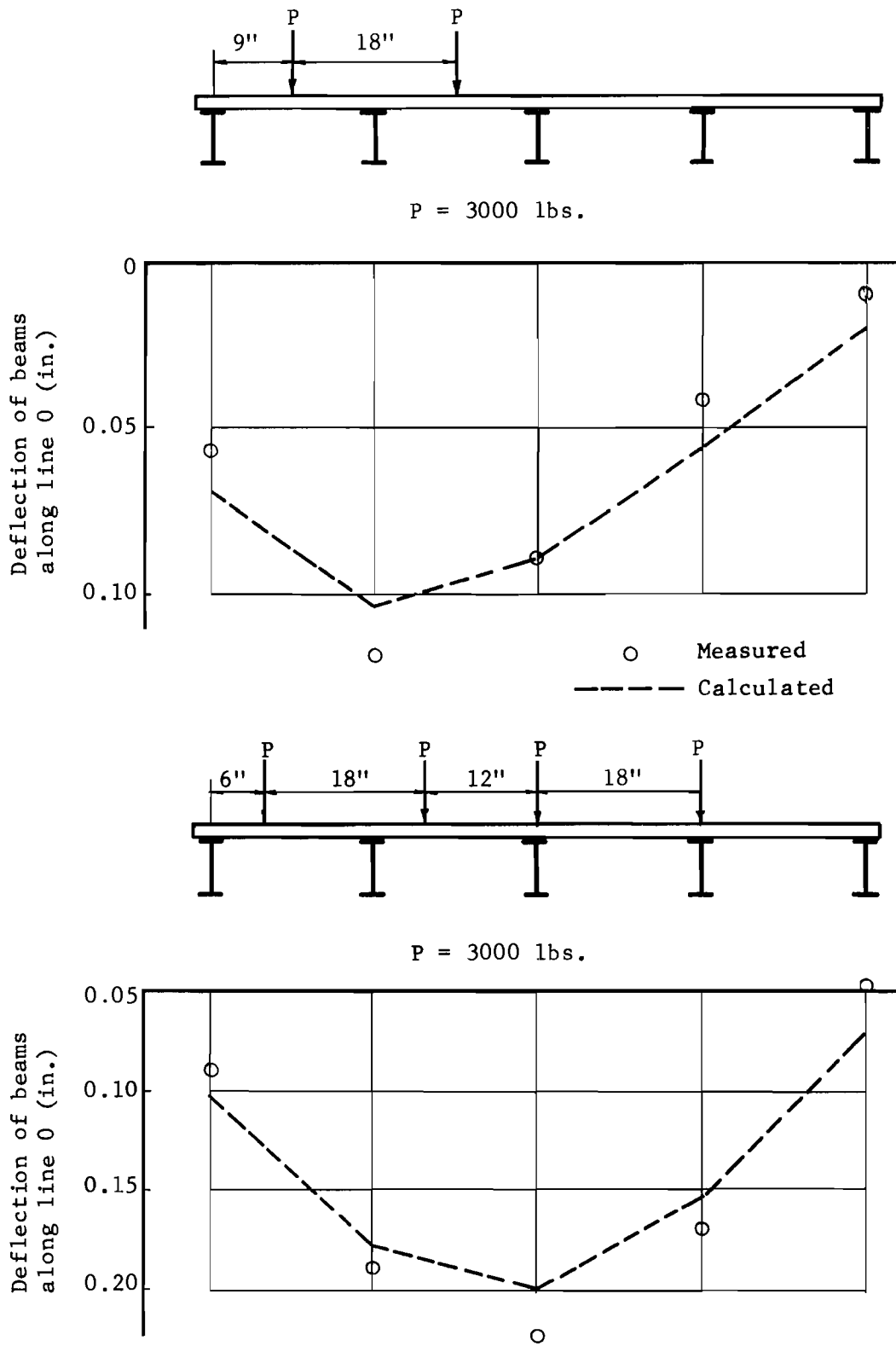
Fig. 6.15 Comparison of girder deflection for loads on line 0
            (Bridge 60N15).

15'-0"   15'-0"

A

B

C

D

E

6'-0"

8'-6"

Sec. 0   Sec. W5
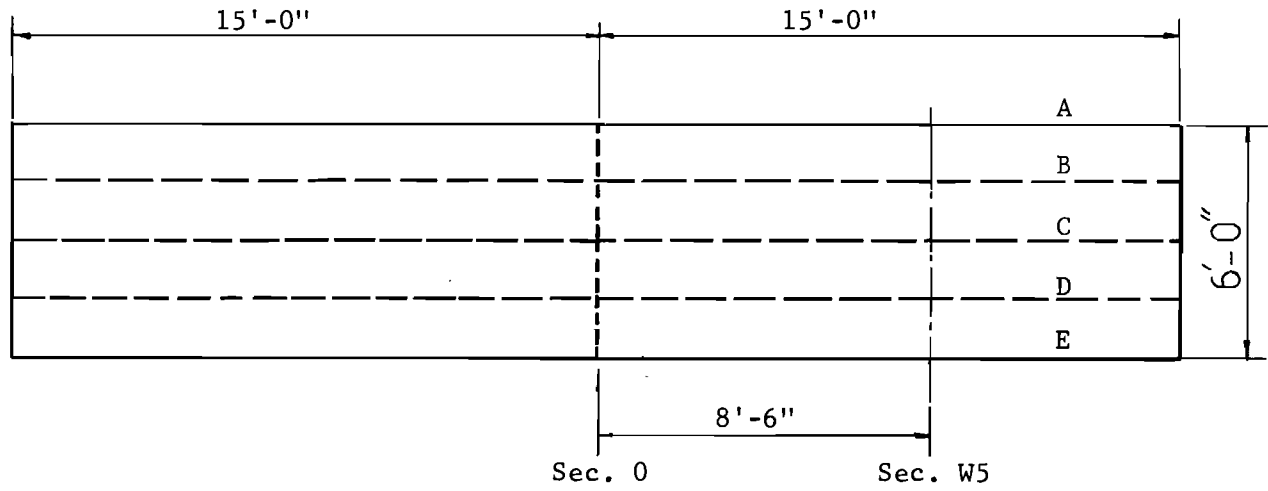
All beams 9JB7.5

Ext. diaphragms 9JB7.5

Int. diaphragms 4⊏5.4

Plan View

1-3/4"

4@ 1'-6" = 6'-0"

Cross Section

1-3/4" Mortar slab

Diaphragm   Diaphragm

15'-0"   15'-0"
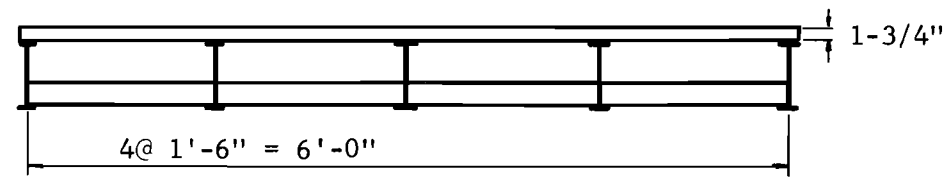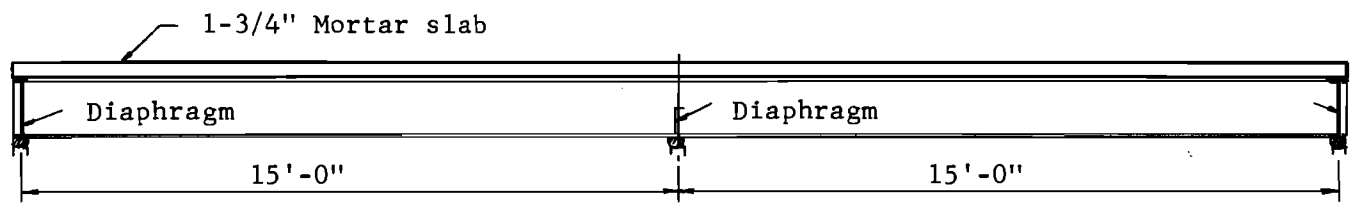
Longitudinal Section

Fig.6.16   Detail of the noncomposite two-span bridge (N30).

sections. Section W5, where the deflection and strain distributions of beams were compared, was the section of maximum positive moment in the beams. The maximum negative moments naturally occur at the interior support and, hence, the strain distribution in the beams was compared along section 0. The results for both load cases are shown in Figs. 6.17 and 6.18. The comparison of test results indicated very good agreement with the analytical solutions.

6.5 The Effect of Composite Action on the Bridge Performance

Table 6.1 presented a summary of the performance of two nearly identical composite and noncomposite bridges. The comparison indicates clearly the favorable effect of the composite action in the performance of the bridge. The comparisons showed that due to the composite action the stiffness of the bridge was tripled and, accordingly, the measured live load deflection of the central beam was only one-third that of the non-composite bridge. The composite action reduced the average impact to 44 percent of the noncomposite bridge.

Comparison of two nearly identical bridges S15 and N15 also show the effect of composite action. Both bridges were tested and reported by Newmark, Siess, and Penman.[42] The composite bridge S15 was presented in Sec. 6.4.1. The similar but noncomposite bridge N15 was analyzed using SLAB36.[30] The deflection of the beams due to four point loads applied at midspan of the bridges is shown in Fig. 6.19. The comparison of the test and analytical results for both bridges are excellent, indicating the accuracy of the theoretical predictions and also the effect of composite action on bridge performance.

The three-span continuous skew and composite bridge presented in Sec. 6.4.3 was reanalyzed on the assumption that no composite action existed between the steel girders and the concrete deck. Girder stiffnesses were evaluated for the noncomposite sections. Analytical results are shown in Fig. 6.20 together with the previous analysis of the bridge and the test values for the deflection along section F1 for a curb lane truck load. The comparison also indicates that the maximum deflection would have been tripled if it had been built noncompositely and that composite action can be modeled.
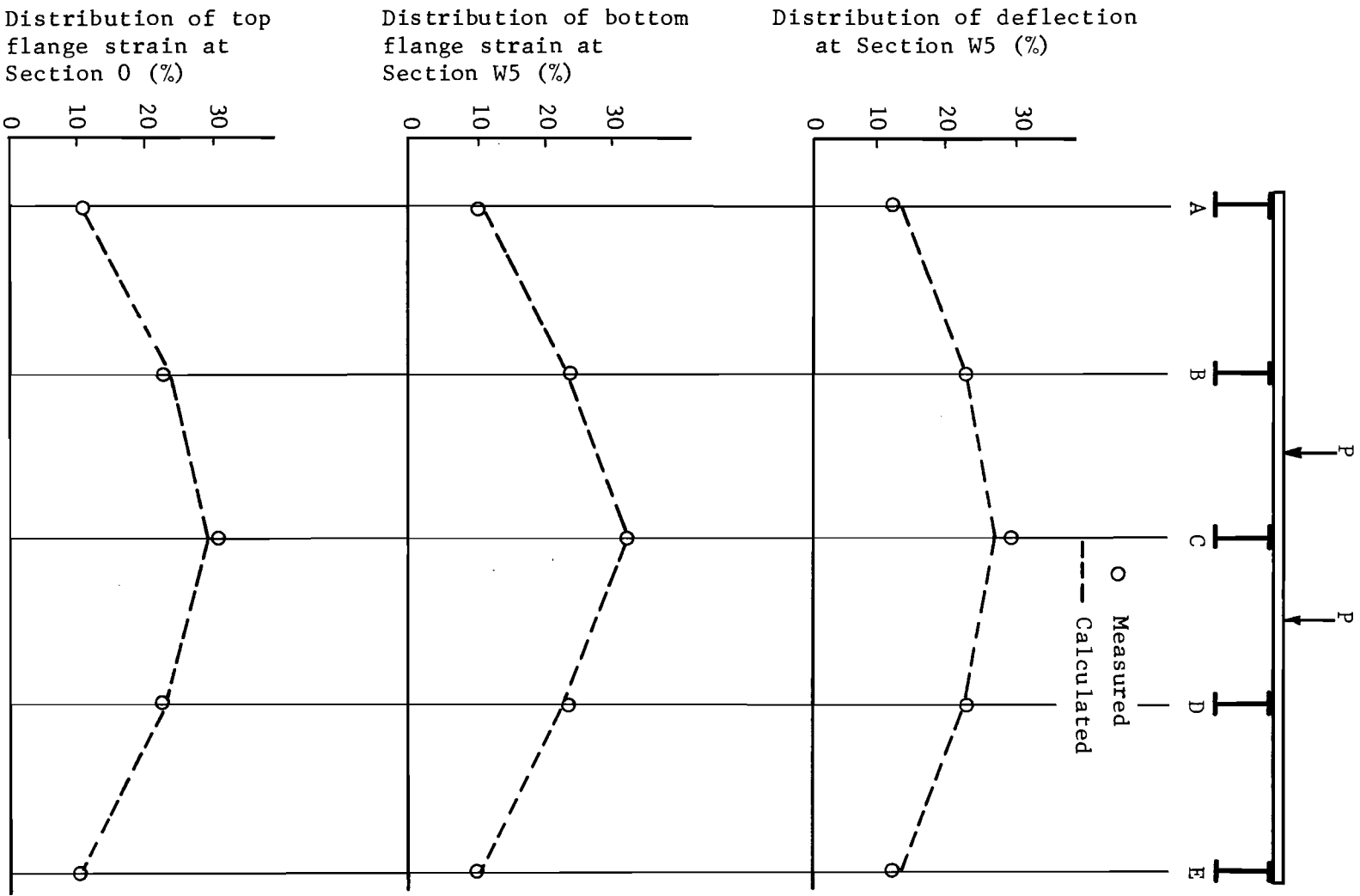
Fig. 6.17 Comparison of measured and calculated deflection and strain distribution of beams for loads applied at Section W5.
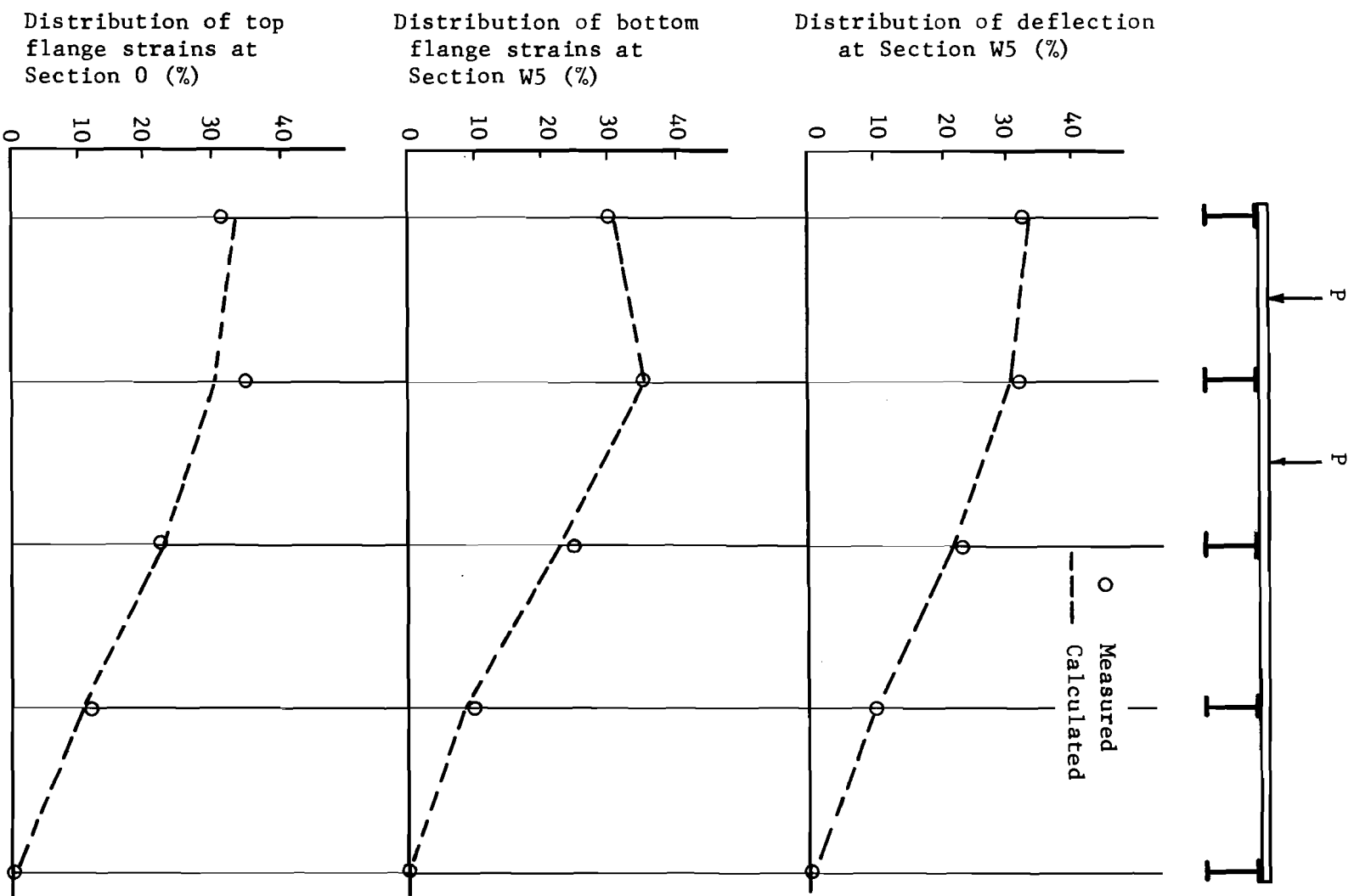
Fig. 6.18 Comparison of measured and calculated deflection and strain distribution of beams for loads applied at Section W5.

P   P   P   P

P = 5000#

①   ②   ③   ④   ⑤

0.40

Noncomposite (N15)

— — — Theory

□   Test

Midspan deflection

0.20

Composite (S15)

——— Theory

○   Test

0
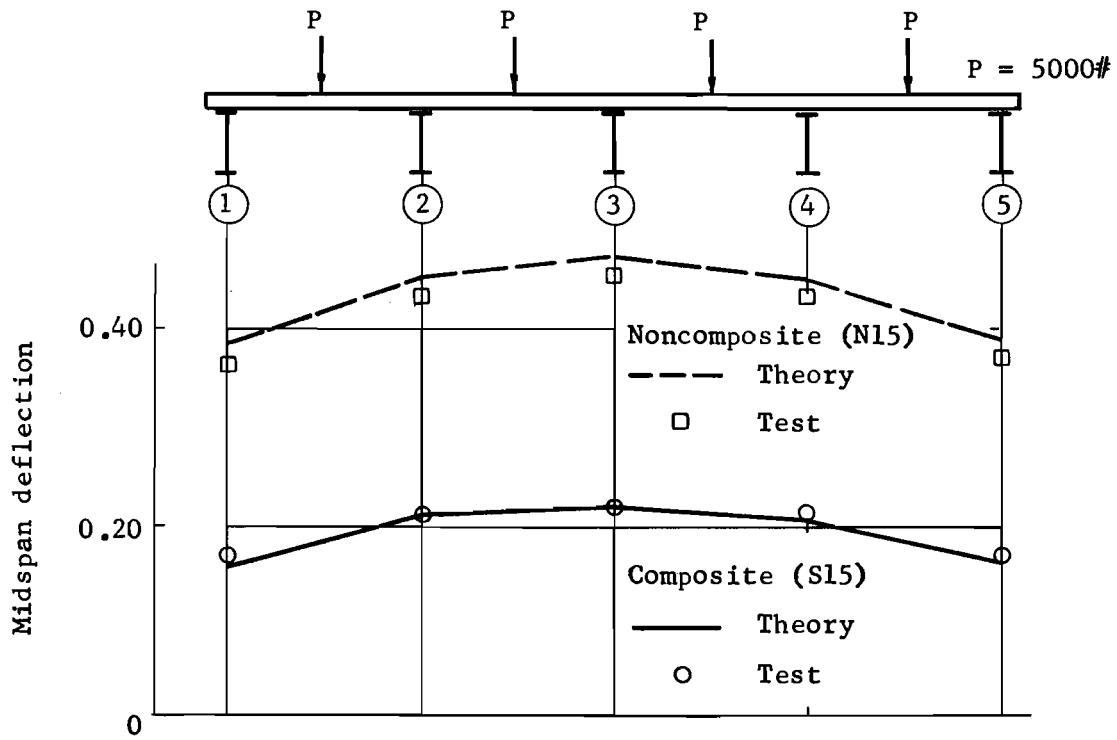
Fig. 6.19   Deflection of beams for bridges S15 and N15.

(H20-S16) Truck

②   ③   ④   ⑤   ⑥   ⑦   ⑧

0.80

○   Test

——— Theory (composite)

0.60

— — — Theory
            (noncomposite)

0.40

Girders deflection at Section F1

0.20

0
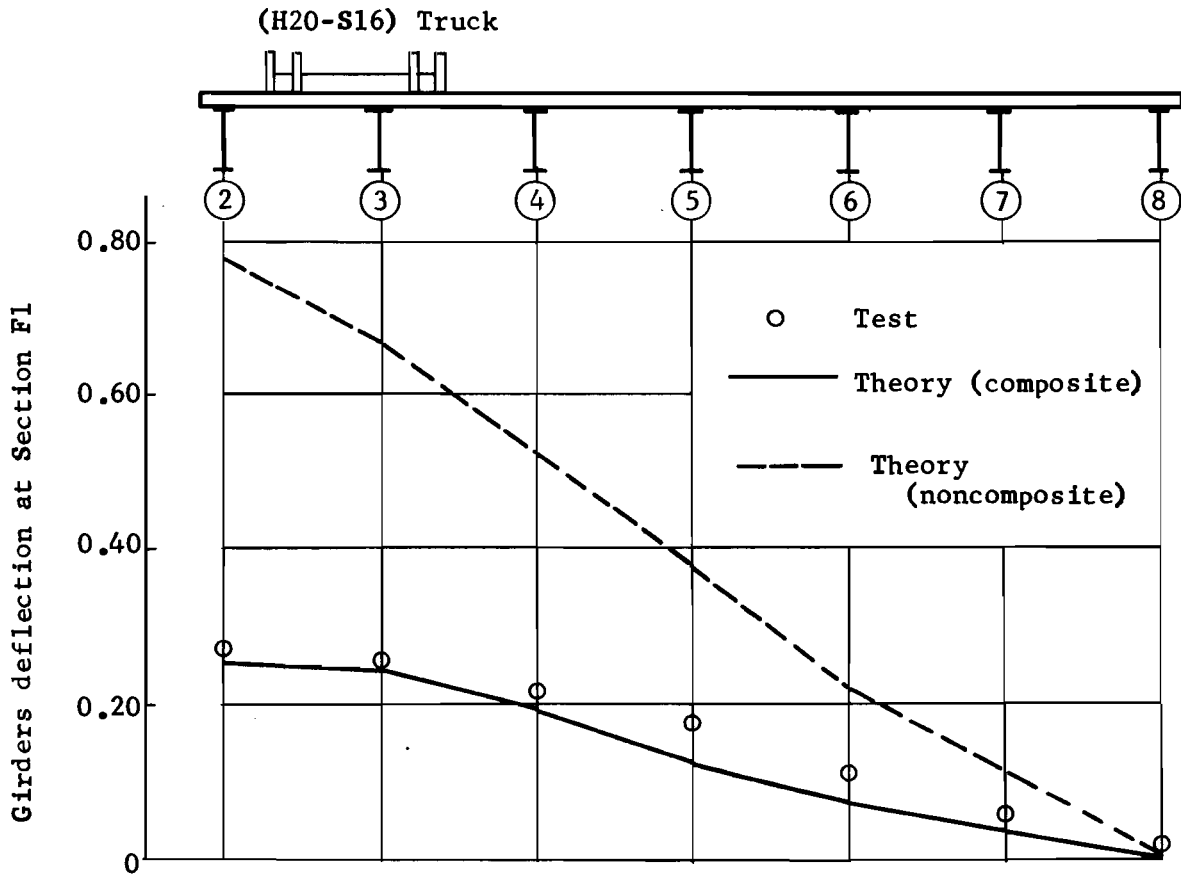
Fig. 6.20   Patuxent River Bridge--3 span continuous, skew and
composite (truck at middle span).

6.6 Recommendation for Analysis of Steel Girder Bridges

The general requirements of computer simulation methods discussed in Sec. 4.5.1 are fully applicable for steel girder bridges. Furthermore, slab stiffnesses and Poisson's ratio can be evaluated from Sec. 4.5.2. Evaluation of flexural and torsional stiffnesses of girders for either composite or noncomposite steel girder bridges can be obtained as follows.

6.6.1 Girder Stiffnesses for a Composite Bridge.

The flexural stiffness of a girder in a composite bridge can be evaluated as an isolated composite steel and concrete section. The elastic transformed section method described in Sec. 6.2.1 may be used for such calculations. The effective width of the concrete slab may be assumed equal to the spacing of the steel girders. For all but one bridge studied in this chapter this assumption agreed with the requirements of the standard AASHO specifications.[1] A reduced effective slab width, corresponding to the AASHO specifications, showed a larger underestimation of the stiffness of the other bridge as presented in Sec. 6.4.2.

If required, the torsional stiffness of the isolated composite section can be obtained directly by using the computer program TORSION. This program is based on the analytical study presented in Sec. 6.2.2.

6.6.2 Girder Stiffnesses of Noncomposite Bridges.

The evaluation of flexural and torsional stiffnesses of the girders in a noncomposite bridge represent a fairly simple case. In this type of bridge construction only the elastic properties of the steel sections need be considered. For a rolled steel section the stiffnesses can be evaluated directly from the handbooks.[4,23] Also, the flexural stiffnesses (EI) of a built-up section can easily be obtained. As described in Eq. 6.7, the torsional stiffness (KG) of such sections is obtained by calculating the torsional rigidity (K) for a thin-walled section.

CHAPTER VII

CONCLUSIONS AND RECOMMENDATIONS

7.1 Summary of the Study

This study investigated the accuracy of treating slab and girder
bridge systems as special cases of orthotropic plates. The general theory
of plates and of the discrete element methods of solution were briefly
presented in order to develop an understanding of the effect of variables.
Computer simulation procedures for physical systems utilizing the SLAB
programs were studied for each type of bridge system. (The previously
developed SLAB program utilizes the discrete element method of solution.)
The bridge types investigated used prestressed concrete, reinforced con-
crete, and both composite and noncomposite steel girders. Evaluation of
solution parameters showed that the flexural stiffness of the girders
dominates the final results. The torsional stiffness of girders was con-
sidered second in importance in the solution, but was found to not be a
primary factor. Methods for evaluating girder flexural and torsional stiff-
ness for each type bridge are discussed in Sec. 7.2.

The computer programs were used to obtain analytical solutions for
comparison with physical measurements from a series of test bridges.
Thirteen bridges were analyzed and comparisons were made with reported
test results. Both simple and continuous span bridges with and without
skew were investigated. The computer simulation methods and the evaluation
of parameters were discussed for each bridge. The comparisons between
measured and computed values in general were excellent, as can be seen from
the data presented in the figures throughout the study.

7.2 Flexural and Torsional Stiffness of Girders

Determination of girder flexural stiffness for each type of bridge
was outlined. For the prestressed concrete and steel girder bridges it was

151

found that elaborate methods (such as nonlinear moment curvature relationships) are ordinarily unnecessary, since adequate estimates can be found from the elastic transformed stiffnesses (EI) of the members. These simpler estimates are generally adequate in the service load and moderate overload regions. More accurate moment-curvature relationships should be used to evaluate the stiffnesses in the ultimate load ranges.

However, the nonlinear behavior of a reinforced concrete girder starts at a much earlier stage of loading and may often include the service load region. This behavior is mainly due to the formation of flexural cracks. In most cases the dead load of the bridge when coupled with shrinkage stresses is enough to produce such cracks in the highly stressed zones. While and upper and lower limits of the flexural stiffness of a reinforced concrete member can be adequately defined by calculating the elastic transformed gross and cracked moments of inertia for the section, neither value can be considered as an adequate estimate of the stiffness of the cracked region for service load conditions. A survey of several computer programs previously written to generate this moment-curvature relationship showed inconsistency with the behavior of tested members. The effective moment of inertia of a cracked section, based on the proposed equation of ACI Committee 435, was used to estimate the flexural stiffness of reinforced concrete members. This method showed better agreement than the previous programs when compared to test results. The ACI Committee 435 method was based on an interpolation between the values of the gross and cracked moment of inertia of the section using an empirical equation for the effective inertia.

Previous work was extended in this study to take into account the effect of crack formation on member behavior. A computer program entitled MPHI was written to generate the theoretical moment curvature relationship for a reinforced concrete member where cracks are anticipated. This theoretical prediction was in excellent agreement with test results shown. The comparisons include both reinforced concrete beams and columns. Values from this MPHI program were shown to give the best correlation in relation to test results. The program was used to generate girder flexural stiffnesses for the test bridges and a good correlation was obtained in the final analysis of these bridges. Poor correlation was obtained when values from

elastic gross or cracked transformed moment of inertia or values from previous moment-curvature programs were used in the analysis.

The girder torsional stiffness was investigated and a method for estimating the stiffness of each bridge type was presented. It was shown that the estimates provided adequate accuracy for analytical purposes.

7.3 Conclusions and Recommendations

Thirteen varied slab and girder bridge types were covered in the present study. Based on the range of variables represented in this representative sample of bridges analyzed using the SLAB programs, the following conclusions can be drawn:

(1) Discrete element computer simulations of slab and girder bridge systems as orthotropic plates yield accurate results when properly evaluated parameters are used in the solution. The most important parameter for such systems was the flexural stiffness of the girders. The torsional stiffness of the girders was considered as the second parameter but was found to be far from critical.

(2) The discrete element method was very accurate for bridges with skew angles up to 45° and only somewhat less accurate at 60° skew angles.

(3) The mesh size needed to accurately simulate the bridges is a function of the number of girders, the number of spans, and the skew angle. Four to seven transverse increments between girders is recommended for general use. A greater number of increments may be used but a number less than four should not be considered. In the longitudinal direction, 16 to 40 increments are suggested for each span.

(4) More accurate results are obtained when applied load points match the mesh nodes. Loads which fall inside a mesh should be statically distributed to the four nodes that bound that mesh.

(5) Program SLAB was very accurate for a variety of continuous bridges.

(6) The flexural stiffness of girders is the dominant parameter affecting the results. The elastic transformed stiffness (EI) can be used in the service load analysis of bridges with either prestressed

concrete or steel girders. The flexural stiffness obtained from the MPHI computer program should be used for reinforced concrete girders.

(7) In the present usage of the SLAB program for reinforced concrete bridges, final results need be obtained by an iterative method. The only variable in each iteration is the flexural stiffness of the girders. Gross stiffness can be used as the first estimate to determine approximate moments on each section. Revised stiffness corresponding to this moment level is determined from the moment-curvature relationship given by the MPHI program and used in the following iteration. Stiffnesses are refined in this fashion until moments converge. Ordinarily only one or two cycles are needed. Moments must correspond to the total moment on the section. Obviously, the dead load moment must be incorporated in the analysis.

(8) Ignoring the girder torsional stiffness produced less than 10 percent deviation in the final results. A method was suggested for each type of bridge to evaluate this parameter with as much accuracy as warranted in view of the lack of sensitivity of the solution to this parameter. For the case of composite steel and concrete sections the computer program TORSION can be used to compute the stiffness. The input of girder torsional stiffness in the DSLAB program requires the simulation of such stiffness into a mesh stiffness. Since the mesh is ordinarily chosen so that the girder axis is on a mesh boundary line, half of the girder stiffness must be placed in the mesh element on each side of the axis. The stiffness is input as a stiffness per unit width by dividing by the width of the mesh.

(9) The average values of Poisson's ratio (ν) for concrete may be used as 0.16, and for steel as 0.30. Ignoring this parameter in the analysis has an effect of only about 1 percent on the final results.

(10) Slab stiffness represents a very small fraction of longitudinal bridge stiffness. In most cases slab flexural stiffnesses are less than 1/1000th that of girders. Therefore, the influence of the variations in slab stiffness on the final results was small. These

stiffnesses can be evaluated using the elastic expressions
presented in Secs. 4.2.1 and 4.2.2.

(11) The effective width of the slab to be considered as acting with
the composite girder for most of the bridges checked in the
study agreed with the requirements of AASHO specifications. For
sections which disagreed with the specification, the best results
were obtained using stiffnesses based on the effective slab width
as equal to the spacing between girders. Further experimental
evidence is required to evaluate this parameter for unusual
conditions.

(12) The effect of the interior diaphragms on the final analytical
solutions depends on their type, location, and method of connec-
tion to girders. Discontinuous diaphragms connecting the girders
seem less effective in the distribution of the loads. A larger
number of continuous diaphragms present in a bridge provides a
better chance of having a diaphragm close to the loaded point and
thus provides a greater effectiveness. The ratio of diaphragm
stiffness to slab stiffness is an important factor which determines
the amount of the influence on the solution. A ratio less than
about 30 may be considered to have a negligible effect on the final
analytical results and, therefore, need not be considered in the
simulation process. This reduces the input data and simplifies
the solution.

R E F E R E N C E S

1. American Association of State Highway Officials, <u>Standard Specifications for Highway Bridges</u>, Tenth Ed., 1969.

2. American Concrete Institute, <u>Building Code Requirements for Reinforced Concrete</u>, Detroit, Mich., June 1963.

3. American Concrete Institute Committee 435, "Deflections of Reinforced Flexural Members," <u>ACI Journal</u>, Proceedings V. 63, No. 6, June 1966, pp. 637-674.

4. American Institute of Steel Construction, <u>Manual of Steel Construction</u>, Sixth Edition, 1963.

5. Antoni, C. M., and Corbisiero, J. A., "Instrumentation and Testing of Concrete Bridges Reinforced with High-Strength Steel," <u>Research Report 68-3</u>, New York State Department of Transportation, Albany, Sept. 1968.

6. Bakir, N. N., "A Study of a 45° Skew Simply Supported Prestressed Concrete Bridge," M. S. Thesis, The University of Texas at Austin, May 1970.

7. Barboza, N. J., "Load Distribution in a Skew Prestressed Concrete Bridge," M. S. Thesis, The University of Texas at Austin, 1969.

8. Beedle, L. S., <u>Plastic Design of Steel Frames</u>, John Wiley & Sons, Inc., New York, 1966.

9. Beedle, L. S., and Tall, L., "Basic Column Strength," Trans. <u>Journal of the Structural Division ASCE</u>, Vol. 127, 1962, Part II, p. 167.

10. Billig, K., <u>Structural Concrete</u>, London, Macmillan & Co., Ltd. 1960.

11. Borges, J. F., and Lima, J. A., "Formation of Cracks in Beams with Low Percentage of Reinforcement," <u>Rilem, Symposium on Bond and Crack Formation in Reinforced Concrete</u>, Stockholm, 1957.

12. Borges, J. F., Lima, J. A., Coelho, A. T., and Monteiro, V., "Analytical Results Concerning the Non-Linear Behavior of Reinforced Concrete Structures," Laboratorio Nacional de Engenharia Civil--<u>Memoria No. 294</u>, Lisboa, 1967.

13. Borges, F. J., and Oliveira, A. E., E. R., "Non-Linear Analysis of Reinforced Concrete Structures" <u>Publications</u>, International Association for Bridge and Structural Engineering, Vol. 23, 1963.

158

14. Breen, J. E., "The Restrained Long Concrete Columns as a Part of a Rectangular Frame," Ph.D. Dissertation, The University of Texas, Austin, June 1962.

15. Chang, D. C., "A Numerical Method of Analyzing Composite Prestressed Concrete Members," M. S. Thesis, The University of Texas at Austin, May 1969.

16. Endres, F. E., and Matlock, H., "An Algebraic Equation Process Formulated in Anticipation of Banded Linear Equations," Research Report 56-19, Center for Highway Research, The University of Texas at Austin.

17. Ferguson, P. M., Reinforced Concrete Fundamentals, John Wiley & Sons, Inc., New York, 1966.

18. Fowler, T. J., "Reinforced Concrete Columns Governed by Concrete Compression," Ph.D. Dissertation, The University of Texas at Austin, 1966.

19. Franz, G., and Karlsruhe, H. B., "Verformugsuersuche an Stahlbeton Balken Mit Hochfestem Bewehrungsstahl," Deutscher Ausschoss fur Stahlbeton--Heft 188, Berlin, 1967.

20. Galambos, T. V., Structural Members and Frames, Prentice-Hall, Inc., Englewood Cliffs, New Jersey, 1968.

21. Gillett, H. W., The Behavior of Engineering Metals, John Wiley & Sons, Inc., New York, 1951.

22. Heins, C. P., Jr., Sartwell, A. D., and Looney, C. T. G., "A Study of a Three Span Continuous Bridge Structure," Progress Report, Civil Engineering Department, The University of Maryland at College Park, Maryland, June 1968.

23. Heins, C. P., Jr., and Seaburg, P. A., "Torsion Analysis of Rolled Steel Sections," Bethlehem Steel Co., Steel Design File No. 13-A-1, 1964.

24. Highway Research Board, "The AASHO Road Test," Special Report 61D, Publication No. 953, National Academy of Sciences--National Research Council, 1962.

25. Hognestad, E., "A Study of Combined Bending and Axial Load in Reinforced Concrete Members," University of Illinois Eng. Exp. Sta., Bulletin No. 399, Nov. 1951.

26. Hudson, W. R., "Discontinuous Orthotropic Plates and Pavement Slabs," Ph.D. Dissertation, The University of Texas, Austin, August 1965.

27. Hudson, W. R., and Matlock, H., "Discontinuous Orthotropic Plates and Pavement Slabs," Research Report 56-6, Center for Highway Research, The University of Texas at Austin, May 1966.

28. Ingram, W. B., and Matlock, H., "A Finite Element Method for Bending Analysis of Layered Structural Systems," <u>Research Report 56-5</u>, Center for Highway Research, The University of Texas at Austin, June 1967.

29. Janney, J. L., and Eney, W. J., "Full Scale Test of Bridge on Northern Illinois Toll Highway," <u>Proceedings, World Conference on Prestressed Concrete</u>, San Francisco, July 1957.

30. Kaczmarek, J. A., "Comparison of Computer Analysis and Experimental Data for Concrete Slab and Steel Girder Bridges," M. S. Thesis, The University of Texas at Austin, January 1970.

31. Keyder, E., "Strength and Behavior in Flexure of Bonded Prestressed Concrete Beams Reinforced in Tension Only," M. S. Thesis, The University of Texas, Austin, May 1965.

32. King, J. W. H., "Discussion on Articles Published in the Magazine of Concrete Research Vol. 7, No. 20, July 1955," <u>Magazine of Concrete Research</u>, Vol. 8, No. 22, March 1956.

33. Kollbrunner, C. F., and Basler, K., <u>Torsion in Structures--An Engineering Approach</u>, Springer-Verlag, Berlin 1969.

34. Leyendecker, E. V., "Behavior of Pan Formed Concrete Slab and Girder Bridges," Ph. D. Dissertation, The University of Texas at Austin, 1969.

35. Lin, T. Y., <u>Design of Prestressed Concrete Structures</u>, John Wiley & Sons, Inc., New York, July 1967.

36. Macchi, G., "Elastic Distribution of Moments on Continuous Beams," <u>Proceedings of the International Symposium on Flexural Mechanics of Reinforced Concrete</u>, Miami, Florida, Nov. 10-12, 1964.

37. Macchi, G., "Proposed Method of Analysis Based on the Theory of Imposed Rotations," European Committee for Concrete, <u>Information Bulletin No. 21</u>, London.

38. Panak, J. J., and Matlock, H., "A Discrete-Element Method of Analysis for Orthogonal Slab and Grid Bridge Floor Systems," <u>Preliminary Research Report 56-25</u>, Center for High Research, The University of Texas at Austin, August 1971.

39. Mattock, A. H., and Kaar, P. H., "Precast Prestressed Concrete Bridges, 6-Test of Half Scale Highway Bridge Continuous Over Two Spans," <u>Journal of the PCA Research and Development Laboratories</u>, Vol.3, No. 3 pp. 30-70, Sept. 1961.

40. McManus, P. F., and Culver, C. G., "Non-Uniform Torsion of Composite Beams," <u>Journal of the Structural Division ASCE</u>, June 1969.

41. Newmark, N. M., Siess, C. P., and Peckham, W. M., "Studies of Slab and Beam Highway Bridges: Part II--Tests of Simple-Span Skew I-Beam Bridges," _Bulletin No. 375_, University of Illinois Eng. Exp. Sta., 1948.

42. Newmark, N. M., Siess, C. P., and Penman, R. R., "Studies of Slab and Beams Highway Bridges: Part I--Tests of Simple-Span Right I-Beam Bridges," _Bulletin No. 363_, University of Illinois Eng. Exp. Sta., 1948.

43. Newton, J. G., and Walker, L. G., "Experimental Use of High-Strength Reinforcing Steel," _Research Report No. 25-1F_, Bridge Division, Texas Highway Department, March 1966, 64 pp.

44. Panak, J. J., and Matlock, H., "A Discrete-Element Method of Multiple-Loading Analysis for Two-Way Bridge Floor Slabs", _Research Report 56-13_, Center for Highway Research, The University of Texas at Austin, Jan. 1970.

45. Private Communications with I. O. Erbug, Graduate Student, and J. E. Breen, Professor of Civil Engineering. Both at The University of Texas at Austin.

46. Rao, P. S., "Die Grundlagen Zur Berechnung Der Bei Statisch Unbestimmten Stahlbetonkonstruktionen Im Plastischen Bereich Auftertenden Umlagerungen Der Schnittkrafte," _Deutscher Ausschuss Fur Stahlbeton--Heft 177_, Berlin, 1966.

47. Repa, J. V., Jr., "Flexural Stiffness Redistribution in Typical Highway Bents," M. S. Thesis, The University of Texas at Austin, August 1970.

48. Roark, R. J., _Formulas for Stress and Strain_, McGraw-Hill Book Company, New York, Fourth Edition, 1965.

49. Rowe, R. E., _Concrete Bridge Design_, John Wiley & Sons, Inc., New York, 1962.

50. Rusch et al, H., "Class Notes of CE 397.78 Special Topics in Reinforced Concrete," Fall 1970.

51. Sartwell, A. D., Heins, C. P., Jr., and Looney, C. T., "The Analytical and Experimental Study of a Simple Girder Bridge," Progress Report, Civil Eng. Dept., The University of Maryland at College Park, Maryland, Feb. 1968.

52. Siess, C. P., and Viest, I. M., "Studies of Slab and Beam Highway Bridges: Part V--Tests of Continuous Right I-Beam Bridges," _Bulletin No. 416_, University of Illinois Eng. Exp. Sta., 1953.

53. Simmons, J. C., "Poisson's Ratio of Concrete: A Comparison of Dynamic and Static Measurements," Magazine of Concrete Research, Vol. 7, No. 20, July 1955, pp. 61-68.

54. Sinha, N. C., "Ultimate Strength of Concrete Members Reinforced with High Strength Steel Without a Definite Yield Point," Ph.D. Dissertation, The University of Texas, Austin, June 1962.

55. Sokolnikoff, I. S., Mathematical Theory of Elasticity, McGraw-Hill Book Company, Inc., New York, 1956.

56. Stelzer, C. F., and Hudson, W. R., "A Direct Computer Solution for Plates and Pavement Slabs," Research Report 56-9, Center for Highway Research, The University of Texas at Austin, Oct. 1967.

57. Subcommittee 4, ACI Committee 435, "Recommendation for ACI Building Code Provision on Deflections," Report Approved by Committee 435 and submitted to ACI Committee 318, Oct. 1967.

58. Timoshenko, S., and Goodier, N., Theory of Elasticity, McGraw-Hill Book Company, Inc., New York, 1951.

59. Timoshenko, S., and Woinowsky-Krieger, S., Theory of Plates and Shells, McGraw-Hill Book Company, Inc., New York, 1959.

60. Troitsky, M. S., Orthotropic Bridges--Theory and Design, The James F. Lincoln Arc Welding Foundation, Cleveland, Ohio, August 1967.

61. Vora, M. R., and Matlock, H., "A Discrete-Element Analysis for Anisotropic Skew Plates and Grids," Research Report 56-18, Center for Highway Research, The University of Texas at Austin, August 1970.

A P P E N D I X   A

LISTING AND INPUT DATA GUIDE FOR

COMPUTER PROGRAMS MPHI AND TORSION

```
      PROGRAM MPHI(INPUT,OUTPUT)
C
C     THIS PROGRAM GENERATES THE THEORETICAL MOMENT-CURVATURE RELATIONSHIP
C     FOR ANY REINFORCED CONCERET SECTION WHICH CAN BE REPRESENTED BY
C     RECTANGLES. THE PROGRAM TAKES INTO ACCOUNT THE EFFECT OF CRACKS ON
C     THE BEHAVIOR OF THE MEMBER.
C
      COMMON /L1/ CYL,EC,TT,RK,ENO
      COMMON /L2/ NUM,YSEG(101),ASEG(101)
      COMMON /L3/ AST(20),D(20),NS
      COMMON /L4/ FY,EY,RATIO
      DIMENSION  T(20),W(20),STRNI(100),STRNO(100),NSEG(101),SEG(101),
     2 TFORT(100),TMOMT(100),PHI(100),RR(100),IK(10),Y(21),RATTOM(100)
  200 FORMAT(1H1,/,5X,*ALL UNITS ARE IN POUNDS AND INCHES*,/)
  201 FORMAT(/,10X,*SECTION PROPERTIES*,/,5X,*CONCERET LAYERS*,/,
     2    5X,*THICKNESS*,11X,*WIDTH*)
  202 FORMAT(/,5X,*STEEL LAYERS*,/,8X,*AREA*,13X,*DEPTH*)
  203 FORMAT(F13.3,F18.3)
  205 FORMAT(/,5X,*AXIAL LOAD          =*,F12.4,/,
     2          5X,*LOAD CLOSURE        =*,F12.4,/,
     2          5X,*DEPTH TO LOAD       =*,F12.4,/,
     2          5X,*N.A.(GROSS SEC.)    =*,F12.4,/,
     2          5X,*CONCERET STRENGTH   =*,F12.4,/,
     2          5X,*STRENGTH FACTOR     =*,F12.4,/,
     2          5X,*E - CONCERET        =*,F12.4,/,
     2          5X,*STEEL YIELD POINT   =*,F12.4,/,
     2          5X,*GROSS INERTIA       =*,F12.4,/,
     2          5X,*CRACKING MOMENT     =*,F12.4,/,
     2          5X,*AS(TENS)/A-GROSS    =*,F12.4,//)
  206 FORMAT(5X,*POINT*,2X,*INNER STRAIN*,3X,*OUTER STRAIN*,3X,
     2    *ACTUAL LOAD*,7X,*MOMENT*,7X,*CURVATURE*,7X,*RIGIDITY*)
  207 FORMAT(I8,8E15.4)
  208 FORMAT(8F10.3)
  210 FORMAT(10A8)
  211 FORMAT(//,5X,10A8)
  212 FORMAT(5X,*LOAD DID NOT CONVERGE (20 ITRATIONS) FOR POINT*,I10)
  214 FORMAT(2I5,7F10.3)
C
      PRINT 200
  100 READ 210,(IK(I),I=1,10)
      KOP=8H
      IF(IK(1)-KOP)  101,102,101
  101 READ 214, NSG,NS,AX,CYL,FY,RK,CLOSURE,EC
      EY=29000000.
      ACI=57400.*SQRT(CYL)
      IF(EC.LT.10.) EC=ACI
      IF(RK.LT.0.01) RK=1.0
      ENO=RK*2.0*CYL/EC
      PRINT 211,(IK(I),I=1,10)
      T(1)=0.
      W(1)=0.
      NN=NSG+1
      READ 208,(T(I),W(I),I=2,NN)
      READ 208,(AST(I),D(I), I=1,NS)
      TT=0.0
```

```
      AREA=0.0
      Y(1)=0.0
      AY=0.0
      PRINT 201
      DO 1 I=2,NN
      PRINT 203,T(I),W(I)
      TT=TT+T(I)
      AREA=AREA+T(I)*W(I)
      Y(I)=Y(I-1)+(T(I)+T(I-1))/2.0
    1 AY=AY+T(I)*W(I)*Y(I)
      YB=AY/AREA
      AS=0.0
      PRINT 202
      DO 2 N=1,NS
      PRINT 203,AST(N),D(N)
      IF(D(N).GT.YB)    AS=AS+AST(N)
    2 CONTINUE
      RATIO=AS/AREA
      DD=0.0
      DO 3 I=2,NN
    3 DD=DD+W(I)*T(I)**3/12.+T(I)*W(I)*(YB-Y(I))**2
      FR=7.5*SQRTF(CYL)
      C=TT-YB
      CRMOM=FR*DD/C
      NSEG(1)=0
      YSEG(1)=0.0
      ASEG(1)=0.0
      NUM=1
      DO 4 I=2,NN
      SEG(I)=(T(I)/TT)*50.
      NSEG(I)=SEG(I)
      SEG(I)=NSEG(I)
      NUM=NUM+NSEG(I)
      N=NUM-NSEG(I)+1
      DO 4 K=N,NUM
      YSEG(K)=T(I)/SEG(I)
      ASEG(K)=YSEG(I)*W(I)
    4 CONTINUE
      IF(CLOSURE.NE.0.0) GO TO 5
      CLOSURE=AX/1000.
      COMPARE=AREA
      IF(COMPARE.GT.CLOSURE) CLOSURE=COMPARE
    5 CALL    LOCATE(AX,CLOSURE,AREA,YB,DEPTH,EINIT)
      PRINT 205,AX,CLOSURE,DEPTH,YB,CYL,RK,EC,FY,DD,CRMOM,RATIO
      PRINT 206
      STRNI(1)=EINIT
      STRNO(1)=EINIT
      RR(1)=0.0
      PHI(1)=0.0
      TFORT(1)=AX
      TMOMT(1)=0.0
      EI=EINIT
      EO=EINIT
      EX =(.0038-EINIT)/50.0
      EXS=5.*EX
      DO 10 I=2,51
```

```
      EI=EI+FX
      VALUE=FXS
      DELTA=FXS
      DO 8 ITRATE=1,20
      EO=EO-DELTA
      CALL          CONC(EI,EO,TFORC,TMOMC)
      CALL          STEEL(EI,EO,TFORS,TMOMS)
      TFORT(I)=TFORC+TFORS
      TMOMT(I)=TMOMC+TMOMS+TFORT(I)*DEPTH
      TEST=TFORT(I)-AX
      IF(ABSF(TEST)-CLOSURE) 14,14,16
   16 IF(TEST.GT.CLOSURE .AND. VALUE.EQ.FXS) GO TO 8
      VALUE=VALUE/2.0
      DELTA=VALUE
      IF(TEST.LT.CLOSURE) DELTA=-VALUE
    8 CONTINUE
      PRINT  212,I
   14 STRNI(I)=EI
      STRNO(I)=EO
      PHI(I)=(EI-EO)/TT
      RR(I)=TMOMT(I)/PHI(I)
      IF(EI.GT.0.0038 .OR. EO.LT. -.010) GO TO 30
   10 CONTINUE
   30 DO 32 J=1,I
   32 PRINT207,J,STRNI(J),STRNO(J),TFORT(J),TMOMT(J),PHI(J),RR(J)
      GO TO 100
  102 CONTINUE
      END
C
      SUBROUTINE LOCATE(AX,CLOSURE,AREA,YB,DEPTH,EINIT)
C  LOCATION OF THE DEPTH TO THE AXIAL LOAD TO GIVE UNIFORM STRAIN ON SECTION
      COMMON /L1/ CYL,EC,TT,RK,ENO
      COMMON /L3/ AST(20),D(20),NS
      COMMON /L4/ FY,EY,RATIO
    2 FORMAT(5X,*DEPTH TO LOAD DID NOT CONVERGE FOR 20 ITRATIONS*)
      IF(AX) 4,15,5
    4 EE=-.0001
      GO TO 6
    5 EE=ENO
    6 DELTA=ABSF(EE)
      DO 12  I=1,20
      CALL  FC(EE,SC)
      CALL  FS(EE,SS)
      ALOAD=SC*AREA
      YLOAD=ALOAD*YB
      DO 8  K=1,NS
      ALOAD=ALOAD+AST(K)*(SS-SC)
    8 YLOAD=YLOAD+AST(K)*D(K)*(SS-SC)
      TEST=ALOAD-AX
      IF(ABSF(TEST)-CLOSURE)  14,14,10
   10 DELTA=DELTA/2.0
      EE=EE+DELTA
      IF(ALOAD.GT.AX)  EE=EE-2.0*DELTA
   12 CONTINUE
      PRINT 2
   14 EINIT=EE
```

```
      DEPTH=YLOAD/ALOAD
      GO TO 16
   15 DEPTH=0.0
      EINIT=0.0
   16 RETURN
      END
      SUBROUTINE CONC(EI,EO,TFORC,TMOMC)
C FOR GIVEN STRAIN GRADIENT ON A CONCRET SECTION THE SURROUTINE  CALCULA:
C   TOTAL FORCE AND MOMENT ON THE SECTION
      COMMON /L1/ CYL,EC,TT,RK,ENO
      COMMON /L2/ NUM,YSEG(101),ASEG(101)
      DIMENSION  SC(101),YY(101)
      YT=0.0
      CALL FC(EI,STRESS)
      SC(1)=STRESS
      TFORC=0.0
      TMOMC=0.0
      DO 10 I=2,NUM
      YT=YT+YSEG(I)
      YY(I)=YT-YSEG(I)/2.0
      EX=EI+(EO-EI)*YT/TT
      CALL FC(EX,STRESS)
      SC(I)=STRESS
      P=(SC(I)+SC(I-1))*ASEG(I)/2.0
      TFORC=TFORC+P
      TMOMC=TMOMC-P*YY(I)-(SC(I)-SC(I-1))*ASEG(I)*YSEG(I)/12.0
   10 CONTINUE
      RETURN
      END
C
      SUBROUTINE STEEL(EI,EO,TFORS,TMOMS)
C CALCULATION OF TOTAL AXIAL LOAD AND MOMENT CARRIED BY STEEL LAYERS
C FOR A GIVEN STRAIN GRADIENT ON THE SECTION
      COMMON /L1/ CYL,EC,TT,RK,ENO
      COMMON /L3/ AST(20),D(20),NS
      COMMON /L4/ FY,EY,RATIO
      TFORS=0.0
      TMOMS=0.0
      DO 10 I=1,NS
      ES=EI+(EO-EI)*D(I)/TT
      CALL FS(ES,SS)
      CALL FC(ES,SC)
      SS=SS-SC
      TFORS=TFORS+SS*AST(I)
      TMOMS=TMOMS-SS*AST(I)*D(I)
   10 CONTINUE
      RETURN
      END
C
      SUBROUTINE FC(EP,STRESS)
      COMMON /L1/ CYL,EC,TT,RK,ENO
C   CONCRETE STRESS USING HOGNESTAD STRESS BLOCK
      EU=0.0038
      ENOT=.0001
      IF (EP) 2,3,4
    2 X=ABSF(EP/ENOT)
```

```
      FT=5.0*SQRTF(CYL)
      SC=-FT/X
      IF(X.LT.1.0)  SC=EP*EC-(FT-ENOT*EC)*X**2
      GO TO 1
    3 SC=0.0
      GO TO 1
    4 SC=RK*CYL*(2.*EP/ENO-(EP/ENO)**2)
      IF(EP.GT.ENO)  SC=RK*CYL*(1.-.1D*(EP-ENO)/(EU-ENO))
    1 STRESS=SC
      RETURN
      END
      SUBROUTINE FS(EP,SS)
C  CALCULATION OF STEEL STRESS FOR A GIVEN STRAIN
      COMMON /L4/ FY,EY,RATIO
      IF(EP.LT.-0.00010)GO TO 8
      SS=EY*EP
      IF(SS.GT.FY) SS=FY
      GO TO 10
    8 X=ABSF(EP/.0001)
      ADD=57.0/RATIO
      IF(RATIO.LT.0.005) ADD=11400.+(ADD-11400.)*(RATIO/.005)
      SS=EP*FY-ADD*(1.0-1./X)
      IF(SS.LT. -FY) SS=-FY
   10 RETURN
      END
```

Input Data Guide for Program MPHI

Identification Card (one alphanumeric card each problem)

Title and description of the problem

1   80

Table 1: One card

NSG	NS	AX	CYL	FY	RK	CLOSURE	E_c	

1   5   10   20   30   40   50   60

Table 2: Concrete layers; 4 layers each card (cards as required)

T_1	W_1	T_2	W_2	---	---		

1   10   20   30   40   50   60   70   80

Table 3: Steel layers = 4 layers each card (cards as required)

A_{s1}	D_1	A_{s2}	D_2	---	---	λ	

1   10   20   30   40   50   60   70   80

Notations (all units are in inches and pounds)

NSG = No. of concrete layers in the section
NS = No. of steel layers in the section
AX = Axial load (negative if it is tension)
CYL = Compressive strength of concrete
F_y = Yield strength of steel
RK = Reduction factor [$f_c'' = (RK)\ f_c'$]

    if not input RK = 1.0 will be considered

CLOSURE = Closure range of calculated and applied
    axial load,if not input the value will
    be the smallest of either 1/1000 of
    applied load if any or a load which
    produces a uniform stress of 1 psi
    over the entire section.

T = Thickness of concrete layer
    the first thickness for the
    layer on the compression face
W = Width of concrete layer
A_s = Steel area of the layer
D = Depth from steel centroid to the
    compression face of the section
E_c = Elasticity of concrete. If not
    input the ACI 318-63 value will
    be taken.

171

```
      PROGRAM TORSION(INPUT,OUTPUT)
C   THIS PROGRAM COMPUTES THE ANGLE OF TWIST AND THE TORSIONAL
C   RIGIDITY FOR A COPMPOSITE STEEL BEAM AND CONCRETE SLAB ALONG THE
C   BEAM.  IF SOLVES FOR THREE END CONDITIONS SIMPLE, CANTILEVER, AND
C   FIXED ENDS
C
      DIMENSION K(10)
   10 FORMAT (10A8)
   11 FORMAT (/,5X,10A8)
   12 FORMAT (7E10.3)
   13 FORMAT (1H1,/,5X,*ALL UNITS ARE IN INCHES, POUNDS,AND RADIANS*//)
   14   FORMAT (/,5X,*SECTION PHOPERTIES*,/,5X,*STEEL SECTION*,/,10X,
      2  *DEPTH =*,E19.3,/,10X,*FLANGE WIDTH =*,E12.3,/,10X,
      3 *FLANGE THICK =*,E12.3,/,10X,*WEB THICK    =*,E12.3,/,5X,
      4*CONCRETE SECTION*,/,10X,*WIDTH =*E19.3,/,10X,*THICKNESS  =*F14.3)
   15 FORMAT(5X,*MATERIALS PROPERTIES*,/,10X,E-STEEL     =*,E14.3,/,10X,
      2 *POISSONS RATIO=*E11.3,/,10X,*E-CONCRETE =*,E14.3,/,10X,
      3 *POISSONS RATIO=*,E11.3,/,5X,*SPAN LENGTH     =*,E14.3,//)
   16 FORMAT(5X,*STATION*,4X,*DISTANCE*,8X,*CASE 2 (CANTILEVER BEAM)*
      2,6X,*CASE 3 (FIXED ENDS BEAM)*,/,32X,*TWIST ANGLE*,5X,*RIGIDITY*
      3  ,6X,*TWIST ANGLE*,5X,*RIGIDITY*)
   17 FORMAT(I10,E14.3,E19.5,5E15.5)
   18 FORMAT(/,5X,*CASE 1 (FREE ENDS BEAM)*,/,*TWIST ANGEL (RAD/IN/ L
      2B-IN ) =*E15.5,/,5X,*RIGIDITY          (LB-SQ.IN)   =*E15.5,/)
  100 READ 10,(K(I),I=1,10)
      NONE=8H
      IF(K(I)-NONE) 1,111,1
    1 READ 12,DEPTH,BS,F,W,BC,TC,SPAN
      READ 12,ES,PS,EC,PC
      PRINT 13
      PRINT  11,(K(I),I=1,10)
      PRINT 14,DEPTH,BS,F,W,BC,TC
      PRINT 15,ES,PS,EC,PC,SPAN
      H=DEPTH-2.*F
      Y=BC*TC*EC*(H+2.*F+.5*TC)+BS*F*ES*(H+2.*F)+H*W*ES*(.5*H+F)
      YBAR=Y/(BC*TC*EC+2.*BS*F*ES+H*W*ES)
      A=YBAR-.5*F
      B=H+.5*TC+2.*F-YBAR
      C=-.5*F
      BS3=BS**3
      BC3=BC**3
      YP=2.*ES*F*BS3*(A-B+C)-EC*TC*(2.*BC3*B+BS3*C-3.*BC*BC*BS*C)
      YPBAR=.5*YP/(2.*ES*F*BS3+EC*TC*BC3)
      D=A-YPBAR
      F3=F**3
      W3=W**3
      TC3=TC**3
      GS=ES/(2.+2.*PS)
      GC=EC/(2.+2.*PC)
      GKT=(2.*GS*BS*F3+GS*H*W3+GC*BC*TC3)/3.0
      ABCD=A+B-C-D
      BB=BS*C-BC*(A+B-D)
      EIW=ES*F*BS3*D*D+EC*TC*BS3*ABCD*ABCD+ES*F*BS3*ABCD*ABCD
      2     +EC*TC*(BC-BS)*(BB*BB+BB*BS*ABCD+(BS*ABCD)**2)
```

```
      EIW=EIW/12.
      R=SQRT(GKT/EIW)
      XL=R*SPAN
      E1=EXP(XL)
      E2=1.0/E1
      EL=E1-E2
      EE=E1*E1
      E3=1.0+EE
      FY1=1.0/GKT
      R1=GKT
      PRINT 18,FY1,R1
      PRINT 16
      DO 3 K=1,21
      AK=K-1
      Z=AK*.05*SPAN
      X=Z*R
      EZ1=EXP(X)
      EZ2=1.0/EZ1
      FY2=(1.0-EZ1-EE+EE*EZ2+R*E3*Z)/(R*GKT*E3)
      R2=(GKT*E3)/(E3-EZ1-EE*EZ2)
      FY3=(2.0-E1-E2+E2*EZ1-EZ1+E1*EZ2-EZ2+R*Z*EL)/(R*GKT*EL)
      R3=(GKT*EL)/(E2*EZ1-EZ1-E1*EZ2+EZ2+EL)
      N=K-1
    3 PRINT 17,N,Z,FY2,R2,FY3,R3
      GO TO 100
  111 CONTINUE
      END
```

Input Data Guide for Program TORSION

Identification Card (one alphanumeric card each problem)

Title and description of the problem
1   80

Table 1: One card (dimensions)

D	B	F	W		B_c	T_c	SPAN	
1	10	20	30	40	50	60	70	

Table 2: One card (material properties)

E_s	ν_s	E_c	ν_c	
1	10	20	30	40

Notations   (all units are in inches and kips)
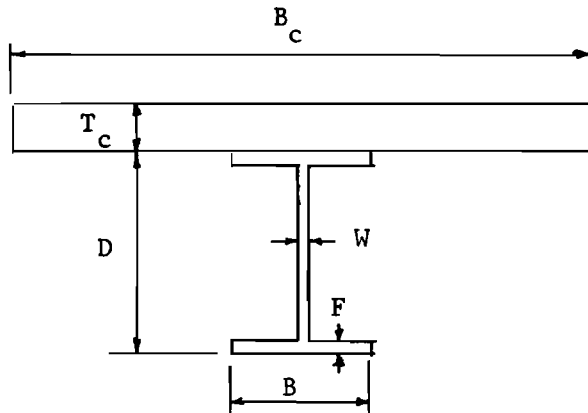
E_s = Steel modulus of elasticity

ν_s = Poisson's ratio of steel

E_c = Concrete modulus of elasticity

ν_c = Poisson's ratio of concrete

SPAN = Span length of the composite beam